EVALUATING THE INFLUENCE OF PRODUCTION PARAMETERS ON THE PERFORMANCE OF MICROSURFACING MIX

A thesis submitted to Indian Institute of Technology Guwahati
for the partial fulfilment of the award of the degree

of

Doctoral of Philosophy

by

Nishant Bhargava
(Roll no.- 176104001)

Under the guidance of

Dr. Anjan Kumar Siddagangaiah
and
Prof. Teiborlang Lyngdoh Ryntathiang

DEPARTMENT OF CIVIL ENGINEERING
INDIAN INSTITUTE OF TECHNOLOGY GUWAHATI
GUWAHATI - 781039, INDIA
JUNE 2022

Certificate

This is to certify that the thesis titled "**Evaluating the Influence of Production Parameters on the Performance of Microsurfacing Mix**" submitted by **Nishant Bhargava** to Indian Institute of Technology Guwahati for the award of the degree of Doctor of Philosophy is a record of bonafide research work carried out by him under our supervision and guidance. In our opinion, the thesis work has reached the requisite standard fulfilling the requirement for the degree of Doctor of Philosophy.

The findings presented in this thesis have not been submitted in part or full to any other university or institute for the award of any degree or diploma.

Dr. Anjan Kumar Siddagangaiah
Associate Professor
Department of Civil Engineering
IIT Guwahati
Guwahati – 781039, Assam, India

Prof. Teiborlang Lyngdoh Ryntathiang
Professor
Department of Civil Engineering
IIT Guwahati
Guwahati – 781039, Assam, India

Place: IIT Guwahati

Date: 28/02/2022

Declaration

I hereby declare that this thesis represents my own research work which has been carried out during my Ph.D. at the Indian Institute of Technology Guwahati. The work presented in this thesis has not been previously included in any other thesis submitted for a degree or other qualifications. Wherever contributions from others are involved, I have provided relevant acknowledgement or reference to the original source. I also declare that I have adhered to all academic ethics and responsibilities and have not misinterpreted or fabricated or falsified any idea/ data/ fact/ source in my submission. This thesis, in any way, does not endorse any proprietary products or technologies.

Place: IIT Guwahati
Date: 28/02/2022

Nishant Bhargava
Roll No. 176104001

Acknowledgment

Firstly, I would like to express my sincere gratitude to my supervisors Dr. Anjan Kumar Siddagangaiah and Prof. Teiborlang Lyngdoh Ryntathiang for providing me guidance throughout the thesis work. Their enthusiasm, encouragement and faith in me all through have been extremely helpful. My indebtedness is for the time they spared and knowledge they endowed while leading me to the right source, theory and perspective towards pavement engineering.

I would also like to extend my heartfelt gratitude to my committee members, Prof. C. Mallikarjuna, Dr. Hrishikesh Sharma and Prof. R. Ganesh Narayanan. Your opinions and inputs are highly appreciated and helped in improving the thesis.

My gratitude goes to Mr. Bhaskar Pratim Das, Mrs. Saswati Das, Mr. Supratim Kaushik, Mr. Santanu Pathak, Ms. Ibaiahun Nongbet Sohlang and Mr. Harish N. for their tremendous support throughout my Ph.D. journey. I would like to thank the technical staff and the staff members of IITG, especially Mr. Kuldeep Kalita, Mr. Mrinal Sarma and Mr. Balan Kalita, who have helped me along the way.

I am thankful to the IITG for providing the research facility for the completions of this research work. Thanks to Om Infracon Pvt. Ltd. and Hincol Pvt. Ltd. for providing the material support and BitChem Asphalt Technologies Ltd. for their help in emulsion production for preliminary investigations. Also, I appreciate the laboratory support provided by IRMS Lab, IIT Kanpur, for sample testing using XRF.

Most importantly, none of this could have happened without my family. Your continuous encouragement, love, and support kept me working hard towards achieving my goal. This thesis stands as a testament to your unconditional love and encouragement.

Nishant Bhargava

Abstract

Microsurfacing is a mixture of crushed mineral aggregates, polymer modified emulsion, mineral filler, water and additive, mixed and produced at ambient temperature. The performance of microsurfacing depends on mix ingredient optimization and process control during production. So, the objective of this study was to investigate the influence of different production parameters on the performance of microsurfacing mix during the *mix design stage*, *production stage*, and *service life*.

Initially, the effect of material properties on the mix design was investigated. The challenges faced during mix design were rapid emulsion breaking, lower cohesion, higher raveling, and rutting. A combination of fillers, harder asphalt binder, and solvent was used to address the compatibility and performance issues. The combination of cement (2%) and fly ash (1%) exhibited the highest cohesion, highlighting the benefits of incorporating waste materials with pozzolanic characteristics in the mix. Incorporation of harder asphalt binder reduced rutting by 36% but resulted in unacceptable raveling. The use of solvent during emulsion production resolved the issue of raveling while further improving the rutting resistance by another 39%. This highlights the importance of proper binder type selection and maintaining equiviscous temperature during emulsion production. Six mix design parameters were evaluated at 4 emulsion contents (total specimens = 72, considering 3 replicates) to determine the job mix formula. A narrow range diagram illustrating the acceptable range of emulsion content was proposed to determine optimum emulsion content (OEC).

For evaluating the effect of process control parameters during production, 35 combinations of aggregate gradation, emulsion content, and water content, were produced. For the control mix, the aggregate gradation, emulsion content, and water content were mean of Type II gradation, OEC (14% by weight of dry aggregate), and optimum water content (OWC, 6.4% by weight of dry aggregate), respectively. Aggregate gradation was varied within mean ± tolerance limit specified by International Slurry Seal Association (ISSA). Emulsion content was varied within OEC ± 1.5%, i.e., 12.5% to 15.5%. Water content was varied from OWC – 1% to OWC + 2%, i.e., 5.4% to 8.4%. Each combination was tested for workability, strength, raveling, rutting, and bleeding in terms of consistency, cohesion, abrasion loss, lateral displacement, and sand adhesion, respectively. A total of 105 specimens (35 combinations with 3 replicates) were tested for workability, and 120 specimens (30 combinations with 4 replicates) were tested for all other performance tests. Finally, the performance during service life was assessed by investigating the synergistic effect of aging and moisture conditioning

on raveling. A total of 30 combinations (4 replicates per combination) of aging and moisture conditioning were considered.

The relative contribution of each parameter was quantified using Artificial Neural Network (ANN) and Garson's algorithm. The parameter having the highest relative contribution on performance was quantified by developing a model using Multigene Symbolic Genetic Programming (MSGP). It was found that the relative contribution of aggregate gradation on strength and raveling, emulsion content on workability, strength at 30-min and rutting, and water content on workability, strength at 60-min and bleeding was more than 35%. Results from MSGP showed that the workability increased at a rapid rate when the emulsion and water content were increased. Minimal variation in cohesion shows that the microsurfacing mix gains sufficient strength if the process control parameters are within the tolerance range. Raveling increased exponentially for coarser aggregate gradation and lower emulsion content. Rutting increased exponentially for emulsion content on either the lower or higher side. Bleeding reduced at a constant rate with the increase in water content.

Reliability analysis showed that the probability of failure due to rutting was the highest when the process control parameters varied within the tolerance limits. The critical combination identified was coarser aggregate gradation and lower emulsion content. The overall reliability increased from 47% to 71% when critical combinations were excluded from reliability analysis. So, this study propose that during mix design, the critical combinations of process control parameters should be identified with the integrated use of ANN and MSGP. The associated risk of failure should be benchmarked using reliability analysis and appropriate quality control measures should be suggested to enhance quality and performance of microsurfacing.

Increasing the aging temperature from 85°C to 105°C led to a 41% reduction in raveling. No significant variation in raveling was noticed with the increase in moisture conditioning time. However, increasing the moisture conditioning temperature from 25°C to 60°C for six days resulted in a 66% reduction in raveling. Until the specimen had the presence of moisture, raveling was influenced by moisture conditioning temperature. But once the specimen was fully cured and subjected to further aging, the effect of moisture on raveling was minimal. Thus, this study recommend that microsurfacing shall be applied during favorable environmental conditions, facilitating faster moisture loss and strength gain to ensure durability.

Keywords: Microsurfacing, process control parameters, aging, moisture.

Table of Contents

List of Tables

List of Figures

List of Abbreviations

AG	Aggregate Gradation
ANN	Artificial Neural Network
ANOVA	Analysis of Variance
ASTM	American Society for Testing and Materials
CoV	Coefficient of Variation
CSS	Cationic Slow Setting
CQS	Cationic Quick Setting
DoT	Department of Transportation
EC	Emulsion Content
FA	Flyash
FPC	Factory Production Control
GP	Genetic Programming
HMA	Hot Mix Asphalt
IRC	Indian Roads Congress
ISSA	International Slurry Seal Association
LWT	Loaded Wheel Test
MBV	Methylene Blue Value
MSE	Mean Squared Error
MSGP	Multigene Symbolic Genetic Programming
OEC	Optimum Emulsion Content
OPC	Ordinary Portland Cement
OWC	Optimum Water Content
PCA	Principal Component Analysis
RAP	Reclaimed Asphalt Pavement
RAS	Recycled Asphalt Shingles
SBRT	Schulze Breuer and Ruck Test
SBR	Styrene Butadiene Rubber
SBS	Styrene Butadiene Styrene
SWOT	Strength, Weakness, Opportunities, and Threat
TAIT	Type Approval Installation Trial
TSA	Total Surface Area
TTI	Texas Transportation Institute
VG	Viscosity Grade

VOC	Vehicle Operation Cost
WC	Water Content
WTAT	Wet Track Abrasion Test
QA	Quality Assurance
QC	Quality Control

List of Symbols

AL_{am}	Abrasion loss of specimens subjected to aging and moisture conditioning, g/m^2
A_T	Aging temperature, °C
A_t	Aging time, hours
AC_t	Temperature of asphalt during emulsion production, °C
AC_{wt}	% of asphalt by total weight of emulsion
AL	Abrasion Loss (Values normalized for MSGP model)
AR	Abrasion resistance as per shaking abrasion test, %
BR	Total bitumen required, %
CH_{30}	Cohesion at 30-min (Values normalized for MSGP model)
CH_{60}	Cohesion at 60-min (Values normalized for MSGP model)
CSA	Corrected surface area of aggregates, m^2/kg
CT	Consistency (Values normalized for MSGP model)
$c_{0,GP}$	Bias/offset coefficient in GP model
$c_{1,GP}$,.. $c_{G,GP}$	Scaling term for respective tree/gene in GP model
DOF	Degree of freedom
E_i	Expected frequency for group i
E_t	Asphalt emulsion manufacturing process temperature, °C
EC	Emulsion content (Normalized values)
f_i	% frequency in group i
$f_n(x)$	Joint probability density function
GD_{cm}	Gap dimension in colloid mill
G_b	Specific gravity of asphalt binder
G_{sa}	Apparent specific gravity of aggregates
G^*	Dynamic shear modulus, MPa
IRI	International Roughness Index, m/km
J_{nr}	Non-recoverable compliance
KA	Kerosene absorbed, %
LCF_{LWT}	Loss correction factor for LWT, g/m^2
LCF_{WTAT}	Loss correction factor for WTAT, g/m^2
LD	Lateral displacement (Values normalized for MSGP model)
M_T	Moisture conditioning temperature, °C
M_t	Moisture conditioning time, hours

m_{LA}	Mass of specimen prior to vacuum application in air, gm
m_{LV}	Mass of specimen after vacuum application in air, gm
m_{WA}	Mass of specimen prior to vacuum application in water, gm
m_{WV}	Mass of specimen after vacuum application in water, gm
m_{ar}	Mass of specimen after abrasion, gm
m_f	Mass of specimen before abrasion, gm
m_p	Mass of specimen in air before testing, gm
N	Total number of observations for reliability analysis
N_i	Number of intervals in group i
n_{ra}	Number of class intervals for reliability analysis
O_i	Observed frequency for group i
$PC_{ij,PCA}$	Weight of component i for test parameter j in PCA
$P(AL)$	Probability of mix passing the specified limits for abrasion loss
$P(CH_{60})$	Probability of mix passing the specified limits for cohesion
$P(LD)$	Probability of mix passing the specified limits for lateral displacement
$P(SA)$	Probability of mix passing the ISSA specified limits for sand adhesion
$P_{ij,ANN}$	Multiplication of $\lvert W_{ij,ANN} \rvert$ and $\lvert W_{i1,ANN} \rvert$
$P_{ra}(n)$	Probability of performance test results falling within specification limits
p_{ra}	Number of model parameters for reliability analysis
$Q_{ij,ANN}$	Ratio of $P_{ij,ANN}$ for each hidden neuron for all input variables j connected to hidden neuron i
$RC_{j,ANN}$	Relative contribution of input variable j
$R(M)$	Overall reliability of mix passing the ISSA specificied limits
R_{cm}	Colloid mill radius
R_d	Stability ratio
R_s	Separation ratio
SA	Sand adhesion (Values normalized for MSGP model)
SAB	Surface area of bitumen, m^2/kg
$Soap_t$	Temperature of soap solution during emulsion production, °C
$Soap_{wt}$	% of soap solution by total weight of emulsion
$S_{j,ANN}$	Sum of $Q_{ij,ANN}$ for input variable j

$S_{m,PCA}$	Score for mix type m using PCA
TSA	Total surface area of aggregates (Normalized values)
t	Asphalt film thickness, µm
$t_{i,GP}$	(N×1) vector of outputs from the ith gene/tree having a multigene individual in GP model
UL_i	Upper limit of class interval for group i
u_i	Mid-point of the range for group i
VOC	Estimated vehicle operating cost per 1000 veh-km
V_A	Volume of specimen after water absoprtion, cm^3
V_V	Volume of specimen before water absoprtion, cm^3
V_{cm}	Velocity of rotation of colloid mill
$V_{i,PCA}$	% of variance of rotated sum of squared loadings for component i
WC	Water content (Normalized values)
W_V	Water absorption, %
$W_{a,LWT}$	Initial width of the LWT specimen, mm
$W_{a,SBRT}$	Initial weight of SBRT specimen, gm
$W_{a,WTAT}$	Initial weight of cured WTAT specimen, gm
$W_{a,aging}$	Weight of WTAT specimen after aging, gm
W_{ac}	Weight of sample and container after centrifuge, gm
$W_{b,LWT}$	Width of the specimen after 1000 cycles of loading, mm
$W_{b,SBRT}$	Weight of SBRT specimen after water absoption, gm
$W_{b,WTAT}$	Weight of WTAT specimen after abrasion, gm
$W_{b,aging}$	Weight of WTAT specimen before aging, gm
W_{bc}	Weight of sample and container before centrifuge, gm
$W_{c,LWT}$	Weight of specimen before sand adhesion, gm
$W_{c,SBRT}$	Weight of SBRT specimen after abrasion test, gm
$W_{d,LWT}$	Weight of specimen after sand adhesion, gm
$W_{d,SBRT}$	Weight of surface dried SBRT specimen after integrity test, gm
$W_{j,PCA}$	Weight for the test parameter j in PCA
W_s	Dry weight of aggregate sample for centrifuge, gm
$\lvert W_{i1,ANN} \rvert$	Absolute of the connection weight between output variable and hidden neuron i (ANN)

$\lvert W_{ij,ANN} \rvert$	Absolute of the connection weight between input variable j and hidden neuron i (ANN)
$X_{mj,PCA}$	Normalized value of results for mix type m and test parameter j
z_d	Upper limit of standard normal for group i
v	Activation function (ANN)
χ^2	Chi-square
μ	Mean of values for a test parameter
δ	Phase angle, °
$\varphi(z)$	Probability integral function
$\dot{\gamma}$	Shear rate
σ	Standard deviation of values for a test parameter
$\varphi_h(v)$	Transfer function for hidden layer (ANN)
$\varphi_o(v)$	Transfer function for output layer (ANN)

CHAPTER 1

Introduction

1.1 General

India has a road network of length 62,15,797 km, according to the annual report published by the Ministry of Road Transport & Highways in 2020-21. In India, the primary road transport system is the National Highways, which are subjected to heavy traffic load applications under varying climatic conditions. Therefore, the pavement must be structurally and functionally sound for safe and smooth travel. The structural strength of the pavement is dependent upon the capacity of the pavement structure to resist traffic loading. In contrast, the functional condition includes the riding quality, safety and comfort at an adequate speed and cost. While structural strength is ensured for the design period during the initial construction and quality control checks, pavement preservation treatments are generally recommended for preserving and improving the functional conditions.

In this regard, timely maintenance with the right treatment choice such as routine maintenance, repair, rehabilitation, or reconstruction needs to be applied to maintain the acceptable serviceability level over a lifetime of a pavement structure. Among these practices, the application of preventive maintenance (routine maintenance or repair) at the proper time had shown to decrease the deterioration rate of pavement condition and delay the requirement of major rehabilitation or reconstruction. Hence, preventive treatments offer a relatively low-cost solution along with improving performance. In this regard, microsurfacing has proven to be a durable solution to improve functional characterisitics and inhibit distresses like raveling and oxidation.

1.2 Problem Statement

To ensure that the microsurfacing mix performs satisfactorily during its service life, it is critical to quantify the effect of each component on the performance of the microsurfacing mix during the mix design stage. Even with a well-designed mix, the performance is dependent on the tightness of the process control methodology and the variables controlled. In the conventional hot mix asphalt (HMA) applications, a significant body of research had been devoted to understanding the variables that would

require the most attention during execution and the associated consequences on the performance of such applications are benchmarked. The focus of the study is to quantify the influence of variation in process control parameters on the performance of microsurfacing mix which is needed to identify the critical combinations that should be taken care of during production.

"Process control" in pavement engineering refers to the tight control of quality control/ quality assurance (QC/QA) during production to assure the fulfilment of quality and regulatory requirements (Mirmiran et al., 2008). The three important process control parameters for microsurfacing include aggregate gradation, emulsion content, and water content. Variation in process control parameters influence the strength development and resistance to ravelling and rutting. It is essential to identify the critical combinations for which the risk of failure of microsurfacing mix increases to an unacceptable limit. Such an understanding would help enhance the process control and performance and point towards developing the pay factors associated with deferred quality.

During in-service life, microsurfacing mix is subjected to the combined action of aging and moisture damage. Consideration of such factors would provide much required rational understanding on the durability of microsurfacing mix. Thus, this research is aimed to propose a systematic approach to address challenges faced during mix design and to quantify the individual and combined effect of process control and environmental factors on the performance of microsurfacing mix. The expected outcome is to propose a methodology to identify the critical combinations that needs to be avoided during production to enhance quality and performance of microsurfacing.

1.3 Research objective

The objective of this dissertation work was to understand and quantify the individual and combined influence of material properties, process control parameters and environmental factors on the performance of microsurfacing mix. Here, the performance was defined in terms of strength, raveling, rutting and bleeding. The tasks for fulfilling the research objective include the following.

- **Task 1**: Quantify the effect of material properties on strength, raveling and rutting of microsurfacing. Subsequently, mix design was finalized considering the material combination providing superior microsurfacing performance.
- **Task 2**: Evaluation of the individual and interactive effect of process control parameters on the performance of microsurfacing in terms of workability, strength, raveling, rutting and bleeding.
- **Task 3**: Investigation on the durability of microsurfacing by assessing the influence of different levels of aging and moisture on the raveling resistance.

1.4 Scope of the study

In this study, one source of locally available aggregate and emulsion was initially selected based on its compatibility. Subsequently, the performance of the microsurfacing mix was evaluated in three tasks to include the mix design stage (Task 1), production stage (Task 2) and in-service performance (Task 3). The factors, levels and responses for Task 1, Task 2 and Task 3 are illustrated in **Figure 1.1**, **Figure 1.2** and **Figure 1.3**, respectively. It should be noted that the word "asphalt" is used in the thesis to signify asphalt binder and not asphalt mixture.

The materials used for finalizing the mix design includes filler type, emulsifier dosage, asphalt type, solvent and mineral filler type and dosage. Initially, trial mix with aggregate source A exhibited rapid breaking with the emulsion used for the study. So, an aggregate source B was selected based on its chemical composition, and the filler was replaced in the mix. Then, based on the range of values recommended by the emulsifier manufacturer, the influence of emulsifier dosage variation from 1.5% to 2.5% was evaluated. The influence of asphalt binder grade was investigated by comparing producing emulsion with VG-10 and VG-30 binder. Since harder binder grade was used, solvent was added to the binder to reduce its viscosity during emulsion production. The rate of addition of solvent, i.e., 1% by weight of asphalt binder, was selected based to achieve 200 cP viscosity at 145°C. Subsequently, cement (OPC-53) and flyash (Class-F) dosages were varied. The range of mineral filler dosages was 0-3% at an increment of 1%. Based on ISSA recommendation, the sum of mineral filler dosages was restricted to a maximum value of 3%. All the 10 possible combinations were tested in this study. Finally, the mix design was conducted for the best combination of material type and dosages. Emulsion content was varied in the range of

12.5% to 17% and performance was evaluated in terms of strength (30-min and 60-min), raveling, rutting, bleeding and moisture damage.

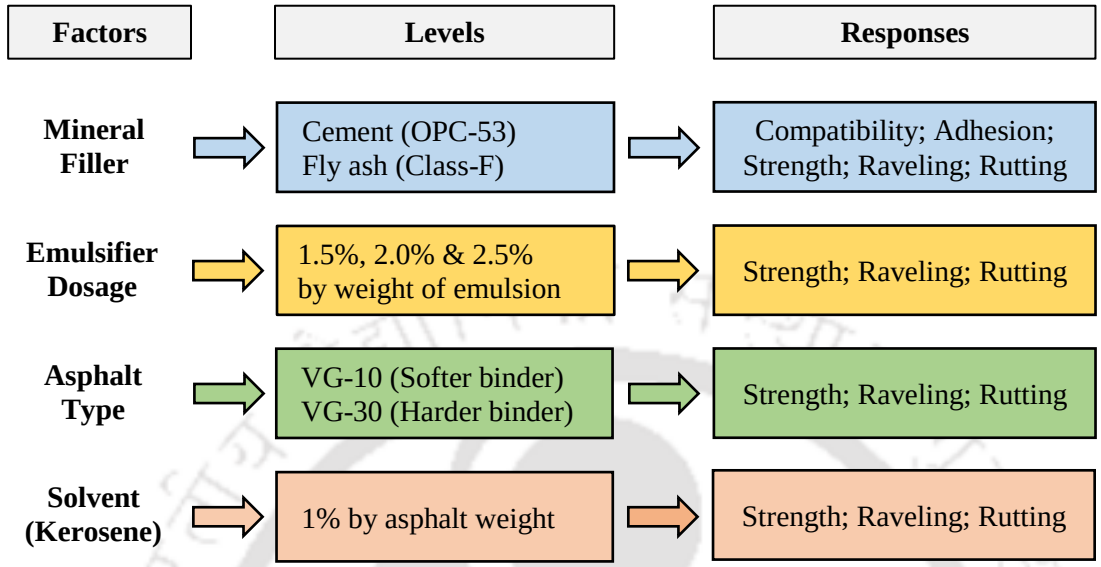

Figure 1.1: Scope of the study for Task 1

In microsurfacing, there are three process control parameters that are monitored during QC/QA. These parameters are aggregate gradation, emulsion content and water content. In this study, the aggregate gradation used for control mix was mid-point of Type II gradation as per ISSA guidelines. The range of variation of aggregate gradation considered was within the extreme limits of tolerance range specified by ISSA guidelines. In terms of emulsion content, variation within optimum emulsion content ± 1.5% was considered at an increment of 0.75%. The range of water content was optimum water content -1.0% to +2.0%. This range was selected based on the workability results of control mix. At water content less than -1% from optimum, the mix exhibited rapid breaking and it was not possible to produce the mix. For water content more than optimum +2%, the water was separating from the mix and a consistency of more than 6 cm was observed. For assessing the synergistic influence, the extreme limits of tolerance range were selected for aggregate gradation and emulsion content whereas water content variation of optimum ± 1% was considered. A total of 30 combinations were tested for workability, strength, raveling, rutting and bleeding.

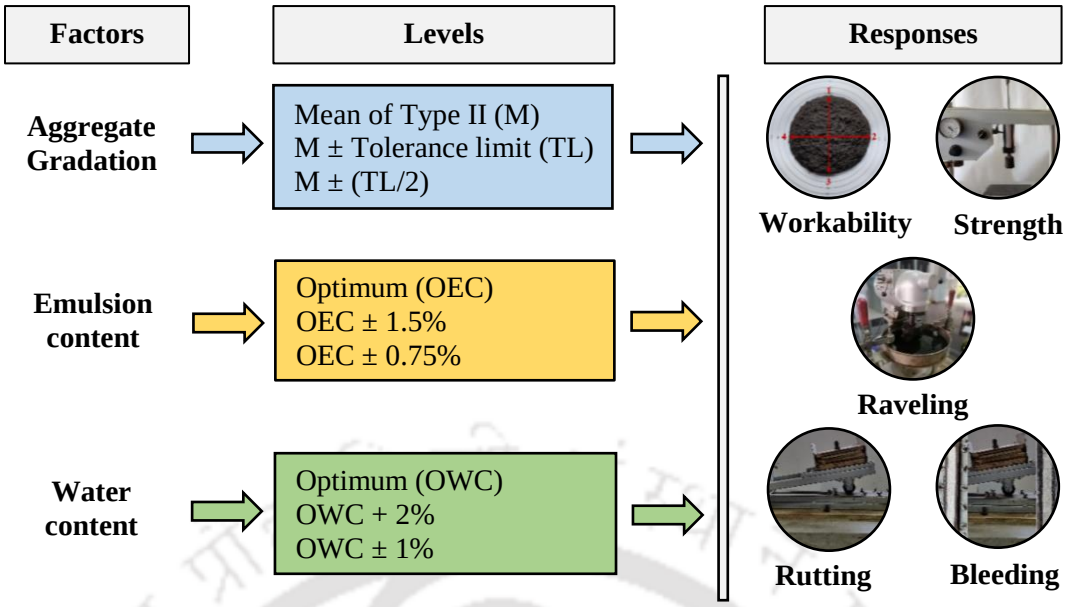

Figure 1.2: Scope of the study for Task 2

The detrimental effect of environmental conditions during service life was evaluated in terms of aging and moisture damage. Aging temperature was varied within range of 85 to 105°C at an increment of 10°C whereas aging time was varied from 1 day to 5 days with an increment of 1 day. On the other hand, moisture conditioning temperature was varied within range of 25 to 60°C (25, 40 and 60°C) and moisture conditioning time was varied from 1 day to 8 days (1, 2, 4, 6 and 8 days). The basis of selection is discussed in detail in **Section 6.2**.

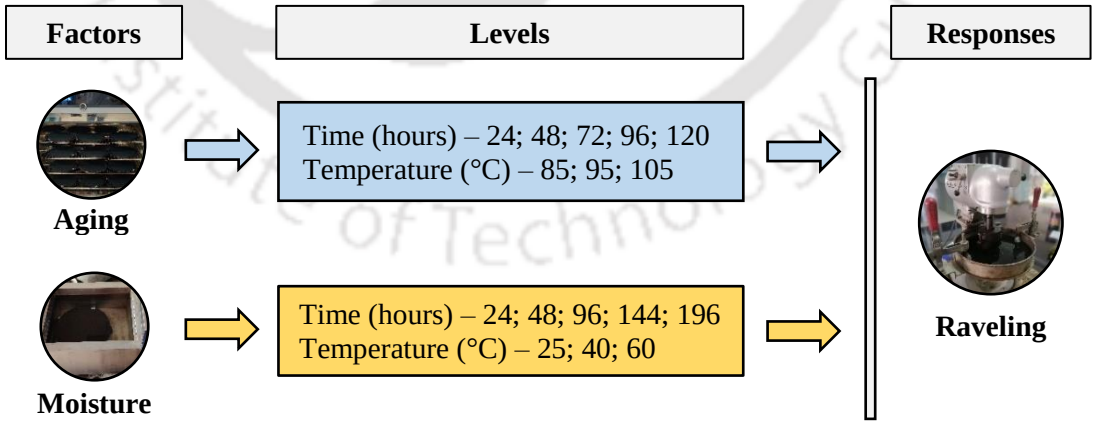

Figure 1.3: Scope of the study for Task 3

1.5 Organization of report

The report is organized into eight chapters as mentioned below:

- **Chapter 1** presents the research background, problem statement, research objectives and scope of the study.
- **Chapter 2** presents the review of previous works on the different parameters associated with the production and performance of microsurfacing mix.
- **Chapter 3** discusses the methodology and experimental protocols of the proposed research work.
- **Chapter 4** describes the effect of material properties, including filler characteristics, mineral filler, emulsifier dosage, asphalt type and solvent on mix design.
- **Chapter 5** presents the detailed investigation on the effect of process control parameters including aggregate gradation, emulsion content and water content on the production and performance in terms of workability, strength, raveling, rutting and bleeding.
- **Chapter 6** includes the durability aspect by subjecting the microsurfacing mix to different aging and moisture conditioning levels.
- **Chapter 7** lists the conclusions drawn from the study and the associated recommendations for minimizing the risk of failure.
- **Chapter 8** discusses about the limitations of the study and proposes methodology for the future studies to address the limitations.
- The list of publications from the dissertation work and bibliographic details are presented.

CHAPTER 2

Literature Review

2.1 General

The growing environmental concern worldwide has led to an increase in the emphasis on sustainable development. In the pavement industry, sustainable transportation is described in terms of safety, affordability, health benefits, proper operation, limited emissions and the inclusion of non-renewable resources for construction (Tighe & Gransberg, 2012). In this respect, one of the critical approaches is the implementation of pavement preservation as an integral part of the maintenance and rehabilitation strategy (Mamlouk & Zaniewski, 1998; Tighe & Gransberg, 2012).

Pavement preservation is defined as "*a program employing a network level, long-term strategy that enhances pavement performance by using an integrated, cost-effective set of practices that extend pavement life, improve safety and meet motorist expectations*" (Geiger, 2005). The application of preservation treatments (minor rehabilitation, preventive treatment or regular maintenance) restores the pavement reliability (Han *et al.*, 2019) by improving the riding quality and pavement condition, which ultimately results in reduced environmental impact (Baladi *et al.*, 2002; Chan *et al.*, 2011; Pellecuer *et al.*, 2014). Van Dam *et al.* (2015) stated that smoother, safer, and quieter riding surfaces of well-maintained pavements result in better vehicle fuel efficiency, decrease the influence of noise on locality, and reduced road crashes. In addition, Zaniewski & Mamlouk (1996) demonstrated that implementing preventive maintenance was 30% to 60% more cost-effective than major rehabilitation or reconstruction only. It has been reported that if the timing of preventive treatment is appropriate, spending $1 on preservation eliminates or delays rehabilitation or reconstruction cost of $6 to $10 (Galehouse *et al.*, 2003).

Several preventive maintenance strategies have been developed for asphalt pavements, as shown in **Table 2.1** (Hicks *et al.*, 1997). One of the prominent "green technology" that has emerged is microsurfacing (Harbi *et al.*, 2015; Santos *et al.*, 2017). Microsurfacing is defined as "a mixture of cationic polymer modified asphalt emulsion, 100% crushed aggregate, water, and other additives properly proportioned and spread

over a prepared surface" (Gransberg, 2010). Microsurfacing is a cold applied treatment that provides a economical and durable solution to address minor distress on pavement surfaces (Broughton *et al.*, 2012). The primary application of microsurfacing is to correct surface friction, bleeding, raveling, oxidation, and/or rutting on a structurally sound pavement (Raza, 1992; Watson & Jared, 1998; Labi & Sinha, 2005; Broughton & Lee, 2012).

Table 2.1: Applicability of preventive treatments for various distresses

Distresses	**Preventive Treatments**						
	Microsurfacing	Crack Sealing	Fog Seal	Slurry Seal	Cape Seal	Chip Seal	Thin Overlay
Roughness: Non-stability related	✓	×	×	×	✓	×	✓
Roughness: Stability related	×	×	×	×	×	×	✓
Rutting	✓	×	×	✓	✓	×	✓
Fatigue cracking (low severity)	✓	×	×	×	×	×	×
Longitudinal and transverse cracking	✓	✓	✓	✓	✓	✓	✓
Bleeding	✓	×	×	×	×	✓	×
Raveling	✓	×	✓	✓	✓	✓	×

Note: ✓ = Applicable; × = Not applicable

The applicability of microsurfacing in addressing various distresses associated with the pavement is highest, as shown in **Table 2.1**. However, the applicability is significantly dependent on the traffic volume and condition of the pavement to be treated (Serigos *et al.*, 2017), where the application of microsurfacing under heavy traffic loads is limited (Du *et al.*, 2018). The performance assessment of 89 microsurfacing projects by Dong *et al.* (2018) showed that performance characteristics are affected by the following factors in the order mentioned:

- **Pavement roughness**: Pre-treatment roughness, aggregate type, and cracking type
- **Friction**: Allowable traffic speed (less than 72 kmph), application rate, pavement surface temperature, and air humidity

- **Rutting**: Traffic level, precipitation, application rate of slurry mixture, humidity, and maximum allowed traffic speed during curing phase
- **Alligator cracking**: Severe weather conditions, unclean pavement surface, mineral filler content, and water content
- **Longitudinal cracks (wheel-path)**: Pavement surface temperature and time to opening for traffic
- **Longitudinal cracks (non-wheel-path)**: Freeze-thaw conditions, application rate, and traffic levels
- **Transverse cracking**: Freeze-thaw condition, pavement condition, application rate, and pavement temperature

The environmental benefits of microsurfacing as pavement preservation are reduced energy consumption, hazardous material exposure and greenhouse gas emissions (Bouteiller, 2010; Babashamsi *et al.*, 2016). Several field and laboratory investigations highlighted the improvement of safety and riding quality along with effective filling of ruts with microsurfacing (Johnson *et al.*, 2007; Uhlam *et al.*, 2010; Jamion *et al.*, 2014; Yu *et al.*, 2017). Therefore, microsurfacing could be suggested as a potential prospect for superior performance with reduced environmental impact. Hence, to understand the effectiveness of microsurfacing and factors affecting its performance, the literature review was divided into four sections, as shown in **Figure 2.1**.

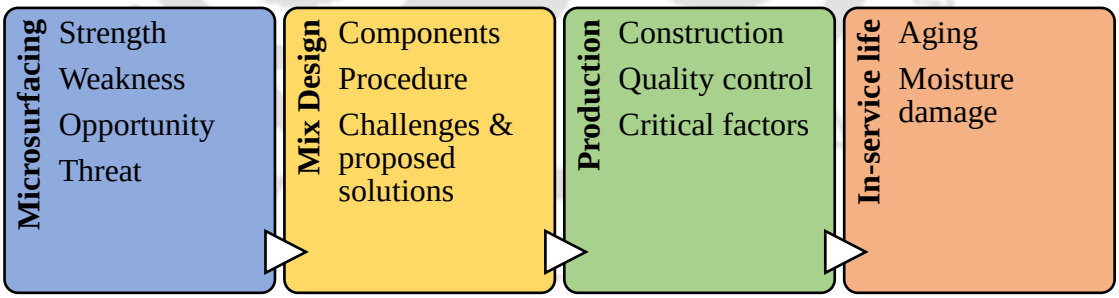

Figure 2.1: Review methodology

2.2 SWOT Analysis of microsurfacing treatment

Strength, weakness, opportunity and threat (SWOT) analysis is a basic, analytical framework primarily used for strategic planning and the decision-making process. SWOT analysis was carried out for microsurfacing treatment utilizing the information from the previous works. Strength and weakness assessment allow to weigh the pros

and cons of treatment selection and implementation. Identifying the opportunities and challenges helps future planning and laying down precautions for better application of microsurfacing treatment. Hence, in the review, the microsurfacing attributes were classified into four categories, i.e., strength, weakness, opportunities and threats, as shown in **Figure 2.2**. An elaborate discussion on the attributes is discussed in the subsequent sections.

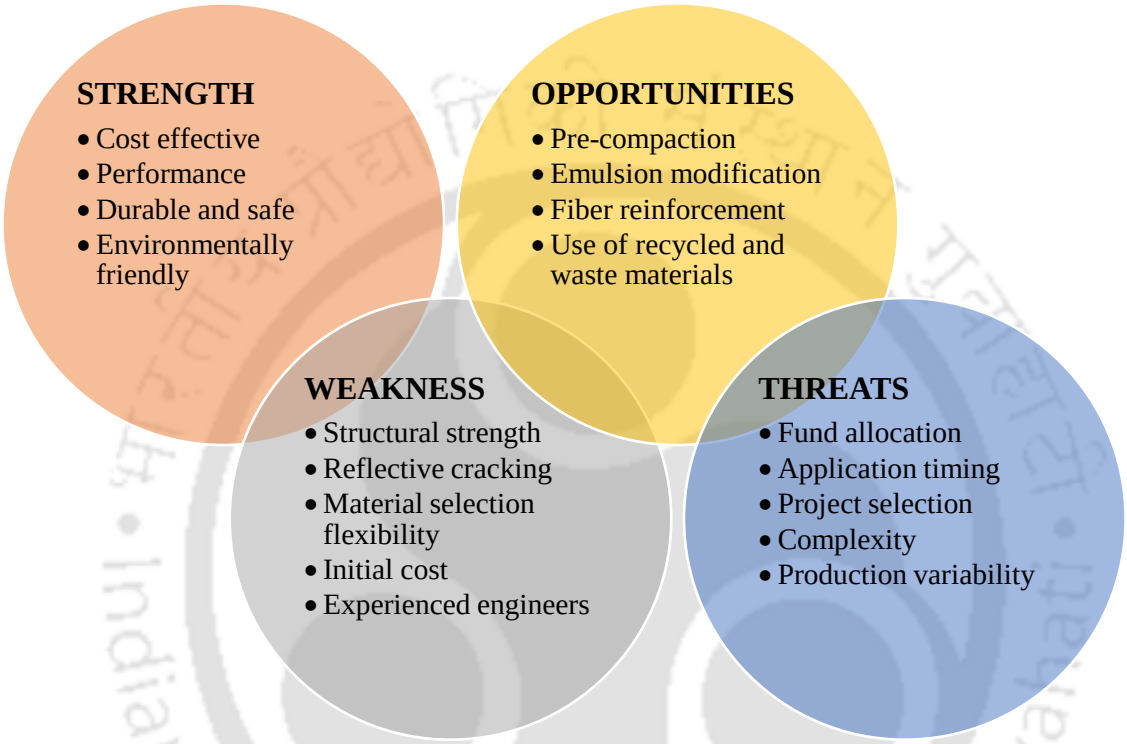

Figure 2.2: SWOT Analysis for microsurfacing treatment

2.2.1 Strength of microsurfacing

Cost-effectiveness

The economic benefits of preservation treatment over the conventional practice of repair after the pavement fails have been widely reported (Mamlouk & Zaniewski, 1998; Wang *et al.*, 2011; Ram & Peshkin, 2014). Galehouse *et al.* (2003) showed that the cost of pavement after 25 years of service life reduced from $304,472 to $86,992 per lane-km with the use of preservation treatment. In addition, numerous studies have compared the equivalent uniform annual cost (EUAC) of microsurfacing with other treatments such as mill and overlay and HMA overlay (Irfan *et al.*, 2011; Pittenger, 2011; Yan *et al.*, 2014). It was found that the EUAC reduced by at least 10% with the use of microsurfacing.

Construction cost comparison between microsurfacing and conventional HMA surface showed that microsurfacing application results in 36% savings over a 30-year period with respect to conventional HMA (Watson & Jared, 1998). In addition, Heritage (2011) stated that the application of microsurfacing as rut filling material instead of the mill and fill with HMA resulted in total savings of approximately $1.8 million.

The application of microsurfacing at night or cooler temperatures results in reduced user costs (Smith *et al.*, 1994; Zhao *et al.*, 2010; Gransberg, 2010). Lower material consumption further enhances the cost-effectiveness of microsurfacing. However, the cost-effectiveness of the treatment is primarily dependent upon distress type and intensity, pavement age, treatment type, climatic conditions, traffic volume, and weight of vehicles (Hicks *et al.*, 1997; Wang *et al.*, 2012; Dong *et al.*, 2013; Zuniga-Garcia *et al.*, 2018).

Improvement in skid resistance and safety

Skid resistance of microsurfacing mix is generally assessed in terms of British Pendulum Number (BPN), macrotexture by sand patch method, and friction number (FN) using a brake force trailer. An increase in BPN improvement in pavement macrotexture, and an increase in FN is generally observed with microsurfacing application (Jahren & Behling, 2004; Uzarowski *et al.*, 2005; Jamion *et al.*, 2014; Patel & Gujar, 2017).

The improvement in skid resistance with microsurfacing application has been summarized in **Table 2.2**. Skid resistance improved by 15% to 200% immediately after the construction of microsurfacing treatment (Hein *et al.*, 1994; Uzarowski *et al.*, 2005; Kim *et al.*, 2013). However, with time, the skid resistance decreased due to polishing and aggregate breaking by traffic action (Jamion *et al.*, 2014). The reduction in skid resistance was significantly influenced by the aggregate type used, where the statistical significance was determined using *t*-test at a significance level of 5% (Temple *et al.*, 2002). Nevertheless, the skid resistance was better than the pre-treated pavement surface even after 36 months of service life (Pederson *et al.*, 1988). Satisfactory skid resistance was observed even after 9 years of service life of microsurfacing treatment, which highlights the durability of microsurfacing treatment (Hixon & Ooten, 1993).

Table 2.2: Variation in skid resistance with microsurfacing application

Author	Method adopted	Skid resistance			
		Before construction	After construction	After service life (months)	
Pederson *et al.* (1988)	Skid Trailer Test	48	--	50 (24)	45 (36)
		51	--	49 (24)	47 (36)
		46	--	48 (24)	46 (36)
		46	--	48 (24)	42 (36)
Hein *et al.* (1994)	British Pendulum Tester	54	75	--	--
Kazmierowski & Bradbury (1995)	ASTM brake force trailer	--	44	45 (8)	53 (20)
		41	--	46 (9)	47 (20)
Jahren & Behling (2004)	Locked Wheel Tester	42.5	51	61 (36)	--
		52.5	--	53 (12)	55 (24)
Uzarowski *et al.* (2005)	ASTM brake force trailer	28	52	--	--
		27-30	58-63	54-58 (10)	
Kim *et al.* (2013)	British Pendulum Tester	62	73	--	--
		63	74	--	--
Patel & Gujar (2017)	British Pendulum Tester	40	80	80 (6)	--

Skid resistance of pavement surface primarily influences the risk of road crashes. An appropriate skid resistance offered by the pavement system enhances safety by minimizing road crashes caused due to poor skid resistance. Studies have shown that the wet road crashed reduced significant with the application of microsurfacing mix. (Erwin, 2007; Lyon *et al.*, 2018). There was an overall reduction in road crashes by 18% with microsurfacing application. In critical locations like intersections, application of microsurfacing resulted in a 24% decrease in the accidents (Erwin, 2007).

In terms of capital loss incurred due to road crashes, it has been reported that, on average, road crashes account for 3.1-3.3% of gross domestic product (GDP) (Elvik,

2000; Wijnen & Stipdonk, 2016). The effective reduction of the total road crashes with the use of microsurfacing would potentially minimize the economic loss to the society. Hence, microsurfacing could be used to restore pavement surface to improve skid resistance and minimize the risk associated with safety, improving safety and reducing economic loss (Gransberg, 2010).

The safety of pavement can also be related to the risk potential during the production stage. Primarily, safety during the production stage is associated with the safety of the worker. Lower production and application temperature of microsurfacing mix minimize the exposure time of construction workers to harmful emissions (Uhlman & Saling, 2010).

Reduction in roughness and better riding quality

A well-constructed microsurfacing mix on a structurally sound pavement has been found to improve the cross-sectional profile and effectively level the transverse cracks, dips, and edge drop off, enhancing the riding quality (Wood & Geib, 2001; Pandey *et al.*, 2011). Generally, the riding quality of the pavement surface is measured in terms of the International Roughness Index (IRI). Bae and Stoffels (2008) showed that when microsurfacing is applied to treat thermally induced cracks, microsurfacing application reduces the IRI by 45-80% depending on the crack severity.

A summary of variation in IRI with microsurfacing application along with the country is presented in **Figure 2.3**. Depending upon the initial roughness, reduction in IRI values after microsurfacing range from 0.4 m/km to 2.6 m/km (MnDOT, 2016; Kim *et al.*, 2013; Moulthrop *et al.*, 1996; Pandey *et al.*, 2011; Gujar *et al.*, 2013). Further assessment of IRI showed that the increase in roughness after a service life of 6-48 months was generally within the specification limits (IRC: SP: 16, 2004) of bituminous concrete (BC), i.e., 2 m/km to be categorized as “good” road surface (Ji *et al.*, 2013; Watson & Jared, 1998; MnDOT, 2016). However, in some cases, the IRI increased more than the specified limits of BC (Hein *et al.*, 1994; Pandey *et al.*, 2011).

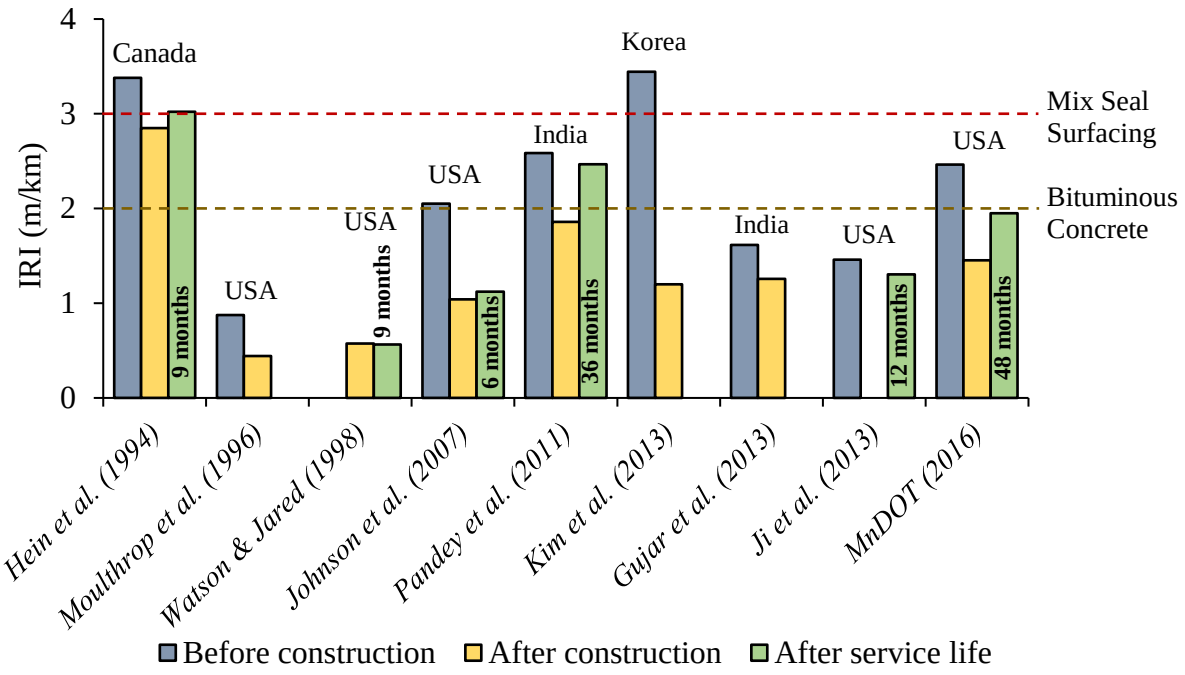

Figure 2.3: Reduction in IRI values immediately after microsurfacing construction

Pavement roughness has been the major contributor to vehicle operating costs (VOC). Study by Bae and Stoffels (2008) showed that depending on the roughness level and cracks treated, microsurfacing application could reduce the annual VOC in the range of $6,513 to $141,132 per km. User-delay costs, related to VOC, also decreases due to minimal traffic delay, which is attributed to quick setting of microsurfacing mix (Gransberg, 2010).

Protection of underlying layers

It is well known that pavement surfaces are exposed to detrimental environmental conditions. This results in oxidative hardening of asphalt from air and water entering pavement layers which causes an increase in stiffness and reduction in adhesiveness of asphalt, leading to distresses like raveling, weathering, and surface cracks (Smith & Beatty, 1999). In this regard, Button (1996) investigated the permeability of microsurfacing using a constant head water permeameter. It was reported that the permeability of microsurfacing was less than 1×10^{-5} cm/sec after achieving maximum compaction. Analysis of the effect of microsurfacing on the aging of underlying pavement layers was also conducted by Button (1996). The results showed that microsurfacing significantly delayed the failure initiation due to oxidative aging of

underlying pavement by 0 to 2 years if the treatment was applied within the first 2 years of service life of underlying pavement (Button, 1996). Therefore, the structural strength of the bituminous layer underneath microsurfacing is preserved, and the pavement service life is extended with microsurfacing application (Gransberg *et al.*, 2012; Vargas-Nordcbeck, 2019).

Effective filling of ruts

One of the primary functions of microsurfacing is also to fill ruts. Start *et al.* (1998) reported that when the rut depths increase above 7.6 mm, there is a substantial increase in accident rates and recommended the pavement treatment at this level to be economically justifiable. In this respect, the application of microsurfacing reduces the risk by quickly filling the ruts (Smith & Beatty, 1999). The material used for microsurfacing is in a semi-liquid state at application. So, when the mix is poured onto the pavement surface having rutting, the mix takes the shape of the rut, hardens upon curing and provides a smooth riding surface (Wood & Geib, 2001). The key point to note is that microsurfacing can only fill ruts caused due to densification of the asphalt layer, not plastic deformation or unstable pavement structure (Smith & Beatty, 1999).

Several field studies have reported that rut filled with microsurfacing on the structurally sound pavement had performed satisfactorily, even after 6 years of service life (Pederson *et al.*, 1988; Baker, 1990; Reinke *et al.*, 1990; Hixon & Ooten, 1993; Kazmierowski & Bradbury, 1995; Ji *et al.*, 2013; Jamion *et al.*, 2014; Vargas-Nordcbeck, 2019). In addition, Ducasse *et al.* (2004) showed that microsurfacing is more economical for rut filling than milling the pavement and overlay if the service life of microsurfacing is greater than 2.5 years.

Environmental benefits

Construction of pavement involves procurement and processing, transportation, production, and placement of large quantities of construction materials. On average, the greenhouse gas emissions and energy consumption for flexible pavement construction is 4.9-6.7 kg/m^2 and 59-77 MJ/m^2, respectively (Chehovits & Galehouse, 2010).

Proper maintenance and rehabilitation (M&R) of pavements could potentially reduce a significant amount of energy consumption and greenhouse gas emission (Simões *et al.*, 2017). A brief comparison of greenhouse gas emission and energy consumption for

microsurfacing in comparison with other treatments is provided in **Table 2.3** and **Table 2.4**, respectively.

Table 2.3: Greenhouse gas emission

Author	Unit	GHG	MS	Chip Seal	HMA_O	HIR	M&O
Takamura *et al.* (2001)	Equivalent per lane-km	CO_2 (t)	0.6		2.4		
		NO_2 (kg)	1.1		4.2		
		Ethene (kg)	7.5		29.8		
Chehovits & Galehouse (2010)	kg/m^2/ year	Total	0.05-0.10	0.08-0.20		0.4-1.0	
Chan *et al.* (2011)	Equivalent per lane-km	CO_2 (t)	1.0			13.5	17.5
		NO_x (kg)	22.5			119	153
		SO_x (kg)	985			3736	4790
Giustozzi *et al.* (2012)	Equivalent per lane-km	CO_2 (t)	7.9				100.2

** GHG – Greenhouse gas; MS – Microsurfacing*; *HMA_O – Hot Mix Asphalt Overlay; HIR – Hot In-place Recycling; M&O – Mill and Overlay*

Table 2.4: Energy consumption

Author	Unit	MS	Chip Seal	HMA_O	HIR	M&O
Chehovits & Galehouse (2010)	MJ/m^2	4.9-6.5	6.5-8.9		49-65	
Chan *et al.* (2011)	MJ	56,451			566,937	674,925
Mosier & Gransberg (2015)	MJ/m^2	4.9-6.5		77.6		

** MS – Microsurfacing*; *HMA_O – Hot Mix Asphalt Overlay; HIR – Hot In-place Recycling; M&O – Mill and Overlay*

Another added advantage associated with microsurfacing is the reduction in material consumption due to its thin application. A summary of aggregate consumption for microsurfacing with respect to other treatments is illustrated in **Figure 2.4**. It could be observed from **Figure 2.4** that for every service life year, aggregate consumption in microsurfacing is the least among other treatments. A study by Heritage (2011) showed

that pavement treatment with microsurfacing would require 28 kg/m^2 of material compared to 119 kg/m^2 material requirement for mill and fill to address the pavement condition. Likewise, Harbi *et al.* (2015) reported that microsurfacing on single mile urban road would require 540-ton lesser material than HMA overlay when a pavement is considered for 40 years analysis period.

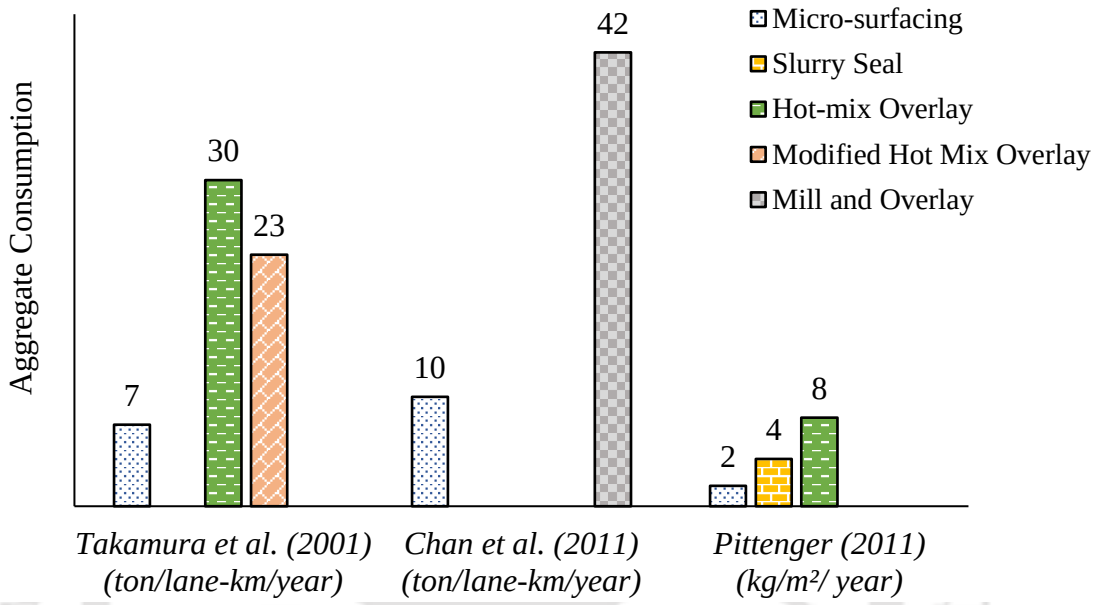

Figure 2.4: Comparison of aggregate consumption

Researchers have also quantified the benefits of microsurfacing using environmental footprint, considering various factors like energy, raw material, emission, land use, risk, toxic potential, and health effects. Investigations showed that the environmental footprint of microsurfacing is significantly lower compared to hot-mix overlay and polymer-modified hot-mix overlay (Uhlam *et al.*, 2010; Takamura *et al.*, 2001).

Another major environmental concern is the tire-pavement noise produced by traffic moving at high speeds. The major factor attributing to the traffic noise are type, age, and wear of the pavement surface (McNerney *et al.*, 1998; Bennert *et al.*, 2005). Hence, to address increased traffic noise with service life, preservation treatment in the form of microsurfacing could provide a viable solution. Studies comparing noise before and after microsurfacing application showed a reduction in noise levels with microsurfacing application within the range of 0.1-4.5 dB(A) (Kim *et al.*, 2013; Bennert *et al.*, 2005). The noise reduction can be attributed to the improved surface profile of pavement.

However, some projects showed increased noise levels (Sangiorgi *et al.*, 2012), probably due to a combination of aggregate gradation, aggregate type, shape, application rate, or mixture consistency (Raza, 1994).

2.2.2 Weakness associated with microsurfacing

Along with numerous benefits, certain limitations are also associated with microsurfacing applications. Projects on microsurfacing had shown premature failures primarily attributed to the inadequate structural strength of underlying layers or base failure (Smith *et al.*, 1994; Broughton & Lee, 2012a; Kazmierowski & Bradbury, 1995). Similarly, problems associated with reflective cracking had been reported (Pederson *et al.*, 1988; Kumar & Ryntathiang, 2012; Yu *et al.*, 2017). The primary reasons for reflective cracking are the thin application and brittle nature of microsurfacing mix (Wood & Geib, 2001). The utilization of softer binder grade for emulsion production or provision of a double microsurfacing layer has shown to minimize the reflective cracking (Johnson *et al.*, 2007; Vargas-Nordcbeck, 2019).

On cracked pavements, the use of crack sealing is recommended, with sufficient time being provided for the sealant to cure before application of microsurfacing (ISSA A143, 2010). Microsurfacing cannot smoothen the projections present in the pavement due to the flowing of mix away from humps during placement. Milling areas with projections is recommended before applying microsurfacing mix (Wood & Geib, 2001).

The influence of material properties on microsurfacing performance has also been widely reported (Lonbar *et al.*, 2015; Lonbar & Nazirizad, 2016; Garfa *et al.*, 2016; Garfa *et al.*, 2018). Specification limits have been laid down for ensuring high durability. Often, locally available materials cannot fulfill the desirable attributes, and the import of aggregates leads to increased production cost (Jahren *et al.*, 2003). Also, the requirement of special equipment for application (Morian, 2011), compatible asphalt emulsion, and additives result in higher initial cost. In addition, adjustments in job mix formula during production is needed to achieve desirable consistency and avoid segregation depending on the climatic conditions and material variability. Hence, the implementation of microsurfacing requires experienced, skilled and knowledgeable engineers (Gransberg, 2010).

2.2.3 Opportunities in microsurfacing

Microsurfacing has evolved over the years. However, there is ample scope for improving the system to suit modern requirements of sustaining higher traffic volume and traffic load. So, researchers have focussed on developing new specifications or production protocols or use of different materials to improve the durability of microsurfacing.

Development of performance-related specifications

Traffic loading and climatic conditions play a major role in microsurfacing design and construction (Peshkin *et al.*, 2004; Cheng *et al.*, 2013; Salleh *et al.*, 2019). In this regard, performance-related specifications were established by Ilias *et al.* (2017) to address the stability and constructability of asphalt emulsion along with rutting and thermal cracking of microsurfacing mix. Specification limits were laid down for varying temperature and traffic conditions to accomodate different scenarios for performance assessment (Kim *et al.*, 2017).

Pre-compaction of microsurfacing mix

Pre-compaction is another interesting area of research in the field of microsurfacing. Generally, no rolling is required for microsurfacing, except in special cases like airport runways and parking areas (Hicks *et al.*, 1997; ISSA A143, 2010). However, Lonbar *et al.* (2015) observed a rapid deformation rate of up to 500 cycles in the loaded wheel test followed by a reduction in the deformation rate. Considering the higher deformation in the initial phase, the primary compaction of microsurfacing before opening to traffic was recommended to ensure durability (Lonbar *et al.*, 2015).

Modification of asphalt emulsion

The performance of microsurfacing is improved by modifying the asphalt emulsion. Generally, synthetic or natural rubber latex is used as a modifier for emulsion during the production process (IRC: SP: 81, 2008). Alternates to latex have been explored for improving performance and reducing cost. One such alternate is waterborne epoxy resin (WER) (Liu *et al.*, 2019). During the curing process, the crosslinking reaction between WER and curing agent results in fully-cured resin macromolecules, which improved the mix's strength, thermal stability, bond strength, and aging resistance (Liu *et al.*, 2019). Laboratory investigations showed an improvement in skid resistance, adhesion between aggregate and binder, cohesion, and raveling and rutting resistance. In contrast,

the low temperature cracking resistance reduced with the incorporation of WER emulsified asphalt (Li *et al.*, 2019; Liu *et al.*, 2019; Luo *et al.*, 2019).

Use of fibers and nanomaterials

Use of fibers in microsurfacing provides a bridging effect, reinforces the mix structure, increases the viscosity of asphalt binder, and provides superior tensile strength. Fibers restricts the movement of aggregates and improves the mix stiffness resulting in better resistance to detrimental effects of traffic and the environment (Luo *et al.*, 2019). Considering these advantages, Luo *et al.* (2019) compared the use of polypropylene fiber, basalt fiber, and hybrid fiber (the two fibers combined in the ratio of 1:1) in microsurfacing. It was reported that the polypropylene fiber had better resistance to raveling, moisture damage, and low temperature cracking resistance, whereas the rutting resistance of basalt fiber was higher.

Tanzadeh and Otadi (2019) showed that combining nanomaterials (nanosilica and nanoclay) and polyethylene fiber provided superior cohesion and resistance to raveling and rutting and low-temperature bending. The nanomaterials were found to accelerate the breaking process and increase the stability of the mix. In contrast, fibers provided flexural tensile strength and resistance to fatigue and reflection cracking.

Incorporation of recycled materials

Aggregates account for around 82-90 % of the microsurfacing mix (Raza, 1994; Gransberg, 2010). Extraction, processing, and transportation consume energy, generate emissions, produce dust and noise, impact water resources, and create traffic safety issues. Therefore, aggregate replacement provides a sustainable solution to the problem associated with the scarcity of virgin aggregates (Van Dam *et al.*, 2015). Additional benefits, including energy conservation, reduced transportation costs, resources preservation, and a decrease in construction debris, enhance the sustainability of the asphalt pavement industry (Copeland, 2011; Wang *et al.*, 2019). Further, the addition of RAP would reduce the environmental impact caused due to the acquisition and refining of petroleum for asphalt production (Van Dam *et al.*, 2015).

Material costs generally account for around 66-70% of the total production cost (Jahren *et al.*, 2003; Copeland, 2011). In addition, 72% of the total carbon footprint in microsurfacing is attributed to raw material consumption (Spray *et al.*, 2014). **Figure 2.5** shows that incorporating recycled materials in HMA has economic and

environmental benefits (Frederick & Tario, 2009; Lee *et al.*, 2010; Aurangzeb & Al-Qadi, 2014). Similarly, including alternate aggregates in the microsurfacing mix could reduced the environmental impact of the treatment by a similar extent or more as HMA.

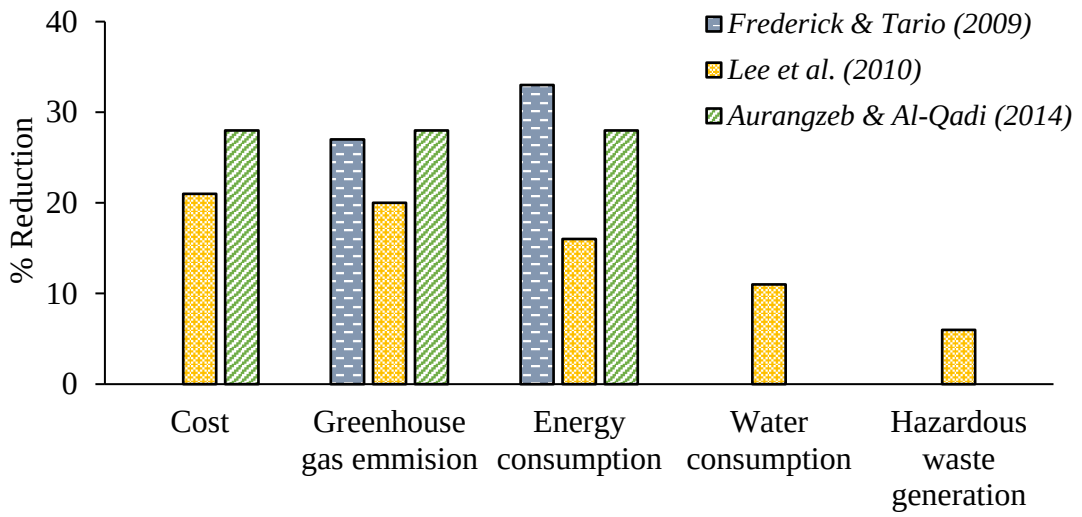

Figure 2.5: Economic and environmental impact of RAP incorporation in HMA

Researchers have focussed on replacing aggregates in microsurfacing with recycled materials (Robati *et al.*, 2013a; Wang *et al.*, 2019). Generally, RAP and recycled asphalt shingles (RAS) are used as an environmentally friendly and economical alternative to virgin aggregates for asphalt mixture production, providing opportunities for microsurfacing studies (Robati *et al.*, 2013a). Laboratory investigations showed that the asphalt emulsion requirement decreases, raveling and rutting decreases, and the bleeding reduces with the incorporation of RAP in place of virgin aggregates. Nevertheless, the microsurfacing mix containing RAP performed satisfactorily as per ISSA specifications (Poursoltani & Hesami, 2020). In another study, Wang *et al.* (2019) showed that the rutting reduced with the increase in RAP content up to an optimal value (RAP content = 20%). Also, the skid resistance and resistance to moisture damage improved with the addition of RAP. So, for consumption of recycled materials in microsurfacing, aggregate-emulsion compatibility needs to be investigated due to the presence of aged bitumen in RAP or RAS (Garfa *et al.*, 2016).

In addition to RAP and RAS, steel slag has also been recommended for use in microsurfacing (Khan, 1998; Xiao *et al.*, 2018; Zalnezhad & Hesami, 2020). Investigation on microsurfacing mix with steel slag showed that the replacement of

100% aggregates with steel slag had the best raveling resistance. In contrast, cohesion and rutting resistance was highest for mix with 61% steel slag (Zalnezhad & Hesami, 2020). Cui *et al.* (2020) also stated that the replacement of aggregates by steel slag improves the mechanical properties (raveling and rutting resistance) and provides better profile characteristics (texture and skid resistance). Since finer steel slag is more prone to expansion, to avoid long-term moisture damage, it is recommended to replace only coarse aggregates (retained on 2.36 mm sieve) with steel slag (Cui *et al.*, 2020)

Waste materials like rice husk, carbon fibers, rubber powder and fly ash are also incorporated in microsurfacing in the form of fillers (Gujar & Chauhan, 2013; Wang *et al.*, 2014; Guo *et al.*, 2017; Patel & Gujar, 2017). In addition, bio-fluxing agent, bio-binder, bottom ash, flue gas desulphurization gypsum, kiln dust, and baghouse fines in microsurfacing has been successfully incorporated in microsurfacing by various researchers (Tighe & Gransberg, 2012). In addition, application of aqueous solutions of alkali earth metal and alkali metal hydroxides or salts has shown to be an effective replacement to filler (Takamura, 2001). Considering the effectiveness of alternate fillers, Gujar & Vakharia (2019) proposed using machine learning techniques including support vector machine, artificial neural network, and isotonic regression for predicting optimal dosage of fillers. Hence, incorporating alternative fillers in the microsurfacing mix could be considered a path forward in enhancing overall sustainability.

2.2.4 Possible threats in microsurfacing application

There is a perception among paving communities about the threat towards adopting microsurfacing as an integral part of pavement management strategy. The net benefit and effectiveness of microsurfacing is dependent on the timing of application (Gransberg *et al.*, 2012; Yao *et al.*, 2019). Even though microsurfacing application in better pre-treatment conditions ensure longer service life (Wang *et al.*, 2012; Giustozzi *et al.*, 2012; Rajagopal, 2010), too early application results in wastage of resources and money (Mamlouk & Zaniewski, 2001). In this respect, the identification and selection of projects for microsurfacing application is a critical parameter.

The aggregate-emulsion interaction and inclusion of additional materials like water, emulsifier, mineral fillers, and additives increase the complexity of the microsurfacing mix (Smith *et al.*, 1994). The important mix design and production parameters influencing the performance include aggregate-emulsion compatibility, aggregate

gradation, asphalt emulsion type, emulsion content and water content (Watson & Jared, 1998; Temple *et al.*, 2002; Hixon & Ooten, 1993; Jahren & Behling, 2004). Hence, a study to understand the combined effect of the abovementioned parameters on the performance of microsurfacing mix in terms of rutting, raveling, and moisture susceptibility is critical for field applications.

2.3 Mix design of microsurfacing

2.3.1 Components of microsurfacing

Microsurfacing mix consists of polymer-modified asphalt emulsion, mineral aggregate, mineral filler, water, and additives (if any), as shown in **Table 2.5** (ISSA A143, 2010). The performance of microsurfacing in terms of aggregate-emulsion compatibility, mixing and setting time, cohesive strength development, stripping, raveling, and rutting resistance is significantly influenced by the quality of materials used. So, understanding the behavior and the parameters influencing the properties of each component is critical for ensuring the durability of the microsurfacing mix.

Table 2.5: Components of microsurfacing mix

Materials	Suggested Limits (ISSA A143, 2010)
Residual Asphalt	5.5 - 10.5% by dry weight of aggregate
Mineral Filler	0.0 - 3.0% by dry weight of aggregate
Polymer Content	Minimum of 3.0% solids based on bitumen weight content
Additives	As needed
Water	As required to produce proper mix consistency

2.3.1.1 Asphalt Emulsion

An emulsion is a colloidal fluid system of two immiscible liquids in which droplets of one liquid are dispersed in another liquid, with the continuous phase being either an aqueous solution or an organic liquid. Asphalt emulsion is a two-phase system with asphalt and water as the dispersed phase and continuous phase, respectively (James, 2006). It acts as a thermodynamically meta-stable system in which the instability is caused by high interfacial tension between asphalt and water phases. Emulsifiers are used to kinetically stabilize the asphalt emulsion (Hunter *et al.*, 2015).

Asphalt emulsion has been divided into four categories based on electrochemistry, i.e., anionic, cationic, non-ionic, and clay-stabilized asphalt emulsion (Smith *et al.*, 1994; Hunter *et al.*, 2015). The positive, negative and neutral electric charge on the asphalt globules is the identification parameter for cationic, anionic and non-ionic asphalt emulsion, respectively (MS-19, 2008; Hunter *et al.*, 2015). In the case of clay-stabilized asphalt emulsion, fine powders (natural or processed clays and bentonites) along with the thixotropic structure of asphalt emulsion protects the coalescence of asphalt droplets (Hunter *et al.*, 2015). The general notations used for asphalt emulsion are shown in **Table 2.6** (James, 2006).

Table 2.6: Classification of asphalt emulsion

Emulsion type/ Symbol/ Notations	**Property**
Cationic (C)	Positively charged droplets
Anionic	Negatively charged droplets
Rapid Setting (RS)	Set quickly in contact with coarser clean aggregates
Medium Setting (MS)	Slower setting than RS; Can be mixed with fine aggregates
Slow Setting (SS)	Mix with reactive aggregates of high surface area
Quick Setting (QS)	Intermediate in reactivity between MS and SS
Number	Asphalt emulsion viscosity (1 – low viscosity)
Text	Residue properties (h – hard asphalt residue)
P or LM	Polymer-modified or latex-modified asphalt emulsion
S	High solvent content
AEP and PEP	Asphalt Emulsion Prime and Penetrating Emulsion Prime
ERA	Recycling Agent Emulsion

The choice of asphalt emulsion is vital and dependent on the treatment application. Some of the conditions encountered in the field and the type of asphalt emulsion suitable is given in **Table 2.7**. The asphalt emulsion commonly used for microsurfacing applications are CSS-1h and CQS-1. However, CQS-1h is preferred to reduce the traffic delay associated with microsurfacing construction (Gransberg, 2010).

Table 2.7: Preference of asphalt emulsion in different conditions

Condition	Asphalt Emulsion type	Preferred Asphalt Emulsion
Low Humidity	Anionic	HFRS-2, HFRS-2P
High Humidity & Quick traffic opening	Cationic	CRS-2, CRS-2P, or CHFRS-2P
Dry dusty aggregate	Anionic	HFRS-2, HFRS-2P
Dusty limestone	Anionic	HFRS-2, HFRS-2P
Hard non-absorptive rock	Cationic/Anionic	CRS (Shorter cure time)

2.3.1.1.1 Components of asphalt emulsion

Asphalt

Asphalt constitutes around 62-65% of the asphalt emulsion used to produce microsurfacing mix (ISSA A143, 2010). The properties of asphalt play a critical role in the production of stable asphalt emulsion (MS-19, 1997; Habeeb *et al.*, 2014). The use of different asphalt grades for different climatic and traffic conditions has provided satisfactory performance (Gransberg, 2010). Studies show that a higher grade of asphalt having higher viscosity improves the resistance towards water displacement, provides better adhesion of asphalt on the aggregate surface and has a higher resistance to deformation (Habeeb et al., 2014). However, higher grades of asphalt binders are not amenable for straight-forward emulsion production. The temperature during emulsion production will vary, the surfactants to be used will vary and it is also difficult to keep the emulsion exit temperature within limits.

Water

Water is the second ingredient of asphalt emulsion, with the stability of asphalt emulsion being affected by the minerals or other matter present in water. The impurities, including calcium and magnesium ions, affect the storage stability of cationic asphalt emulsion, whereas carbonate and bicarbonate ions react with water-soluble amine hydrochloride emulsifiers and destabilize cationic asphalt emulsion. The presence of particulate matter (usually negatively charged particles) could cause premature breaking (MS-19, 2008).

Emulsifier

Emulsifiers are large organic molecules with head and a tail portion being hydrophilic (water-soluble) and lipophilic (oil-soluble), respectively (James, 2006). Emulsifier lowers the surface tension by preferential adsorption at asphalt surface (Baumgardner, 2006). The head portion consists of positively and negatively charged areas resulting in polarity, making the head water-soluble. The tail portion contains a long chain of a hydrocarbon soluble in asphalt (Hunter *et al.*, 2015). In an asphalt emulsion, the head portion of the emulsifier aligns itself at the surface of the asphalt droplet, whereas the tail orients itself on the surface of the asphalt (Hunter *et al.*, 2015). Along with the emulsifier being water-soluble, a balance between hydrophilic and lipophilic properties is essential for the emulsifier to be effective. The classification of emulsifiers according to the dissociation of characteristics in water is shown in **Table 2.8** (MS-19, 2008).

Table 2.8: Classification of emulsifying agents

Asphalt emulsion	Description	Chemical Formula
Anionic	Electrovalent and polar hydrocarbon group part of negatively charged ion	$CH_3(CH_2)_nCOO^-Na^+$
Nonionic	Hydrophilic group is covalent and polar	$CH_3(CH_2)_nCOO(CH_3CH_2O)_xH$
Cationic	Electrovalent and polar hydrocarbon group part of positively charged ion	$CH_3(CH_2)_nNH_3^+Cl^-$

Acid

Hydrochloric acid (HCl) is generally added to soap solution at 20-22°C to convert emulsifier (water-insoluble) into water-soluble salts and to regulate the final asphalt emulsion pH (Baumgardner, 2006). When HCl is incorporated to modify the pH of the soap solution, counterions of Cl^- get dissolved in the solution. These counterions then actively migrate and attach to the headgroups of the ionic emulsifier and compress the electrical double layer of the headgroups. As a result, the electrostatic interaction among the headgroups of emulsifier get weakened because of which the adsorption layer forms a relatively compact structure, and the interfacial tension reduces (Cui & Pang, 2017).

Additives

Polymers, solvents, additives, and salts are also added to enhance the properties of asphalt emulsion. Polymers such as latex or styrene butadiene styrene (SBS), either as water dispersion or solids, are dissolved in asphalt to improve asphalt's elastic and flow properties. Polymer modification of asphalt allows thicker sections, effective for rut filling, reduce temperature susceptibility and aggregate loss, improve elastic and flow properties, adhesion and cohesion properties, and cracking and rutting resistance (Smith *et al.*, 1994; Hogendoorn, 2016; Gransberg, 2010).

Hydrocarbon solvents and fluxes like fuel oil or kerosene are used to improve emulsification, curing at a lower temperature, reduce the viscosity of asphalt emulsion residue and provide workability to microsurfacing mix (James, 2006; Hogendoorn, 2016). Generally, aluminum sulfate crystals, inorganic salts, ammonium sulfate, and amines are used as additives for adjusting breaking and setting time. Anti-stripping agent is used to reduce moisture susceptibility of the microsurfacing mix (Gransberg, 2010).

Additives and salts improve storage stability and control viscosity changes by reducing the osmosis of water into bitumen, respectively (James, 2006; Hogendoorn, 2016). The parameter influencing the additive type is its compatibility with the other components of microsurfacing mix. It can be ensured by conducting laboratory tests including mix time and workability test for assessing constructability and cohesion, raveling, rutting and bleeding as performance parameters for microsurfacing mix (Smith *et al.*, 1994).

2.3.1.1.2 Production of asphalt emulsion

Colloid mill is the most commonly used equipment for manufacturing asphalt emulsions (Smith *et al.*, 1994; Hunter *et al.*, 2015). The mill consists of a high-speed rotor revolving at 1000-6000 revs/sec around a stator with a gap between rotor and stator being 0.25-0.50 mm (Hunter *et al.*, 2015). The shearing action of the rotor breaks asphalt into small droplets of size from one-tenth of mm to few tenths of mm. The asphalt droplets are coated with an emulsifier providing the surface electric charge, which prevents the particles from coalescing (Hunter *et al.*, 2015). In microsurfacing, cationic asphalt emulsions are most commonly manufactured worldwide. Usually, the pH range for cationic asphalt emulsion is between 2 to 3 (Hunter *et al.*, 2015). The parameters influencing the manufacturing of asphalt emulsion include:

- **Dispersion energy**: Mechanical energy and physicochemical energy causes asphalt emulsion dispersion which is provided by colloid mill and emulsifier, respectively. The mechanical energy should be sufficient to reduce the asphalt particle size distribution to desirable limits, along with the presence of sufficient physicochemical energy to maintain stability (Baumgardner, 2006).
- **Particle size distribution**: The asphalt particle size and its distribution influence asphalt emulsion stability, breaking, and curing rate along with coating on the aggregate surface. Particle size is related to the shear rate in the mill. Shear rate ($\gamma^{\cdot}$) is a function of colloid mill radius (R_{cm}), the angular velocity (V_{cm}), and gap dimension (GD_{cm}) as shown in **Equation 2.2** (Baumgardner, 2006).

$$\gamma^{\cdot} = \frac{2\pi\, R_{cm}\, V_{cm}}{60 \times GD_{cm}} \tag{2.2}$$

- **Component viscosity and temperature**: The dispersion of asphalt in the aqueous phase is dependent on its viscosity. Equiviscous temperature (EVT) is defined as the temperature at which asphalt viscosity is 200 cP (Baumgardner, 2006).
- **Asphalt emulsion temperature**: The asphalt emulsion manufacturing process temperature (E_t) should be less than 95°C at the mill outlet, which can be approximated using **Equation 2.3** (Baumgardner, 2006).

$$E_t = \frac{[(AC_{wt} \times AC_t \times 0.5) + (Soap_{wt} \times Soap_t \times 1)]}{[(AC_{wt} \times 0.5) + (Soap_{wt} \times 1)]} \tag{2.3}$$

where, AC_{wt} = % of asphalt by total weight of emulsion; AC_t = Temperature of asphalt during emulsion production, °C; $Soap_{wt}$ = % of soap solution by total weight of emulsion; $Soap_t$ = Temperature of soap solution, °C.

2.3.1.1.3 Breaking and curing of asphalt emulsion

Breaking of asphalt emulsion refers to the loss of water from the asphalt emulsion, which is identified by the change of asphalt emulsion color from brown to black, resulting in a continuous asphalt film (Hunter *et al.*, 2015). The stability of the emulsion could be described by DLVO-theory (Derjaguin-Landau-Verwey-Overbeek theory). According to this theory, the interaction between the droplets are the summation of the

electrostatic repulsion and Van-der-Waals attraction. Van-der-waal attraction is due to the intermolecular attraction between the like molecules whereas electrostatic repulsion arises due to the presence of electrical charges in the polar heads of the emulsifier. No breaking occurs when the electrostatic repulsion overcomes the attraction as the asphalt droplets are prevented from approaching each other. Alternatively, the asphalt droplets coalesce when the attraction overcomes repulsion (Lesueur & Potti, 2004).

When the asphalt emulsion comes into contact with aggregates, breaking of emulsion could be described as a consequence of two causes (Lesueur & Potti, 2004):

a) Gel contraction – In gel contraction, the breaking of emulsion takes place due to the disappearance of electrostatic repulsion between asphalt droplets. This breaking mode is activated by action of aggregates. When the asphalt droplets come in contact with the reactive aggregates, the emulsion droplets break and coalesce around the aggregate. In this case, the kinetics is governed by binder viscosity, particle size and binder-water interfacial tension.
b) Film forming – When the emulsion breaks because of evaporation of water, the coalescence occurs due to the high crowding pressure which results in the breaking of water film between the asphalt droplets. The kinetics of film formation is imposed by the evaporation rate.

In microsurfacing, the breaking and curing process involves the adsorption of free emulsifiers to the aggregate surface making the surface lipophilic and increase in pH. Then, asphalt droplets flocculate due to loss of charge on the droplets and neutralization of acids. Finally, water evaporates, after which displacement of water film on the lipophilic aggregate surface leads to the formation of asphalt coating on the aggregate surface (James, 2006). The factors influencing the breaking and curing rates include the following (MS-19, 2008; Hunter *et al.*, 2015; Hogendoorn, 2016).

- Type and quantity of emulsifier
- pH of the aqueous solution
- Asphalt source and content
- Particle size distribution of asphalt droplets
- Aggregate type and gradation, water absorption and moisture content
- Wind speed, temperature, and humidity
- Use of breaking agents

2.3.1.1.4 Properties of asphalt emulsion

The vital physical properties of the produced asphalt emulsion are stability and viscosity (Ibrahim, 1998). In microsurfacing, the quality tests for asphalt emulsion adopted by various agencies are shown in **Table 2.9**.

Table 2.9: Quality tests on asphalt emulsion for microsurfacing

Tests on asphalt emulsion	**ISSA**[1]	**ASTM**[2]	**India**[3]	**Texas**[4]
Viscosity, Saybolt Furol at 25°C, SFS	20-100	20-100	20-100	20-100
Viscosity, Rotational Paddle Viscometer at 25°C, mPa-s	45-220	40-250	--	--
Particle Charge test	Positive	Positive	Positive	Positive
Sieve test, % *max*	0.1	--	0.05	0.1
Settlement and storage stability, % *max*				
24 hours	1	1	2	1
168 hours	--	--	4	--
Distillation of asphalt emulsion, % *min*	62	57	--	62
Residue by evaporation, % *min*	--	--	60	--
Coagulation at low temperature	--	--	Nil	--
Tests on asphalt emulsion residue				
Ductility, 25°C, 5 cm/minute, cm *min*	40	40	50	70
Solubility in trichloroethylene, % *min*	97.5	97.5	97	97
Softening point of asphalt, °C *min*	57		57	57.2
Penetration of asphalt (25°C)	40-90	40-90	40-100	55-90
Elastic recovery, %			50 *min*	5-60

[1] (ISSA A143, 2010); [2] (ASTM D2397, 2020); [3] (IRC: SP: 81, 2008); [4] (TxDOT, 2014)

Asphalt emulsion stability

Cui and Pang (2017) defined the stability of asphalt emulsion as "the resistance of the dispersed droplets to coalescence." It is generally characterized by properties such as creaming or sedimentation, coalescence between drops, and flocculation of drops or phase separation (Borwankar *et al.*, 1992). Stability is a vital physical property of asphalt emulsion, which affects the surface viscosity and rheology of the interface of two phases. Generally, asphalt emulsion stability is measured using settlement and storage stability (24 hrs or 5 days) (ASTM D6930, 2019) and sieve test (ASTM D6933, 2018). In addition, researchers have used advanced technologies like atomic force

microscopy, microelectrophoresis, imaging techniques, laser diffraction, and dynamic shear rheometer for the measurement of asphalt emulsion stability (Loeber, et al., 2000; Jada *et al.*, 2004; Rodríguez-Valverde *et al.*, 2008; Wang *et al.*, 2012; Mercado & Fuentes, 2017).

Several factors influence asphalt emulsion stability, including pH of asphalt emulsion, particle size distribution, temperature, and viscosity (Gorman *et al.*, 1998). It has been reported that the stability of asphalt emulsion reduces with an increase in pH of asphalt emulsion from 3 to 7 (Cui & Pang, 2017). It was found that after 50 days, the non-Newtonian effects disappear, and the asphalt emulsion becomes unstable (Mercado & Fuentes, 2017). The stability of asphalt emulsion also reduces with the increase in storage temperature above 35°C and excessive movement during storage. The storage of asphalt emulsion in aluminum or plastic containers were recommended whereas storage in iron container led to reduction in the asphalt emulsion stability (Liu & Hou, 2017).

The slightly higher density of asphalt with respect to water leads to the settlement of asphalt. Also, lower binder content and lower viscosity result in quicker settlement. Hence, the settlement could be decreased by equalizing the density, increasing the viscosity of the aqueous phase, reducing mean particle size, or ensuring a uniform particle size of asphalt droplets (Hunter *et al.*, 2015).

Asphalt emulsion viscosity

Asphalt emulsion viscosity refers to the resistance to the flow of asphalt emulsion, which affects the asphalt film thickness and workability of microsurfacing mix. Saybolt Furol viscometer is used to determine the viscosity of the asphalt emulsion. The efflux time for asphalt emulsion to reach receiving flask is termed Saybolt Furol viscosity (ASTM D7496, 2018). An increase in the viscosity can be achieved by increasing the quantity or viscosity of asphalt, reduction in particle size distribution of asphalt, decrease in the acid content or an increase in the emulsifier content (Hunter *et al.*, 2015).

2.3.1.2 Aggregate

Aggregates are the mineral materials accounting for the major volume of the microsurfacing mix (Gransberg, 2010). Crushed stone such as granite, limestone, sandstone or high-quality aggregates are used for microsurfacing application (ISSA

A143, 2010; Broughton & Lee, 2012a). Since aggregates play a critical role in achieving the design life of microsurfacing, several key characteristics of aggregates need to be assessed for better performance. These characteristics include the following (Hicks *et al.*, 1997; Lesueur & Josè Potti, 2004; Gransberg, 2010):

- **Geology**: The aggregate-emulsion compatibility is primarily dependent on the mineralogical composition of the aggregates, which influence the adhesive and cohesive properties of the microsurfacing mix.
- **Shape and texture**: Aggregate shape influences the interlocking matrix of the microsurfacing mix. Aggregates with fractured faces and rough texture are preferred over rounded aggregates and smoother texture for achieving desirable strength.
- **Age and reactivity**: Reactivity and surface charge of aggregates influences the breaking and set time of asphalt emulsion. Hence, freshly crushed aggregates with higher surface charges are preferred over weathered ones to achieve the desired reaction rate.
- **Cleanliness**: The presence of deleterious materials like clay, dust, or silt on the aggregate surface significantly influences the reaction rate due to emulsifier adsorption on the deleterious materials.
- **Soundness and abrasion resistance***:* Soundness and abrasion resistance of aggregates influence the resistance of microsurfacing to weathering action of freeze-thaw cycle and traffic and hence, contributes to mix durability.

Additionally, aggregate gradation and moisture content also influence the performance. It is recommended to cover aggregate stockpile to avoid the detrimental effects of high water content on the mix performance (Smith *et al.*, 1994; Gransberg, 2010). European standard (BS EN 12273, 2008) recommends using polished stone value to ensure the durability of microsurfacing skidding resistance. The quality tests for aggregates and aggregate gradation adopted by various agencies are shown in **Table 2.10** and **Table 2.11**, respectively.

Table 2.10: Quality tests for aggregates

Test	ISSA[1]	ASTM[2]	India[3]	Caltrans[4]	Texas[5]	Australia[6]
Sand Equivalent Value, *min*	65	65	50	70	65	60
Aggregate soundness, % *max*:						
Na_2SO_4	15	15	12	--	--	--
$MgSO_4$	25	25	18	--	25	--
LA Abrasion, % *max*	30	30	--	35	30	30
Water Absorption, % *max*	--	--	2	--	--	--
Durability Index, % *min*	--	--	--	65	--	--
Crushed particles, % *min*	--	--	--	95	95	--
Acid Insoluble, % *min*	--	--	--	--	55	--
Degradation factor, % *min*	--	--	--	--	--	50
Aggregate wet strength, kN *min*	--	--	--	--	--	150
Wet/Dry strength, % *max*	--	--	--	--	--	30
Polished aggregate friction, *min*	--	--	--	--	--	45

[1] (ISSA A143, 2010); [2] (ASTM D6372, 2015); [3] (IRC: SP: 81, 2008); [4] (Caltrans, 2015); [5] (TxDOT, 2014); [6] (Patrick, 2018)

Table 2.11: Aggregate gradation for microsurfacing mix

Sieve Size (mm)	ISSA[1]		Texas, USA[2]	Georgia, USA[3]		India[4]		Australia[5]	
	Type II	Type III		Type I	Type II	Type II	Type III	Size 5	Size 7
9.50	100	100	100	100	100	100	100	100	100
6.70	--	--	--	--	--	--	--	100	85-100
6.30	--	--	--	--	--	100	90-100	--	--
4.75	90-100	70-90	86-94	90-100	60-95	90-100	70-90	90-100	70-90
2.36	65-90	45-70	45-65	65-90	45-75	65-90	45-70	50-70	45-70
1.18	45-70	28-50	25-46	--	--	45-70	28-50	30-50	28-50
0.60	30-50	19-34	15-35	--	--	30-50	19-34	20-35	19-34
0.30	18-30	12-25	10-25	20-45	15-35	18-30	12-25	12-25	12-25
0.15	10-21	7-18	7-18	--	--	10-21	7-18	7-18	7-18
0.075	5-15	5-15	5-15	5-15	5-15	5-15	5-15	4-10	5-15

[1] (ISSA A143, 2010); [2] (TxDOT, 2014); [3] (GDOT, 2013); [4] (IRC: SP: 81, 2008); [5] (Patrick, 2018)

2.3.1.3 Mineral Filler

Mineral filler, generally Portland cement (IRC: SP: 81, 2008), influence the performance of the microsurfacing mix (Smith *et al.*, 1994; Gransberg, 2010). The pre-wetting water added to cold mix asphalt reacts with the mineral filler and results in the formation of hydration products. The hydration products, in turn, results in the acceleration of the breaking process of asphalt emulsion (García et al., 2013). On the other hand, when asphalt emulsion is added to the mix having cement, filler particles (basic) and asphalt particles (acidic) come into contact because of chemical compatibility. This results in the occurrence of two concurrent reactions. Firstly, the water phase of the emulsion reacts with cement particles to cause the primary hydration reaction. Then, asphalt particles encapsulate the cement particles in a secondary reaction, which causes a delay in the hydration process (Du, 2014).

Mineral filler is primarily used to increase the stiffness of mastic, minimize segregation, enhance resistance to fracture and crack propagation, improve consistency, and adjust breaking and curing time (Raza, 1994; Little & Petersen, 2005; ISSA A143, 2010). The filler properties, including size, shape, surface area and particle distribution, influence the stiffening effect of asphalt-filler mastic (Smith *et al.*, 1994; Robati *et al.*, 2015a).

Since the role of mineral filler is vital, it is essential to understand the mechanism associated with the interaction of filler with asphalt emulsion. The addition of cement to asphalt emulsion increases asphalt emulsion pH and the reaction of cement release Ca^{2+} ions, leading to the destabilization of asphalt emulsion (Takamura & James, 2015; Fang *et al.*, 2016). The hydration products formed by the interaction between cement and asphalt emulsion increase the asphalt binder stiffness and adhesion at the mastic-aggregate interface (Du, 2014).

2.3.1.4 Water

Water is introduced into microsurfacing mix in three ways, i.e., moisture present in aggregate, mixing water and water present in asphalt emulsion (Raza, 1994). The primary purpose of mixing water is to wet the aggregate surface to reduce the surface tension. It allows better coating of emulsion on the aggregate surface (Smith *et al.*, 1994; MS-19, 2008). The use of potable water free of harmful salts and contaminants is recommended for microsurfacing application (Smith *et al.*, 1994; ISSA A143, 2010).

The factors influencing the water content required are moisture content in aggregates, temperature, relative humidity and amount of moisture absorbed by pavement surface (Smith & Beatty, 1999). Hence, considering the above-mentioned factors, field adjustments to water content is recommended for achieving desirable consistency (Smith *et al.*, 1994).

2.3.2 Mix Design

Mix design involves the determination of an optimum job mix formula ensuring the compatibility among ingredients of mixture and satisfying the mix design parameters. In microsurfacing, every formulation laid down is a chemical system which is affected by the components used for producing mix. Hence, an empirical approach for analysing the laboratory specimens to field simulated tests under project specific conditions become critical for assessment of microsurfacing mix design (Andrews, 1994).

Several mix design procedures have been developed by several agencies like ISSA, ASTM, Indian Roads Congress (IRC), Texas Transportation Institute (TTI) and Australian specifications. In European practices, tests like consistency, cohesion, abrasion loss and shaking abrasion tests have been recommended (BS EN 12273, 2008). The sequence of tests specified for obtaining optimum job mix formula is shown in **Figure 2.6** (ISSA A143, 2010). A brief description of the test procedures is summarized in **Table 2.12** (Andrews, 1994; ISSA A143, 2010).

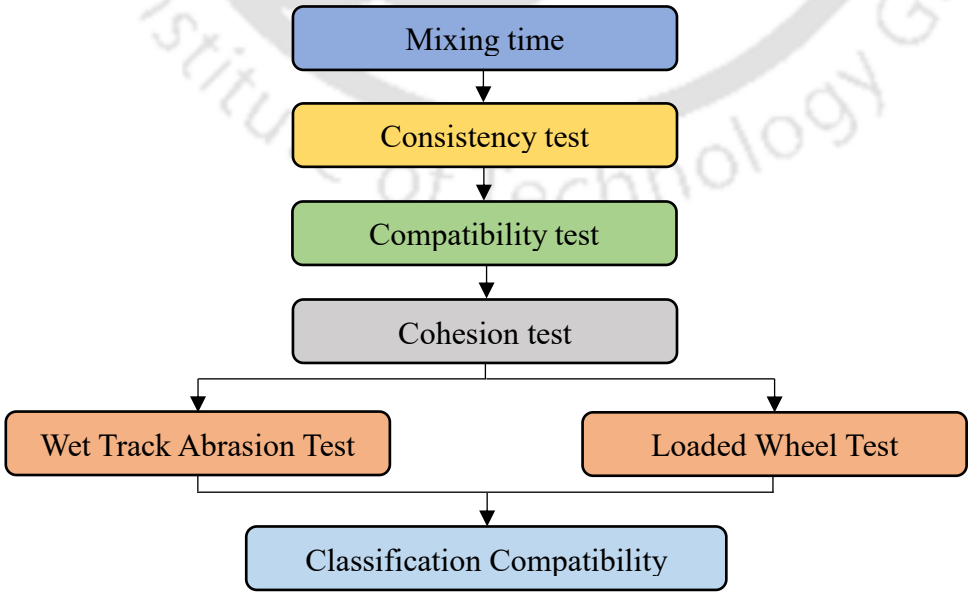

Figure 2.6: Microsurfacing mix design process as per ISSA

Table 2.12: Significance of tests on microsurfacing

Tests	Description	Significance
Mixing time test	Adequate formulation providing mixing time within range of 120-300 sec. is established	Establishing formulation and verifying initial compatibility
Consistency test	Water content providing outflow of 2.5 cm is determined	Determination of optimum amount of water
Compatibility test	Description of compatibility using split consistency, split cup compatibility and adhesion of mix	Assessment of mutual compatibility of aggregates
Cohesion test	Set time and early rolling traffic is defined as a function of torque	Provides minimum mineral filler content
Wet track abrasion 1-hour soak	Evaluation of internal mat adhesion and resistance to aggregate loss due to mechanical abrasion	Determination of minimum asphalt content
Wet track abrasion 6-day soak		Assessment of moisture susceptibility
Loaded Wheel Test	Traffic simulation of resistance to deformation and flushing under heavy loads	Determination of maximum asphalt content
Schulze-Breuer and Ruck Test	Aggregate passing 2 mm sieve and mineral filler compatibility with asphalt emulsion tested.	Assessment of asphalt emulsion affinity to aggregate filler

2.3.2.1 Procedure for obtaining job mix formula for microsurfacing mix

Material Selection and Characterization

The first step in microsurfacing mix design is to assess the quality of aggregates and asphalt emulsion used in its production. In addition to quality tests mentioned in **Table 2.9**, **Table 2.10** and **Table 2.11**, performance-related specifications are also explored by researchers to address constructability of microsurfacing in terms of stability of asphalt emulsion and its mixing ability with aggregates (Ilias *et al.*, 2017).

Theoretical Binder Content Determination

For a job mix formula, the theoretical binder content is initially determined using surface area method (ISSA TB No. 118, 2005). **Equation 2.4** and **Equation 2.5** are used to determine the surface area of bitumen (SAB). The kerosene absorbed (KA) is calculated from centrifuge kerosene equivalent test using **Equation 2.6**. The total bitumen required (BR) is then computed by adding SAB and KA ($BR = SAB + KA$).

$$CSA = SA \times (2.65/G_{sa}) \tag{2.4}$$

$$SAB = CSA_{m^2/kg} \times t \times 0.09996 \times G_b \tag{2.5}$$

$$KA = \frac{W_{ac} - W_{bc}}{W_s} \times 100 \tag{2.6}$$

where, CSA = Corrected surface area of aggregates; G_{sa} = Apparent specific gravity of aggregates; G_b = Specific gravity of asphalt binder; t = Asphalt film thickness, μm; W_{ac} and W_{bc} = Weight of sample and container after and before centrifuge, gm and W_s = Dry weight of aggregate sample, gm. Alternatively, centrifuge kerosene equivalent test (ASTM D5148, 2010) can also be adopted for trial binder content assessment.

Mix and Set Time Test

The trial formulation is then evaluated using mix and set time test (ISSA TB No. 113, 2017). In microsurfacing, it is essential to maintain adequate mixing time in order to avoid premature breaking of asphalt emulsion. But, despite simple test procedure, mixing test has shown high variability because of difference in hand mixing from one operator to another and subjective nature of breaking and setting time assessment.

To overcome the problem, Caltrans (2010) recommended carrying out mixing using an automated motor and measuring variation of viscosity (torque) with time to assess mix and spreadability indices (Caltrans, 2010). In addition, IRC (IRC: SP: 81, 2008) and ASTM (ASTM D6372, 2015) recommended the use of paper blot method to examine set time. For a quick slurry system, a set time of 1 hour is considered acceptable.

Consistency Test

In the next step, optimum water content (OWC) is determined using consistency test (ISSA TB No. 106, 2015) to evaluate the workability and segregation potential of microsurfacing mix. It is important to note that the water content of aggregates obtained from consistency test can have both beneficial and detrimental effect on the mix

performance based on the aggregate type used (MS-19, 2008). In case of high-water content, the binder affinity towards an aggregate surface significantly reduces whereas poor coating is associated with low water content (Smith *et al.*, 1994). Hence, for incorporating field conditions, varying temperature (10°C, 25°C and 50°C) for OWC determination was proposed by Caltrans (2010).

However, the inability of the consistency test to provide adequate results for quick set, quick traffic system is a major drawback. In this regard, Smith *et al.* (1994) recommended use of modified cup flow test for determination of OWC. OWC is selected based on three criteria, i.e., avoid flushing of the surface, presence of excessive fluids on the edge of the specimen mould and provide uniform and smooth surface texture (Smith *et al.*, 1994).

Compatibility Test

Aggregate-emulsion compatibility evaluation is conducted for analysing the coating ability of asphalt emulsion on an aggregate surface (Baker, 1990). The curing process of microsurfacing is chemically controlled. The physical and chemical properties of asphalt emulsion and aggregates significantly influence the aggregate-emulsion compatibility. The compatibility characteristics, in turn, affects the adhesion characteristics of microsurfacing mix. Hence, ISSA had laid down test protocols to assess the compatibility of aggregates and asphalt emulsion using split consistency or split cup consistency test (ISSA TB No. 115, 2005). In addition, boiling compatibility test (ISSA TB No. 149, 2005) can also be used to determine mix compatibility. For a good mix compatibility, more than 90% of the aggregate surface should be coated after boiling water test.

Cohesion Test

The compatible emulsion-aggregate systems are subjected to cohesion test for ensuring adequate strength development prior to opening to traffic (ISSA TB No. 113, 2017). Various mineral filler contents are analysed for torque measurements, and minimum mineral filler content is defined. The major difficulty with the procedure is the operator dependency of torque application. Hence, automated cohesion test was developed to minimize the variability. The amount of rotation of foot is controlled by software and torque measurements are graphically displayed on computer (Caltrans, 2010).

Performance Tests

Next, the microsurfacing mix is subjected to performance test, i.e., raveling (Wet Track Abrasion Test, WTAT) (ISSA TB No. 100, 2017) and sand adhesion (Loaded Wheel Tester, LWT) (ISSA TB No. 109, 2005; ISSA TB No. 147, 2005). The optimum asphalt emulsion content (OEC) is determined by plotting the aggregate loss and sand adhesion as shown in **Figure 2.7** (ISSA TB No. 111, 2005).

Generally, an increase in sand adhesion and decrease in aggregate loss is observed as the asphalt emulsion content increases. Hence, to avoid raveling and minimize rutting simultaneously, assigning an acceptable asphalt emulsion content range is critical for ensuring satisfactory microsurfacing mix performance. Currently, a 3% tolerance range is deducted from maximum allowable asphalt emulsion content from LWT and the mid-point of tolerance range is defined as OEC (Andrews, 1994).

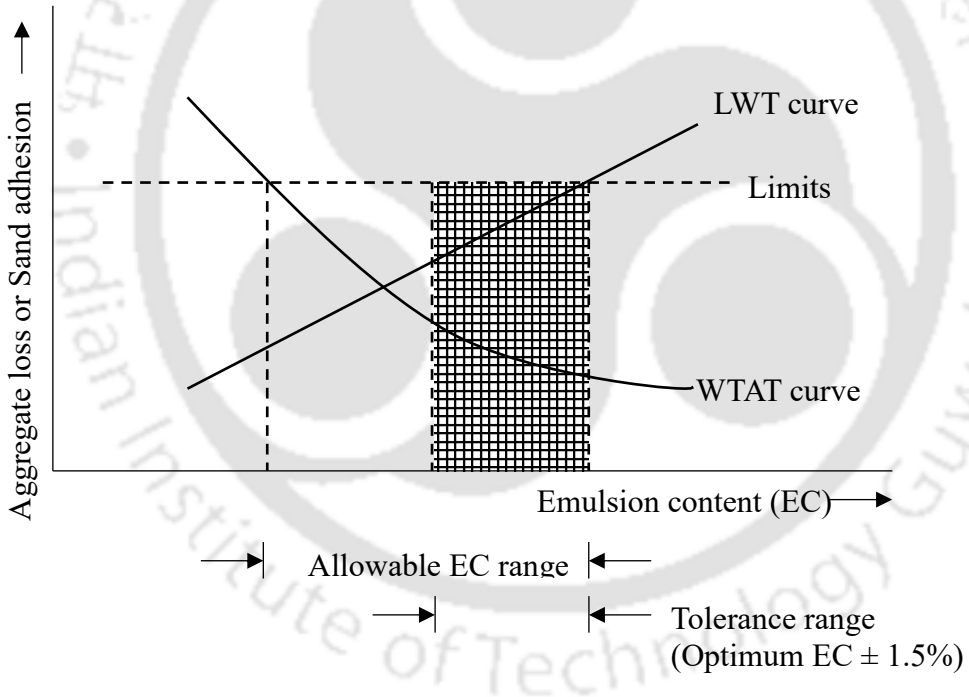

Figure 2.7: Optimum asphalt emulsion content determination

However, certain limitations have been reported for WTAT and LWT test. Smith *et al.* (1994) observed that for two material combinations, 1-hr soaked WTAT specimens exhibited substantial within materials imprecision. It indicates that for certain formulations, WTAT shows consistently imprecise results. Also, the current ISSA specification does not include aggregate retained on 4.75 mm for abrasion resistance

assessment. Cohesion-abrasion test was developed by Caltrans (2004) in which the rubber hose was replaced by a two-wheel fixture for better replication of traffic action. In addition, for assessing early curing and cohesion build up, it was recommended to evaluate the performance at various curing conditions. It was also reported that the limits for excessive asphalt emulsion content from sand adhesion may not be indicative of flushing in microsurfacing mix (Smith *et al.*, 1994).

Another performance parameter, long-term moisture susceptibility, is determined by WTAT on 6-day soaked specimens (Caltrans, 2004). Caltrans (2010) recommends moisture damage assessment by evaluting the ratio of abrasion loss of 6-day soaked specimen to 1-hour soaked specimen. European Standard (BS EN 12274-7, 2005) recommends the use of shaking abrasion test to determine the water sensitivity of microsurfacing mix consisting of aggregates passing 2 mm sieve. Water absorption is determined using **Equation 2.7** or **Equation 2.8** and abrasion resistance is determined using **Equation 2.9**.

$$W_V = \frac{m_{LV} - m_p}{m_{LA} - m_{WA}} \times 100 \qquad for\ V_V \leq V_A \qquad (2.7)$$

$$W_V = \frac{(m_{WV} - m_p) + (m_{LA} - m_{WA})}{m_{LA} - m_{WA}} \times 100 \qquad for\ V_V > V_A \qquad (2.8)$$

$$AR = \frac{m_f - m_{ar}}{m_f} \times 100 \qquad (2.9)$$

where, W_V = Water absorption, %; AR = Abrasion resistance, %; V_V and V_A = Volume of specimen before and after water absoprtion, cm^3; m_p = Mass of specimen in air before testing, gm; m_{LA} and m_{WA} = Mass of specimen prior to vacuum application in air and water, gm; m_{LV} and m_{WV} = Mass of specimen after vacuum application in air and water, gm; m_f and m_{ar}= Mass of specimen before and after abrasion, gm.

Classification Compatibility Test

After the microsurfacing mix passes the performance test, final job mix formula is assessed for classification compatibility by Schulze-Breuer and Ruck test (ISSA TB No. 144, 2013). The compatibility is quantified in terms of abrasion loss, integrity and adhesion (ISSA A143, 2010).

2.3.2.2 Challenges and proposed solutions to mix design

Microsurfacing mix design is a complex process as each component of the mix and their interaction play a critical role in coating quality and strength characteristics. It is well established that asphalt emulsion plays a critical role in microsurfacing performance. However, the current specifications for asphalt emulsion properties are empirical and do not directly relate to field performance. In this regard, Ilias *et al.* (2017) introduced asphalt emulsion performance grade (EPG) which directly correlated the asphalt emulsion specifications to field performance. EPG specifications defined the climatic and traffic conditions for which a particular asphalt emulsion could be used for microsurfacing production based on fresh asphalt emulsion properties and resistance of the asphalt emulsion residue to rutting, bleeding and thermal cracking. The proposed EPG specifications for different grades are presented in **Table 2.13** (Ilias *et al.*, 2017).

Various researchers have also reported the challenges with the existing mix design processes. The most commonly reported issues are as follows (Raza, 1994; Smith *et al.*, 1994; Andrews, 1994; Robati *et al.*, 2013b; Wu, 2015):

- Subjective determination of mixing time
- Operator dependency of torque application for cohesion measurement
- Poor reproducibility of LWT
- Weak relation between laboratory results and field performance
- Inability of wet track abrasion to delineate the influence of aggregate type
- Variation in the optimum asphalt emulsion content with different procedures
- Exclusion of 4.75 mm retained aggregates in WTAT and LWT test procedure

In order to overcome these shortcomings, several modifications proposed by TTI and Caltrans have been discussed in detail in **Section 2.3.2**. **Table 2.14** describes the drawbacks of conventional ISSA test procedures and the alternate test protocols suggested by different agencies to overcome the listed issues. Additionally, the recommendation of incorporation of field conditions in mix design by Caltrans could further help in enhancing the durability of microsurfacing.

Table 2.13: Proposed EPG specifications for microsurfacing

Parameter	**Temperature (°C)**		
	EPG 61-XX	**EPG 67-XX**	**EPG 73-XX**
High-temperature grade [a]	61	67	73
Low-temperature grade [b]	-7; -13; -19; -25; -31	-7; -13; -19; -25; -31	-7; -13; -19; -25; -31
Test Methods for Asphalt Emulsion	**Test T(°C)**		
Storage Stability A - 24-h separation ratio (R_s): 0.2 to 1.5 B - 24-h stability ratio (R_d): max. 1.5	25	25	25
Emulsion Viscosity: max. 600 cP at 5 rpm	25	25	25
Particle Charge: Positive (Cationic)	25	25	25
Sieve Test: Max. 0.1%	25	25	25
Solubility: Min. 97.5%	25	25	25
Float: Min. 1,200 s	60	60	60
Percent Residue: Min. 57%	25	25	25
Test Methods on Asphalt Emulsion Residue			
Resistance to Rutting and Bleeding			
Max. J_{nr} at 3.2 kPa, 5 kPa^{-1} (low traffic)	61	67	73
Max. J_{nr} at 3.2 kPa, 1.5 kPa^{-1} (medium - high traffic)	61	67	73
Resistance to Thermal Cracking			
Max. |G*| at δ_c: 16 MPa δ_c values at low-temperature grade: δ_c = 50° at -7°C, δ_c = 48° at -13°C, δ_c = 46° at -19°C, δ_c = 44° at -25°C, δ_c = 42° at -31°C, δ_c = 40° at -37°C	5 and 15	5 and 15	5 and 15

[a] *Average 7-day maximum pavement surface design temperature should be less than High-temperature grade.*

[b] *Minimum pavement surface design temperature should be greater than Low-temperature grade*

Table 2.14: Alternate test protocols to conventional ISSA test procedures

ISSA Specified Tests and Drawbacks	Alternate Test Protocols			
	ASTM[1]	**Caltrans**[2]	**Texas**[3]	**Europe**[4]
Mix and Set Time Test				
• Operator variability for hand mixing. • Subjective nature of breaking and setting time assessment.	• Paper blot method	• Automatic Mixing Test	• Procedure similar to ISSA • Different cement content	• No provision
Consistency Test				
• Water content variation with temperature not considered. • Unable to provide adequate results for quick set system, quick traffic system.	• No provision	• Temperature variation (10°C, 25°C and 50°C) for OWC determination	• Modified cup flow test	• Procedure similar to ISSA
Cohesion Test				
• Operator dependency of torque application	• Procedure similar to ISSA	• Automated cohesion test	• Procedure similar to ISSA. • Minimum cement content determination	• Procedure similar to ISSA except mixing time: – Quick set: 45 sec – Slow set: 60-180 sec

ISSA Specified Tests and Drawbacks	**Alternate Test Protocols**			
	ASTM[1]	**Caltrans**[2]	**Texas**[3]	**Europe**[4]
Performance Tests				
Raveling, Rutting and Moisture Damage • Low correlation with field performance • Absence of provision for different curing conditions • Variability in test results	1. Raveling • Similar to ISSA except the absence of provision for air curing after specimen preparation. 2. Rutting • Similar to ISSA 3. Moisture Damage • No provision	1. Raveling • Cohesion-abrasion test for different curing conditions 2. Rutting • Procedure similar to ISSA but conditioning of specimens based on traffic conditions 3. Moisture damage • Ratio of abrasion loss of 6-day soaked specimen to 1-hour soaked specimen	1. Raveling • Procedure similar to ISSA. 2. Rutting • No provision 3. Moisture damage • Minimum residual asphalt content (RAC) • Optimum RAC = Minimum RAC + 0.5%	1. Raveling • Procedure similar to ISSA 2. Rutting • Not Applicable 3. Moisture damage • Shaking abrasion test
Classification Compatibility Test	• Procedure similar to ISSA	• No provision	• No provision	• No provision

[1] (ASTM D6372, 2015); [2] (Caltrans, 2010); [3] (Smith *et al.*, 1994); [4] (BS EN 12274-3, 2002; BS EN 12274-4, 2003; BS EN 12274-5, 2003; BS EN 12274-7, 2005)

Some researchers have also recommended modifications to improve the current mix design procedure. It was suggested to use LWT (ISSA TB No. 147, 2005) to determine optimum asphalt emulsion content. The formulations with greater cohesion (ISSA TB No. 113, 2017) were subjected to compaction, and the formulation with the least vertical and lateral displacement was termed as optimum asphalt emulsion content (Robati, 2014). In addition, studies had proposed evaluating peak flexural tensile strain using a bending test of a small beam of microsurfacing mix at -10°C along with conventional ISSA procedure to determine the optimum emulsion content (Wu, 2015).

A modified mixing method for specimen preparation during mix design was also proposed (Kumar & Ryntathiang, 2016). In this method, the pre-wet coarse aggregates were mixed with the required asphalt emulsion quantity estimated from the surface area method. After a homogeneous coating of coarse aggregates, 50% moistened fine aggregate and 50% asphalt emulsion estimated for fine aggregate were added and mixed. Then, additives were added, after which the remaining 50 % moistened fine aggregates and 50% asphalt emulsion estimated for fine aggregate were poured and mixed. The modifications adopted in the study were reported to eliminate the formation of lumps in the microsurfacing mix during the production stage.

Researcher have also explored the binder rheological property (complex shear modulus - G* and phase angle - δ), mixture interfacial adhesion property (bond strength at the interface), and bulk cohesive property of microsurfacing (Susanto *et al.*, 2019). The rheological properties, G* and tan δ, were measured using a frequency sweep test in the temperature range of 20-70°C (6°C intervals). The Leutner shear test was used to determine the interface bond strength. For specimen preparation, a core of 100 mm diameter was cut from an asphalt concrete slab, a ring mold was placed over it, and the microsurfacing mix was poured and allowed to cure. Since microsurfacing thickness is only 10 mm, the test set-up was modified by gluing 34 mm thick steel cylinder to microsurfacing mix. Then, the sample was placed horizontally, and vertical loading and lateral force were applied to measure the adhesion of microsurfacing with asphalt specimen at different temperatures, applied shear stress and shear rate. For measuring the bulk cohesive properties, displacement controlled cyclic sinusoidal loading was applied strain amplitude of 50 μm instead of uniaxial monotonic load. The delayed load response was recorded, and results were analyzed similar to the dynamic modulus test. Hence, incorporating the modifications suggested by the researchers and agencies, the

most commonly adopted ISSA mix design could be improved for ensuring better durability of the microsurfacing mix.

2.3.3 Effect of material properties on mix design and performance

The important factors contributing to the curing process which require detailed understanding are described in **Figure 2.8** (MS-19, 2008; Esfahani & Khatayi, 2020; Zalnezhad & Hesami, 2020). The detailed description of the effect of these components is discussed in **Section 2.3.1**.

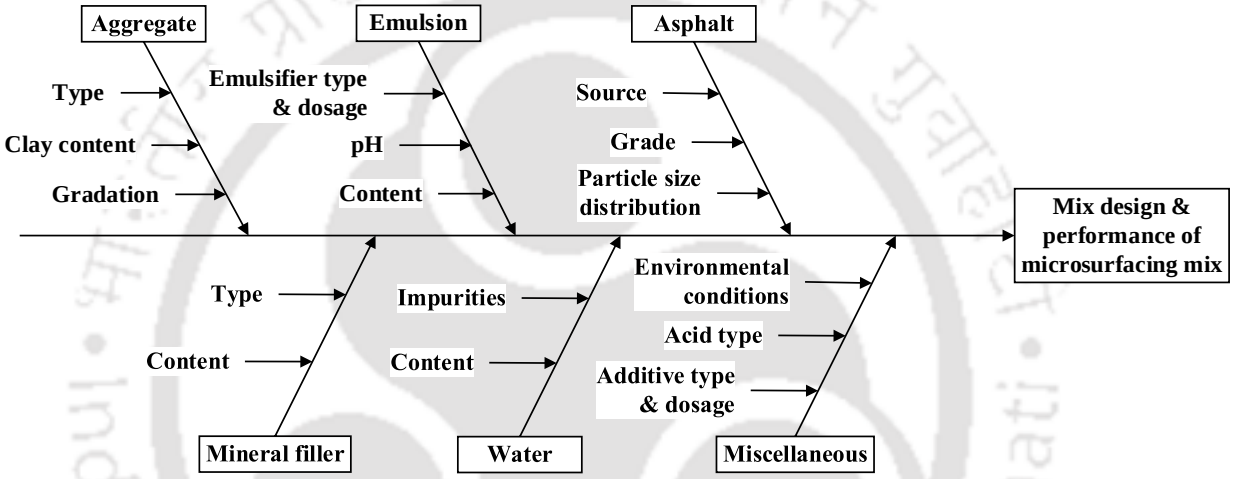

Figure 2.8: Factors influencing mix design and performance of microsurfacing mix

A summary of laboratory and field investigations on microsurfacing performance is presented in **Table 2.15** and **Table 2.16**, respectively. Studies have shown that the cohesion of microsurfacing mix is dependent on the combination of water content, cement content and additive used for mix production. It was also observed from Schulze Breuer and Ruck test that mineral filler content and compatibility rating were related (Andrews, 1994). In addition, the water damage was found to be dependent on the cleanliness of mineral aggregate. It was recommended that Methylene blue value (MBV) test should be used to assess the cleanliness of aggregates. Prewetting of aggregates was also recommended to allow dust particles to absorb water and allow asphalt emulsion to adhere to the aggregate surface (Wu *et al.*, 2011). The remaining coated area (wet stripping test) was found to be dependent on both aggregate type and asphalt emulsion content (Robati *et al.*, 2015b).

Table 2.15: Microsurfacing performance – Laboratory investigations

Author	Parameters	Property	Influence on microsurfacing property
Holleran *et al.* (1997)	• Additive type (Latex and crumb rubber in emulsion)	• Set time • Raveling • Rutting • Flexural strength	– Marginal improvement with crumb rubber addition – Raveling – Polymer < Rubber < Neat asphalt – Rutting – Polymer < Rubber < Neat asphalt – Rubber modified material – Better crack resistance
Nikolaides and Oikonomou (2000)	• Mineral filler type • Test temperature	• Raveling	– OPC as filler – Not influenced by temperature – Flyash as filler – Increase in aggregate loss at 35°C
Robati *et al.* (2013c)	• Aggregate gradation • Emulsion content	• Raveling	– Dependent on total surface area of aggregates – Emulsion content ↑ - Raveling ↓
Lonbar *et al.* (2014)	• Aggregate type • Emulsion content	• Skid resistance	– Improved with rough texture aggregates – Emulsion content ↑ - Skid resistance ↓
Robati *et al.* (2015a)	• Filler-mastic interaction	• Cohesion	– Higher stiffening rate - Faster cohesion development for higher pH of filler, higher zeta potential and higher MBV
Ilias (2015)	• Binder type • Temperature • Moisture	• Raveling • Moisture damage	– Raveling reduces with binder modification – Increase in temperature increases raveling – Poorly performing mix – Aggregate loss increases significantly

Author	Parameters	Property	Influence on microsurfacing property
Lonbar *et al.* (2015)	• Aggregate type • Emulsion type • Emulsion content	• Rutting	– Rut depth - Riverine > Mountainous aggregates – Rut depth - CSS-1h polymer modified > Resin epoxy modified – Emulsion content ↑ - Rutting ↑
Garfa *et al.* (2016)	• Aggregate gradation • Emulsion type • Mineral filler content	• Raveling • Rutting • Cohesion	– Dependent on both aggregate gradation and emulsion content – Coarse gradation showed best rutting resistance – Coarse gradation – Best cohesion – Dependent on emulsion type and mineral filler content – Curing time ↑ - Cohesion ↑
Lonbar and Nazirizad (2016)	• Aggregate type • Emulsion content • Emulsion type	• Raveling • Moisture damage • Rutting	– Raveling - Mountainous > Riverine aggregates – Raveling - CSS-1h > CQS-1h emulsion – Emulsion content ↓ - Raveling ↑ – Moisture damage - Mountainous > Riverine aggregates – Rut depth - Riverine > Mountainous aggregates – Emulsion content ↑ - Rutting ↑ (Dependent on emulsion type)
Yang and Liu (2017)	• Packing degree of aggregates • Asphalt film thickness	• Raveling • Rutting	– 1-hour soaked > 6-day soaked (Increases up to 48 hours) – Short-term raveling – Dependent on aggregate packing degree – Long-term raveling – Dependent on asphalt film thickness – Highest packing degree – Not obtaining best rutting resistance

Author	Parameters	Property	Influence on microsurfacing property
Ye *et al.* (2017)	• Aggregate gradation	• Cohesion • Raveling • Rutting • Moisture damage	– Coarser gradation - Lower cohesion value – Intermediate gradation – Best raveling resistance – Proportion of fine aggregates ↑ - Flushing ↓ – Intermediate gradation – Best moisture resistance
Hou *et al.* (2018)	• Aggregate gradation • Temperature • Water content • Cement content • Sand equivalent • Emulsion content	• Mixing time • Demulsification time • Raveling	– Finer gradation - Mixing & demulsification time ↓ – Temperature ↑ - Mixing & demulsification time ↓ – Water content ↓ - Mixing & demulsification time ↓ – Cement ↑ - Mixing time (first ↑ then ↓); Demulsification time ↓ – Sand equivalent ↓ - Mixing & demulsification time ↓; Raveling ↑ – Emulsion content ↓ - Raveling ↑
Garfa *et al.* (2018)	• Water content	• Rutting	– Significantly influenced by rut depth before rehabilitation and added water percentage
Xiao *et al.* (2018)	• Aggregate gradation	• Skid resistance • Raveling	– Use of single graded aggregates: Feasible solution considering - Skid resistance: 1.18–2.36 and 2.36–4.75 grade - Raveling: 0.6–1.18 and 1.18–2.36 grade
Zalnezhad and Hesami (2020)	• Emulsion type	• Cohesion • Raveling • Rutting	– Quick setting emulsion (CQS-1h) – Better cohesion, raveling and rutting resistance than slow setting emulsion (CSS-1h).

Author	Parameters	Property	Influence on microsurfacing property
Hafezzadeh and Kavussi (2021)	• Latex dosage • Cement content • Emulsion content	• Cohesion • Raveling • Rutting	– Latex dosage ↑ - Cohesion ↑; Abrasion ↓; Rutting ↓ – Cement content ↑ - Cohesion ↑; Abrasion ↓; Rutting ↓ – Emulsion content ↑ - Abrasion ↓; Rutting (first ↓ then ↑)

Note: ↑ denotes increase in parameter value; *↓ denotes decrease in parameter value*

Table 2.16: Field investigations on microsurfacing performance

Author	Parameter	Property	Influence on microsurfacing property
Hixon and Ooten (1993)	• Alternate materials • Aggregate type and gradation • Application	• Rate of rutting • Rut filling • Skid resistance • Raveling resistance • Reflective cracking	– Effectively reduced to 4 years – Effective upto 38 mm depth – Improved with skid resistance – Improved with customized gradation – Inadequate for application on PCC – Observed for application over PCC
Smith *et al.* (1994)	• Water content • Filler content	• Breaking and setting time • Abrasion • Sand adhesion	– Unacceptable for higher water content and lower mineral filler content and vice-versa – Decrease with increase in water content – Increase with increase in water content
Watson and Jared (1998)	• Aggregate size • Emulsion content	• Surface quality • Flushing	– Improved by removal of oversized stone – Reduced with lowering emulsion content by 0.8%

Author	Parameter	Property	Influence on microsurfacing property
Temple *et al.* (2002)	• Aggregate type	• Skid resistance	– Sandstone aggregates perform better than limestone.
Johnson *et al.* (2007)	• Asphalt grade • Binder content	• Transverse reflective cracking • Longitudinal reflective cracking • Rut filling and scratch coarse	– Softer asphalt grade - Reduced moderately – Softer asphalt grade - Effective reduction – Binder content reduction (1-2%) – Effective
Kucharek *et al.* (2010)	• Aggregate gradation	• Satisfactory performance - Structural strength, macrotexture and noise level	– Moderate traffic – Type II gradation – Heavy traffic – Fine Type III gradation – Minimum binder content – 7%
Broughton and Lee (2012b)	• Asphalt type • Application rate • Pavement condition • Environmental condition • Workmanship	• Aggregate loss • Flushing and bleeding • Debonding • Crack propagation • Performance • Ensuring performance	– Recommendation - Use harder grade binder – Reason - Higher application rate – Recommendation – Use continuous paving machine – Insufficient structural strength of underlying pavement – Accelerated with cold weather – Poor – Base failure – Preparation of test strip and equipment calibration

2.4 Production of microsurfacing mix

2.4.1 Construction of microsurfacing

The construction of microsurfacing on a structurally sound pavement involves cleaning of the surface, application of tack coat (optional), sealing of cracks and spreading of homogeneous, stable microsurfacing mix at a pre-defined application rate. The construction equipment generally used for microsurfacing production is provided in **Table 2.17** (ISSA A143, 2010). The continuous-flow mixing unit minimizes the number of transverse joints incurred due to the start-and-stop paving operation (Patrick, 2018). The mechanical devices in the spreader box ensure agitation and uniform spreading of mix throughout the spreader box (ISSA A143, 2010). Front seal prevents the loss of mix from the spreader box and rear seal provides a strike-off. After the mix is spread, a secondary strike-off ensures that the desired surface texture is achieved (ISSA A143, 2010). It is important to note that the cracks on the pavement surface wider than 6.4 mm should be treated using a sealant with sufficient time to cure before applying microsurfacing. In addition, providing adequate construction joints and ensuring acceptable edges are vital for successful microsurfacing performance (ISSA A143, 2010).

Table 2.17: Construction equipment used in microsurfacing as per ISSA

Category	Equipment type
Mixing and Proportioning Devices	• Automatic-sequenced, self-propelled mixing machine. • Continuous-flow mixing unit with revolving multi-blade, double-shafted mixer. • Individual volume or weight controls for proportioning
Spreading Equipment	• Spreader box – Twin-shafted paddles or spiral augers • Front and rear seal
Secondary Strike-off	• Adjustable to match the width of the spreader box • Allow for varying pressures
Rut-Filling Equipment	• Rut depth < 12.7 mm – Full width scratch course • Rut depth: 12.7 mm to 38.1 mm – Independent filling with a rut-filling box • Rut depth > 38.1 mm – Multiple applications with the rut-filling box with curing under traffic for at least 24 hours between two layers application

2.4.2 Quality Control

Quality refers to the degree to which the job conforms to the specification requirements. In order to ensure a durable pavement, quality assurance (QA) and quality control (QC) have to be planned and performed systematically. Since the projects involving microsurfacing are on a large scale, the inherent variability in nature over the course of time results in changes in the material properties, including quality of aggregates and asphalt emulsion. It has to be controlled to ensure microsurfacing mix performs as desired (Gransberg, 2010).

Several agencies laid down criteria for the frequency of testing for QC. Typical QC guidelines by MoRT&H, 2013 are shown in **Table 2.18** (MoRT&H, 2013). The guidelines laid down for tolerance limits concerning aggregate gradation and residual asphalt content by various agencies are presented in **Table 2.19** and **Table 2.20,** respectively (West & Smith, 1996; OkDOT, 2009; ISSA A143, 2010; MoRT&H, 2013; GDOT, 2013; Sholar & Kim, 2013; MnDOT, 2016; Patrick, 2018). It could be inferred from **Table 2.19** and **Table 2.20** that although the importance of quality control is well-known, the tolerance limits established by different agencies vary. For instance, the tolerance limits for aggregate gradation by Texas Department of Transportation (DoT) and Australian specifications are more stringent than ISSA or Indian specifications.

Table 2.18: Quality control tests with minimum frequency for microsurfacing mix

Parameter	Property	Frequency
Aggregates	Physical properties	One per source/ site
	Moisture content	Two per day
	Gradation	Two per day
Asphalt emulsion	Physical properties	One per lot of 20 t
	Binder content	Two per lane per km
Construction	Machine calibration	Once per project
	Quantity of slurry	Daily

Table 2.19: Tolerance limits for aggregate gradation

Sieve Size (mm)	ISSA[1]	Texas[2]	Georgia[3]	India[4]	Australia[5]
4.75	± 5%	± 5%	± 6%	± 5%	± 6%
2.36	± 5%	± 5%	± 5%	± 5%	± 5%
1.18	± 5%	± 5%	--	± 5%	± 5%
0.60	± 5%	± 3%	--	± 5%	± 4%
0.30	± 4%	± 3%	± 4%	± 4%	± 3%
0.15	± 3%	± 3%	--	± 3%	± 2%
0.075	± 2%	± 3%	± 3%	± 2%	± 1.5%

[1] (ISSA A143, 2010)*; [2]* (TxDOT, 2014)*; [3]* (GDOT, 2013)*; [4]* (IRC: SP: 81, 2008)*; [5]* (Patrick, 2018)

Table 2.20: Tolerance limits for residual asphalt content

Source	Residual asphalt content (by weight of dry aggregate)	Tolerance limits of residual asphalt content
ISSA*	5.5 – 10.5 %	± 1.5 %
India: Type II	6.5 – 10.5 %	--
Type III	5.5 – 10.5 %	--
USA: Florida	5.5 – 10.5 %	± 0.5 %
Oklahoma	6.0 – 9.0 %	± 0.5 %
Texas	6.0 – 9.0 %	± 0.5 %
Minnesota	7.0 – 10.5 %	--
Georgia	6.0 – 9.0 %	± 0.5 %
Australia	--	- 0.5% to + 1%

* *Tolerance limits for OEC from job mix formula*

Studies have also recommended narrowing the range of aggregate gradation provided in ISSA guidelines (Robati *et al.*, 2013b). For residual asphalt content, Minnesota DoT and Georgia DoT suggests reducing the allowable range to 7.0-10.5 % and 6.0-9.0%, respectively. The Australian specifications permit a wider tolerance range for asphalt content in comparison to other specifications. Understanding the variability in performance associated with deviation in process control parameters is critical to analyze project-specific microsurfacing durability.

It is important to control the variability in material delivery rate during the production stage. The California DoT (Caltrans, 2015) laid down the criteria for maximum allowable deviation of 2% for the delivery rate of both aggregate and asphalt emulsion from aggregate belt feeder and asphalt emulsion pump, respectively. Ohio DoT (ODOT, 2018) specified that the binder to dry aggregate proportioning should conform within a tolerance range of Job Mix Formula (JMF) ± 6.4 L/metric ton.

Assessment of the microsurfacing surface characteristics for conforming to performance requirements is vital. According to the European Standard (BS EN 12273, 2008), the evaluation of conformity to stated performance characteristics should be demonstrated by Factory Production Control (FPC) and Type Approval Installation Trial (TAIT). In FPC system, the producer shall establish, document and maintain the record of procedures, regular inspections and tests conducted to ensure quality control of procured material, equipment, production process and the finished product. In TAIT, the test section of a minimum length of 200 m is installed using FPC, and the performance characteristics are defined after one year of completion of microsurfacing application.

In addition, European Standard (BS EN 12274-8, 2005) provides a guideline for qualitative (estimated) and quantitative (measured) assessment of defects. The defects are estimated or measured in terms of areas and lengths for 100 m section every 11-13 months. The defects mentioned below are then categorized according to performance characteristics of microsurfacing (PD 6689, 2009; BS EN 12273, 2008):

- Bleeding, fatting up and cracking
- Delamination, loss of aggregate, wearing, rutting, lane joint gaps and slippage
- Corrugation, bumps and ridges
- Small repetitive defects
- Longitudinal grooves

Even after rigorous quality control during production stage, there is a possibility of non-compliance of material properties or construction activities from the specified tolerance ranges. In such cases, the payment of the work is reduced in conjunction with the non-compliance of that particular work. Several agencies have defined pay reduction factors for different parameters during the microsurfacing production and construction stage as follows:

- **Residual asphalt content**: 2% reduction in unit price for each 0.1% variation in residual asphalt content outside mixture control tolerance range (GDOT, 2013).
- **Application rate**: 5% reduction in unit price for each 0.5 kg/m^2 lesser mix spread rate than specified tolerance range (GDOT, 2013).
- **Aggregate properties**: Deduction of $2/ton for each non-compliant aggregate gradation and cleanliness (sand equivalent) test (Caltrans, 2015).
- **Defects**: 2% to 20 % reduction in price depending upon the number of defects including binder or aggregate properties, aggregate gradation, binder content, surface shape, skid resistance and texture depth (Patrick, 2018).

2.4.3 Production parameters influencing microsurfacing performance

The main process control variables include aggregate gradation, asphalt emulsion content and aggregate moisture content. In this context, the durability of microsurfacing mix should be assessed in terms of laboratory performance tests by subjecting the mix to variability encountered in field.

Workability

Workability of microsurfacing mix is defined in terms of its flow characteristics. During production, the proper spreading and laying of the mix is dependent on the workability of the mix. A mix with very low workability often breaks within the paver whereas very high workability might lead to segregation. In microsurfacing, the workability characteristics are generally established using consistency test (ISSA A143, 2010). Several factors contribute to the variation in the workability of the microsurfacing mix, as shown in **Figure 2.8**. The variabilities associated with the use of different aggregate type, emulsifier dosage and chemistry, emulsion pH, mineral filler type and use of recycled or waste materials is accounted during mix design. During the production stage, there is a inevitable variation of aggregate gradation, emulsion content, and water content. In terms of environmental factors, difference in temperature and humidity is generally countered by varying the quantity of water added to the mix. Laboratory investigations on the effect of process control parameters also showed that the mixing time and workability reduced for finer gradation and increased for coarser gradation (Ye *et al.*, 2017). Hou *et al.* (2018) found that the mixing and demulsification time substantially reduces for lower water content and emulsion content.

Strength

Microsurfacing mix should gain adequate strength after application for opening to traffic. Lower rate of strength development might result in tire marks with the traffic movement and increased risk of raveling. As a result, premature distresses would be observed on the pavement surface. In such cases, the durability of microsurfacing mix is substantially reduced. Generally, the strength evolution of the microsurfacing mix is assessed with the help of a cohesion test (ISSA A143, 2010). Study on filler-mastic interaction pointed out that the rate of cohesion development was higher for higher pH of filler, higher zeta potential and higher methylene blue value (Robati *et al.*, 2015a). The cohesion was found to be dependent on the combination of emulsion type and mineral filler content (Garfa *et al.*, 2016). Several factors contribute to the strength evolution in the microsurfacing mix, as shown in **Figure 2.8**. Among these factors mentioned, the process control parameters vary during the production stage. As a result, the strength development prior to opening to traffic is affected. Laboratory investigations also highlighted that the cohesion decreased for coarser aggregate gradation and lower emulsion content (Ye *et al.*, 2017; Buss & Pinto, 2019). In contrast, the effect of water content on cohesion was not significant (Buss & Pinto, 2019).

Raveling

Raveling is one of the key performance parameters of the microsurfacing mix. It has been reported that the resistance to raveling is better for finer aggregate gradation (Robati *et al.*, 2013c; Ye *et al.*, 2017). On the other hand, a decrease in the emulsion content increases the potential for raveling (Lonbar & Nazirizad, 2016; Hafezzadeh & Kavussi, 2021). Another critical aspect, pre-wetting water content, influences the production and performance of microsurfacing (Garfa *et al.*, 2018; Hou *et al.*, 2018). Poor coating, raveling, and delamination are generally observed when there is a substantial reduction in the water content from the optimum. On the other hand, when the water content is substantially high, issues related to the reduction of binder affinity towards the aggregate surface, delayed setting, raveling, flushing, and segregation are observed (Gransberg, 2010).

Rutting

In microsurfacing, the air voids generally vary between 9-11% (Reinke *et al.*, 1990; Sangiorgi *et al.*, 2012). The load application might result in the densification of the mix

along the wheel path, i.e., rutting. These ruts often lead to difficulties in the steering of the vehicle and hydroplaning-related road crashes. Laboratory investigations were conducted on rutting of microsurfacing laid over HMA slab and a regression model was developed to predict rutting (Garfa *et al.*, 2018). Significance testing of model parameters highlighted that the water content added to the aggregates significantly affected the rut depth observed. In addition, it has been reported that for finer aggregate gradation and very high-water content, the susceptibility to rutting increases (Garfa *et al.*, 2016). In terms of emulsion content, the rutting decreases till optimum emulsion content, after which the rutting increases (Wang *et al.*, 2019; Fooladi & Hesami, 2021; Hafezzadeh & Kavussi, 2021).

Bleeding

Bleeding refers to a smooth, shiny, and reflective pavement surface caused due to the migration of asphalt to the surface when traffic load is applied over it. As a result, safety concerns arise due to reduced surface friction and visibility difficulties (Krishnan & Rao, 2001). Laboratory investigations showed that the risk of bleeding increases for higher emulsion content (Lonbar *et al.*, 2015; Esfahani & Khatayi, 2020) and a decrease in the finer proportion of aggregates (Ye *et al.*, 2017). Robati *et al.* (2013c) also found that the bleeding potential increases with the increase in the total surface area (TSA), i.e., for finer aggregate gradation.

Cracking

Cracking, especially reflective cracking, is also one of the major concerns observed in the field (Wood & Geib, 2001; Johnson *et al.*, 2007; Nair *et al.*, 2020). Smith and Beatty (1999) stated that if the cracks are on a structurally inadequate or unstable pavement layer, the microsurfacing treatment would generally be ineffective. In such cases, alternate repair methods are recommended in place of microsurfacing to treat pavement. In addition, Shackil *et al.* (2020) reported that the microsurfacing might not be appropriate even for pavements with low severity cracks as the chances of proper adhesion between the mix and crack sides is low.

A brief summary of possible distresses in microsurfacing, and their causes is presented in **Table 2.21** (Kucharek *et al.*, 2010; Broughton & Lee, 2012a; Ilias, 2015). Aggregate type and gradation, emulsion and water content are process control parameters. Construction factors include application rate and environmental conditions (Hixon &

Ooten, 1993; Watson & Jared, 1998; Temple *et al.*, 2002; Jahren & Behling, 2004; Sangiorgi *et al.*, 2012; Tabatabaee *et al.*, 2012).

Table 2.21: Possible causes for distresses in microsurfacing

Distress	Cause
Raveling and surface wear	• Aggregate binder incompatibility • Inadequate binder content or oxidation of binder • Effectiveness of polymer modification • Insufficient fines in the mix • Abrasion action of tires • Premature wear - Heavy traffic or snow ploughs
Rutting	• Filling ruts greater than 0.5'' in single pass, not crowning the ruts • High binder content • Excessive traffic loading
Cracking	• Low temperature • Reflective cracking from existing cracks • Aging of microsurfacing mix
Stripping	• Presence of moisture • Degradation of bond between binder and aggregate
Delamination	• Inadequate cleaning of original surface or presence of moisture at the interface between existing pavement and microsurfacing • Early asphalt emulsion break • Inadequate binder content
Bleeding, shoving and flushing	• High binder content • High temperature or high humidity • Loss of aggregate from surface
Miscellaneous	• Drag Marks - Asphalt emulsion is breaking too fast • Scratch marks and tears - Poorly maintained equipment or improper application rates • Poor edges and joints - Contractor inexperience • Early traffic damage - Insufficient cure time, conditions or mix design

2.5 Durability of microsurfacing treatment

Durability is defined in terms of the ability of the pavement structure to fulfil the structural and functional requirements throughout the service life. Microsurfacing is applied on the surface course and its durability is generally assessed in terms of its functional characteristics. Being a cold mix, the mechanical behaviour of microsurfacing mix continues to evolve with time (Lambert *et al.*, 2018). The evolutive behavior is generally attributed to the gradual loss of water from the mix. As the water drains off, there is an improvement in the stiffness of the mix (Thiriet *et al.*, 2021). But, over time, the detrimental environmental conditions and traffic loading deteriorate the performance of microsurfacing mix. The predominant environmental factors include aging and moisture damage. A detailed discussion on the effect of aging and moisture damage on the behaviour of microsurfacing mix is provided below.

Aging

Asphalt aging is attributed to the changes in rheological and mechanical properties as time elapse due to the changes in the chemical composition of asphalt. Aging is associated with three mechanisms: volatilization of light oils during mixing, oxidation during service life, and steric hardening. It causes a change in relative proportions of saturates, aromatics, resins and asphaltenes (SARA) fractions which result in a change in the colloidal structure of asphalt resulting in changes in its viscoelastic properties. In conventional HMA, volatilization is considered to be the primary cause of short term aging which occurs during mixing, laying and compaction of asphalt at elevated temperatures. Oxidation results in long term aging of the asphalt mixture that occurs throughout the pavement service life due to its exposure to the environment (Petersen & Glaser, 2011; Menapace *et al.*, 2015).

Unlike conventional HMA, the microsurfacing mix does not undergo aging during the production process. However, stiffening of the binder occurs during the curing process and aging during subsequent service life. Hence, to understand the aging kinetics, Peterson and Glaser (2011) and Poulikakos *et al.* (2019) recommended assessing the carbonyl and sulfoxide functional group as a parameter for asphalt oxidation. In this respect, investigations on the Infra-red oxidation levels showed a significant increase in the carbonyl and sulfoxide oxidation indexes with time for curing at 35°C at 20% relative humidity. It highlights that the oxidation of the binder increases with time during the warm period (Thiriet *et al.*, 2021).

Further, laboratory investigations on the performance of microsurfacing mix showed that the oxidation and aging resulted in the increase in the degree of raveling of microsurfacing mix (Ji *et al.*, 2013). In another study, Garfa *et al.* (2018) subjected HMA slabs rehabilitated with microsurfacing to aging at 85°C for 2 days and 5 days to simulate thermal aging. Laboratory testing of aged specimens showed that the rutting resistance improved with the increase in curing as well as aging times. Recently, Liu *et al.* (2021) mimicked aging using ultraviolet high-pressure mercury lamp. It was found that the raveling potential and moisture susceptibility increased with the increase in aging time.

Moisture damage

In addition to aging, it is vital to assess the damage associated with moisture ingress. Moisture damage is defined as the loss of stiffness and strength of the asphalt mixtures as the moisture enters into the aggregate binder interface. The mix undergoes loss of adhesive properties and softening of the binder due to the rupture of the bond between molecules of the asphalt film (Little & Jones, 2003). Subsequently, under the application of mechanical loading, stripping, and in turn, distresses like raveling and cracking are observed.

Hence, to investigate moisture damage in microsurfacing, specimens are generally soaked for 6-days in a water bath at 25°C (Caltrans, 2010; ISSA A143, 2010), and WTAT is carried out. Since the conventional test protocol is time-consuming (approximately 9 days), Zhai and Rosales (2017) explored the effect of time and temperature of moisture conditioning to rapidly assess the effect of moisture on raveling resistance of microsurfacing. It was found that the conditioning time and temperature of 3 hours and 60°C respectively in the water bath mimicked the moisture damage exhibited to WTAT specimens using conventional test protocol, i.e., 6 days at 25°C. Alternatively, Ilias (2015) suggested that to differentiate a poorly performing mix from a well-performing mix, the specimens could be subjected to 24 hours of moisture conditioning in a water bath at 40°C.

2.6 Summary of literature review

Microsurfacing has emerged as a green technology owing to its performance, cost and environmental benefits. So, to analyse the pros and cons of microsurfacing, SWOT analysis was initially conducted by utilizing information from literature. Then, the parameters affecting mix design, production and durability were determined by literature review on the role of each component and variable associated with microsurfacing production and performance. The summary of the literature review is as follows:

- SWOT analysis highlighted that the benefits associated with microsurfacing are cost-effectiveness, improved safety for both user and construction worker, superior aesthetics, and reduction in energy consumption, greenhouse gas emission, and aggregate consumption. However, certain challenges like insufficient fund allocation, implementation or performance issues and production variability need to be addressed. Also, skilled and knowledgeable engineers should be able to rectify commonly faced issues during the construction phase.
- Interesting opportunities, including pre-compacting microsurfacing before opening to traffic, could be a way forward for decreasing permeability, reducing rutting and moisture infiltration to underlying layers. Incorporation of recycled and waste materials improves sustainability along with a reduced overall construction cost.
- Good mix design and systematic quality control during production are the keys to ensure the effectiveness and durability of microsurfacing. ISSA's conventional microsurfacing mix design covers various performance parameters, including aggregate-emulsion compatibility, early traffic damage, raveling, rutting, and bleeding.
- Repeatability and reproducibility of test results are the main concern expressed in the vast literature body. Concerns on particle size restriction, field performance correlation, curing time consideration, temperature and humidity ranges are also reported.
- Premature distress, such as disintegration, deformation, cracking and bleeding, is primarily attributed to deviation in process control parameters and construction factors considered during mix design.

2.7 Research gaps

The following research gaps are identified from the review of the existing literature.

- Section 2.3.2 highlights that the quantification of the effect of material properties on microsurfacing performance is still not fully understood. Also, there is a need to present a systematic approach to address the challenges faced during microsurfacing mix design.
- Application of microsurfacing according to project-specific conditions and appropriate adjustments required to the job mix formula is based on experience only, as described in Section 2.3.3. In this regard, there is a gap in the literature related to the understanding on the synergistic influence of process control parameters, including aggregate gradation, emulsion content, and water content, on the performance of the microsurfacing mix.
- Quality control in microsurfacing mix does not specify critical combinations of production parameters that need to be avoided during construction, as shown in Section 2.4. So, identifying the critical combinations of factors influencing the production and performance of microsurfacing mix and assigning the contribution of each parameter is vital.
- From Section 2.5, it could be said that even though the importance of establishing the durability of microsurfacing is well-acknowledged, limited studies in this area restrict the boundaries of understanding related to the effect of environmental conditions on the performance of microsurfacing mix during its service life.

CHAPTER 3

Experimental Methodology

3.1 General

This chapter discusses the experimental methodology adopted in this study to evaluate the performance of the microsurfacing mix. Initially, the flow chart and relevant information regarding the laboratory investigations are presented. For each testing protocol followed, a detailed discussion on the selection basis is provided.

3.2 Experimental Methodology

The scope of the study was divided into three phases, as described in **Section 1.4**. The schematic representation of the experimental methodology adopted for fulfilling the scope of the study is shown in **Figure 3.1**. Physical tests and chemical composition analysis were conducted to characterize the aggregates, asphalt emulsion and mineral filler. The obtained results were compared with the requirements of the specification. Then, the influence of material properties on cohesion, raveling, and rutting resistance was determined. **Table 3.1** provides the summary of different variable considered, notations used and description for each variable. The mix design was conducted as per ISSA guidelines (ISSA A143, 2010) using the best material combination. The mix design involves testing the microsurfacing mix for the design parameters, i.e., abrasion loss and sand adhesion. In addition, a narrow range diagram considering cohesion at 30-min and 60-min, abrasion loss (1 hr and 6-day soaked), lateral displacement and sand adhesion was plotted for obtaining OEC.

Subsequently, the performance of the microsurfacing mix was evaluated for different combinations of process control parameters. A total of 35 combinations of aggregate gradation, emulsion content and water content were selected, as shown in **Table 3.2**. The performance tests were conducted as per ISSA guidelines, where four replicates were casted for each test to ensure repeatability of test results (Ilias, 2015). The relative contribution of process control parameters was assessed using Artificial Neural Network (ANN) and modeling of test results was conducted using Multigene Symbolic

Genetic Programming (MSGP). Reliability analysis was also conducted to assess the risk of failure of microsurfacing mix.

The durability of microsurfacing treatment was assessed in terms of resistance to aging and moisture damage. Different combinations of time and temperature were selected for aging and moisture conditioning to account for different environmental conditions encountered depending on the project location. The performance was described in terms of raveling.

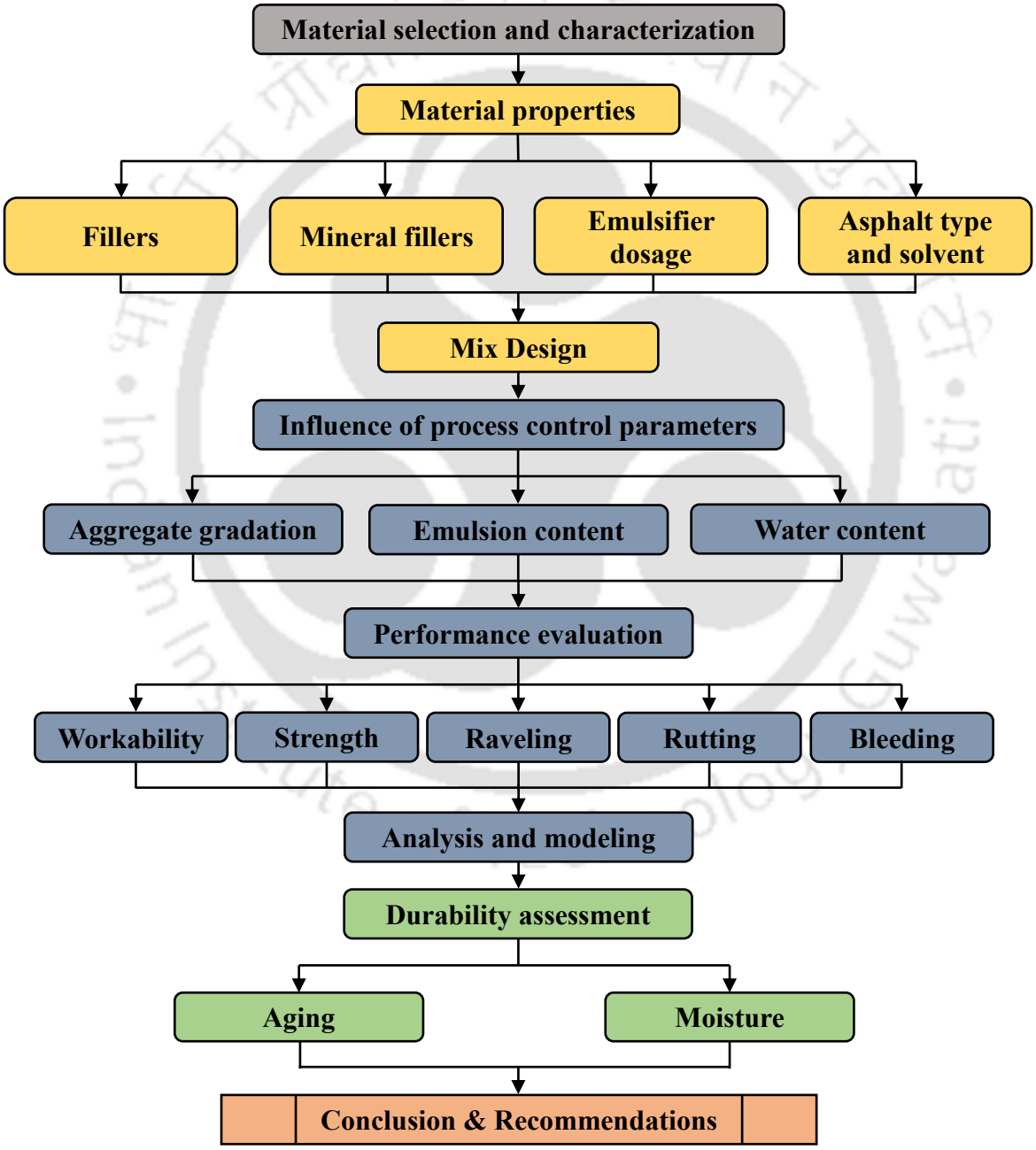

Figure 3.1: Flow chart representing the experimental matrix

Table 3.1: Summary of different variables considered and its description

Variables	Notations	Description
Fillers	Filler A	Material passing 75 μm sieve for aggregate source A
	Filler B	Material passing 75 μm sieve for aggregate source B
Mineral fillers	OPC	Ordinary Portland Cement (Grade – 53)
	FA	Flyash (Class-F)
Asphalt type	VG-10	Softer binder grade (Viscosity Grade – 10)
	VG-30	Harder binder grade (Viscosity Grade – 30)
Solvent	Kerosene	Solvent addition in asphalt @ 1% by weight of asphalt
Emulsion types	E1	VG-10 binder, 1.5% emulsifier dosage and no solvent
	E2	VG-10 binder, 2.0% emulsifier dosage and no solvent
	E3	VG-10 binder, 2.5% emulsifier dosage and no solvent
	E4	VG-30 binder, 1.5% emulsifier dosage and no solvent
	E5	VG-30 binder, 1.5% emulsifier dosage and 1% solvent

Table 3.2: Process control parameters combinations for performance evaluation

Mix ID	TSA (m^2/kg)	EC (%)	WC (%)	Mix ID	TSA (m^2/kg)	EC (%)	WC (%)
C1	10.2	14.00	6.4	**C19**	8.7	15.50	5.4
C2	11.7	14.00	6.4	**C20**	8.7	15.50	6.4
C3	10.9	14.00	6.4	**C21**	8.7	15.50	7.4
C4	9.4	14.00	6.4	**C22**	8.7	12.50	5.4
C5	8.7	14.00	6.4	**C23**	8.7	12.50	6.4
C6	10.2	15.50	6.4	**C24**	8.7	12.50	7.4
C7	10.2	14.75	6.4	**C25**	11.7	14.00	5.4
C8	10.2	13.25	6.4	**C26**	11.7	14.00	7.4
C9	10.2	12.50	6.4	**C27**	11.7	15.50	5.4
C10	10.2	14.00	5.4	**C28**	11.7	15.50	6.4
C11	10.2	14.00	7.4	**C29**	11.7	15.50	7.4
C12	10.2	14.00	8.4	**C30**	11.7	12.50	5.4
C13	10.2	15.50	5.4	**C31**	11.7	12.50	6.4
C14	10.2	15.50	7.4	**C32**	11.7	12.50	7.4
C15	10.2	12.50	5.4	**C33**	11.7	12.50	8.4
C16	10.2	12.50	7.4	**C34**	10.2	12.50	8.4
C17	8.7	14.00	5.4	**C35**	8.7	12.50	8.4
C18	8.7	14.00	7.4				

** Note: TSA = Total Surface Area (m^2/kg); EC = Emulsion content (% by weight of dry aggregates); WC = Water content (% by weight of dry aggregates); C1 = Control mix.*

3.3 Material selection and characterization

3.3.1 Aggregates and mineral filler

Properly selecting aggregates and assessing aggregate characteristics is required to achieve desired strength and durability of the microsurfacing mixture. The primary factor that influences the performance is the gradation of aggregate used for the production of microsurfacing mix. Type II gradation, as per ISSA guidelines, is generally used in rural and urban roads to fill surface voids, address surface distresses, and provide a durable wearing surface (IRC: SP: 81, 2008; ISSA A143, 2010). Hence, mid-point of Type II gradation (ISSA A143, 2010) was adopted in the study for control mix, as shown in **Figure 3.2**.

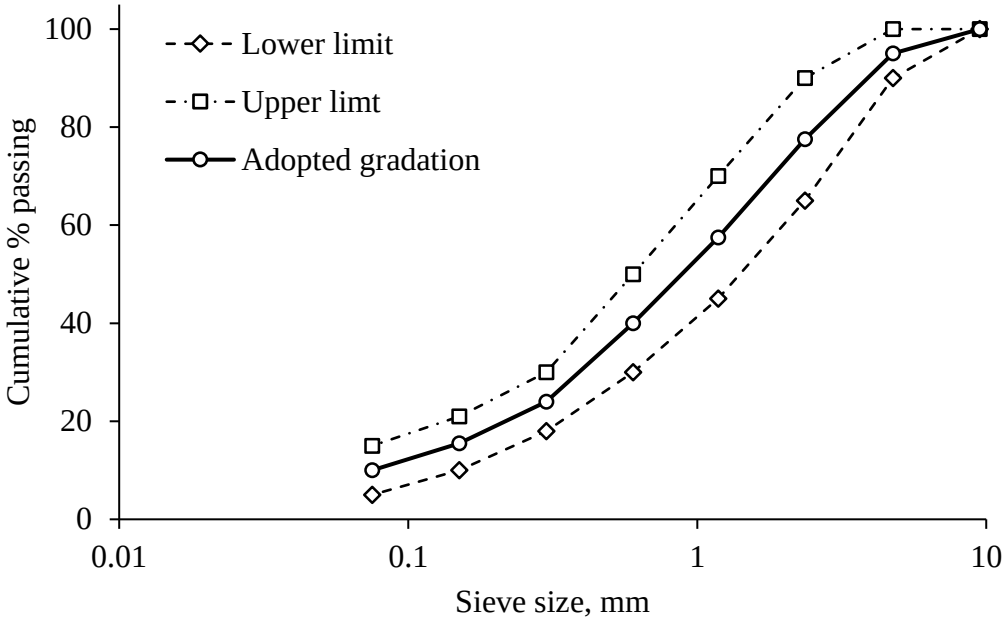

Figure 3.2: Aggregate gradation

The fundamental requirements defined by a combination of engineering and physical properties were studied. The microsurfacing mix cures chemically and acts as a surface course. The properties like durability, abrasion resistance, cleanliness (sand equivalent value), and water absorption of aggregate are critical for ensuring a durable mix. The physical properties of aggregates used are presented in **Table 3.3**.

Table 3.3: Physical properties of aggregates

Property	Results	Specification Limits
Bulk specific gravity of aggregates	2.888	--
Water absorption	1.0 %	--
Soundness with Na_2SO_4	8.9 %	15 % *max.*
Abrasion value	17.7 %	30 % *max.*

The mineral fillers used are Ordinary Portland Cement (OPC-53) and Flyash (Class-F). The mineral fillers are included as a part of the gradation, where the amount of mineral filler added replaces the equal amount of material passing 75 μm sieve.

Aggregates were procured from 2 sources: Source A and Source B. For production of microsurfacing mix, aggregates from Source A were considered initially. Then, to rectify the issue of rapid breaking (explained in detail in **Section 4.3.1**), filler (material passing 75 μm sieve) from Source A were replaced by filler from aggregate Source B. The physical properties of aggregate fillers from Source A (Filler A) and Source B (Filler B) are presented in **Table 3.4**. Sand equivalent values of aggregate source was also determined having Filler A and Filler B. It could be observed from **Table 3.4** that the MBV of Filler A was greater than 15 whereas Filler B had an MBV of 2.55 and a relatively lower pH value. Also, the sand equivalent value increased to an acceptable value of more than 65, which shows that the clay content in Filler B is relatively lower than Filler A. In general, the physical properties of fillers, including MBV and sand equivalent value, indicate that the breaking and setting process would be faster for mixes produced with Filler A due to the high clay content of aggregate (Robati *et al.*, 2015a). It would ultimately result in a lower mixing time.

Table 3.4: Physical properties of fillers

Properties	Filler A	Filler B
Specific Gravity of filler	2.915	2.794
Methylene blue value (MBV)	15.5	2.55
Rigden voids, %	34.2	37.3
pH	8.05	7.88
Sand Equivalent Value*	55.4	81.7

** Sand Equivalent Value: For combination of aggregates passing 4.75 mm*

In addition, the chemical composition of aggregate fillers and mineral fillers was conducted using an X-ray fluorescence spectrometer. The equipment used was Rigaku made WD-XRF Machine (Power: 4KW, 60kV-150mA). Results of the investigations are shown in **Table 3.5**. XRF results showed that the SiO_2 content of Filler A was substantially higher than Filler B. Since there is a negative charge on the aggregate surface with high silica content, adding cationic asphalt emulsion to aggregates having Filler A would break the mix early. Aggregates having a higher CaO/SiO_2 ratio generally provide better adhesive properties with asphalt binder (Abo-Qudais & Al-Shweily, 2007). In this study, Filler B had a relatively higher CaO/SiO_2 ratio (4.23) than Filler A (0.14), indicating the better adhesivity with Filler B.

Table 3.5: Chemical composition of material passing 75 µm, % by mass

Oxide	Filler A	Filler B	Cement	Flyash
CaO	6.1	39.4	63.6	1.2
SiO_2	44.6	9.3	19.5	59.4
Fe_2O_3	19.0	1.6	3.9	3.6
Al_2O_3	14.5	2.7	3.1	28.1
MgO	5.2	10.9	2.9	0.6
TiO_2	2.3	0.2	0.3	1.9
Na_2O	2.1	0.0	0.0	0.1
K_2O	1.7	1.5	0.3	1.2
P_2O_5	0.5	0.0	0.0	0.3
MnO	0.2	0.1	0.1	0.1
NiO	0.0	0.0	0.0	0.0

From **Table 3.5**, it could be seen that cement had CaO as the major component occupying 63.6% by mass of the total weight. Higher CaO content present in cement promotes hardening of cold mix asphalt by removing water from the mixture through cement hydration. On the other hand, fly ash exhibited very high SiO_2 content, which shows that the incorporation of fly ash alone might not sufficiently strengthen the mix. In addition, Class-F type flyash requires an alkaline environment, for e.g., $Ca(OH)_2$, to react and form cementitious compounds (Thomas, 2007). Since asphalt emulsion is

acidic (pH = 2), flyash addition might not improve the adhesion characteristics of the microsurfacing mix.

The reaction kinetics of cement and flyash was divided into two phases. Firstly, the cement hydration forms calcium silicate hydrate (C-S-H) and calcium hydroxide (CaOH). Secondly, the CaOH reacts with the silica present in the fly ash to again produce C-S-H. This reaction leads to the higher production of the cementitious product (C-S-H), and the adhesion improves (American Coal Ash Association, 2003). Hence, both cement and flyash are required to be added to compliment the strength requirement of microsurfacing mix.

3.3.2 Asphalt emulsion

3.3.2.1 Production of asphalt emulsion

Asphalt emulsion (cationic quick setting) was produced in the laboratory using a colloid mill. The materials used in the study are shown in **Table 3.6**. In this study, two viscosity grade (VG) binder grades were used: VG-10 and VG-30. The physical properties of the binders is described in **Table 3.7**. The temperature, binder grade and formulations used for the study are presented in **Table 3.8**.

Table 3.6: Description of asphalt emulsion components

Component	Description
Asphalt	Unmodified VG-10 and VG-30 asphalt
Asphalt additive	Ingevity Peral® 600 (P600)
Emulsifier	Cationic quick setting emulsifier: Ingevity Peral® 417 (P417)
Latex	SBR latex
Acid	Hydrochloric acid
Water	Potable water

Table 3.7: Properties of VG-10 and VG-30 binder

Parameter	VG-10		VG-30	
	Result	**Limits**	**Result**	**Limits**
Penetration value, 0.1 mm	95	*min.* 80	54	*min.* 45
Softening point, °C	43	*min.* 40	53	*min.* 47
Ductility value, cm	100+	*min.* 75	100+	*min.* 40
Specific Gravity	1.018	--	1.062	--
Flash point, °C	320+	*min.* 220	320+	*min.* 220
Solubility, %	99.3	*min.* 99%	99.2	*min.* 99%
Kinematic Viscosity, cSt	303.0	*min.* 250	485.7	*min.* 350
Absolute Viscosity, Poise	1080	800-1200	3380	2400-3600

Table 3.8: Formulations of asphalt emulsion

Parameter	Emulsion ID				
	E1	**E2**	**E3**	**E4**	**E5**
Temperature of asphalt, °C	140	140	140	145	145
Temperature of soap solution, °C	50	50	50	50	50
Binder grade	VG-10	VG-10	VG-10	VG-30	VG-30
Weight of binder, gm	620	620	620	620	620
Weight of kerosene, gm	0	0	0	8	8
Weight of bitumen additive, gm	3.1	3.1	3.1	3.1	3.1
Weight of emulsifier, gm	15	20	25	15	15
Weight of Latex, gm	35	35	35	35*	35*
Weight of HCl, gm	to pH 2	to pH 2	to pH 2	to pH 2	to pH 2
Weight of water, gm	330	330	330	330	330

* *Post-addition of latex*

After the formulation was fixed, the production of asphalt emulsion using a colloid mill (**Figure 3.3a**) involves the following steps:

- Preparation of rinse and soap solution
- Running colloid mill to produce the emulsion
- Curing of emulsion
- Cleaning of colloid mill

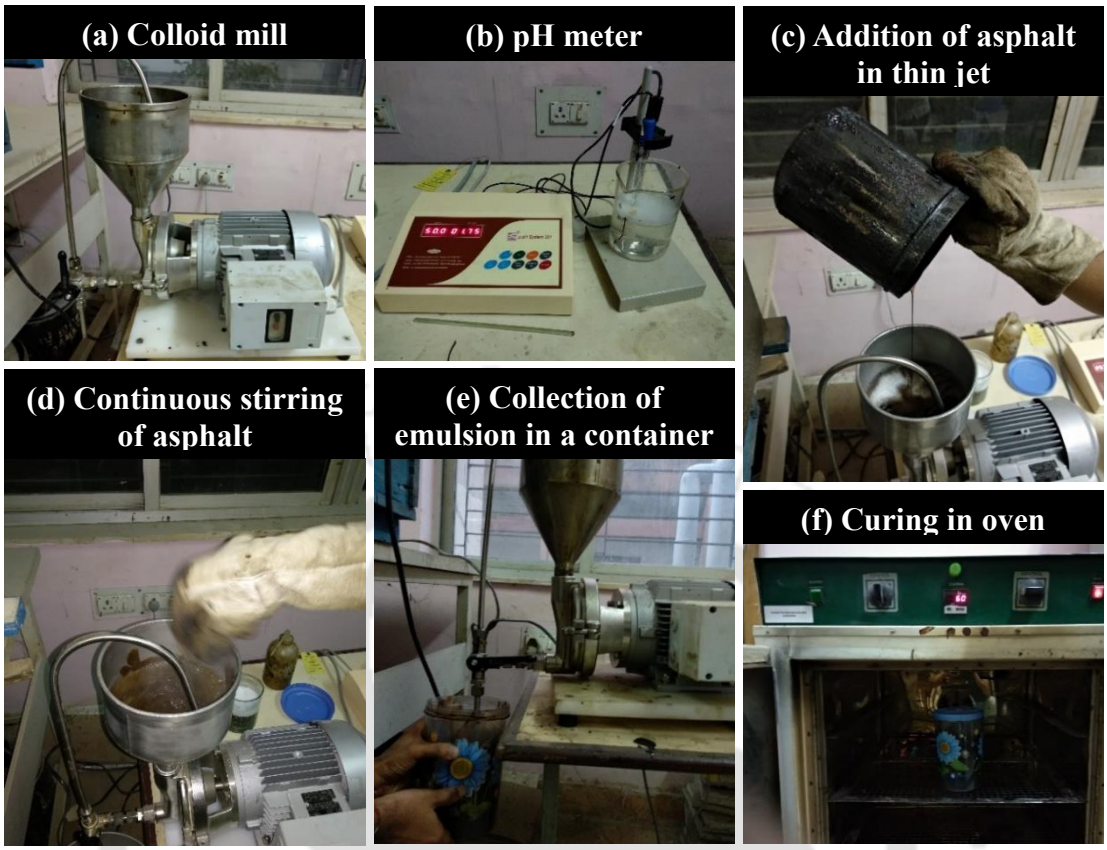

Figure 3.3: Production of emulsion in the laboratory using a colloid mill

Preparation of rinse solution

Rinse solution was prepared using emulsifier, acid and water in the proportion mentioned in **Table 3.8**. Initially, the desired amount of water at 60°C was poured into a 1000 ml glass beaker. Emulsifier was added and mixed thoroughly. Once the emulsifier completely dissolves in water, the pH of the solution was determined using a pH meter (**Figure 3.3b**). Then, the desired quantity of HCl obtained using the trial and error method was added to the solution to bring the pH to 2.

Preparation of soap solution

Soap solution was prepared using emulsifier, latex (if required), acid and water in the proportion mentioned in **Table 3.8**. Initially, the desired amount of water at 60°C was poured into a 1000 ml glass beaker. Emulsifier was added and mixed thoroughly. Latex was added to the beaker for emulsion E1, E2 and E3 only. Once the solution was homogeneous, the pH of the solution was determined using a pH meter. The desired quantity of HCl was added to the solution to bring the pH to 2.

Running colloid mill to produce the emulsion

Initially, hot water was poured into the colloid mill, and the mill was run in switch on mode for conditioning of the mill. Then, rinse solution was poured into the mill and run to reduce the influence of water on the pH during emulsion production. After that, the rinse solution was removed, and soap solution was poured into the colloid mill. Additive was added to the asphalt and mixed thoroughly. If required, kerosene was added to asphalt just before pouring it in the colloid mill having soap solution. Next, asphalt at the desired temperature was poured into the colloid mill in an even jet within 1 min (**Figure 3.3c**). The asphalt emulsion was continuously stirred (**Figure 3.3d**) and circulated for less than 1.5 min. The valve was opened, and the prepared asphalt emulsion was collected in a container (**Figure 3.3d**). Special attention was paid to turning off the mill before the entire emulsion was taken out to avoid choking the mill.

Curing of the emulsion

For curing of emulsion, the prepared emulsion was placed in an oven overnight at 60°C (**Figure 3.3e**). After the curing period, the emulsion was subsequently cooled down at room temperature for at least 2 hours before testing. Since latex addition in soap solution was not feasible for emulsions E4 and E5, addition of latex was carried out on the produced emulsion at a later stage.

Cleaning of the colloid mill

The cleaning of the colloid mill was carried out using rinse solution and hot water. First, rinse solution was poured into the colloid mill, allowed to run for 1 minute and then exit through the valve. Then, hot water was poured into the mill, and the water was allowed to exit through the valve slowly. The addition of water was continued until clear water comes out of the mill.

3.3.2.2 Characterization of asphalt emulsion

The physical properties of asphalt emulsion used for the study were tested according to American Standards to conform to the specifications laid down in ISSA guidelines. The physical properties of the emulsion and residual asphalt for the different formulations (**Table 3.8**) are shown in **Table 3.9**. Here, the different formulations were associated with different emulsifier dosages (1.5%, 2% and 2.5%), asphalt type (VG-10 and VG-30) and solvent (with and without solvent).

Results in **Table 3.9** for emulsions E1, E2 and E3 showed that all the physical properties satisfy the specification limits laid down by ISSA (ISSA A143, 2010). In addition, variation in properties of both asphalt emulsion and its residue was minimal. Therefore, it could be said that the physical properties of asphalt emulsion do not vary substantially within the recommended range (as per the manufacturer's recommendation) of emulsifier dosage.

In addition, it could be observed from **Table 3.9** that the asphalt emulsion properties did not change substantially with asphalt type (E1 and E4). However, the difference in properties of asphalt emulsion residue of E1 and E4 was noticed with different asphalt types. Higher softening point and lower penetration values for emulsion E4 prove the hypothesis that the stiffness of asphalt emulsion residue increases by replacing softer grade binder with harder grade binder for asphalt emulsion production.

Table 3.9: Physical properties of asphalt emulsion and asphalt emulsion residue

Emulsion Component	Results					Specified Limits
	E1	E2	E3	E4	E5	
Test on emulsion						
Viscosity (SFS)	39	32	37	39.5	45	20-100
Particle Charge	+ve	+ve	+ve	+ve	+ve	Positive
Sieve test, %	0.01	0.00	0.02	0.15	0.02	0.1% *max*
Storage stability, 24h, %	0.3	0.5	0.5	2.3	0.3	1% *max*
Residue, %	65	64.4	64.6	65.1	65.0	62% *min*
Test on emulsion residue						
Ductility, 25°C, cm	>100	>100	>100	> 100	> 100	40 cm *min*
Softening Point, °C	61	58	60	65.5	65	57°C *min*
Penetration (25°C), 0.1 mm	54	56	55	43	45	40-90

Note: *+ve denotes positive*

3.4 Performance testing

3.4.1 Mix Time

In this test, 100 gm of dried aggregate was mixed with the desirable amount of mineral filler and water until uniform distribution. Emulsion was added and mixed thoroughly. The time at which the mix breaks was noted as mixing time (ISSA TB No. 113, 2017).

3.4.2 Consistency Test

Consistency test was conducted as per ISSA guidelines (ISSA TB No. 106, 2015). In this test, a cone of height 75 mm and diameter of 40 mm at top and 90 mm at bottom, respectively, was placed on a concentric flow scale (**Figure 3.4**). Specimen was prepared similar to the mix time test and the homogeneous mix was poured into the cone. The excess material was struck off and the cone was immediately removed with a smooth vertical motion. The specimen was allowed to flow freely. The outflow was then measured at 4 points 90° apart. The average of the four values was termed as the consistency value. A typical case is shown in **Figure 3.4**.

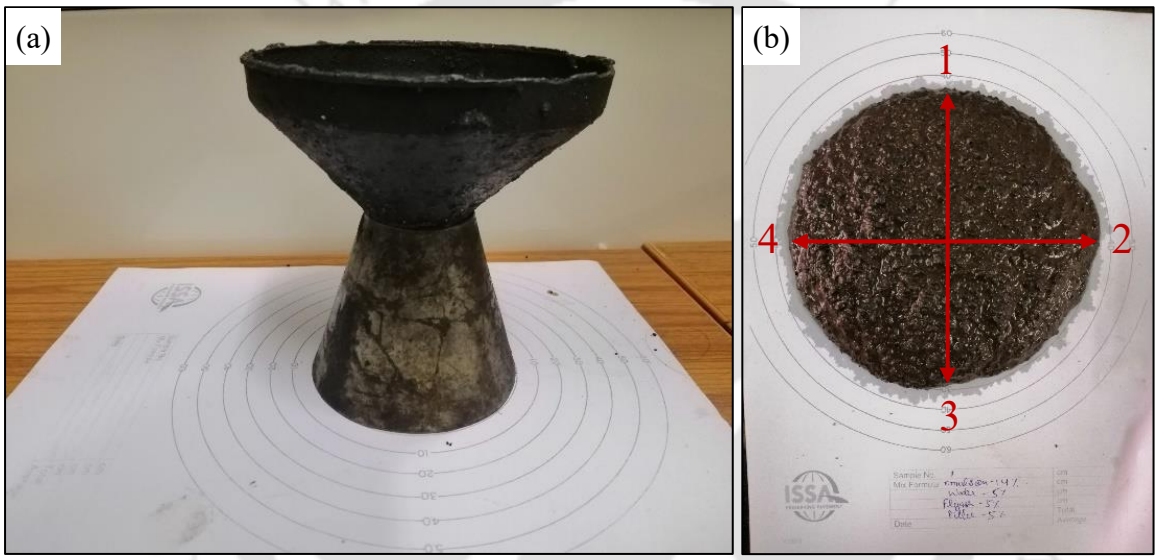

Figure 3.4: Consistency: (a) testing set-up and (b) tested specimen

3.4.3 Cohesion Test

Cohesion test was performed as per ISSA guidelines (ISSA TB No. 139, 2017). In this test, dried aggregates were screened through a 4.75 mm sieve. Then, the mix was prepared as per the mix time test procedure with 200 gm dried aggregate. After mixing for 30 seconds, the specimen was poured onto the 6 mm ring mold. The excess material was trimmed off. Ring mold was removed after the specimen attained sufficient stability to resist flow. The specimen was then kept for air curing at room temperature for desired amount of time. Subsequently, the specimen was placed in the cohesion testing machine and centered under the neoprene foot. The air pressure was set at 200 kPa. The neoprene foot was lowered and allowed to stay in contact with the specimen for 5-6 sec. For testing, the specimen substrate was held with one hand while the other

hand was used for rotating torque meter through an arc of 90-120° within 0.5 to 0.7 seconds. The torque reading and rupture mode were noted. The test setup, along with untested and tested specimens, is shown in **Figure 3.5**.

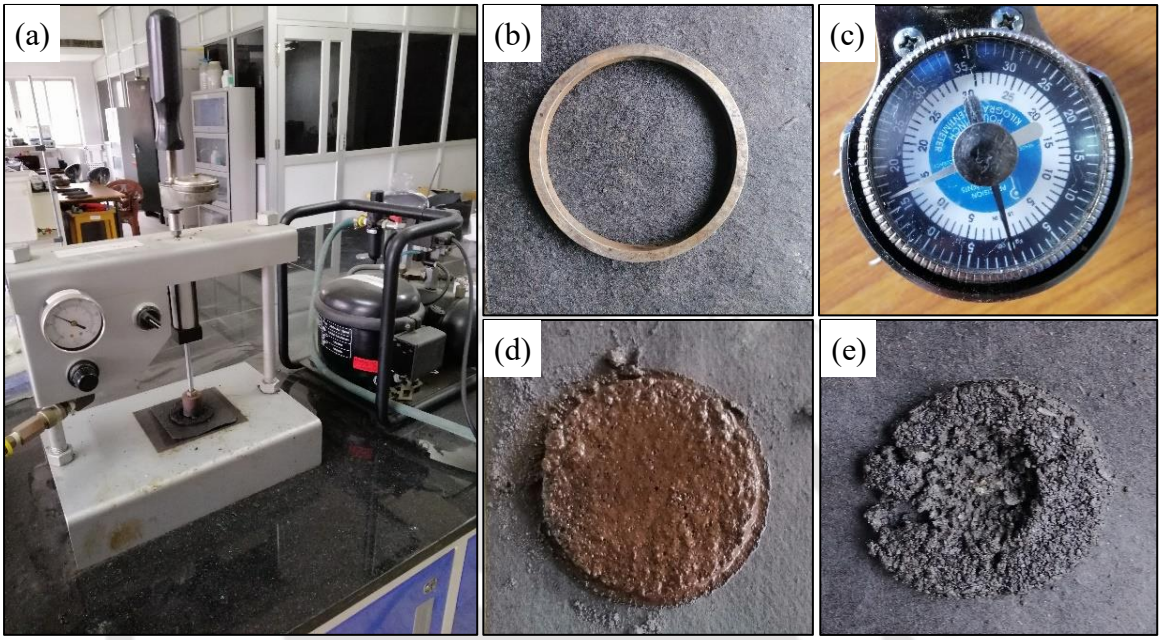

Figure 3.5: Cohesion test: (a) test set-up; (b) ring mould; (c) torque meter; (d) untested specimen; and (e) tested specimen

3.4.4 Wet Track Abrasion Test (WTAT)

WTAT was conducted as per ISSA guidelines (ISSA TB No. 100, 2017). In WTAT, the specimens were prepared by adding water and mineral filler to 800 gm of dry aggregates. The emulsion was added and the mix was stirred for 30 seconds. The mix was poured onto the aluminium plate with a specimen mold on top. After the specimen achieved the initial setting, the mold was removed, and the specimens were allowed to cure in the air for 2-3 hours at room temperature. Next, specimens were cured in an oven for 24 hours at 60°C ± 3°C. The cured specimens were allowed to cool down to room temperature for 2 hours.

For testing, cured specimens were kept in the water bath at 25°C ± 3°C for 60-75 min for raveling test or 6 days for moisture damage assessment. Subsequently, the specimens were kept in WTAT machine and turned on for testing. The machine was allowed to run for 315 ± 2 sec where the rubber hose abraded the specimen. The loose debris was then washed off from the abraded specimen. The change in weight of the

specimen due to abrasion was noted down and the abrasion loss was calculated using **Equation 3.1**.

$$Abrasion\ loss = (W_{a,WTAT} - W_{b,WTAT}) \times LCF_{WTAT} \quad (3.1)$$

where $W_{a,WTAT}$ = Initial weight of cured specimen, gm; $W_{b,WTAT}$ = Weight of specimen after abrasion, gm; and LCF_{WTAT} = Loss correction factor (32.9 g/m^2). The test setup, along with untested and tested specimens, is shown in **Figure 3.6**.

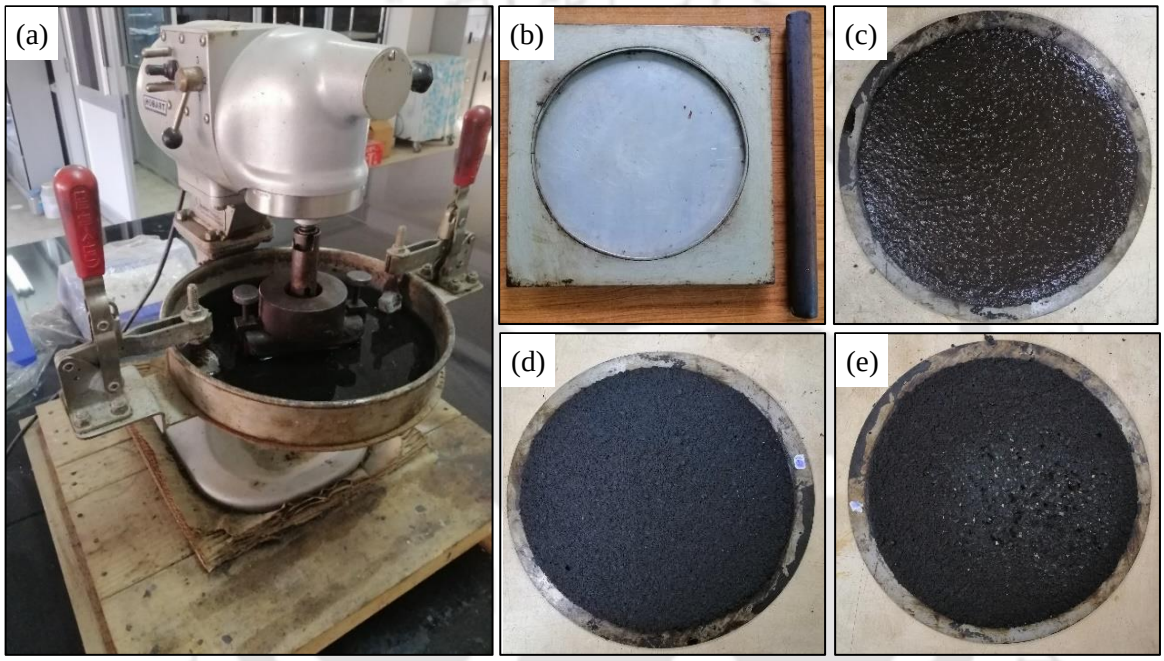

Figure 3.6: Wet track abrasion test: (a) test set-up; (b) specimen preparation set-up; (c) specimen after casting; (d) cured specimen; and (e) tested specimen

3.4.5 Loaded Wheel Test (LWT)

LWT was carried out as per ISSA guidelines (ISSA TB No. 109, 2005; ISSA TB No. 147, 2005). In LWT, the mix was casted in a mold to get specimen dimensions of 381 mm × 50.8 mm with a height of 12.7 mm. After casting, the specimen was air-cured at room temperature for 24 hours followed by oven-curing at 60°C for 18-24 hours. The cured specimen was then cooled to room temperature for 2 hours and mounted on the testing machine. In the test, 56.7 kg load was applied, and the specimen was compacted at the rate of 44 cycles/minute for 1000 cycles. The change in width was noted down to assess the lateral displacement using **Equation 3.2**. The specimens were then mounted on the testing machine, and a sand frame was centered over the specimen. Then, 300

gm heated (82.2°C) sand of size range 0.15 mm to 0.6 mm was uniformly spread on the specimen and compaction was immediately started for 100 cycles. The sand adhesion was determined using **Equation 3.3**.

$$Lateral\ Displacement = \frac{(W_{b,LWT} - W_{a,LWT})}{W_{a,LWT}} \times 100 \quad (3.2)$$

$$Sand\ adhered = (W_{d,LWT} - W_{c,LWT}) \times LCF_{LWT} \quad (3.3)$$

where $W_{a,LWT}$ = Initial width of the specimen, mm; $W_{b,LWT}$ = Width of the specimen after 1000 cycles of loading, mm; $W_{c,LWT}$, $W_{d,LWT}$ = Weight of specimen before and after sand adhesion. The correction factor (LCF_{LWT}) for LWT can be determined using the area that the sand adheres. The test setup along with untested and tested specimens are shown in **Figure 3.7**.

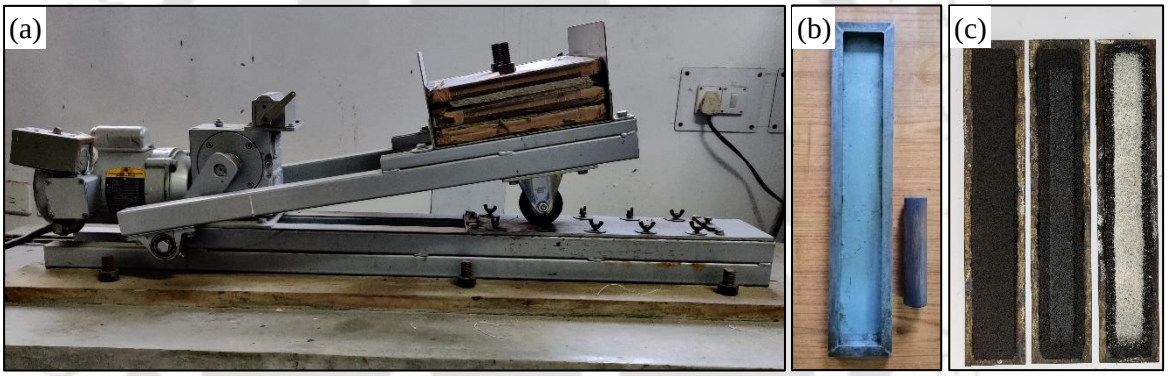

Figure 3.7: Loaded wheel test: (a) test set-up; (b) mould and wooden rod; (c) untested, tested specimen, and specimen after sand adhesion (from left to right)

3.4.6 Schulze Breuer and Ruck Test

The Schulze Breuer and Ruck test (SBRT) was used to determine the compatibility of aggregate fines with emulsion residue (ISSA TB No. 115, 2005). The Schulze Breuer and Ruck test setup is illustrated in **Figure 3.8**. In this test, 200 gm of dry aggregate (including mineral filler) was mixed with the desired amount of water until the aggregates get uniformly wet. Then, emulsion equivalent to 8.125 % asphalt residue was added, and the mix was stirred until it breaks. The broken mix was allowed to air cure for 1 hour followed by oven curing in a forced draft oven at 60°C for 18 hours. Immediately after oven curing, 40 gm of the mix was crumbled and placed in a pre-heated mold for compaction. The pressure of 200 kPa was applied and maintained for

1 minute. Subsequently, the specimen was extracted from the mold and allowed to cool at room temperature. The specimens were then tested for absorption, abrasion, and integrity.

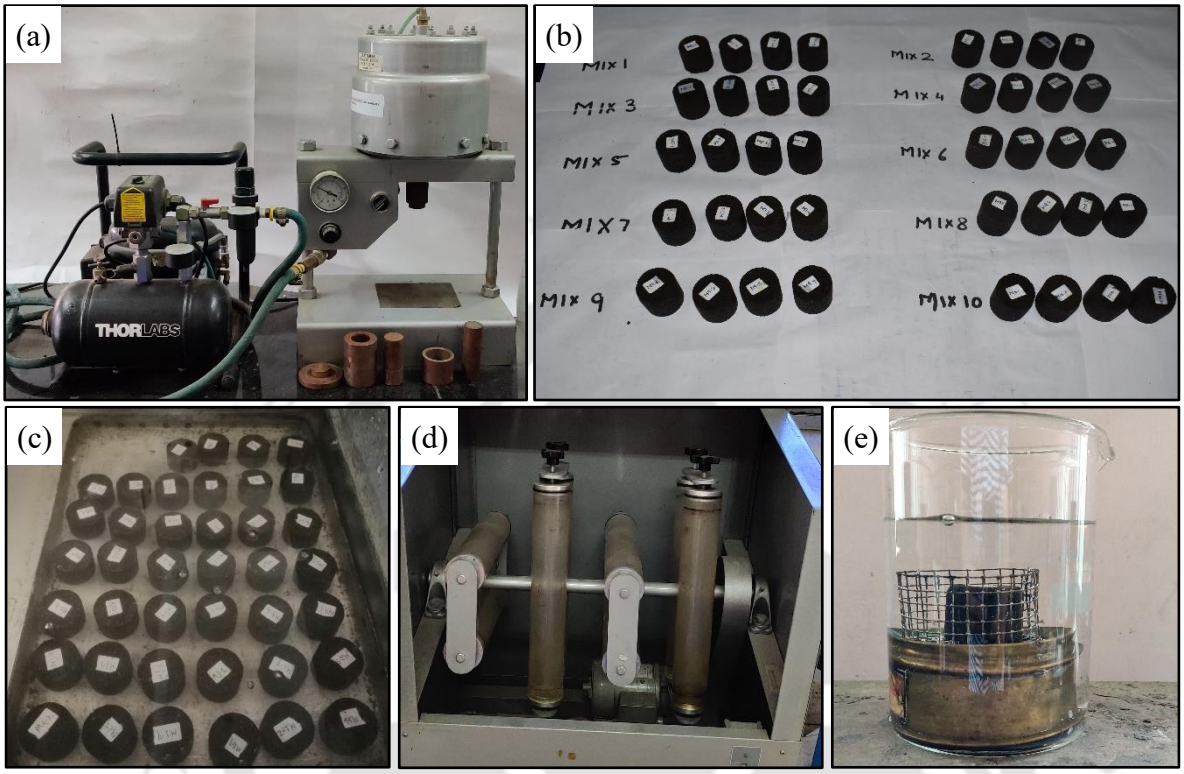

Figure 3.8: Schulze Breuer and Ruck test: (a) specimen production set-up; (b) untested specimens; (c) absorption test; (d) abrasion test; and (e) integrity test

Absorption

The specimens prepared were weighed ($W_{a,SBRT}$) and placed in a water bath at 25°C ± 3°C for six days. After soaking, the specimens were removed, surface-dried, and weighed ($W_{b,SBRT}$). The percent absorption was then evaluated using **Equation 3.4**.

$$\%\ Absorption = \frac{W_{b,SBRT} - W_{a,SBRT}}{W_{a,SBRT}} \times 100 \qquad (3.4)$$

Abrasion

After determining % absorption, the specimens were placed in a separate shuttle cylinder filled with 750ml ± 25ml water at 25°C ± 3°C. The cylinders having the specimens were closed and placed in the abrasion machine. Subsequently, the abrasion

machine was rotated for 3600 cycles at 20 RPM. After the completion of 3600 cycles, the specimen was removed from the abrasion machine, surface dried, and weighed ($W_{c,SBRT}$). The abrasion loss (in grams) was determined using **Equation 3.5**.

$$Abrasion\ Loss = W_{b,SBRT} - W_{c,SBRT} \quad (3.5)$$

Integrity

The abraded specimen was subjected to boiling water for 30 minutes to assess the specimen's integrity. It was ensured that a cover of 6.35 mm was provided above and below the specimen. The integrity weight was recorded by surface drying the largest remaining piece after boiling the specimen and noting down its weight ($W_{d,SBRT}$). The percentage integrity was calculated using **Equation 3.6**.

$$Integrity, \%\ retained = \frac{W_{d,SBRT}}{W_{b,SBRT}} \times 100 \quad (3.6)$$

3.4.7 Boiling water test

The boiling water test was used to demarcate the adhesion characteristics of the microsurfacing mix with different mineral filler types and dosages (ISSA TB No. 149, 2005). The test set-up for the boiling water test is illustrated in **Figure 3.9**. In this test, 150 gm dry aggregates passing 4.75 mm sieve along with mineral filler were batched according to gradation. Water was added and mixed until the mix gets homogeneously wet. The emulsion was added to the mix and stirred for 30 seconds. Immediately, the mix was poured onto an aluminum foil having a template placed over it. The template's length, width, and height were 88.9 mm, 114.3 mm, and 6.35 mm, respectively. The mix was allowed to air cure for 24 hours at room temperature.

After the curing period, excess aluminum foil was removed, and the air-cured specimen was placed in boiling water for 10 minutes. While placing the specimen in boiling water, care was taken to ensure that the mix was 12.7 mm above the bottom of the glass beaker to avoid direct contact between the specimen and heat source. After 10 minutes, excess water was removed, and the mix was placed on a level surface . The mix was allowed to dry in air overnight and subjected to stripping evaluation using Asphalt Compaibility Tester (ACT).

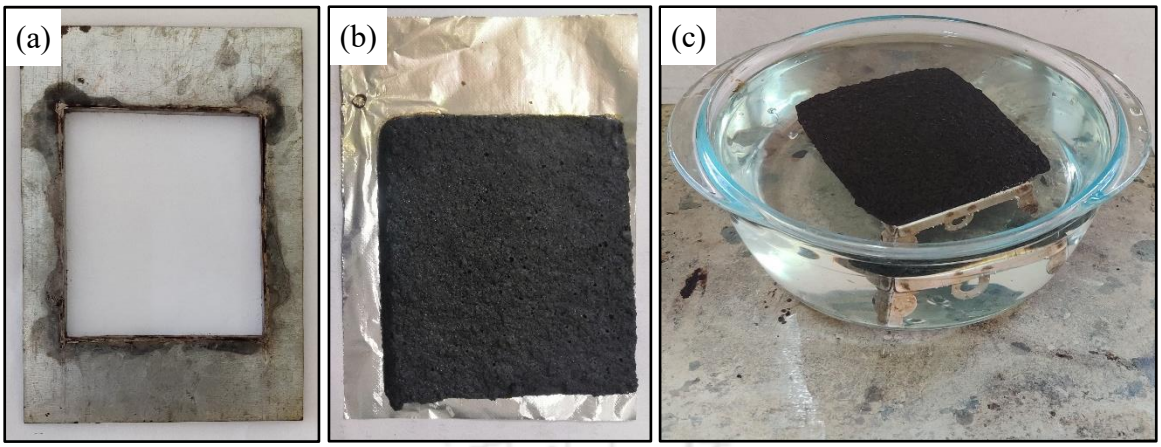

Figure 3.9: Boiling water test: (a) template for specimen preparation; (b) untested specimen; (c) test set-up

3.4.7.1 Stripping evaluation: Asphalt compatibility tester

After completing the boiling water test, a photo-detection technique using ACT was explored instead of visual inspection to characterize the moisture susceptibility and adhesive properties of asphalt mixtures (InstroTek, Inc., 2019). ACT equipment consists of a control box, sensor, standard felt, stand, testing tray, sample, and pan, as shown in **Figure 3.10**. ACT was used in conjunction with boiling water test to quantify the stripping potential of asphalt mixtures in terms of change in color of the mixture. It uses a photodetector to measure reflected light, and the percentage loss in reflected light was evaluated. The percentage loss was then used to demarcate the stripping potential of different asphalt mixtures.

Calibration of ACT equipment

Initially, the ACT equipment had to be calibrated for each aggregate source because there would be a variation in calibration for different aggregate sources as brighter aggregates reflect more light. For calibration, three different counts, i.e., fully coated sample (0% loss), saturated surface dry aggregate (100% loss) and standard felt, were measured for the aggregate source. Then, using this information, a linear relationship was calculated for percentage (%) loss and counts. The respective calibration factors obtained from the linear relationships were used for further evaluation.

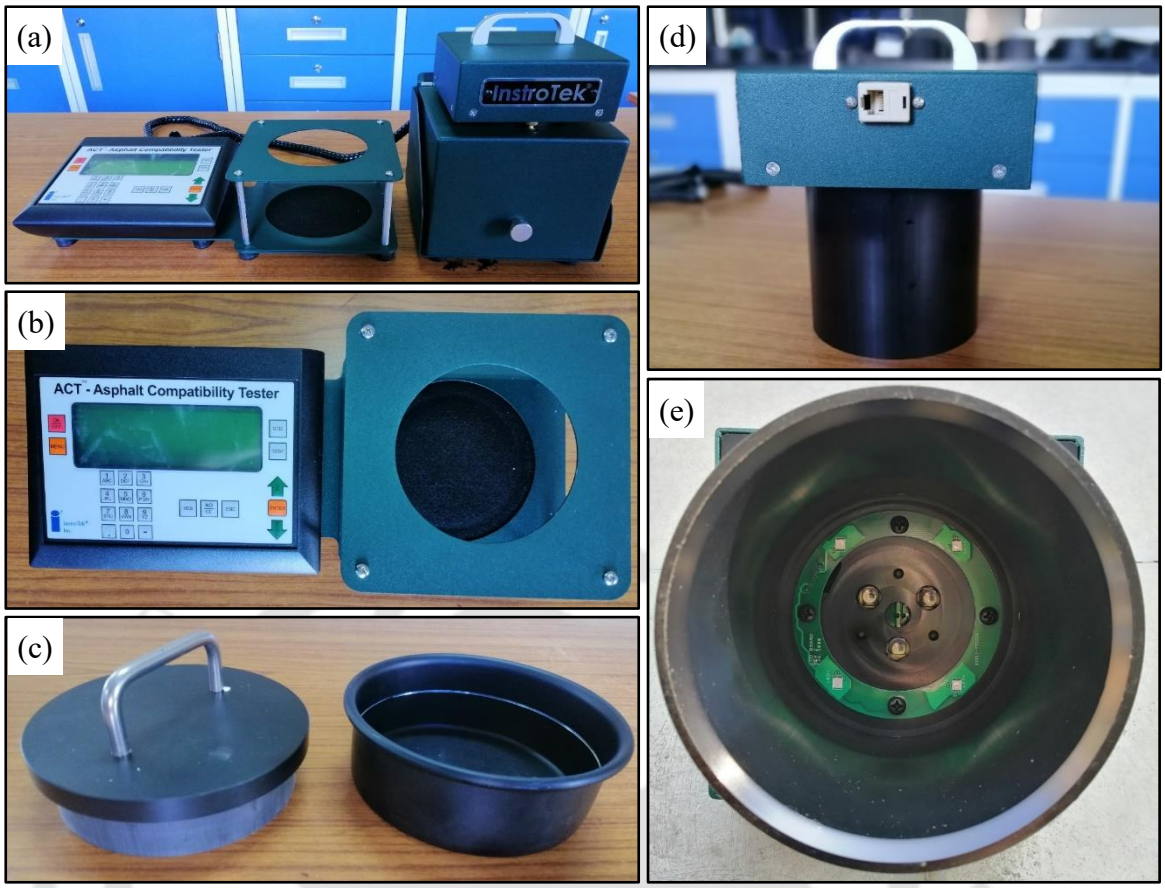

Figure 3.10: Asphalt compatibility tester: (a) complete set-up; (b) controller and standard felt; (c) tamper and pan; (d) sensor; and (e) photo detectors in sensor

Evaluation of Loss Index

After the calibration process, the loose mix after subjecting to boiling water test were dried using a heat gun. The boiled mix was spread in a tray and the hot air was allowed to blow from a height of 30 cm. The mix was stirred at regular intervals for exposing the damp aggregate surface to hot air until the mixture gets surface dry uniformly. The dried mix was then placed in the sample pan and stirred using a spoon to ensure that the mix was not segregated. The mix was then compressed using a tamper to smoothen the surface. It is important to note that the mix should not be shaken vigorously or grinded while compressing. This might lead to the binder getting removed from the aggregate surface due to the shear force applied, or the coarse aggregates coming on top, producing unreliable results. Then, the prepared specimen was kept in the testing tray, and a sensor was placed over the specimen. The test was initiated using the controller, during which the intensity of light reflected by the mix was quantified by photodetectors in sensors. The results were then described in terms of the Loss Index.

3.5 Summary

In this chapter, a brief summary of the experimental methodology adopted was discussed. Subsequently, a detailed discussion on material selection and characterization was conducted. The physical properties of aggregates, mineral filler and asphalt emulsion was evaluated and compared with the specified limits of ISSA. Finally, the procedure followed for different performance tests conducted in the study were described in detail.

In addition, to demonstrate the repeatability of the test results, **Table 3.10** describes the summary of replicates considered in the study. Coefficient of variation (CoV) observed is also included. An average CoV of less than 10% highlights that the results were repeatable and the number of replicates considered for each test were acceptable.

Table 3.10: Summary of replicates and repeatability of different tests considered

Parameters	Replicates	Average coefficient of variation, %
Mix design		
Mix time	3	9.0
Cohesion	3	4.8
Raveling	3	7.8
Rutting	3	7.0
Compatibility	4	2.7
Adhesion	3	5.3
Production parameters		
Workability	4	6.2
Strength	4	3.4
Raveling	4	8.6
Rutting	4	9.5
Bleeding	4	8.5
Aging and moisture damage		
Raveling	4	7.9

CHAPTER 4

Effect of Material Properties on Mix Design

4.1 Introduction

The composition of microsurfacing mix were finalized during mix design to optimize mix performance. It is a complex process due to the inclusion of multiple components and nature of the curing process. Understanding the role of each component is vital to address issues faced during mix design. In this regard, this chapter discusses the effect of material properties on microsurfacing mix design. The materials investigated includes filler (aggregates passing 75 μm sieve) type, mineral filler type (cement and flyash) and dosage, emulsifier dosage, asphalt type and solvent. The performance was quantified in terms of cohesion, raveling and rutting. Then, mix characteristics (compatibility, cohesion and adhesion) and performance (raveling and rutting) was optimized by varying type and dosage of mineral filler. Finally, the optimum emulsion content was assigned using a narrow range diagram considering all the design parameters.

4.2 Methodology

The experimental methodology adopted is illustrated in the form of a flow chart in **Figure 4.1**. Initially, it was observed that the emulsion was breaking rapidly after its addition to aggregates. The material passing 75 μm sieve contribute substantially to the reactivity of emulsion due to larger surface area. Hence, the filler of the Source A aggregate was replaced by the filler of the Source B (refer **Section 3.3.1** for details).

Next, mineral filler types (OPC and FA) and dosages (0% to 3%) were added to the mix to address insufficient strength development. Cohesion test was used as a parameter to demarcate the strength developed among different mixes. After that, different emulsifier dosages were used to produce emulsion to ensure stability of emulsion and mix. Three emulsifier dosages, i.e., 1.5%, 2.0% and 2.5%, were selected. The performance was assessed in terms of cohesion, raveling and rutting.

In order to address the issue of inadequate rutting resistance, a harder asphalt grade, VG-30, was used in place of a softer asphalt grade, VG-10. During emulsion

production, solvent was added to the asphalt just before pouring it into the colloid mill to improve the storage stability of emulsion produced with VG-30. The addition of solvent reduces the viscosity of asphalt. When the asphalt having lower viscosity is used for production of emulsion, the particle size distribution of asphalt particles is finer. As a result, slower rate of coalescence is observed. Performance parameters included cohesion, raveling and rutting.

Before finalizing the mix design, the effect of mineral filler type and dosages on the mix characteristics and performance was investigated. The mix characteristics and performance includes the following:

- Mix characteristics
  - Compatibility – Schulze Breuer and Ruck test;
  - Strength – Cohesion test (15, 30, 45, 60, 90, 120, 180, and 240 minutes);
  - Adhesion – Boiling water test.
- Performance
  - Raveling – WTAT;
  - Rutting – LWT.

The purpose behind the investigation of cohesion at different curing times was to understand the rate of strength development with different combinations of mineral filler types and dosages. The maximum curing time of 240 minutes was selected based on the recommendation of the IRC to ensure that a stable torque reading is achieved (IRC: SP: 81, 2008). In general, a compatible mix with better cohesion and adhesion is likely to perform better during service life. Subsequently, the performance was correlated with mix characteristics. The combination exhibiting superior mix characteristics and performance was determined and subjected to further investigation for obtaining the job mix formula.

Mix design was conducted using emulsion components and mineral filler dosages that provides superior performance as per ISSA guidelines (ISSA A143, 2010). A narrow range diagram was used to determine the OEC. The tests included in narrow range diagram are cohesion (30 and 60-min), WTAT (1 hr and 6 days soaked), LWT, and sand adhesion. The experimental matrix for assessing the effect of material properties is described in **Table 4.1**.

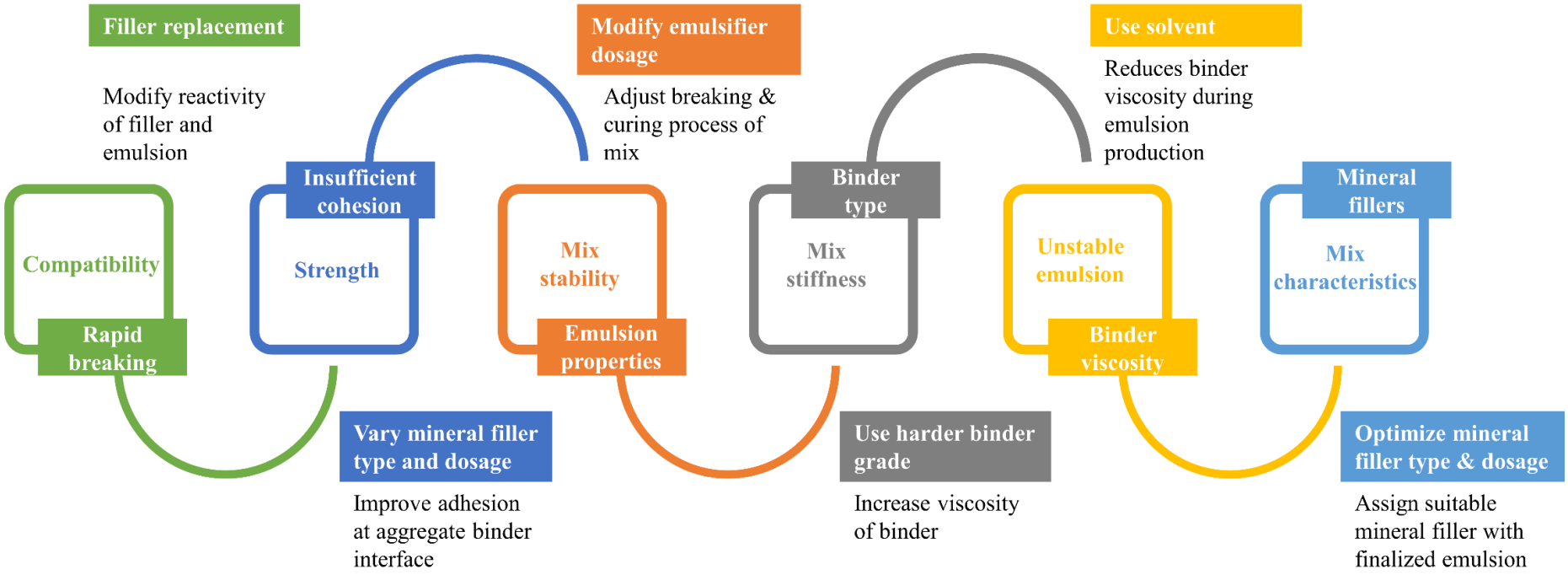

Figure 4.1: Methodology for systematically addressing challenges in mix design

Table 4.1: Experimental matrix for assessing the effect of material properties

Parameter	Combinations	No. of tests	No. of specimens*
Replacement of filler	6	1	18
Mineral filler type and dosage	7	2	42
Emulsifier dosage	3	4	36
Asphalt type and solvent	3	4	36
Optimizing mineral fillers	10	14	390**
Mix design	4	6	72

** Number of replicates for each test = 3*

*** For 2 tests (raveling and rutting), only 5 selected combinations were tested.*

4.3 Trial formulation

Initially, mix time test was conducted on the trial formulation, i.e., the ratio of dry aggregate: water: emulsion: cement was 100:5:14:1. Subsequently, the water content was increased to achieve a mixing time of a minimum of 120 seconds. It was observed that even with a water content of 20%, rapid breaking was observed, due to which the mix could not be produced. The rapid breaking could be attributed to one or a combination of reasons listed below (MS-19, 2008).

a) Emulsifier chemistry
b) Insufficient emulsifier dosage
c) pH of soap solution
d) Filler-emulsion compatibility

4.3.1 Importance of filler characteristics

In a microsurfacing mix, fillers contribute significantly to the breaking and curing process due to their large surface area. To mitigate the problem associated with premature breaking, the old filler (Filler A with 45% SiO_2) was replaced with a new filler (Filler B with 39% CaO). The physical properties (**Table 3.4**) and mineralogical composition (**Table 3.5**) of both the fillers were assessed to understand the influence of filler characteristics on the breaking process. As discussed in **Section 3.3.1**, the physical properties and mineralogical composition analysis showed that the mixes produced with aggregates having Filler A should have relatively lower mixing time

than mixes produced with aggregates having Filler B (Abo-Qudais & Al-Shweily, 2007; Robati *et al.*, 2015a).

After examining the physical properties and mineralogical composition, a mix time test was conducted on the mixes produced with Filler A and Filler B. Based on the total surface area of aggregates calculations, trail emulsion content of 14% was selected. Water content was varied from 5% to 20% by weight of dry aggregate for Filler A. Then, Filler A was replaced by Filler B and the mix time was investigated at water content of 5% and 7%. Results of mix time test with both fillers is illustrated in **Figure 4.2**. Error bars refer to ± standard deviation. The repeatability of the test results was investigated in terms of coefficient of variation (CoV). For the 6 combinations tested (with 3 replicates), the CoV varied from 7.4-10.8%, with the average CoV being 9%.

It was observed that the mixing time increased to 160 seconds even with emulsion and water content of 14% and 7%, respectively, by replacing the filler. Improvement in mix time indicates that filler plays a major role in the breaking process of microsurfacing mix. Therefore, for subsequent testing, filler with lower MBV (Filler B) was included in the gradation to replace the filler initially adopted in the study (Filler A).

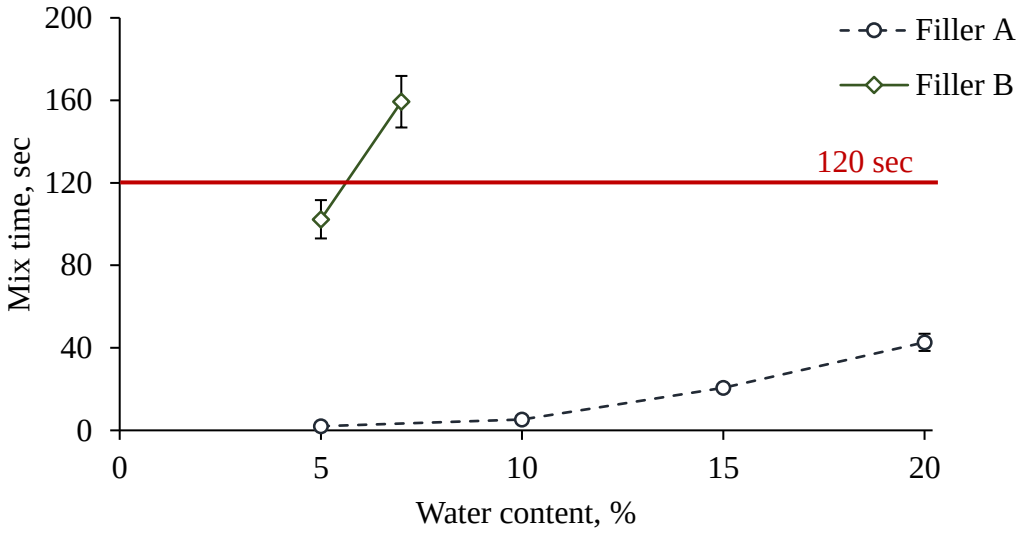

Figure 4.2: Variation of mix time with water content and filler type

4.4 Effect of mineral filler

Cement is used in microsurfacing as a mineral filler. However, in this study, to enhance sustainability, fly ash was also incorporated along with cement. In order to assess the

effect of mineral filler in the microsurfacing mix, cohesion was evaluated for 30-min and 60-min (ISSA TB No. 139, 2017). The formulations are presented in **Table 4.2**.

Table 4.2: Mineral filler combinations assessed at trial formulation

Filler type	% by weight of dry aggregate weight						
	Mix 1	Mix 2	Mix 3	Mix 4	Mix 5	Mix 6	Mix 7
Stone-dust	10	9	8	7	7	7	7
Fly ash	0	0	0	0	1	2	3
Cement	0	1	2	3	2	1	0

The cohesion test results and specification limits (ISSA A143, 2010) are illustrated in **Figure 4.3**. Error bars refer to ± standard deviation. The repeatability of the test results was investigated in terms of CoV. For the 7 combinations tested (with 3 replicates) for 30-min and 60-min cohesion, the CoV varied from 2.0-7.2%, with the average CoV being 4.7%. It could be observed from **Figure 4.3** that all the mixes passed the specification limit for 30-min cohesion. But, Mix 1 and Mix 7 could not meet the 60-min cohesion requirement. The higher cohesion for mixes with OPC could be attributed to the hydration products formed by the reaction of OPC with the water phase of the emulsion (García *et al.*, 2013; Yang *et al.*, 2019; Fooladi & Hesami, 2021).

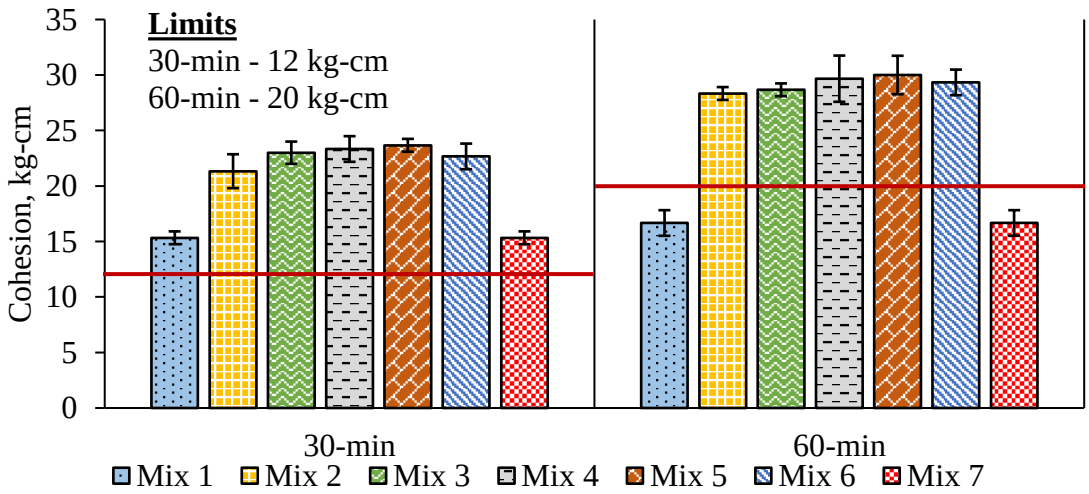

Figure 4.3: Influence of mineral filler on the cohesion of microsurfacing

Mixes with both cement (2%) and fly ash (1%) as mineral filler had the highest cohesion. The mechanism behind higher cohesion was divided into two phases. Firstly, the cement hydration forms calcium silicate hydrate (C-S-H) and calcium hydroxide (CaOH). Secondly, the CaOH reacts with the silica present in the fly ash to again produce C-S-H. This reaction leads to the higher production of the cementitious product (C-S-H), and the adhesion improves (American Coal Ash Association, 2003).

Statistical analysis of the observed means was conducted using Tukey's *post-hoc* multiple comparisons using SPSS software. The significance level was 5%, and the mixes were grouped according to test results. Some of the key points associated with Tukey's *post-hoc* multiple comparisons include the following:

- Groups were assigned such that the difference between the means of the observations in a group was statistically significant than the observed means of other groups.
- Group number 1 represented the best performing mix, and subsequent numbering denoted relatively inferior performance.
- Numbering 1/2 implied that the mean of the observations for that mix was not significantly different from observed means of group 1 and 2.

Results of the statistical analysis are described in **Table 4.3**. It could be observed that the mixes with cement, i.e., Mix 2 to 6, were assigned group 1 whereas group 2 was assigned to Mix 1 and Mix 7 for both 30-min and 60-min. It shows that the cohesion of mixes with cement was significantly higher than the cohesion of mixes without cement.

Table 4.3: Grouping of mixes according to mineral filler

Mix type	Cohesion, kg-cm	
	30 min	60 min
Mix 1	2	2
Mix 2	1	1
Mix 3	1	1
Mix 4	1	1
Mix 5	1	1
Mix 6	1	1
Mix 7	2	2

4.5 Variation in emulsifier dosage

Emulsifier dosage was varied within the manufacturer's recommended range of 1.5-2.5% by weight of the emulsion. The physical properties for the emulsion prepared with three emulsifier dosages, i.e., 1.5% (E1), 2.0% (E2) and 2.5% (E3) were discussed in **Section 3.3.2.2**. Performance was assessed in terms of cohesion, raveling and rutting.

Results of the the influence of emulsifier dosage on performance is illustrated in **Figure 4.4**. Error bars refer to ± standard deviation. The repeatability of the test results was investigated in terms of CoV. For the 3 combinations tested (with 3 replicates) for cohesion, WTAT and LWT, the CoV varied from 2.4-11.4%, with the average CoV being 5.7%, 5.7% and 8.7%, respectively.

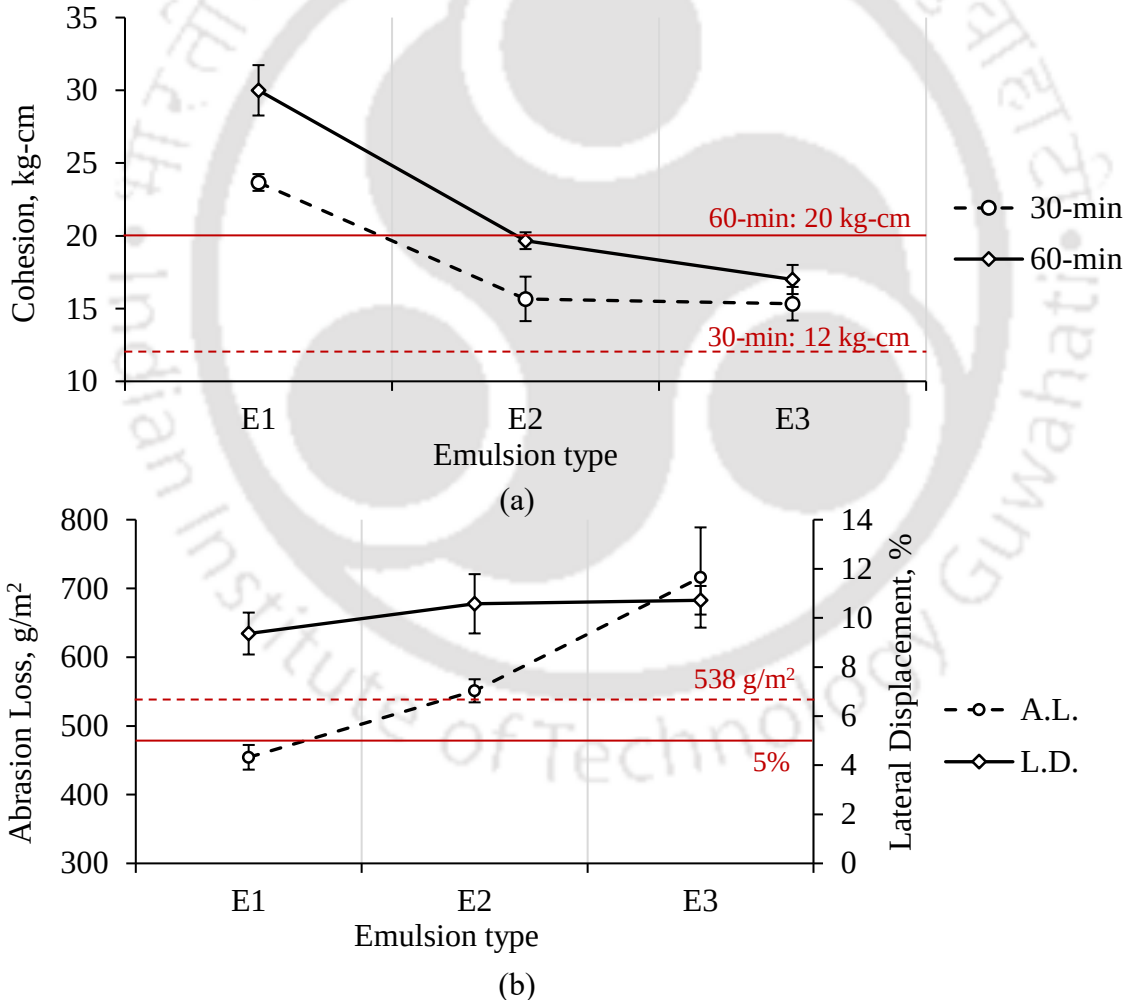

Figure 4.4: Effect of emulsifier dosage: (a) cohesion; and (b) raveling and rutting

Figure 4.4 shows that, in general, performance degrades with the increase in emulsifier dosage. The cohesion at 1.5% emulsifier dosage was 34% to 43% greater than cohesion at 2.0% and 2.5% emulsifier dosage, as shown in **Figure 4.4a**. Cohesion variation shows that higher emulsifier dosage hinders the curing process and delays strength development.

Figure 4.4b shows that the susceptibility of mix to raveling and rutting also increased with the increase in the emulsifier dosage. With respect to 1.5% emulsifier dosage, raveling increased by 21% and 58%, whereas rutting increased by 13% and 14% for 2% and 2.5% emulsifier dosage, respectively. The reason behind higher raveling and rutting could be due to the delay in the curing process and lower adhesion at the aggregate-binder interface caused by excessive emulsifier in the emulsion. When the emulsifier dosage is very high, the aggregate surface is covered by a bilayer of the excess emulsifier. It results in the aggregate surface being hydrophilic rather than hydrophobic. Due to the hydrophilic nature, asphalt particles cannot spread over the aggregate surface, and the adhesion at the aggregate-binder interface becomes substantially low (Ronald & Luis, 2016).

Statistical analysis of test results using Tukey's *post-hoc* multiple comparisons is presented in **Table 4.4**. The anlysis show that the cohesion at 1.5% emulsifier dosage was significantly higher than cohesion at 2.0% and 2.5% emulsifier dosages. Raveling at 2.5% emulsifier dosage was significantly higher than 1.5% and 2.0% emulsifier dosage. In contrast, variation in emulsifier dosage did not have a significant influence on rutting.

Table 4.4: Grouping of mixes according to emulsifier dosage

Mix type	Cohesion, kg-cm		Abrasion Loss	Lateral Displacement
	30-min	60-min		
E1	1	1	1	1
E2	2	2	1	1
E3	2	2	2	1

4.6 Influence of asphalt type and solvent

Cohesion and raveling were within the specified limits at 1.5% emulsifier dosage whereas rutting was more than the specified limit of 5%, as shown in **Figure 4.4**. One

way to rectify issues related to rutting is to increase the stiffness of the emulsion residue. For this purpose, laboratory investigations were conducted on emulsion prepared with harder asphalt grade (VG-30), i.e., emulsion E4.

Preparation of emulsion using colloid mill was difficult with VG-30 because of its higher viscosity. Baumgardner (2006) recommended that the outlet temperature of emulsion, calculated using **Equation 2.2**, should be less than 95°C. It was found that the maximum allowable temperature for emulsion exit temperature of 95°C was found to be 145°C. Hence, for production of emulsion E4, asphalt temperature was kept at 145°C. Since harder binder grade was used for emulsion production, it was found that the storage stability of emulsion exceeded the specification limit of 1% (**Table 3.9**). The higher storage stability, i.e., a faster coalescence rate, was primarily attributed to the high viscosity of asphalt during emulsion production.

Hence, to rectify this issue, there was a need to reduce the asphalt viscosity. For this purpose, kerosene was added in asphalt at the rate of 1% by weight of asphalt just before it was poured in the colloid mill. Baumgardner (2006) recommended that during emulsion production, the equiviscous temperature should be maintained, i.e., the viscosity of asphalt should be the same (200 cP) irrespective of asphalt type. It ensures that the asphalt particles in the emulsion have desirable particle size distribution. Thus, for production of emulsion E5, the kerosene content was selected such that the viscosity of asphalt at 145°C was 200 cP.

Latex could not be added to soap solution with the use of VG-30 as binder because of choking problems encountered during emulsion production. Hence, post-addition of latex at the rate of 3.5% by the total weight of emulsion was conducted for emulsion E4 and E5.

Results of the influence of asphalt type and solvent on performance is illustrated in **Figure 4.5**. Error bars refer to ± standard deviation. The repeatability of the test results was investigated in terms of CoV. For the 3 combinations tested (with 3 replicates) for cohesion, WTAT and LWT, the CoV varied from 0.7-15.0%, with the average CoV being 3.2%, 7.7% and 6.4%, respectively.

It could be observed from **Figure 4.5a** that the variation in cohesion was minimal with the difference in both asphalt type and solvent. Mixes produced with emulsion having VG-10 (emulsion E1) and VG-30 with solvent (emulsion E5) as binder had relatively

lower raveling than VG-30 without solvent (emulsion E4) as the binder, as shown in **Figure 4.5b**. In addition, replacing softer binder (E1) with harder binder (E4) reduced rutting by 36%. Moreover, with the addition of solvent in VG-30 asphalt (E5), rutting was reduced by another 39%. It could be said that harder binder grade improves the stiffness of the mix and, in turn, provides better rutting resistance. But, coarser particle size distribution of asphalt due to its higher viscosity during emulsion production deteriorates the performance of the mix (Hou *et al.*, 2018). Hence, it is vital to select proper asphalt binder grade for achieving desirable stiffness of the mix. For the selected asphalt binder, maintaining equiviscous temperature during emulsion production is critical for ensuring satisfactory performance.

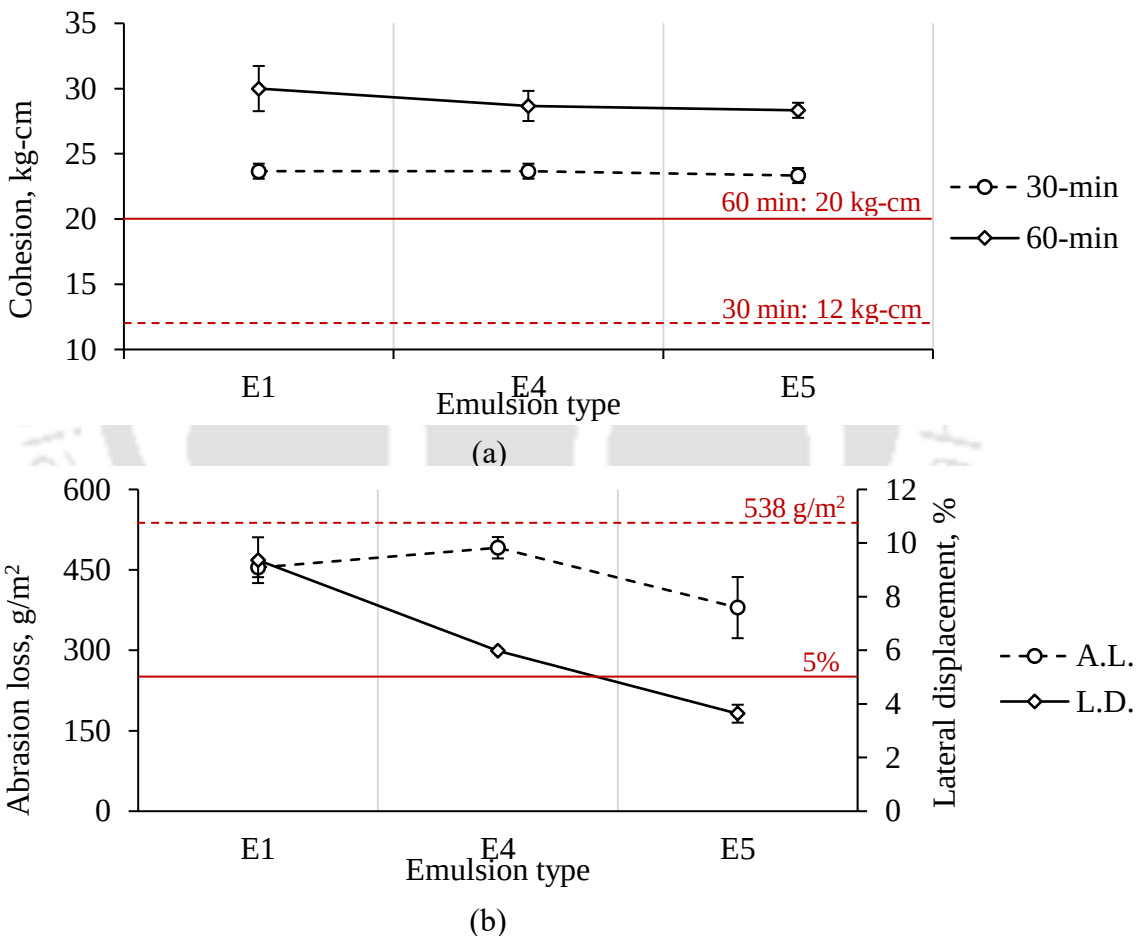

Figure 4.5: Effect of asphalt type and solvent: (a) cohesion; (b) raveling and rutting

Statistical analysis of test results using Tukey's *post-hoc* multiple comparisons is presented in **Table 4.5**. It could be observed from **Table 4.5** that the cohesion did not

vary significantly with asphalt type and solvent. In terms of raveling, mix produced with harder binder grade (E4) had significantly higher raveling than the mix which has harder binder grade and solvent (E5). Rutting reduced significantly with the use of harder binder (E4) instead of softer binder grade (E1). The use of solvent with harder binder grade (E5) also resulted in a significant reduction in rutting when compared to emulsion E4.

Table 4.5: Grouping of mixes according to asphalt type and solvent

Mix type	Cohesion, kg-cm		Abrasion Loss	Lateral Displacement
	30-min	60-min		
E1	1	1	1/2	3
E4	1	1	2	2
E5	1	1	1	1

4.7 Optimizing the mix characteristics and performance

Selection of suitable type and optimum dosage of mineral filler is vital to optimize the mix characteristics and performance of the microsurfacing mix. A total of 10 different combinations of mineral fillers at varying dosages were used to produce mix, as shown in **Figure 4.6**. The dosages of mineral filler were selected as follows.

- Mix 1 – Control mix (No mineral fillers)
- Mix 2 to Mix 4 – OPC as mineral filler
- Mix 5 to Mix 7 – FA as mineral filler
- Mix 8 to Mix 10 – Both OPC and FA as mineral filler

Mix characteristics were defined in terms of compatibility, cohesion and adhesion. The test results were ranked using principal component analysis to identify the combinations of mineral filler that are likely to perform better and the critical combinations that should be avoided during the mix design. Performance was assessed in terms of raveling (WTAT) and rutting (LWT) for the five selected best combinations from the principal component analysis. The performance was correlated with the mix characteristics. Based on the correlation analysis, the mix characteristic that could predict the performance of the microsurfacing mix was identified.

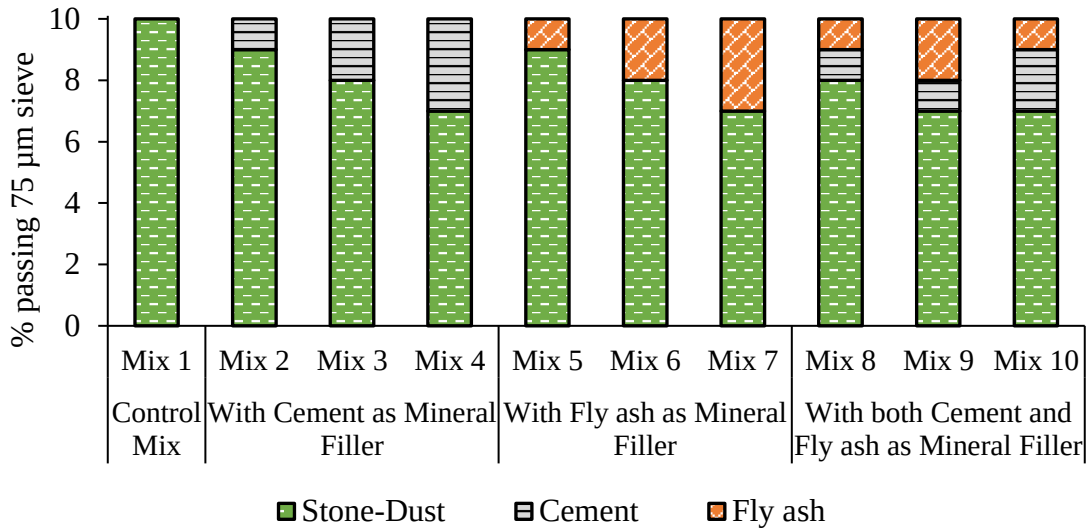

Figure 4.6: Mineral filler combinations for optimizing mix characteristics

4.7.1 Compatibility assessment of filler with asphalt emulsion

Schulze-Breuer and Ruck test was conducted to quantify the variation in compatibility. The results for absorption, abrasion loss, and integrity for the 10 mixes are presented in **Figure 4.7**. Error bars refer to ± standard deviation. The repeatability of the test results was investigated in terms of CoV. For the 10 combinations tested (with 4 replicates), the CoV varied from 0.2-14.6%, with the average CoV being 2.7%, 4.9% and 0.4% for absorption, abrasion loss, and integrity respectively.

Higher water absorption indicates a higher likelihood of moisture-induced distresses like stripping, raveling, and cracking. It could be seen from **Figure 4.7a** that water absorption varied in the range of 4.7% to 6.3%. The control mix had the highest water absorption, followed by mixes with OPC and FA. In terms of mineral filler dosage, lower absorption values were observed when higher mineral filler dosages were used.

After evaluating water absorption, saturated specimens were subjected to abrasion to mimic traffic action. Higher abrasion loss indicates weaker adhesion at the aggregate-binder interface. Results of abrasion loss presented in **Figure 4.7b** showed that incorporating mineral filler improved the resistance to abrasion for the microsurfacing mix. According to the ISSA, mixes having abrasion loss less than 0.7 gm were considered to have excellent abrasion resistance (ISSA TB No. 115, 2005). Therefore, the mixes having superior abrasion resistance were Mix 3, Mix 4, Mix 9, and Mix 10. In general, mixes with OPC or FA or both OPC and FA had better abrasion resistance than the control mix.

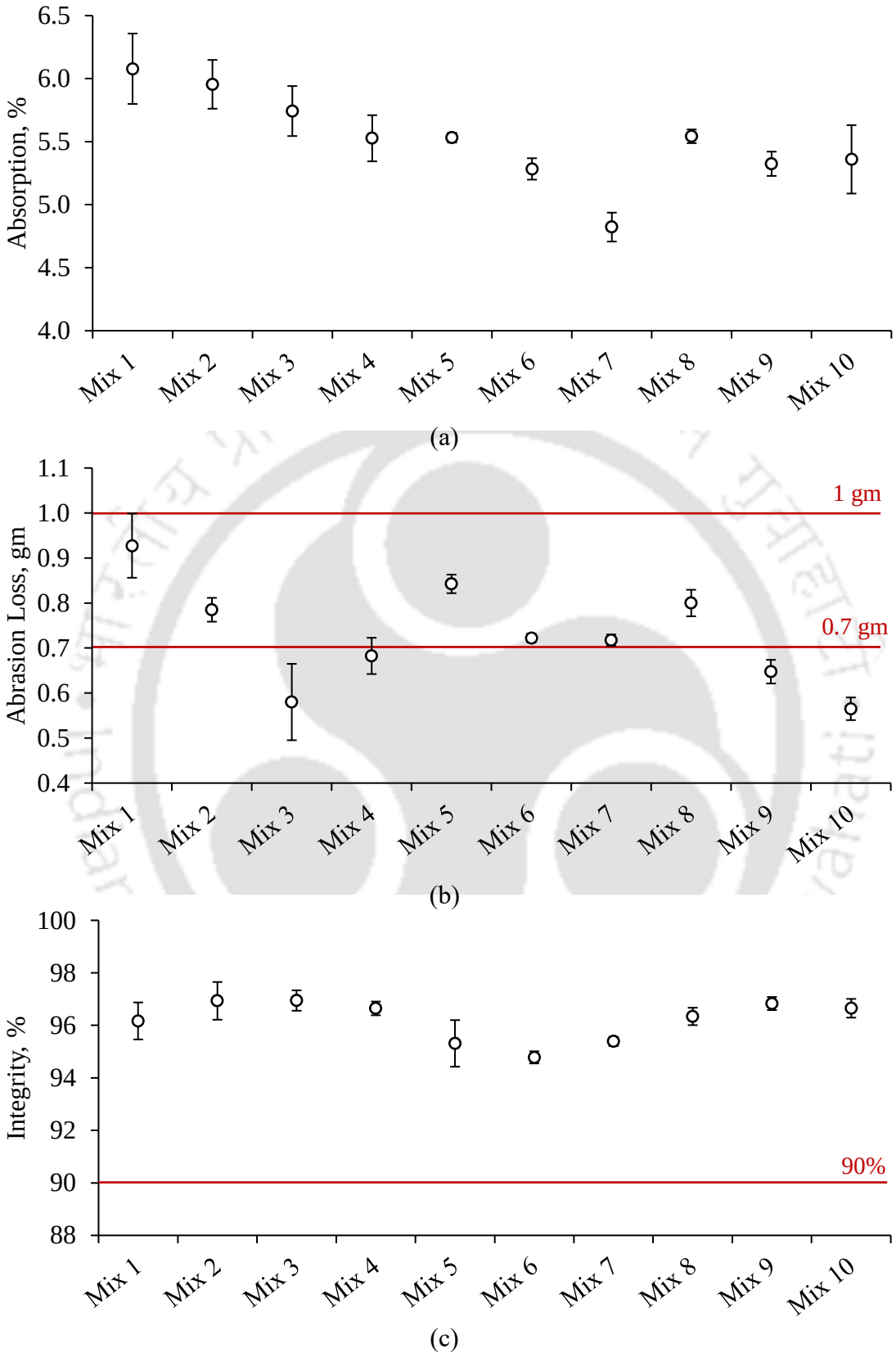

Figure 4.7: Compatibility: (a) Absorption; (b) Abrasion loss; (c) Integrity

Evaluation of adhesion characteristics of the filler-emulsion system were assessed for all mixes by subjecting the abraded pill to boiling. Higher integrity indicates better resistance to moisture-induced stresses. Results in **Figure 4.7c** showed that the mixes with OPC had superior resistance to the detrimental effect of moisture. The integrity of mixes with FA was found to be the lowest. The presence of SiO_2 is generally associated with higher moisture susceptibility of asphalt mixture (Abo-Qudais & Al-Shweily, 2007). So, higher SiO_2 content in FA (**Table 3.5**) explains the higher loss in weight due to moisture damage. Mixes with a combination of OPC and FA had similar moisture resistance to mixes with OPC.

4.7.2 Influence of mineral filler on cohesion development

Cohesion is one of the primary contributors to the resistance to traffic action during the initial phase of the microsurfacing mix. The results of the investigations on cohesion development (ISSA TB No. 139, 2017) are presented in **Figure 4.8**. The repeatability of the cohesion test results was investigated in terms of CoV. For the 80 combinations tested (with 3 replicates), the CoV varied from 1.8-10.6%, with the average CoV being 5.5%.

Similar to **Section 4.4**, it could be observed from **Figure 4.8** that the inclusion of OPC improved cohesion with respect to the control mix. Also, mixes with higher OPC dosage exhibited higher cohesion. **Figure 4.8** also showed that for mixes having OPC as mineral filler, cohesion values were observed to be similar during the initial phase, irrespective of the OPC dosage and the use of FA. The inclusion of FA in the mix also showed an increase in cohesion. The cohesion at the end of 240 minutes increased by 4%, 7%, and 10% for mixes with 1% FA, 2% FA, and 3% FA, respectively, when compared to the control mix. Cohesion for mixes with FA was less than mixes with OPC. The reason behind the lower cohesion could be the relatively lower cementitious content of FA with respect to OPC (Du, 2013). Because of the low cementitious content, the stiffness imparted by FA would be lower than OPC, and hence, the mix would have lower torque resistance. As a result, lower cohesion values were observed for mixes with FA.

Mixes containing both OPC and FA exhibit the best cohesion among the combinations considered. Higher cohesion values in these mixes could be due to the reaction of silica present in FA with available lime and alkali in OPC. This reaction results in the

production of cementitious compounds (C-S-H), as shown in **Equation 4.1** and **4.2** (American Coal Ash Association, 2003).

$$\text{Cement reaction:} \quad C_3S + H \rightarrow C-S-H + CaOH \tag{4.1}$$

$$\text{Pozzolanic reaction:} \quad CaOH + S \rightarrow C-S-H \tag{4.2}$$

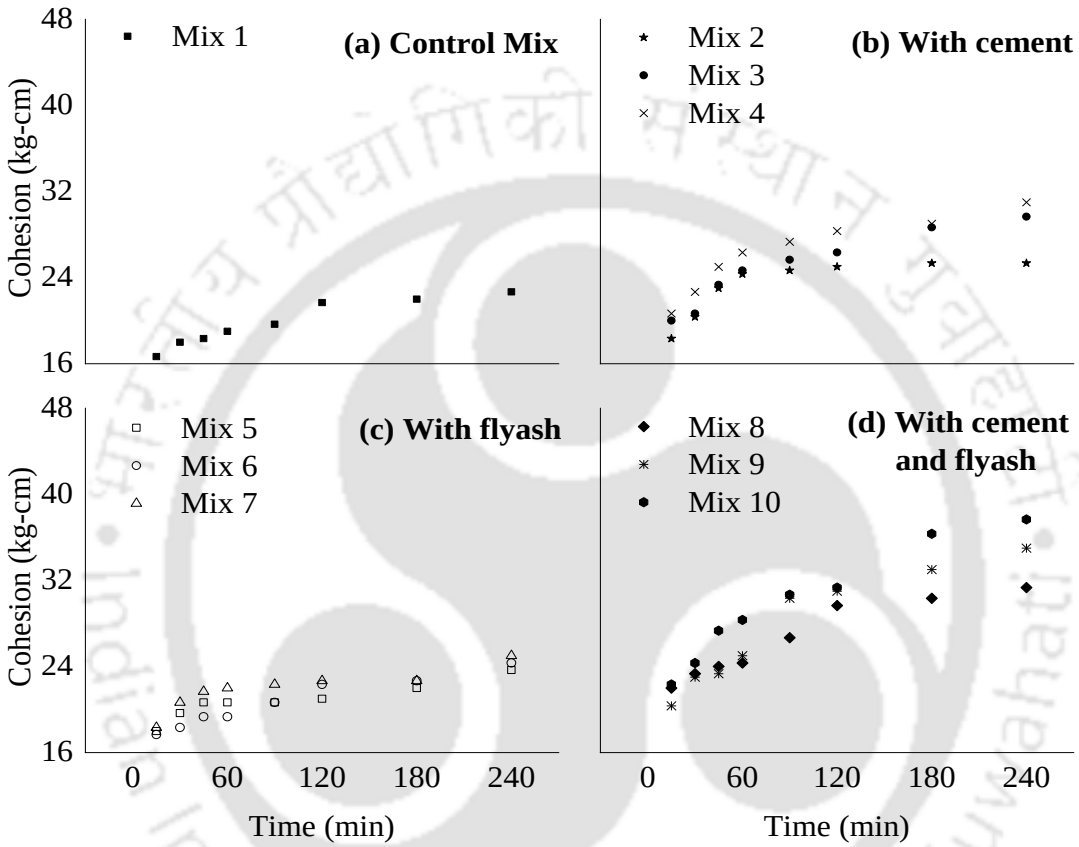

Figure 4.8: Cohesion development for different mineral filler types and dosages

Since the difference in cohesion development with time was observed for different mix types, interpretation of results by modeling the data would provide better insight on the extent of variation. For this purpose, a Power-Law Model (**Equation 4.3**) was used in the study to describe the rate of cohesion development. Here, time (minutes) was the only independent variable, and cohesion (kg-cm) was the dependent variable.

$$Cohesion = a \times (Time)^b \tag{4.3}$$

where *a* and *b* were regression coefficients. The model parameters, *p*-value, and R^2 are presented in **Table 4.6**. The value of R^2 for all mix types was higher than 0.85, which indicates that the Power-Law Model provides an excellent fit for cohesion development

with time for all mix types. Results from the statistical analysis show that the *p*-value was less than even 0.001 for all cases, which indicates that the rate of cohesion development was statistically significant for all the mix types.

Table 4.6: Power-law model coefficients for cohesion development

Mix Type	Model Parameters		*p*-value		R^2
	a	b	a	b	
Mix 1	12.05	0.115	0.000	0.000	0.96
Mix 2	14.01	0.118	0.000	0.001	0.85
Mix 3	13.03	0.150	0.000	0.000	0.97
Mix 4	14.26	0.142	0.000	0.000	0.98
Mix 5	14.72	0.081	0.000	0.000	0.90
Mix 6	12.43	0.117	0.000	0.000	0.95
Mix 7	14.91	0.090	0.000	0.000	0.89
Mix 8	14.51	0.140	0.000	0.000	0.94
Mix 9	11.24	0.208	0.000	0.000	0.96
Mix 10	12.94	0.193	0.000	0.000	0.98

The variation in model parameters was used to recognize the dependence of cohesion on mineral filler. An increase in the value of *b* implies a higher rate of cohesion development. From **Table 4.6**, it could be observed that mixes having OPC as a mineral filler (Mix 2, Mix 3, and Mix 4) had a higher rate of cohesion development than both control mix (Mix 1) and mixes having FA (Mix 5, Mix 6 and Mix 7) as mineral filler. With the increase in mineral filler dosage for both OPC and FA, the value of parameter *b* first increased and then decreased. This shows that there exists an optimum mineral filler dosage for which the rate of cohesion development is maximum. Mixes with both OPC and FA (Mix 9 and Mix 10) had the highest value of parameter *b*, which points towards better cohesion development in these mixes. Hence, it could be said that careful selection of the type and dosage of mineral filler combination could maximize the strength of the microsurfacing mix.

4.7.3 Adhesion properties of microsurfacing mix

Adhesion is a measure of the aggregate-binder bond which is generally evaluated using boiling water test (ISSA TB No. 149, 2005). It was observed that during the boiling

water test, some amount of binder came to the surface for the control mix as well as mixes with FA (Mix 5, Mix 6, and Mix 7). In contrast, no loss of binder was observed with the addition of OPC. Hence, it could be inferred that OPC helps accelerate the curing process in the microsurfacing mix.

Further, the mixes subjected to boiling were dried using a hot-air gun, and the loss index was measured using ACT. The results of the loss index are presented in **Figure 4.9**. Error bars refer to ± standard deviation. The repeatability of the cohesion test results was investigated in terms of CoV. For the 10 combinations tested (with 3 replicates and 3 trials per replicate), the CoV varied from 1.1-12.5%, with the average CoV being 5.3%.

Higher loss index values represent a higher loss of coating and lower aggregate-binder adhesion in the mix. As expected, mixes with OPC (Mix 2, Mix 3 and Mix 4) had better adhesion than both control mix (Mix 1) and mixes with FA (Mix 5, Mix 6 and Mix 7). Better adhesion with OPC is due to the improvement in interfacial bonding in the asphalt mastic, which results in better resistance to damage caused by water (Li *et al.*, 2019). FA, which has higher content of SiO_2, contributes to the moisture susceptibility of the mix. Like cohesion test results, a mix containing both OPC and FA (Mix 8, Mix 9 and Miix 10) had the least loss index indicating superior adhesion.

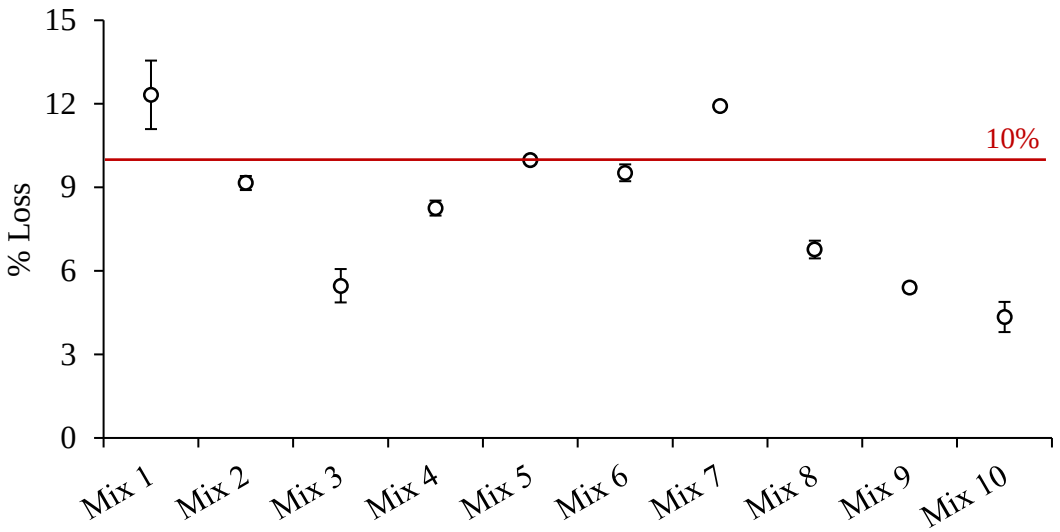

Figure 4.9: Variation of Loss Index with mineral filler type and dosage

4.7.4 Statistical analysis of mix characteristics

4.7.4.1 Analysis of Variance

The test results were statistically analyzed using a one-way analysis of variance (ANOVA) at a 5% significance level. ANOVA is a tool to compare the means of several populations based on random, independent samples from each population. It provides a statistical test to determine if population means are equal or not (i.e., came from the same distribution). The hypotheses of interest in an ANOVA are as follows:

H0: $\mu_1 = \mu_2 = \mu_3 \ldots = \mu_k$

H1: Means are not all equal.

where k = the number of independent comparison groups.

The results of the analysis presented in **Table 4.7** show that the *p*-value was less than even 0.001 for all cases. Hence, a statistically significant difference was noticed among 10 mix types considered in the study for compatibility, cohesion, and adhesion.

Table 4.7: Significance test for assessing the effect of mineral filler

Source	Parameter	Test/Time	df	*F*	*p*-value	Significant
Mix type	Compatibility	Abrasion Loss	9	26.2	0.000	Yes
		Integrity	9	6.5	0.000	Yes
	Cohesion	15 min	9	6.7	0.000	Yes
		30 min	9	7.9	0.000	Yes
		45 min	9	9.3	0.000	Yes
		60 min	9	14.5	0.000	Yes
		90 min	9	17.3	0.000	Yes
		120 min	9	28.9	0.000	Yes
		180 min	9	38.5	0.000	Yes
		240 min	9	25.4	0.000	Yes
	Adhesion	Loss Index	9	91.7	0.000	Yes

4.7.4.2 Principal Component Analysis

Principal Component Analysis (PCA) is a multivariate statistical method primarily used for data reduction by identifying variables contributing to the total variance's

significant portion. In PCA, the intercorrelated variables are minimized. The PCA allows the selection of the variables which capture the maximum variation in the pavement performance (Bianchini, A., 2014). Then, the covariance matrix is computed for the standardized data. Eigenvectors and eigenvalues are determined for the covariance matrix to identify the critical components. Based on the eigenvalues, percentage variance is calculated by dividing the eigenvalues of each component by the sum of all eigenvalues. The parameters are then arranged in descending order according to % variance. The number of principal components which explain the threshold % variance, say 95%, are selected for further analysis.

In this study, the data was initially normalized using **Equation 4.4** and **Equation 4.5** to eliminate the effect of the difference in the magnitude of different test results. Since the increase in adhesion test results (Loss Index) and abrasion loss represents a deterioration in performance, the formula of computing normalized value was modified, as shown in **Equation 4.5**.

$$y_i = \frac{x_i - x_{min}}{x_{max} - x_{min}} \qquad \text{for cohesion and integrity} \qquad (4.4)$$

$$y_i = \frac{x_{max} - x_i}{x_{max} - x_{min}} \qquad \text{for adhesion and abrasion} \qquad (4.5)$$

The correlation matrix was obtained for all test parameters, as shown in **Table 4.8**. For analysis purpose, the cohesion was considered at ISSA recommended curing times of 30 and 60 minutes only. Results show that compatibility characteristics had a good correlation with cohesion and adhesion characteristics. It was also observed that cohesion at 60-min had a better correlation with adhesion and compatibility than cohesion at 30-min. Based on the correlation analysis, cohesion at 60-min was found to be a better parameter to assess a microsurfacing mix's strength characteristics than cohesion at 30-min.

Table 4.8: Correlation matrix

Condition	Parameter	Cohesion	Adhesion	Compatibility	
				Abrasion	Integrity
Correlation (with 30-min cohesion)	Cohesion	*1.00*	0.77	0.60	0.57
	Adhesion	0.77	*1.00*	0.76	0.61
	Abrasion Loss	0.60	0.76	*1.00*	0.37
	Integrity	0.57	0.61	0.37	*1.00*
Correlation (with 60-min cohesion)	Cohesion	*1.00*	0.80	0.72	0.74
	Adhesion	0.80	1.00	0.76	0.61
	Abrasion Loss	0.72	0.76	*1.00*	0.37
	Integrity	0.74	0.61	0.37	*1.00*

Bartlett's test of sphericity was used to assess the statistical significance of correlation values. Correlation matrix (**Table 4.9**) was assumed to be an identity matrix, i.e., the null hypothesis: *correlation matrix = identity matrix*. At a significance level of 5%, it could be observed from **Table 4.9** that the null hypothesis could be rejected for both cases since the significance value was less than 0.05. Thus, the correlation between the test parameters is statistically significant, and the multivariate analysis could be considered for the decision-making process.

Table 4.9: Bartlett's test of sphericity

Parameters	Cohesion at 30-min	Cohesion at 60-min
Approx. Chi-Square	15.70	20.35
df	6	6
Significance	0.015	0.002

Eigen values of the principal components were evaluated using SPSS software. It could be observed from **Table 4.10** that the cumulative percent of variance was more than 95% for the first 3 components. So, for the present analysis, 3 components were extracted. For better interpretation of results, orthogonal rotation using Varimax method was conducted. Each parameter's rotated loadings on each component were calculated and the result is shown in **Table 4.11**.

Table 4.10: Total variance considering rotated sums of squared loadings

Cond.	Cmp	Initial Eigenvalues			Rotated Sums of Squared Loadings		
		Total	% of variance	Cmv. %	Total	% of variance	Cmv. %
With cohesion at 30-min	1	2.85	71.3	71.3	1.49	37.2	37.2
	2	0.65	16.2	87.5	1.20	30.0	67.2
	3	0.34	8.5	96.0	1.15	28.9	96.0
	4	0.16	4.0	100.0			
With cohesion at 60-min	1	3.02	75.5	75.5	1.52	38.0	38.0
	2	0.65	16.3	91.8	1.50	37.5	75.5
	3	0.20	4.9	96.7	0.85	21.2	96.7
	4	0.13	3.3	100.0			

* ***Note****: Cond.: Condition; Cmp = Component; Cmv = Cumulative.*

Table 4.11: Rotated component matrix from Principal Component Analysis

Parameter	Component (considering cohesion at 30-min)			Component (considering cohesion at 60-min)		
	1	**2**	**3**	**1**	**2**	**3**
Cohesion	0.33	0.89	0.28	0.67	0.63	0.28
Adhesion	0.68	0.52	0.40	0.39	0.50	0.78
Abrasion	0.94	0.25	0.13	0.15	0.92	0.33
Integrity	0.18	0.26	0.95	0.95	0.13	0.24

Weights associated with each parameter were evaluated using **Equation 4.6**. Next, the normalized values for each mix type were multiplied with the weights, and the scores were calculated using **Equation 4.7**.

$$W_{j,PCA} = \sum_{i=1}^{3} PC_{ij,PCA} \times V_{i,PCA} \tag{4.6}$$

$$S_{m,PCA} = \sum W_{j,PCA} \times X_{mj,PCA} \tag{4.7}$$

Here, i = component number (1 to 3); j = test parameter (cohesion, adhesion, abrasion, and integrity); m = mix type (Mix 1 to Mix 10); PC = component weights; V = % of variance of rotated sum of squared loadings; W = Weight for the parameter.

The scores of each mix type and associated ranking among the 10 mix types are presented in **Table 4.12**. A higher score represented better performance of the mix. Rankings showed that mixes with OPC performed better than mixes with FA. The probable reason behind the inferior characteristics and performance of the mix with FA was the pH environment of the asphalt emulsion (pH = 2). Class F type FA requires an alkaline environment, for e.g., $Ca(OH)_2$, to react and form cementitious compounds (Thomas, 2007). Since asphalt emulsion is acidic (pH = 2), FA's addition does not improve the compatibility and strength characteristics of the microsurfacing mix. Overall, combination of OPC and FA as mineral filler performed the best.

Table 4.12: Ranking of mix type based on Principal Component Analysis

Mix type	Considering cohesion at 30-min		Considering cohesion at 60-min	
	Score	Rank	Score	Rank
Mix 1	0.27	10	0.29	10
Mix 2	0.98	6	1.15	6
Mix 3	1.51	3	1.67	2
Mix 4	1.29	4	1.40	4
Mix 5	0.49	8	0.47	8
Mix 6	0.47	9	0.46	9
Mix 7	0.61	7	0.60	7
Mix 8	1.23	5	1.16	5
Mix 9	1.58	2	1.58	3
Mix 10	1.82	1	1.92	1

4.7.5 Performance of microsurfacing mix

In this study, the performance of the microsurfacing mix was assessed for 5 mixes (Mix 2, Mix 3, Mix 8, Mix 9, and Mix 10) that had superior mix characteristics. **Figure 4.10** shows the raveling and rutting of the 5 mixes tested. Error bars refer to ± standard deviation. The repeatability of the cohesion test results was investigated in terms of CoV. For the 5 combinations tested, the CoV varied from 2.1-12.3%, with the average CoV being 10.1% and 6.0% for WTAT and LWT respectively.

Similar to the mix characteristics, it was observed that the mixes having higher cement content (Mix 3 and Mix 10) performed better than other mixes. Also, it could be seen

that the mix produced with 1% OPC along with 0%, 1%, and 2% FA (Mix 2, Mix 8 and Mix 9) failed in both raveling and rutting. Hence, it could be said that the role of mineral filler is to provide adequate strength and stiffness to the microsurfacing mix to resist the shear and compressive action of traffic.

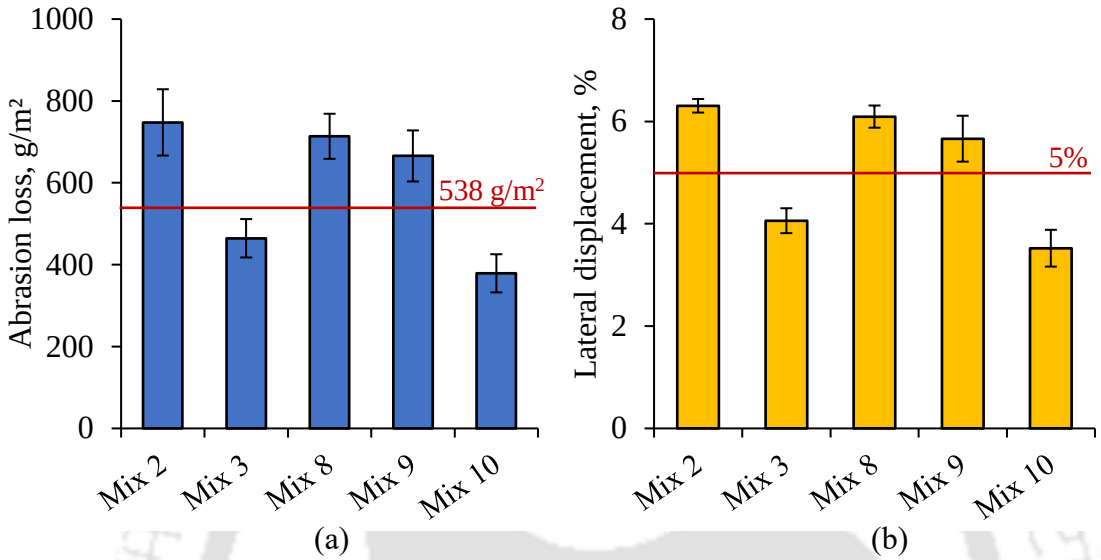

Figure 4.10: Influence of mineral filler on (a) raveling and (b) rutting

Performance parameters including raveling and rutting were correlated with the mix characteristics including cohesion at 30-min and 60-min, adhesion and compatibility (absorption, abrasion and integrity). Results of the correlation analysis, presented in **Figure 4.11**, showed that the mix characterisitics including 60-minute cohesion, adhesion, and compatibility (abrasion loss) correlated well with the raveling and rutting of microsurfacing mix. Hence, establishing the mix characteristics during mix design could help in selecting the suitable type and optimum dosage of mineral filler.

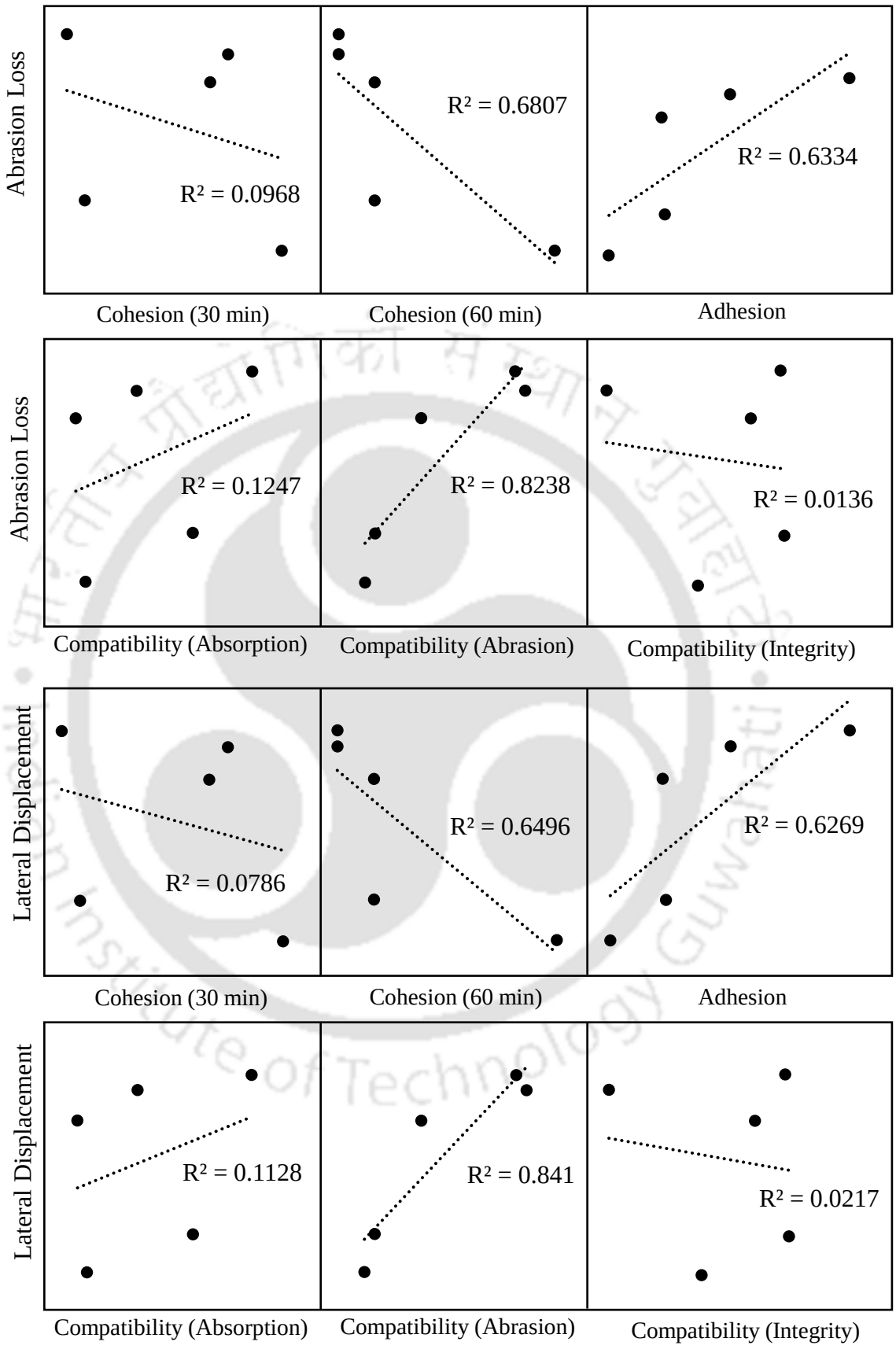

Figure 4.11: Correlation of mix characteristics with performance

4.8 Mix Design

After addressing the related issues and finalizing the production variables, mix design was conducted as per ISSA guidelines (ISSA A143, 2010). In this study, instead of determining OEC using abrasion loss and sand adhesion, a narrow range diagram was proposed to represent the acceptable emulsion content range satisfying the specification limits laid down by ISSA (ISSA A143, 2010).

In conventional practice, the emulsion content 1.5% less than the maximum acceptable emulsion content from the sand adhesion test is termed as OEC (ISSA A143, 2010). In this study, the OEC would be 13.6% (=15.1% - 1.5%), and the acceptable range was 12.5% to 15.1%, as shown in **Figure 4.12**. If the lateral displacement is considered at 12.5%, it had exceeded the specification limit. Alternatively, for narrow range diagram, all the parameters, including cohesion (30-min and 60-min), abrasion loss (1-hr and 6 days), lateral displacement and sand adhesion, would be considered.

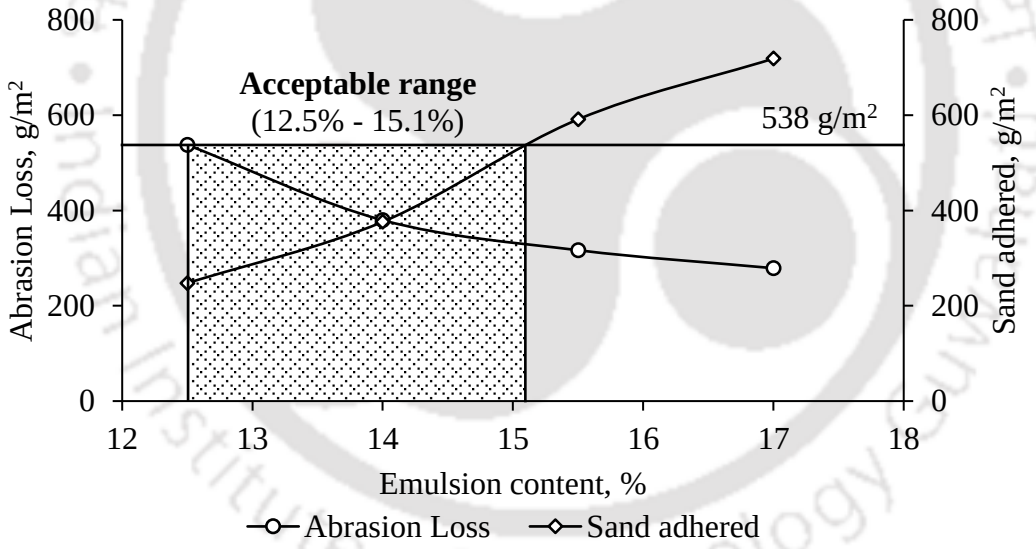

Figure 4.12: Acceptable range for emulsion content as per ISSA

The acceptable limits of each design parameter were obtained by fitting a second-degree polynomial to the test results, as shown in **Figure 4.13**. Error bars refer to ± standard deviation. The range of emulsion content with satisfactory results was termed as an acceptable range. Results showed that the mix passed the specification limits for cohesion and abrasion loss (1-hr soaked specimens) for all emulsion contents. However, an acceptable emulsion content range exists for which the lateral displacement and sand adhesion was satisafactory.

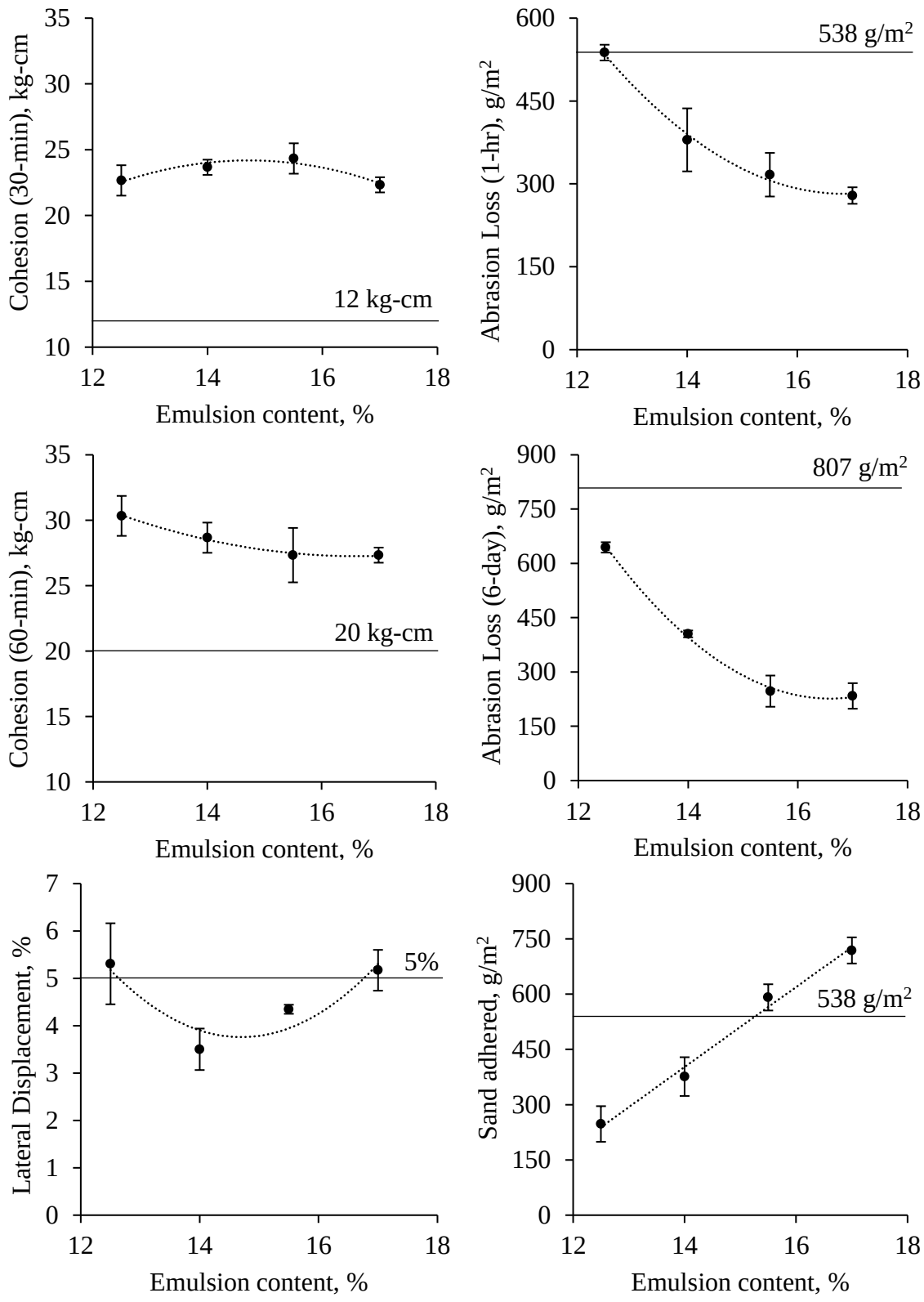

Figure 4.13: Design parameters for microsurfacing mix design

After determining the acceptable range from the graph, a narrow range diagram was plotted and shown in **Figure 4.14**. The acceptable range was determined by drawing a vertical line through the minimum and maximum acceptable emulsion content, considering all the design parameters. For the materials used and performance tests conducted in the study, an acceptable range of emulsion content varied from 12.6% to 15.2%. So, an OEC of 14% was selected for the materials investigated in this study.

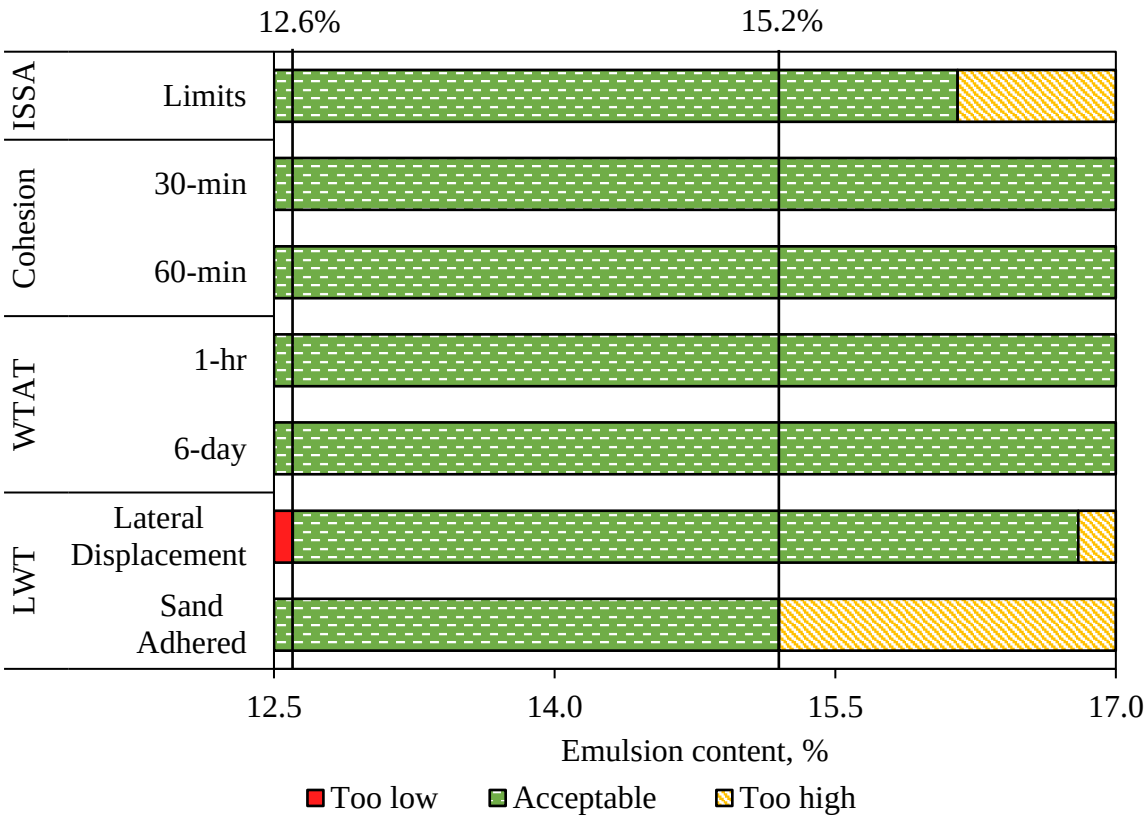

Figure 4.14: Narrow range diagram for microsurfacing mix design

The mix design formulation is presented in **Table 4.13**. The properties of the microsurfacing mix at the design formulation are described in **Table 4.14**. It could be observed from table that all the requirements of ISSA guidelines (ISSA A143, 2010) were satisfied at OEC.

Table 4.13: Mix design formulation

Component	Quantity	Allocation of component quantity
Emulsion		
Asphalt (VG-30)	62%	by weight of the emulsion
Asphalt additive	0.5%	by weight of asphalt
Solvent (Kerosene)	1%	by weight of asphalt
Emulsifier	1.5%	by weight of the emulsion
pH of soap solution	2	by addition of HCl
Latex (post-addition)	3.5%	by weight of the emulsion
Mix		
Emulsion Content	14%	by weight of dry aggregate
Water Content	6.4%	by weight of dry aggregate

Table 4.14: Verification of mix properties at design formulation

Test	Results	Specification
Cohesion		
30 min (Set)	23.7 kg-cm	12 kg-cm *min.*
60 min (Traffic)	28.7 kg-cm	20 kg-cm *min.*
Wet Track Abrasion Loss		
1-hr soaked	380 g/m^2	538 g/m^2 *max.*
6-day soaked	405 g/m^2	807 g/m^2 *max.*
Loaded Wheel Test		
Lateral Displacement	3.5%	5% *max.*
Sand adhered	376 g/m^2	538 g/m^2 *max.*
Classification compatibility	12-grade pts.	11-grade pts. m*in.*

4.9 Summary

Microsurfacing mix design is a rigorous and complicated process due to multiple components associated with the production process. In this chapter, a systematic procedure was adopted to mitigate the common problems encountered during mix design. Analysis and interpretation of test results highlight the following findings.

- Rapid breaking of microsurfacing mix can be mitigated by selecting the aggregates with low clay content, measured using MBV and Sand Equivalent test. In addition, the use of a filler with low silica content could also solve the issue of the high reactivity of aggregates.

- Cohesion was significantly higher for mixes having cement as mineral filler. Highest cohesion was exhibited by mix produced with the combination of cement and fly ash.
- Increasing emulsifier dosage from 1.5% to 2.0% resulted in a significant reduction in cohesion and an increase in raveling and rutting by 21% and 13%, respectively.
- Asphalt type and solvent didn't effect the cohesion significantly. With the addition of 1% solvent with harder grade asphalt during emulsion production, raveling and rutting reduced by 23% and 39%, respectively.
- Recommended tests to obtain suitable type and optimal dosage of mineral filler at the trial emulsion content is presented in **Figure 4.15**. In this study, mix with 1% flyash with 2% cement showed superior mix characteristics and performance (raveling and rutting).

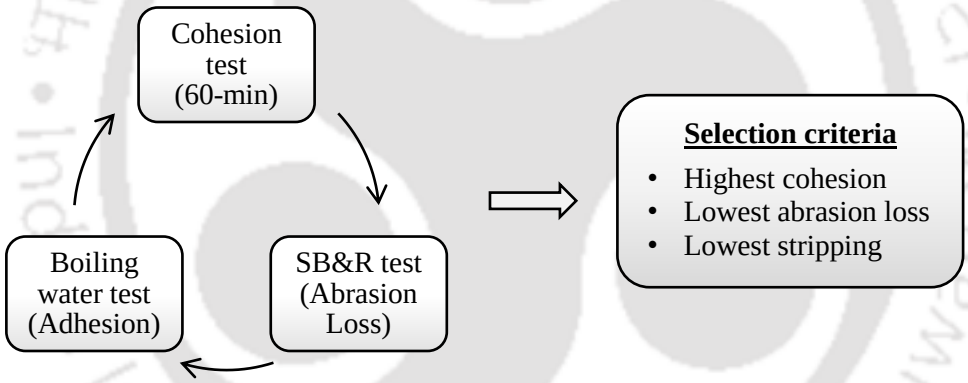

Figure 4.15: Approach to identify type and optimal dosage of mineral filler

- A narrow range diagram was proposed to identify the acceptable emulsion content range considering all the design parameters.

CHAPTER 5

Influence of Production Parameters on Performance

5.1 Introduction

This chapter discusses the variation in the microsurfacing mix performance due to the factors associated with the production stage. A total of 35 combinations of varying process control parameters, including aggregate gradation, emulsion content, and water content, were produced. Performance parameters including workability, strength, raveling, rutting and bleeding were determined in terms of consistency, cohesion, abrasion loss, lateral displacement, and sand adhesion, respectively.

Using the test results, the relative contribution of process control parameters on microsurfacing mix performance was evaluated with the help of Artificial Neural Network and Garson's algorithm. The effect of the parameter having highest relative contribution was quantified by developing a model using Multigene Symbolic Genetic Programming. Sensitivity analysis was used to interpret the model formulation. Reliability analysis was also conducted for each test to determine the risk of failure. The overall reliability was quantified using the limits specified by ISSA.

5.2 Methodology

The methodology adopted for assessing performance of microsurfacing mix is illustrated in **Figure 5.1**. The mixes were produced for 35 different combinations of process control parameters, including aggregate gradation (AG), emulsion content (EC) and water content (WC) as mentioned in **Table 3.2** (Mix C1 to C35). AG was described in terms of total surface area (TSA).

The selection criteria for these combinations is discussed below:

1. **Phase 1**: The individual effect of process control parameters was investigated in this phase. The parameters including TSA (C2 to C5), EC (C6 to C9), and WC (C10 to C12) were varied one-by-one while keeping the other 2 parameters constant at the optimum value. For TSA, EC and WC, the number of levels selected were 4, 4, and 3 (excluding control mix), respectively. The levels were

selected based on the tolerance limits range specified by ISSA. A total of 12 combinations (including the control mix) were tested.

2. **Phase 2**: In this phase, the synergistic effect of process control parameters was investigated by varying TSA, EC, and WC to 3 levels each (C13 to C32). For TSA and EC, the investigations were conducted at the optimum and boundary conditions of the tolerance limits range. For WC, the levels included optimum and optimum ± 1%. A 3^3 factorial design was adopted. Each level of one input variable was combined with each level of other two input variables to produce all possible combinations. A total of 20 additional combinations were tested in this phase.
3. **Phase 3**: In addition to the 32 combinations, 3 more combinations were tested in this phase at optimum WC + 2% and optimum EC – 1.5% (C33 to C35). The reason behind these investigations was that when the EC was optimum EC – 1.5% and WC was optimum WC – 1%, the mix was breaking rapidly. In field, to counter such situations, it recommended to adjust the WC. So, optimum WC + 2% was considered. For these 3 combinations, aggregate gradations mid-point (M), upper limit (UL), and lower limit (LL) were considered.

For each combination, performance was assessed, as described in **Figure 5.1**. A total of 4 replicates were produced for each test to ensure repeatability. The results were statistically analyzed was conducted at a significance level of 5% using univariate ANOVA. Subsequently, the following analysis was conducted:

1. ANN – Backpropogation algorithm was used to formulate model. The goodness-of-fit of the model was validated. The connection weights were extracted and Garson's algorithm was used to quantify the relative contribution of input parameters.
2. MSGP – Input and output parameters were normalized with respect to control mix to mitigate the biasedness based on the magnitude of the results. Parameters for MSGP model formulation were selected using trial and error method. Sensitivity analysis was conducted to interpret the model formulation.
3. Reliability - Frequency distribution of the test results was assumed to follow a normal distribution. Chi-square test was used for evaluating the goodness-of-fit. Reliability was determined by integrating the distribution function using the limits specified in ISSA guidelines (Chakroborty *et al.*, 2009).

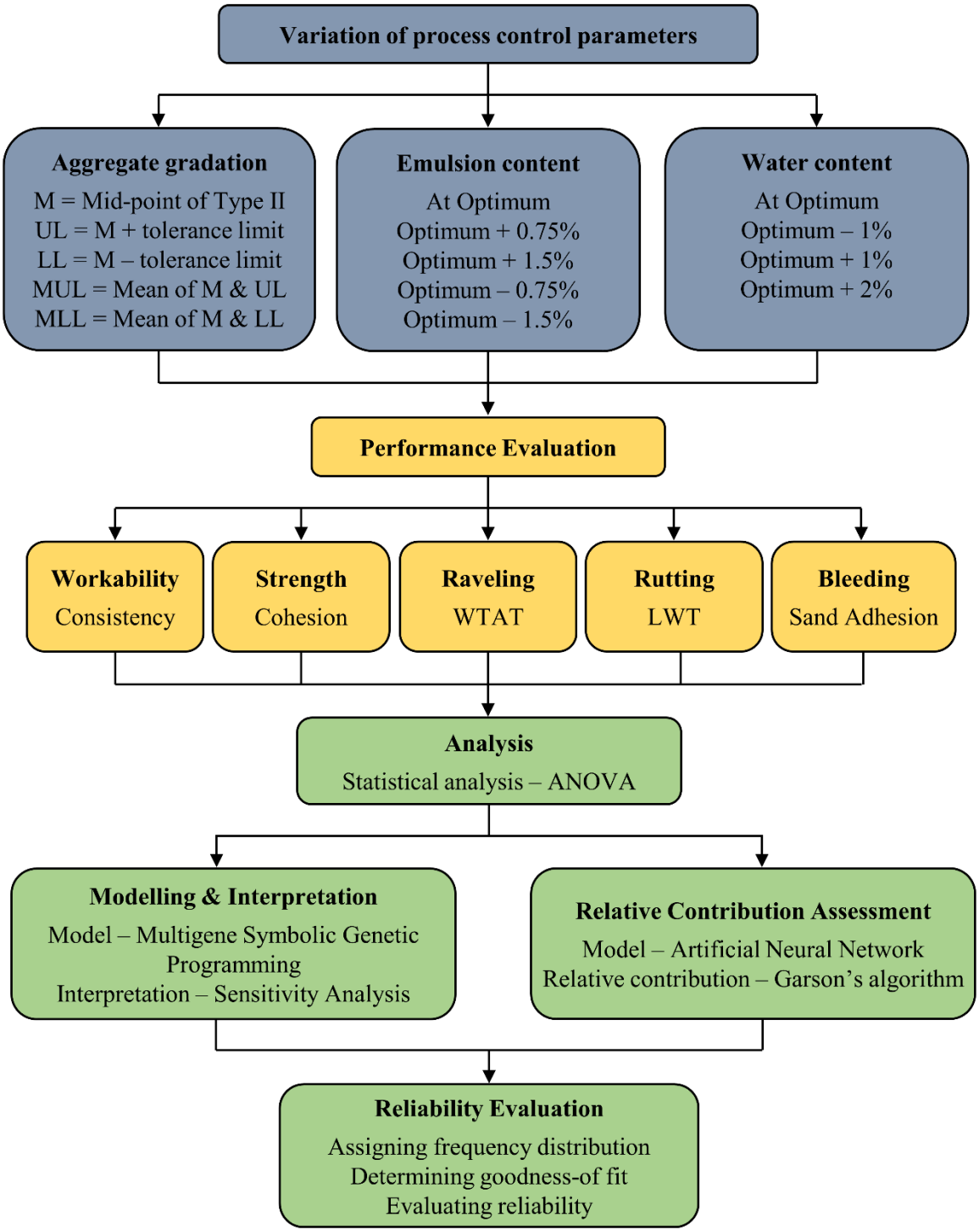

Figure 5.1: Methodology for assessing influence of production parameters

5.3 Performance evaluation with variation in process control parameters

5.3.1 Workability

The workability of the microsurfacing mix was defined in terms of consistency. **Figure 5.2** shows the results of the consistency test for 35 combinations of aggregate gradation, emulsion content, and water content. Error bars refer to ± standard deviation. For control mix, the consistency observed was 2.7 cm. The repeatability of the test results was investigated in terms of CoV. For the 35 combinations tested (with 3 replicates), the CoV varied from 1.1% to 16.6%, with the average CoV being 6.2%.

Aggregate gradation

The variation of consistency with aggregate gradation is described in **Figure 5.2a**. The consistency of the mix increased from 2.3 cm for 11.7 m^2/kg TSA to 3.6 cm for 8.7 m^2/kg TSA. This shows that when the aggregate gradation is varied from finer to coarser gradation, there is a substantial increase in the workability. The increase in the workability could be explained by the difference in the TSA for different aggregate gradations. For finer gradation, the TSA is higher, due to which higher water or emulsion content is required to achieve the same workability. As a result, the mix with finer gradation had lower consistency for similar water and emulsion content.

Emulsion content and water content

The variation of consistency with emulsion content and water content is described in **Figure 5.2b** and **Figure 5.2c**, respectively**.** It could be observed from both figures that the consistency decreased with the decrease in emulsion or water content. For instance, as the emulsion content decreased from 15.5% to 12.5%, the consistency reduced from 4.1 cm to 1.8 cm, i.e., a reduction of 56% was noticed (**Figure 5.2b**). On the other hand, **Figure 5.2c** shows that a 79% reduction in the consistency was noticed when the water content reduced from 8.4% to 5.4%. The primary reason for increase in the workability with the increase in water content was the reduction in surface tension on the aggregate. Similarly, thicker asphalt film around aggregate surface facilitate movement of aggregates and the workability of the mix is increased.

Critical parameters for workability

The synergistic effect of process control parameters on workability is illustrated in **Figure 5.2d**. It could be observed from **Figure 5.2d** that the consistency varied between 0 to 5.2 cm, i.e., a variation of -100% to +90% with respect to the control mix was

noticed. The mixes exhibiting a negligible consistency (close to 0 cm) were mix C15, C22, C25, C30, and C31. It was observed that for all the mixes except mix C31, the water content was decreased by 1% from optimum. For mix C31, water content was optimum, but the emulsion content was on the lower end of the acceptable range, and aggregate gradation was on the upper end of the tolerance range (finer gradation). Hence, rapid breaking would occur, and the mix would not be workable enough for laying on the pavement surface if the mentioned parameters are encountered in the field during the microsurfacing mix production.

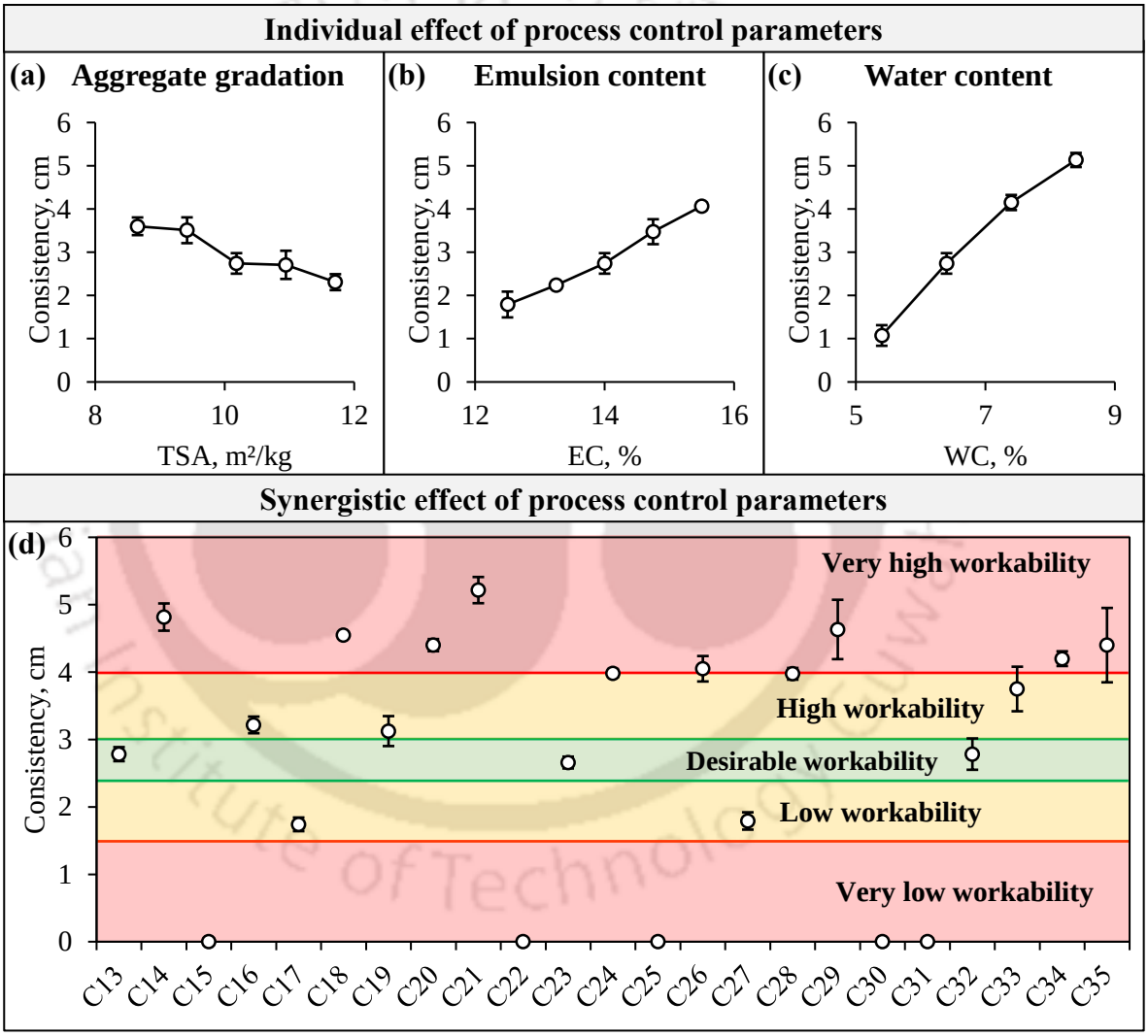

Figure 5.2: Workability characteristics of microsurfacing mix

Mix C21, C14, C29, and C18 had very high workability (consistency > 4.5 cm). For all these mixes, the water content was at 1% more than the optimum. The increment of consistency to a very high value leads to segregation, i.e., asphalt-rich fines come on

the surface, and coarse aggregates settle down, leading to a higher risk of bleeding and issues related to surface friction (Raza, 1994).

Hence, the following two scenarios should be avoided to ensure that the mix has desirable workability during production.

- Variation of the water content of more than ±1% from optimum
- Mix with TSA on the upper limit and emulsion content on the lower limit of the tolerance range

5.3.2 Strength evolution

Strength evolution of microsurfacing mix was characterized in terms of cohesion. Mixes C15, C22, C25, C30, and C31 were not considered because these mixes exhibited rapid breaking and very low workability (**Figure 5.2d**). Hence, for the assessment of strength evolution, only 30 combinations were considered. The results of the cohesion test conducted after 30 minute and 60 minutes of specimen preparation is illustrated in **Figure 5.3** and **Figure 5.4** respectively. Error bars refer to ± standard deviation. For control mix, the cohesion at 30-min and 60-min was 25.5 and 29.5 kg-cm, respectively. For the 30 combinations tested (with 4 replicates), the CoV varied from 1.7% to 6.5%, with the average CoV being 3.4% for both 30-min and 60-min cohesion.

Aggregate gradation

The variation of cohesion at 30-min and 60-min are presented in **Figure 5.3a** and **Figure 5.4a**, respectively. The cohesion at 30-min and 60-min of mix with 11.7 m^2/kg TSA was 2 kg-cm and 4 kg-cm higher than mix with 8.7 m^2/kg TSA, respectively. It implies that the cohesion after 30-min and 60-min was higher for the finer gradation compared to coarser gradation. The higher cohesion for finer gradation could be due to two factors, i.e., higher TSA and higher mineral filler content. Due to the higher TSA of finer gradation, the water gets absorbed, and emulsion gets cured faster (Robati *et al.*, 2013c). Also, higher mineral filler content results in stiffer filler mastic, which leads to higher cohesion (Li *et al.*, 2019).

Emulsion content

The variation of cohesion at 30-min and 60-min are presented in **Figure 5.3b** and **Figure 5.4b**. It could be observed that with emulsion content, minimal variation was observed for cohesion at 30-min and 60-min. The variation of cohesion with respect to

the control mix was within the range of -2% to 0% and 0% to 3% for cohesion at 30-min and 60-min, respectively. Interestingly, during the initial strength evolution, i.e., the first 30-min, a decrease in cohesion was observed with the increase in emulsion content. But, as the curing time increased to 60-min, higher cohesion was observed for higher emulsion content. Hence, it could be said that the influence of emulsion content on the strength evolution of the microsurfacing mix was dependent on the curing time.

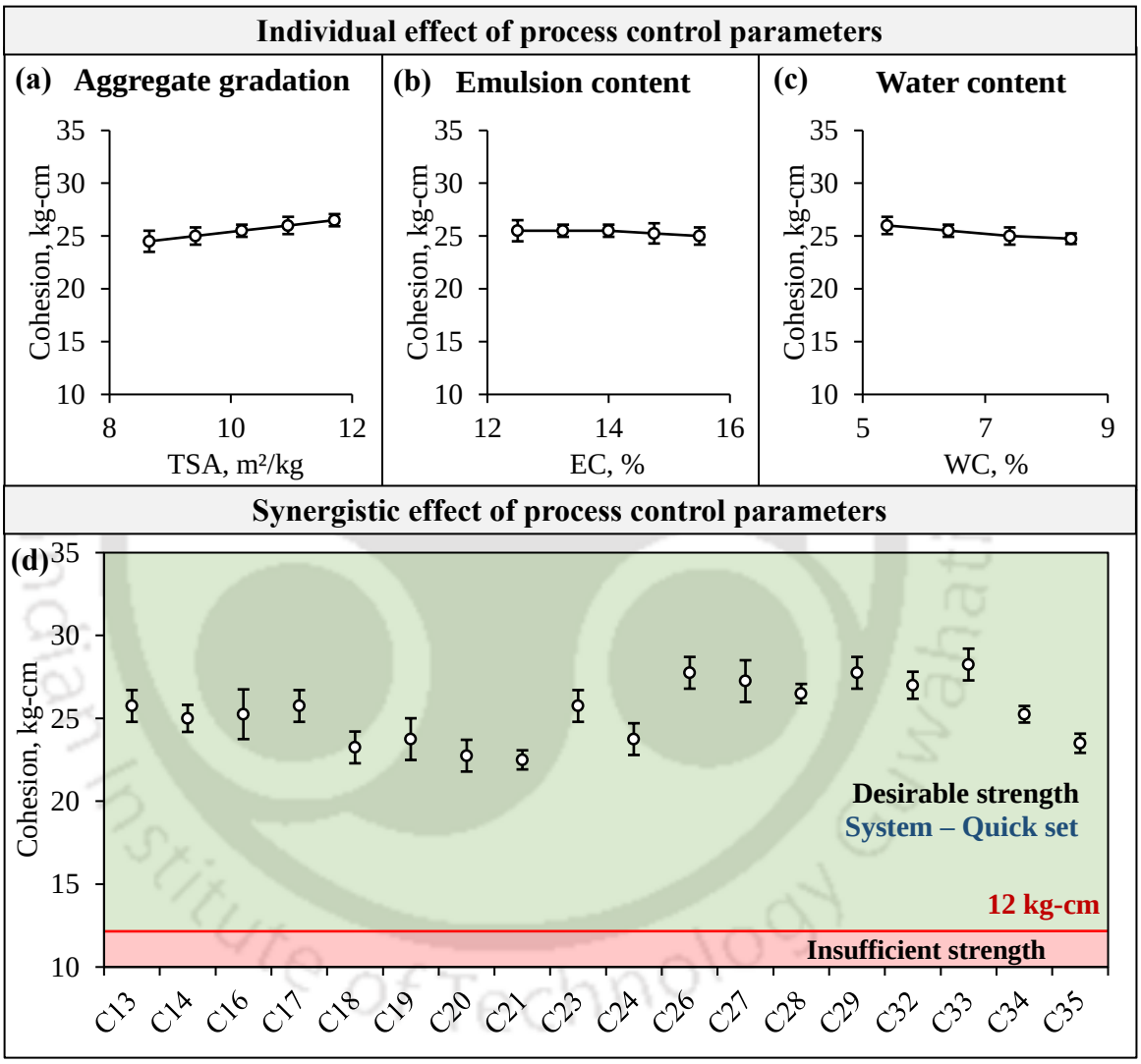

Figure 5.3: Strength development after 30-minutes of air curing

Water content

The variation of cohesion with water content is presented in **Figure 5.3c** and **Figure 5.4c**. It was found that with the decrease in the water content by 1% from the optimum resulted in minimal increase in the cohesion (< 3%). Increasing water content by 1% from optimum also led to a minimal reduction in cohesion (< 2%). The reduction in

cohesion with an increase in water content could be attributed to a combination of three reasons. First, the higher water content present in the mix requires more time to cure. Secondly, the coarser particles settle at the bottom for higher water content, and asphalt-rich fines move to the top (Raza, 1994). The third reason could be the reduction in the affinity of the binder towards the aggregate with the increase in water content (Smith *et al.*, 1994). As a result, the resistance of the mix to torque reduces. So, due to the higher curing time requirement in conjunction with segregation of mix and reduction in binder affinity, lower cohesion was observed for mixes with higher water content.

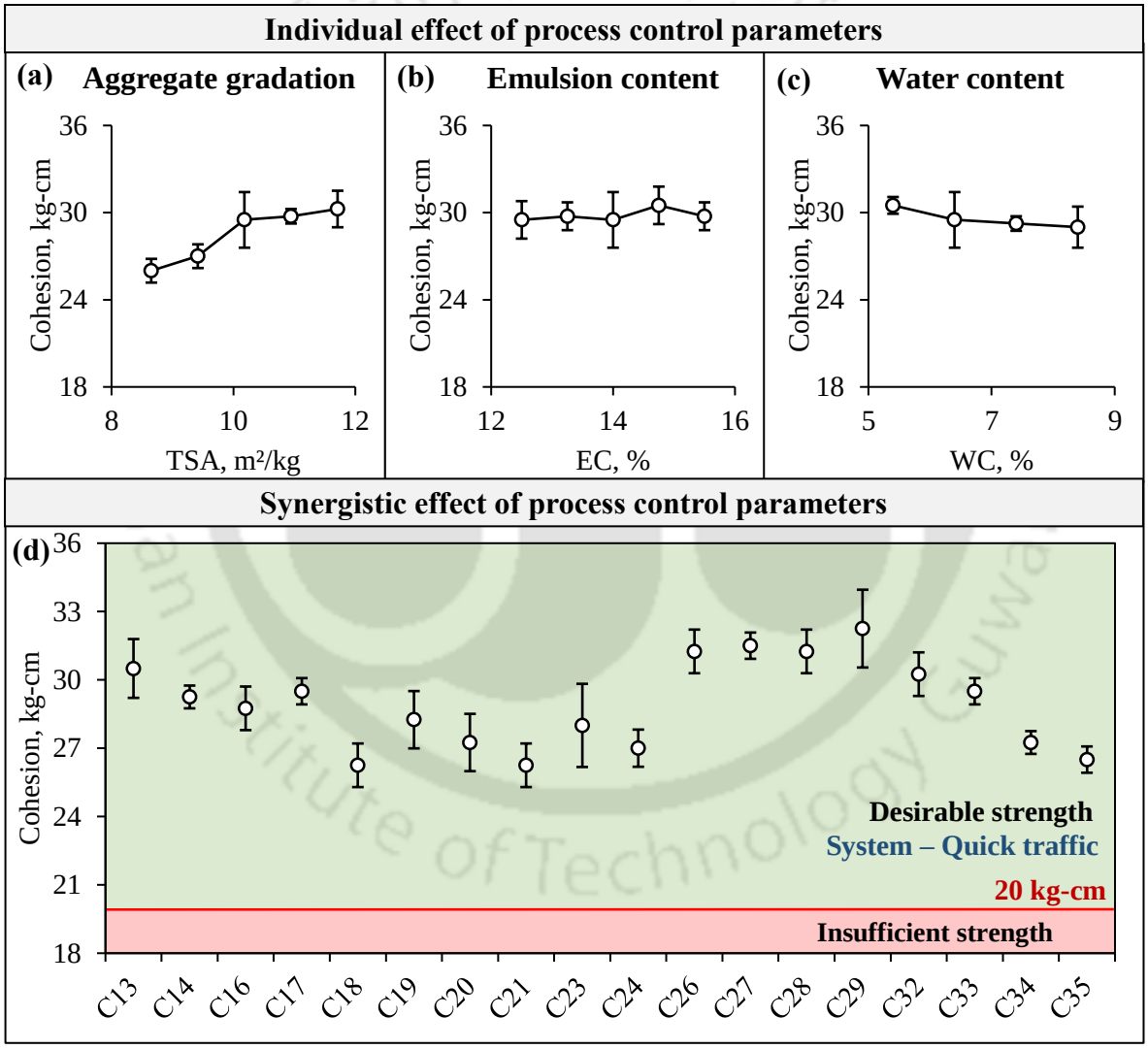

Figure 5.4: Strength development after 60-minutes of air curing

Critical parameters for strength evolution

The synergistic effect of process control parameters on cohesion at 30-min and 60-min is illustrated in **Figure 5.3d** and **Figure 5.4d**, respectively. Overall, the cohesion values

varied between 22.5-28.3 kg-cm for cohesion at 30-min and 26.0-32.3 kg-cm for cohesion at 60-min. The mix with relatively lower cohesion, i.e., C18, C20, C21, C24, and C35, had a common factor, i.e., coarser aggregate gradation. Alternatively, mix with relatively higher cohesion, i.e., C26, C27, C28, C29, and C33, had finer aggregate gradation. Variation in emulsion and water content did not contribute substantially to cohesion (**Figure 5.3d** and **Figure 5.4d**). Hence, it could be said that the aggregate gradation (including mineral filler content) should not be allowed to be at the lower limit of the tolerance range to ensure that the mix achieves sufficient strength within one hour of production.

5.3.3 Raveling

Results of raveling for 30 different combinations of aggregate gradation, emulsion content, and water content are illustrated in **Figure 5.5**. Error bars refer to ± standard deviation. For control mix, abrasion loss observed was 380 g/m^2. For the 30 combinations tested (with 4 replicates), the CoV varied from 3.0-18.1%, with the average CoV being 8.6%.

Aggregate gradation

The effect of aggregate gradation on raveling is presented in **Figure 5.5a**. It was found that the coarser gradation exhibited an 85% higher abrasion loss in comparison to finer gradation. Higher abrasion loss for coarser gradation highlights that the raveling resistance of the mix is dependent on the adhesion at aggregate-binder interface. Since coarser gradation had a relatively lower finer portion, the packing of the aggregates was relatively poor. Also, the stiffness of the asphalt mastic and aggregate-binder adhesion reduces due to lower cement content (Li *et al.*, 2019).

Emulsion content

The variation in raveling with emulsion content is illustrated in **Figure 5.5b**. A decrease in abrasion loss from 554 g/m^2 to 274 g/m^2 was observed when the emulsion content increased from 12.5% to 15.5%. The lower abrasion loss with higher emulsion content was probably due to the higher asphalt film thickness and better adhesion at the aggregate-binder interface (Hou *et al.*, 2018; Hafezzadeh & Kavussi, 2021). Most importantly, the wide range of abrasion loss values with respect to control mix (-27% to +46%) highlights the need to ensure minimal variation in the emulsion content from the job mix formula.

Water content

Water content also had a substantial contribution to the raveling of the microsurfacing mix, as shown in **Figure 5.5c**. When the variation of water content was within ± 1% from optimum, the difference in the abrasion loss of the mix was minimal. However, the abrasion loss was observed to be reduced for very high-water content (Optimum + 2%). This is probably because at higher water content, asphalt-rich fines comes to the surface, leading to lower abrasion loss. But, it is not recommended to have substantially high-water content due to the increased segregation potential and issues related to surface texture and friction (Raza, 1994).

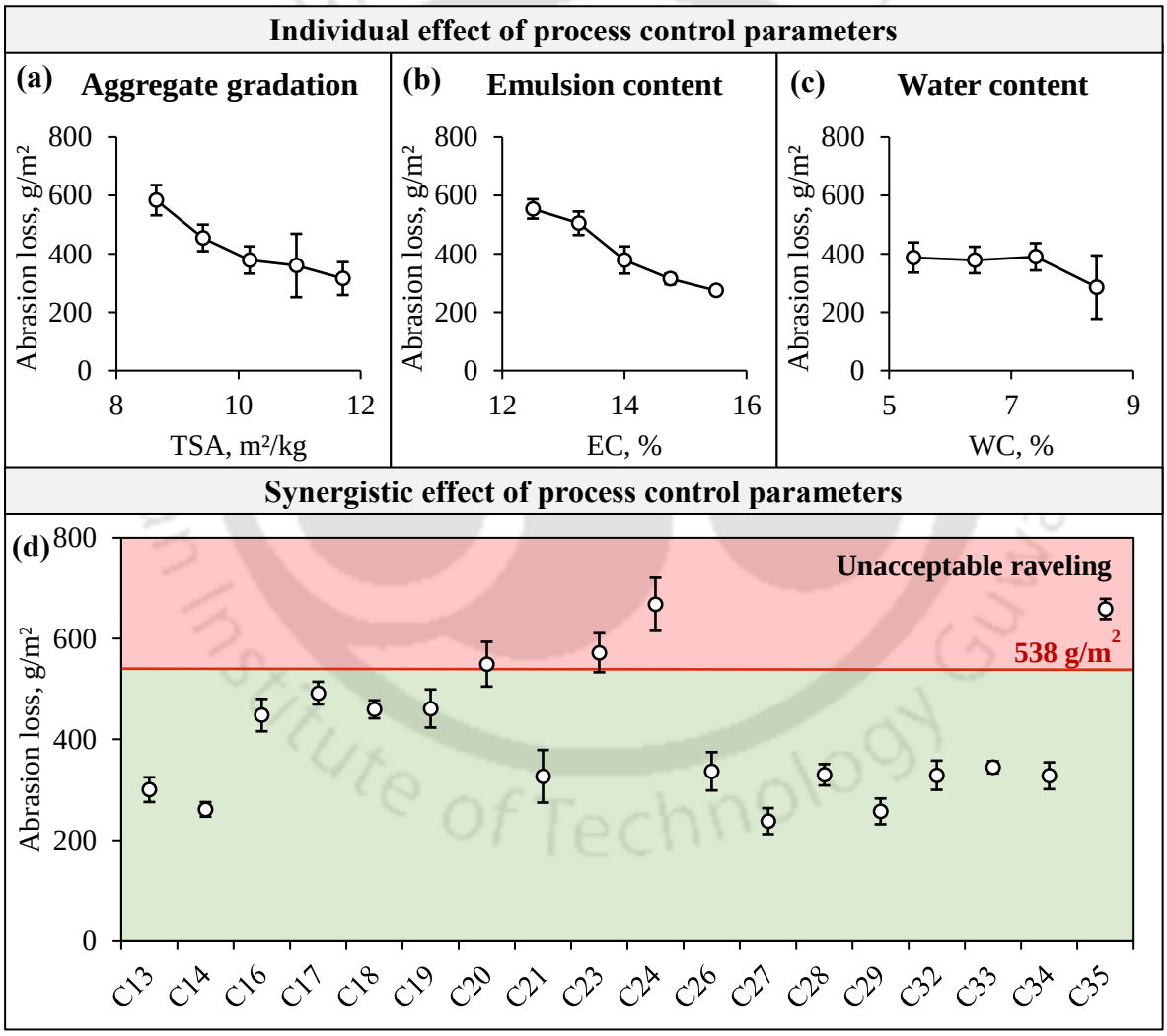

Figure 5.5: Synergistic influence of process control parameters on raveling

Critical parameters for raveling

The synergistic effect of process control parameters on raveling is illustrated in **Figure 5.5d**. Overall, the mixes with minimum abrasion loss were mix C14, C27, and C29. The common factor among the mixes was the higher emulsion content. This shows that higher emulsion content ensures that the adhesion between the aggregate and binder is strong enough to resist the abrasive action of traffic load, even with the variation of aggregate gradation and water content within the tolerance limits. Hence, the wearing qualities of microsurfacing mix under wet abrasion conditions improve by ensuring higher emulsion content in the tolerance limits range. Mix C23, C24 and C25 had the maximum abrasion loss. These mixes had coarser gradation and lower emulsion content. Hence, it could be said the combination of aggregate gradation on the coarser side and emulsion content on the lower side should be avoided during the production of microsurfacing mix.

5.3.4 Rutting

Results of rutting for 30 different combinations of aggregate gradation, emulsion content, and water content are illustrated in **Figure 5.6** in terms of lateral displacement. Error bars refer to ± standard deviation. For control mix, the lateral displacement was 3.5%. For the 30 combinations tested (with 4 replicates), the CoV varied from 3.8-16.7%, with the average CoV being 9.5%.

Aggregate gradation

Results of the influence of aggregate gradation on rutting is presented in **Figure 5.6a**. It was found that the lateral displacement increases for coarser gradation having relatively lower mineral content. On the other hand, compared to the control mix, the difference in lateral displacement is minimal for finer gradation. Proper aggregate interlock and better packing degree allow the mix to resist higher load and exhibit better rutting resistance. In microsurfacing, coarse aggregates provide a skeleton to resist deformation. Fine aggregates complete the aggregate structure by filling the void spaces in coarse aggregates. In the coarser gradation, the void spaces left by the coarse aggregates are not properly filled due to the lesser amount of fine aggregates. So, when the load is applied onto the mix having coarser gradation, higher lateral displacement was observed. In addition, the hydration of mineral filler, including cement and flyash, imparts stiffness and improves the resistance to compressive stresses. Hence, with a

relatively lower packing degree and lower mineral filler content, coarser gradation exhibited higher lateral deformation with the application of dynamic loading.

Emulsion content

The effect of emulsion content on rutting is shown in **Figure 5.6b**. It could be seen that the lateral displacement was minimal at an optimal value of emulsion content. With the increase in emulsion content, the lateral displacement decreased initially and then started increasing. This could be attributed to the higher air void content for lower emulsion content as the voids was not filled by asphalt. The void spaces would reduce on the application of load, and therefore, higher deformation was observed. Alternatively, with the increase in emulsion content, asphalt film thickness on the aggregate surface increases. Due to the increased asphalt film thickness, there is a reduction in friction and interlocking between aggregates, therefore higher deformation was observed.

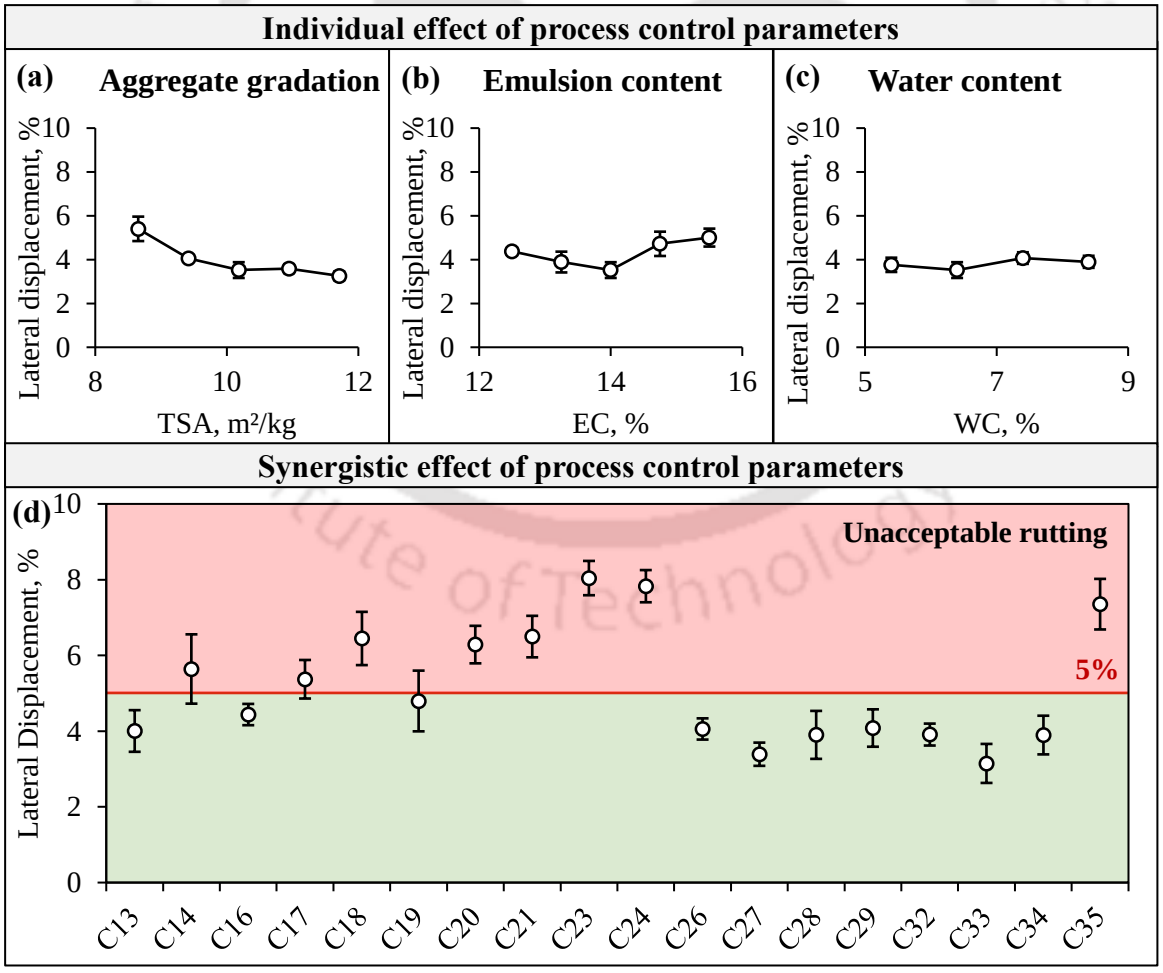

Figure 5.6: Synergistic influence of process control parameters on rutting

Water content

Even though aggregate gradation and emulsion content variation led to the difference in lateral displacement, there was no substantial impact of water content on the lateral deformation, as shown in **Figure 5.6c**.

Critical parameters for rutting

The investigations on the synergistic influence of process control parameters on rutting is illustrated in **Figure 5.6d**. It could be observed that the lateral displacement varied from 2.5% to 8.6%. In particular, the rutting was minimum for finer gradation having the combination of higher emulsion content and relatively lower water content or lower emulsion content and relatively higher water content. On the other hand, mixes having coarser gradation and lower emulsion content had relatively higher rutting. Hence, avoiding such scenarios in the field minimize the risk of rutting of microsurfacing mix.

5.3.5 Bleeding

Results of bleeding for 30 different combinations of aggregate gradation, emulsion content, and water content are illustrated in **Figure 5.7** in terms of sand adhesion. Error bars refer to ± standard deviation. For the control mix, the sand adhesion was 376 g/m^2. For the 30 combinations tested (with 4 replicates), the CoV varied from 1.6-16.6%, with the average CoV being 8.5%.

Aggregate gradation

Figure 5.7a shows the influence of aggregate gradation on bleeding. It could be seen that the sand adhesion increases with the decrease in the TSA of aggregates from 11.7 m^2/kg to 8.7 m^2/kg. Sand adhesion on the mix with a TSA of 8.7 m^2/kg was substantially higher than the other four. The lower sand adhesion with the increase in TSA was due to reduction in the asphalt film thickness as the emulsion has to coat more aggregate surface.

Emulsion content and water content

The effect of emulsion content on bleeding was not evident, as shown in **Figure 5.7b**. On the other hand, **Figure 5.7c** shows that the sand adhesion reduced considerably with the increase in water content. It could be due to the combined effect of residual asphalt content and surface texture of the microsurfacing mix. When the mix had higher consistency, i.e., the emulsion content or water content or both are on the higher side of optimum, the chances of segregation increase. In such cases, the finer particles tend

to move to the top whereas coarse particle settles down at the bottom. So, the sand does not stick to the smooth surface, and lower sand adhesion was observed. With the increase in emulsion content, excess asphalt was countered by the smoother surface texture, and hence, minimal variation in sand adhesion was noticed.

Critical parameters for bleeding

The synergistic influence of process control parameters on bleeding is shown in **Figure 5.7d**. It was found that the range of variation of sand adhesion was 208 g/m^2 to 692 g/m^2. The combination of finer gradation, lower emulsion content and higher water content had the least potential for bleeding. On the other hand, the combination of coarser gradation, higher emulsion content and relatively lower water content led to an increased risk of bleeding.

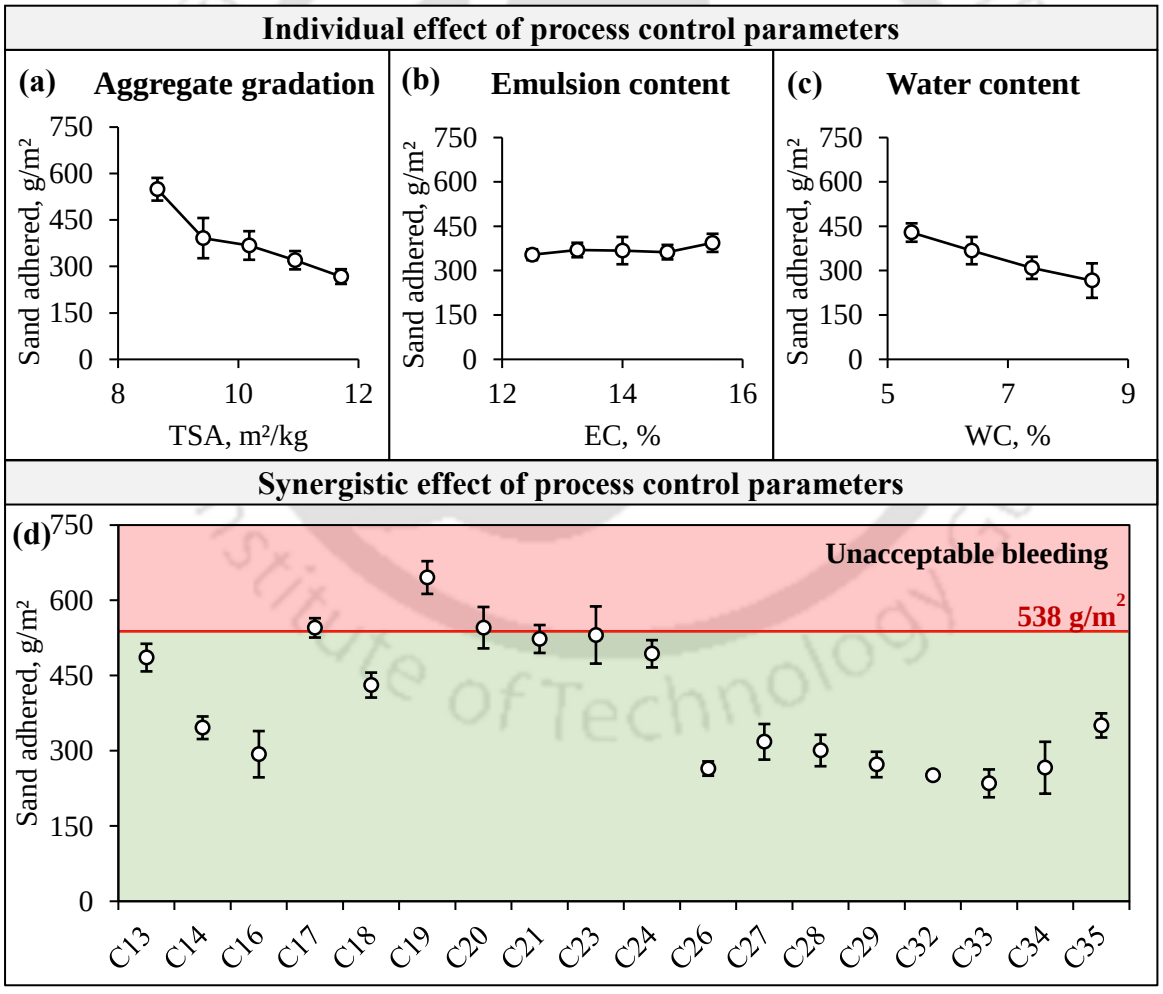

Figure 5.7: Influence of process control parameters on bleeding

5.4 Statistical analysis

The test results were statistically analyzed using univariate ANOVA at a significance level of 5%. The results of statistical analysis are shown in **Table 5.1**. It could be observed that the interaction of process control parameters had a significant influence on the consistency of the microsurfacing mix. In terms of cohesion, the interaction of aggregate gradation, expressed in terms of TSA, and emulsion content had a significant influence. In contrast, the interaction of emulsion content and water content did not contribute significantly. The individual effects of all process control parameters on the performance were significant, except emulsion content on cohesion at 60-min.

Table 5.1: Statistical analysis of the influence of process control parameter

Input parameter	Statistical parameter	Result					
		CT	**CH-30**	**CH-60**	**AL**	**LD**	**SA**
TSA	*p*-Value	0.000	0.000	0.000	0.000	0.000	0.000
	F	81.7	56.2	58.4	135.9	135.1	159.5
	Sig.	Yes	Yes	Yes	Yes	Yes	Yes
EC	*p*-Value	0.000	0.017	0.289	0.000	0.000	0.000
	F	404.7	3.2	1.3	48.3	8.2	7.2
	Sig.	Yes	Yes	No	Yes	Yes	Yes
WC	*p*-Value	0.006	0.001	0.000	0.000	0.000	0.000
	F	1281.0	5.6	7.6	10.5	15.7	48.7
	Sig.	Yes	Yes	Yes	Yes	Yes	Yes
TSA * EC	*p*-Value	0.000	0.003	0.027	0.000	0.000	0.399
	F	4.0	4.2	2.9	11.5	15.9	1.0
	Sig.	Yes	Yes	Yes	Yes	Yes	No
TSA * WC	*p*-Value	0.000	0.002	0.065	0.000	0.245	0.000
	F	7.1	3.7	2.1	10.6	1.3	5.4
	Sig.	Yes	Yes	No	Yes	No	Yes
EC * WC	*p*-Value	0.000	0.564	0.487	0.000	0.000	0.211
	F	19.0	0.7	0.9	7.5	6.1	1.5
	Sig.	Yes	No	No	Yes	Yes	No

** Note: CT = Consistency; CH-30 = 30-min Cohesion; CH-60 = 60-min Cohesion; AL = Abrasion Loss; LD = Lateral Displacement; SA = Sand adhesion; TSA = Total surface area; EC = Emulsion content; WC = Water content; Sig. = Significant*

In addition, it could be observed in **Table 5.1** that the interaction of all parameters contributes significantly to the raveling resistance of the microsurfacing mix. From the *F*-value, it could be said that the aggregate gradation had the highest impact on raveling. In contrast, the effect of WC on raveling was minimum among the parameters considered in the study.

The interaction of EC with TSA and WC resulted in significant differences in the lateral displacement results. Sand adhesion was significantly influenced by the interaction between TSA and WC. For all process control parameters, the individual effect on the rutting and bleeding characteristics of the microsurfacing mix was significant.

Owing to the significant difference in the production and performance parameters due to variation in process control parameter, it is vital to develop a model and quantify the relative contribution of each parameter to understand the changes in the behavior of microsurfacing mix when the variation of process control parameters is encountered in the field.

5.5 Relative contribution assessment using Artificial Neural Network

Artificial Neural Network (ANN) is an information-processing system that processes information by elements called neurons (Sivanandam & Deepa, 2006). The schematic diagram of a three-layer feed-forward network with three input variables, *n* hidden variables, and one output variable is represented in **Figure 5.8**.

In this network, the raw information is represented by the activity of neurons in the input layer. In contrast, the activity of neurons in the hidden and output layer is evaluated using activities of the previous layer and connection weights and bias. The activations in the input layer are fixed and propagated throughout the network until the determination of output layer values (Sivanandam & Deepa, 2006). ANN trains the available data to minimize the total square error. Hence, the developed model can effectively predict the output within the range of input variables values considered during training.

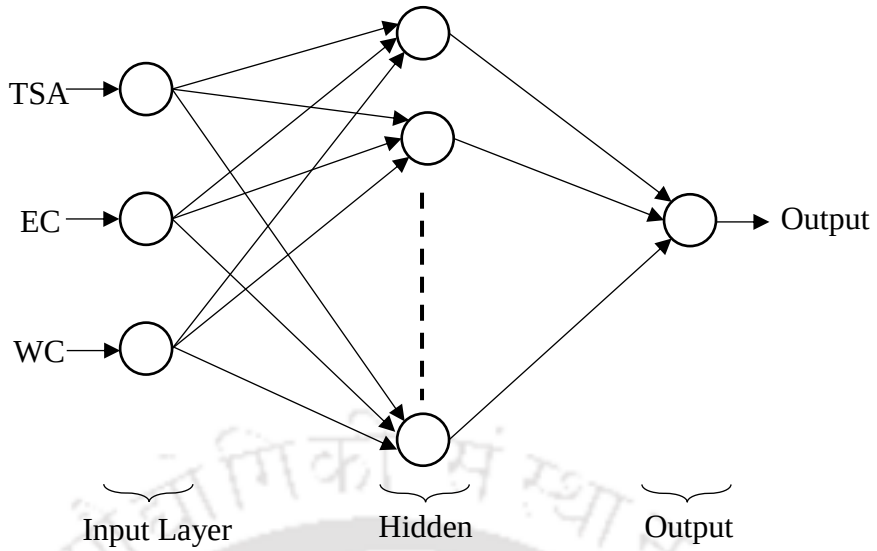

Figure 5.8: Schematic diagram of the feed-forward neural network

5.5.1 Input and output layers

The process control parameters which includes TSA of aggregates, emulsion content (EC), and water content (WC), were used for describing the input layer of the neural network. A total of 30 combinations were selected for input layer. Performance parameters, i.e., consistency, cohesion, raveling, rutting and bleeding, were used for describing the output layer.

Model construction with ANN involves minimizing the prediction error by effectively modifying the connection weights. Studies have also used ANN for modeling when the input-output relationship is complex and dataset is limited (Topçu & Saridemir, 2008; Xiao *et al.*, 2009; Firouzinia & Shafabakhsh, 2018). Hence, developing a model with 30 dataset using ANN should provide a good relation between input andoutput parmaeters.

5.5.2 Training

Levenberg-Marquardt backpropagation algorithm which is an advanced non-linear optimization algorithm (Hagan & Menhaj, 1994), was used for training the network with the support of MATLAB. In the feed-forward network (**Figure 5.8**), weights were assigned to all connections randomly. The weighted inputs were processed in each node, as shown in **Figure 5.9**. The transfer functions for hidden ($\varphi_h(v)$) and output layers ($\varphi_o(v)$) were tan-sigmoid (**Equation 5.1**) and a linear function (**Equation 5.2**) respectively (Tarefder *et al.*, 2005; Liu *et al.*, 2018).

$$\varphi_h(v) = \frac{2}{1 + e^{-2v}} - 1 \tag{5.1}$$

$$\varphi_o(v) = v \tag{5.2}$$

where, v = activation function. Subsequently, network layer connection weights were modified to minimize the error between network output and target values utilizing learning rules (Sivanandam & Deepa, 2006; Ozsahin & Oruc, 2008).

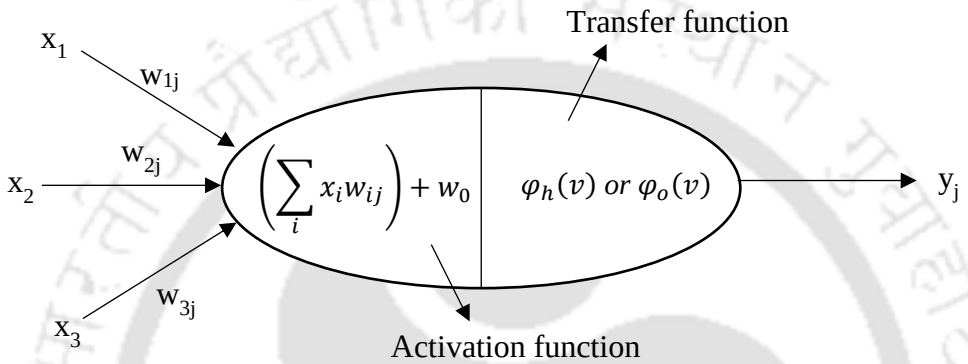

Figure 5.9: Schematic structure of a single neuron

5.5.3 Algorithm

The algorithm for ANN is shown in **Figure 5.10**. The data set containing 30 combinations were divided into 3 subsets: 20 for training, 5 for validation, and 5 for testing. Weights and bias were updated according to the error in the training dataset. The validation dataset was used to measure generalization. The network training was stopped when the generalization, i.e., validation performance, stops improving. The mean square error (MSE) between ANN predicted and laboratory determined raveling was defined as the network performance. The performance of network was assessed independently using a testing subset during and after training, where the network's performance was not affected by the testing subset.

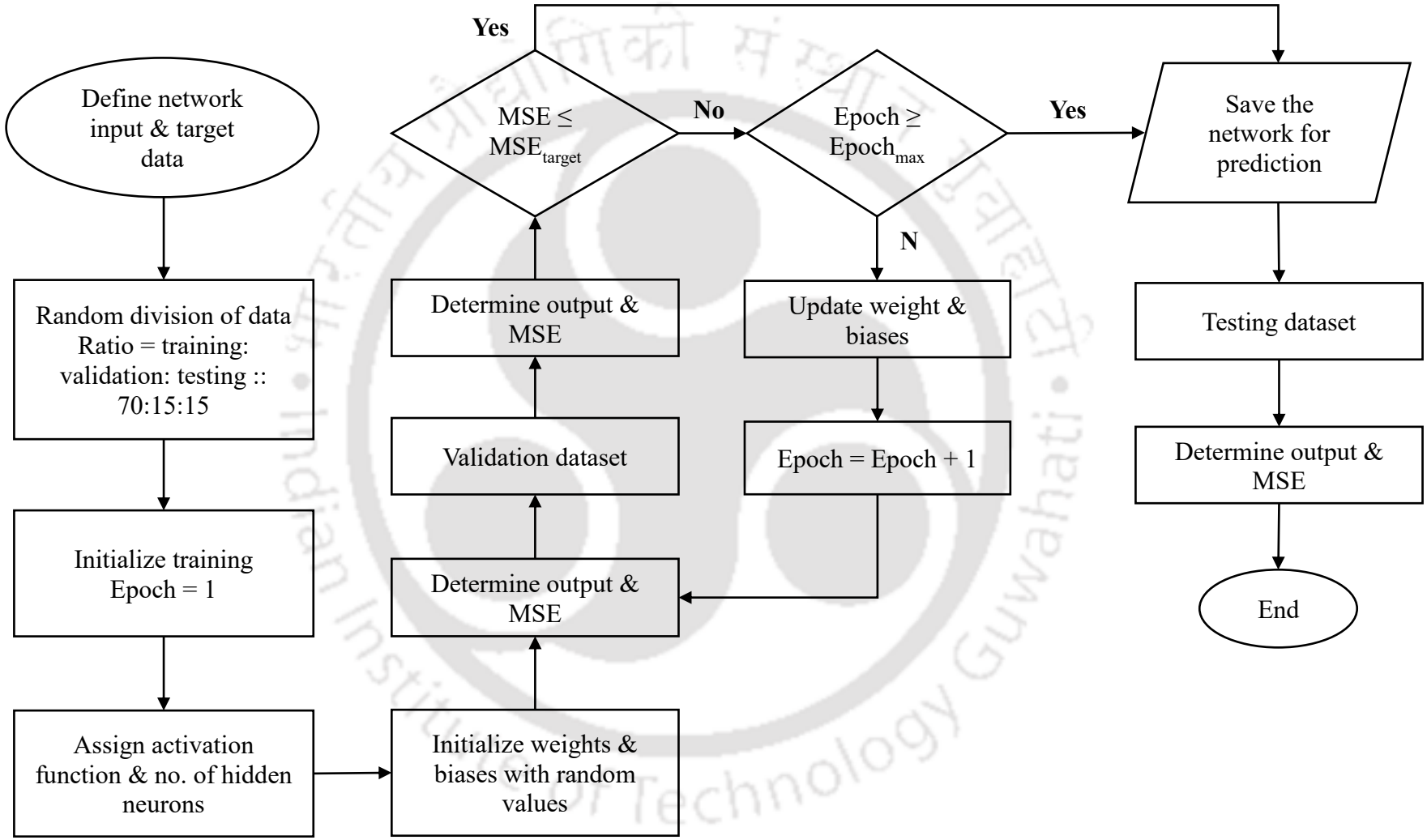

Figure 5.10: Architecture for Artificial Neural Network

5.5.4 Implementation of ANN for modeling microsurfacing performance

In this study, a three-layer feed-forward network with three input variables, *n* hidden variables, and one output variable was used for evaluating the network. Hidden variables were decided based on the MSE of the validation and testing data sets. Sivanandam and Deepa (2006) recommended that the number of hidden variables should be less than one plus two times number of input variables. Hence, for this study, since the number of input variables are 3, the number of hidden layer nodes was varied from 3 to 6, and the respective MSE was calculated. Here, an epoch was defined as the number of times the learning algorithm would read the input dataset and apply different calculations in one cycle through the training dataset. For each combination, the number of epochs was decided based on the MSE of the validation dataset. A typical example of the relation between MSE and the number of epochs is shown in **Figure 5.11**.

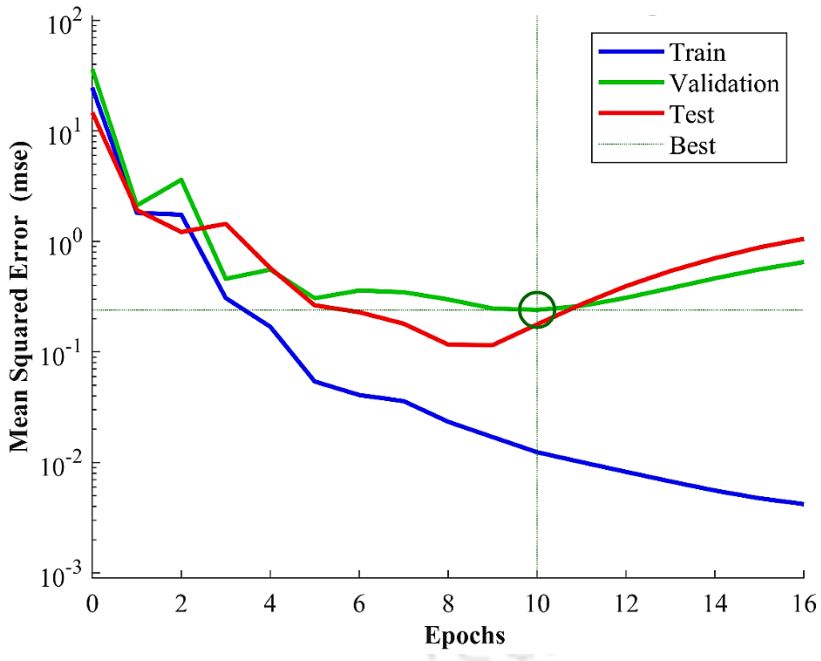

Figure 5.11: Variation of mean squared error with the number of epochs

The variation of ANN performance with number of hidden layer nodes is described in **Table 5.2.** It could be observed that the MSE for consistency, cohesion at 30-min, coesion at 60-min, raveling, rutting and bleeding was minimum with 6, 5, 6, 4, 6, and 4 hidden nodes, respectively. Hence, for further investigations, the desired number of hidden nodes was used along with three input variables and one output variable.

Table 5.2: Variation of ANN performance with hidden layer nodes

Parameter	Input node	Hidden node	Epoch	Mean Squared Error (MSE)			
				Training	Test	Validation	Overall
Consistency	3	3	9	0.03	0.26	0.00	0.06
	3	4	3	0.13	0.12	0.03	0.12
	3	5	4	0.04	0.11	0.04	0.05
	3	*6*	*11*	*0.03*	*0.05*	*0.06*	*0.04*
Cohesion	3	3	7	0.06	0.21	0.05	0.09
(30-min)	3	4	10	0.01	0.37	0.12	0.09
	3	*5*	*10*	*0.01*	*0.18*	*0.24*	*0.08*
	3	6	23	0.00	1.49	0.11	0.27
Cohesion	3	3	9	0.12	0.64	0.30	0.24
(60-min)	3	4	9	0.06	1.69	0.78	0.45
	3	5	8	0.11	2.53	0.38	0.56
	3	*6*	*8*	*0.06*	*0.41*	*0.71*	*0.22*
Raveling	3	3	4	2086	2244	5981	2761
	3	*4*	*10*	*188*	*4855*	*1941*	*1258*
	3	5	12	249	1068	8174	1707
	3	6	3	2273	1602	8515	3201
Rutting	3	3	11	0.07	0.29	0.55	0.18
	3	4	12	0.09	0.93	1.03	0.38
	3	5	3	0.07	0.45	0.17	0.15
	3	*6*	*9*	*0.01*	*0.12*	*0.18*	*0.06*
Bleeding	3	3	3	445	1438	230	575
	3	*4*	*13*	*723*	*219*	*191*	*550*
	3	5	4	81	3496	1532	892
	3	6	5	579	1001	634	658

After training the network and ensuring minimum error, the neural network output was compared with the target values. The correlation between the experimental results and predicted output from ANN is shown in **Appendix A**. It could be observed from these figures that the predicted output from ANN had a good correlation with the experimental results confirming the relevance of ANN for predicting performance.

5.5.5 Garson's algorithm

Garson's algorithm was used in the study for assessing the relative contribution of the input variable on the values of the output variable. In this method, the connection weights between the hidden and output layer of every hidden neuron were partitioned into components associated with every input neuron (Gevrey *et al.*, 2003). The effect of each input variable on the output variable was assessed by multiplying the connection weight direction. If the connection weight direction for both steps was positive, the input factor had a positive effect. Similarly, the input factor had a positive effect if the connection weight direction for both steps was negative. Otherwise, the effect was negative (Olden & Jackson, 2002).

Initially, the values of the connection weights for different links shown in **Figure 5.8** were derived from the network diagram. Then, the absolute of the connection weight between input variable *j* and hidden neuron *i* ($|W_{ij,ANN}|$) was multiplied by the absolute of the connection weight between the output variable and hidden neuron *i* ($|W_{i1,ANN}|$), as shown in **Equation 5.3**.

$$P_{ij,ANN} = |W_{ij,ANN}| \times |W_{i1,ANN}| \tag{5.3}$$

Subsequently, the relative contribution of each input neuron *j* to the outgoing signal for each hidden neuron i was determined. To do so, $Q_{ij,ANN}$ was calculated by dividing the $P_{ij,ANN}$ for each hidden neuron i to the sum of $P_{ij,ANN}$ for all input variables j connected to hidden neuron i, as shown in **Equation 5.4**. Then, using **Equation 5.5**, the sum of $Q_{ij,ANN}$ was determined for each input variable j and denoted as $S_{j,ANN}$. Finally, to determine the relative contribution of each input variable j, $RC_{j,ANN}$, the $S_{j,ANN}$ for the input variable j was divided by the sum of $S_{j,ANN}$ for all input variables (**Equation 5.6**).

$$Q_{ij,ANN} = \frac{P_{ij,ANN}}{\sum_j P_{ij,ANN}} \tag{5.4}$$

$$S_{j,ANN} = \sum_i Q_{ij,ANN} \tag{5.5}$$

$$RC_{j,ANN} = \frac{S_{j,ANN}}{\sum_j S_{j,ANN}} \tag{5.6}$$

Application of Garson's algorithm for relative contribution assessment

The relative contribution of aggregate gradation, emulsion content, and water content were determined using Garson's algorithm. For this purpose, the connection weights were initially determined using the Simulink diagram provided in the Neural Network fitting app of MATLAB. The connection weights of input-hidden layers and hidden-output layers obtained in the study are provided in **Table 5.3**. Subsequently, using the connection weights, the relative contribution of each parameter was determined using Garson's algorithm. The step-by-step procedure adopted is described below (Olden & Jackson, 2002; Gevrey *et al.*, 2003):

a) Connection weight of input-hidden layer was multiplied to the connection weight of hidden-output layer for each hidden neuron *i*.
b) The process was repeated for all input variables *j* and calculate the product P_{ij} using **Equation 5.3** to assess input variables' contribution to the output layer.
c) The absolute of P_{ij} was divided by the sum of absolute values of P_{ij} for all input variables to determine Q_{ij} (**Equation 5.4**).
d) For each input neuron, the values of Q_{ij} were added to determine the Sum (S_j) (**Equation 5.5**).
e) The relative contribution of each input variable was determined by dividing S_j by summation of S_j for all input variables (**Equation 5.6**).

The parameters P_{ij} and Q_{ij} for all the parameters is described in **Table 5.4**. Subsequently, using the values of P_{ij} and Q_{ij}, the value of parameter S_j was calculated, as shown in **Table 5.5**. The results of the relative contribution of input parameters using Garson's algorithm are described in **Figure 5.12**. It could be observed from **Figure 5.12** that the relative contribution of the following parameters on the performance of the microsurfacing mix was more than 35%:

- Workability – Emulsion content (44%) and water content (42%).
- Strength (30-min) – Aggregate gradation (40%) and emulsion content (37%).
- Strength (60-min) – Water content (44%) and aggregate gradation (35%).
- Raveling – Aggregate gradation (40%).
- Rutting – Emulsion content (40%).
- Bleeding – Water content (42%).

Table 5.3: Connection weights

Parameter (Output)	Hidden neuron	Weights			
		AG	EC	WC	Output
Consistency	Hidden 1	-0.392	1.215	1.012	0.706
	Hidden 2	0.171	1.132	-2.743	-0.596
	Hidden 3	-0.409	3.860	-1.182	0.122
	Hidden 4	1.240	1.340	-4.027	-0.259
	Hidden 5	2.827	-2.377	3.449	0.052
	Hidden 6	0.123	-2.268	0.813	-0.976
Cohesion (30-min)	Hidden 1	0.009	-3.679	-0.432	0.050
	Hidden 2	-1.437	-0.413	-1.774	-0.856
	Hidden 3	0.749	-0.314	-0.065	1.443
	Hidden 4	-1.365	1.278	-0.583	0.415
	Hidden 5	-2.458	-0.749	-1.563	0.431
Cohesion (60-min)	Hidden 1	-0.853	1.784	0.583	0.393
	Hidden 2	0.945	4.817	3.405	-0.365
	Hidden 3	3.321	-0.568	4.769	0.154
	Hidden 4	-2.164	-0.044	1.379	-0.650
	Hidden 5	3.189	0.342	4.327	0.174
	Hidden 6	0.942	0.075	-1.583	0.407
Raveling	Hidden 1	4.381	8.484	-0.790	-0.094
	Hidden 2	-2.638	-0.869	-1.733	0.514
	Hidden 3	-6.704	0.347	-7.956	0.268
	Hidden 4	8.089	-7.418	8.921	0.372
Rutting	Hidden 1	0.090	0.485	3.425	0.146
	Hidden 2	-2.705	-2.147	0.766	0.535
	Hidden 3	2.159	3.221	-0.354	0.588
	Hidden 4	-3.556	1.393	1.893	0.403
	Hidden 5	-1.163	-0.815	-0.388	1.599
	Hidden 6	-0.034	0.762	0.200	-1.285
Bleeding	Hidden 1	0.182	1.121	-6.039	-0.012
	Hidden 2	0.694	-0.113	0.472	-1.189
	Hidden 3	-20.054	16.023	-0.101	-0.047
	Hidden 4	-1.401	4.333	5.402	0.053

Table 5.4: Different parameters (P_{ij} and Q_{ij}) of Garson's algorithm

Parameter	Hidden neuron	P_{ij}			Q_{ij}		
		AG	EC	WC	AG	EC	WC
Consistency	Hidden 1	0.28	0.86	0.71	0.15	0.46	0.39
	Hidden 2	0.10	0.68	1.64	0.04	0.28	0.68
	Hidden 3	0.05	0.47	0.14	0.08	0.71	0.22
	Hidden 4	0.32	0.35	1.04	0.19	0.20	0.61
	Hidden 5	0.15	0.12	0.18	0.33	0.27	0.40
	Hidden 6	0.12	2.21	0.79	0.04	0.71	0.25
Cohesion (30-min)	Hidden 1	0.00	0.18	0.02	0.00	0.89	0.10
	Hidden 2	1.23	0.35	1.52	0.40	0.11	0.49
	Hidden 3	1.08	0.45	0.09	0.66	0.28	0.06
	Hidden 4	0.57	0.53	0.24	0.42	0.40	0.18
	Hidden 5	1.06	0.32	0.67	0.52	0.16	0.33
Cohesion (60-min)	Hidden 1	0.33	0.70	0.23	0.26	0.55	0.18
	Hidden 2	0.34	1.76	1.24	0.10	0.53	0.37
	Hidden 3	0.51	0.09	0.74	0.38	0.07	0.55
	Hidden 4	1.41	0.03	0.90	0.60	0.01	0.38
	Hidden 5	0.55	0.06	0.75	0.41	0.04	0.55
	Hidden 6	0.38	0.03	0.64	0.36	0.03	0.61
Raveling	Hidden 1	0.41	0.80	0.07	0.32	0.62	0.06
	Hidden 2	1.36	0.45	0.89	0.50	0.17	0.33
	Hidden 3	1.80	0.09	2.13	0.45	0.02	0.53
	Hidden 4	3.01	2.76	3.32	0.33	0.30	0.37
Rutting	Hidden 1	0.01	0.07	0.50	0.02	0.12	0.86
	Hidden 2	1.45	1.15	0.41	0.48	0.38	0.14
	Hidden 3	1.27	1.90	0.21	0.38	0.56	0.06
	Hidden 4	1.43	0.56	0.76	0.52	0.20	0.28
	Hidden 5	1.86	1.30	0.62	0.49	0.34	0.16
	Hidden 6	0.04	0.98	0.26	0.03	0.76	0.20
Bleeding	Hidden 1	0.00	0.01	0.07	0.02	0.15	0.82
	Hidden 2	0.83	0.13	0.56	0.54	0.09	0.37
	Hidden 3	0.94	0.75	0.00	0.55	0.44	0.00
	Hidden 4	0.07	0.23	0.29	0.13	0.39	0.49

Table 5.5: Parameter S_j of Garson's algorithm

Parameter	*Sum, S_j*		
	AG	**EC**	**WC**
Consistency	0.82	2.64	2.54
Cohesion (30-min)	0.00	0.89	0.10
Cohesion (60-min)	0.40	0.11	0.49
Raveling	1.60	1.11	1.28
Rutting	0.02	0.12	0.86
Bleeding	0.48	0.38	0.14

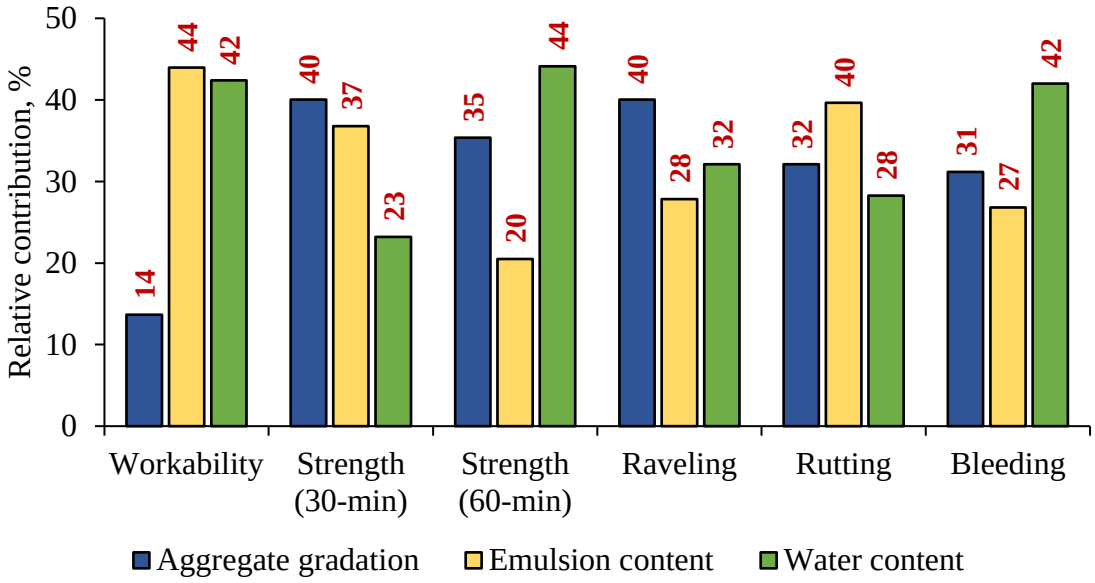

Figure 5.12: Relative contribution of process control parameter on performance

5.6 Multigene Symbolic Genetic Programming (MSGP)

Genetic programming (GP) is a symbolic optimization technique that utilizes automated computer programs to find the best solution to a complicated problem based on the principle of Darwinian Natural Selection (Koza, 1992; Gandomi & Alavi, 2012). Unlike conventional regression, a predetermined functional form is not required in GP. Instead, GP uses the library of operators, and the best expression is determined by the evolution of the generation of expressions using genetic operators like mutation and crossover (Kumar *et al.*, 2014). Multigene symbolic genetic programming (MSGP), a robust variant of GP, automatically evolves the model structure and its coefficients from

the multiple genes, where each gene represents a tree expression. In MSGP, a search heuristic is evolved where each expression generated performs better, i.e., provides a better correlation coefficient, than the previous generation (Searson *et al.*, 2010). Owing to its accuracy and ease of computation, the use of MSGP to develop mathematical models has gained popularity in recent times, especially in the field of transportation systems engineering (Alavi *et al.*, 2017; Das *et al.*, 2020; Pattanaik *et al.*, 2020).

Symbolic regression is an inductive learning process in which a symbolic mathematical function is identified to best describe the output in terms of minimal input parameters (Das *et al.*, 2020). A pictorial representation of the general multigene symbolic regression model is illustrated in **Figure 5.13**.

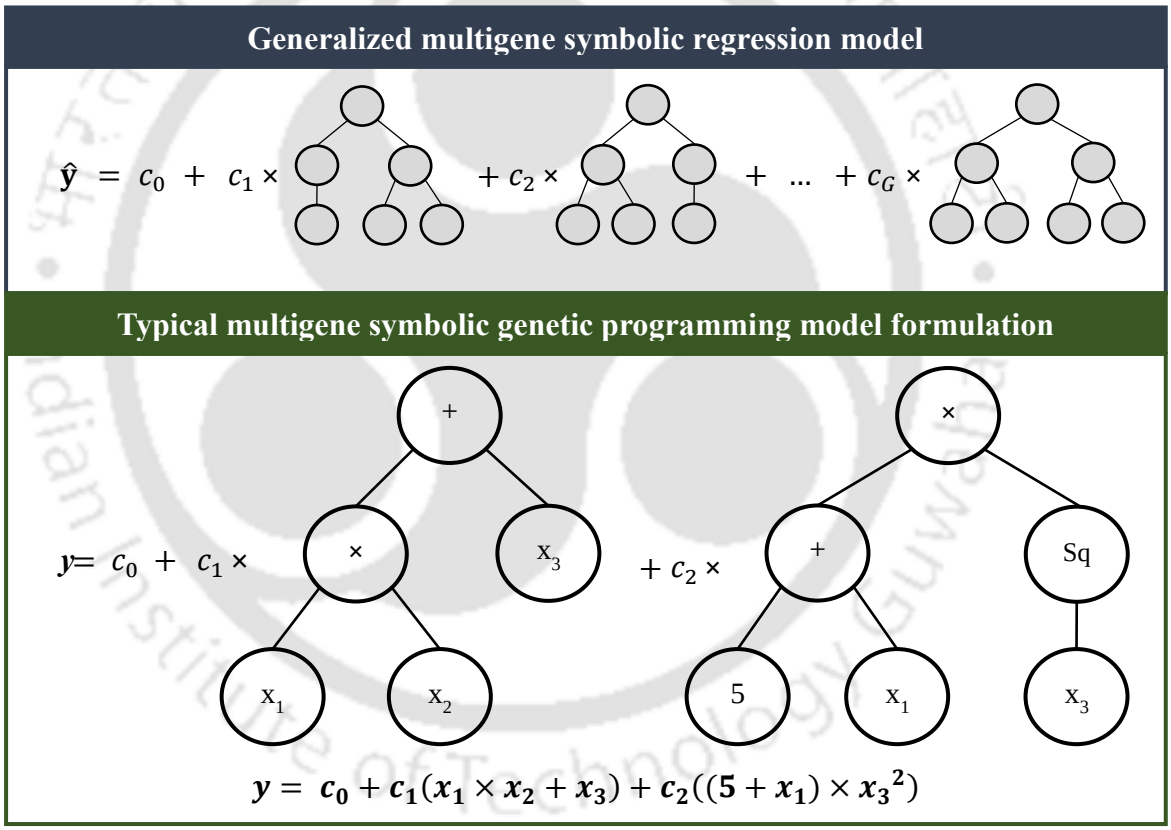

Figure 5.13: Typical MSGP model formulation

The prediction of output (**y**) from training data could be mathematically written as described in **Equation 5.7** (Searson, 2015).

$$\hat{\boldsymbol{y}} = c_{0,GP} + c_{1,GP}\boldsymbol{t}_{1,GP} + c_{2,GP}\boldsymbol{t}_{2,GP} + \cdots + c_{G,GP}\boldsymbol{t}_{G,GP} \quad (5.7)$$

where, $\boldsymbol{t}_{i,GP}$ = (N×1) vector of outputs from the ith gene/tree having a multigene individual; $c_{0,GP}$ = bias/offset coefficient; $c_{1,GP}$,.. $c_{G,GP}$ = scaling term for respective tree/gene.

In this study, the prediction model was formulated using MATLAB toolbox entitled GPTIPS. GPTIPS is a command-line-driven open-source toolbox with several in-built functions to simplify the post-run analysis of results. Besides, GPTIPS enforces the use of a maximum number of genes (G_{max}) and maximum tree depth (D_{max}) that allows the user to control the maximum complexity and promotes the evolution of comparatively compact models (Searson *et al.*, 2010; Gandomi & Alavi, 2012).

5.6.1 Model development

The architecture for model development using MSGP in GPTIPS is illustrated in **Figure 5.14**. In GPTIPS, the initial population of multi-tree solutions was constructed by creating individuals having GP trees that were randomly generated, where the number of genes was between *1* and G_{max} (Gandomi & Atefi, 2020). The population was then evolved for several generations (iterations) by copying, mutation, and recombination operators, as shown in **Figure 5.15**.

In MSGP, three recombination operators were used: tree crossover, sub-tree crossover, and sub-tree mutation. A tree crossover operator, known as a two-point high-level crossover, was used for acquiring and deleting genes. Sub-tree crossover or low-level crossover was performed for randomly selected genes from each parent individual. The parent trees were replaced with the resulting trees in the otherwise unchanged individual in the next generation (Searson *et al.*, 2010). In a sub-tree mutation, a randomly selected sub-tree of the parent was deleted, and a new sub-tree was randomly generated using the initial tree building algorithm. The resulting expression was introduced into the new population. The relative probabilities of each of the recombinative processes were grouped into categories known as events. The sum of the events (crossover, direct reproduction, and mutation) was 1 (Searson *et al.*, 2010).

At each generation, individuals were selected for breeding based on either its fitness (regular tournament) or both fitness and complexity (Pareto tournaments) (Searson, 2015). The fitness function adopted in this study was a root mean square error (RMSE) between the observed and predicted results.

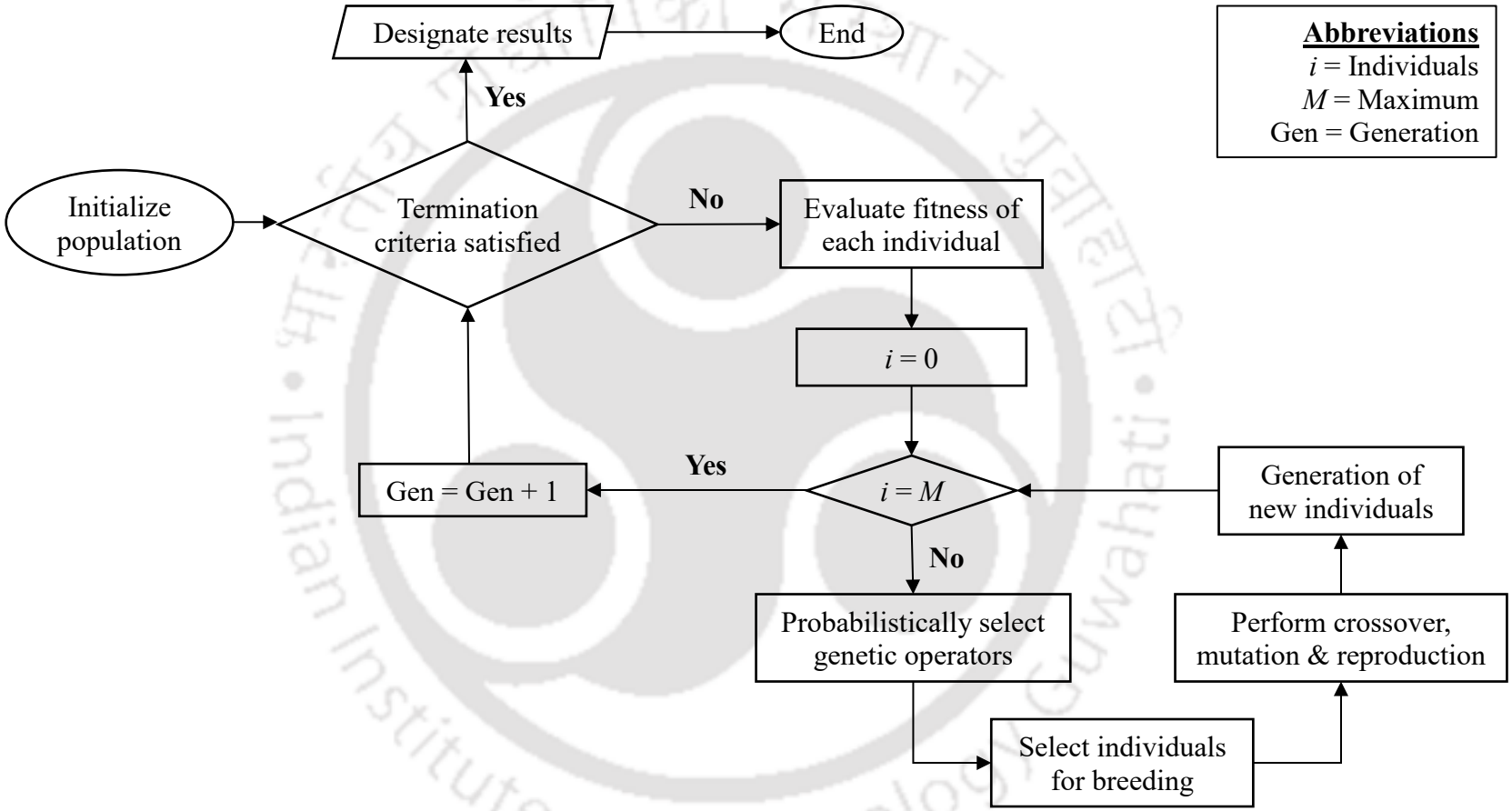

Figure 5.14: Architecture for model development using MSGP

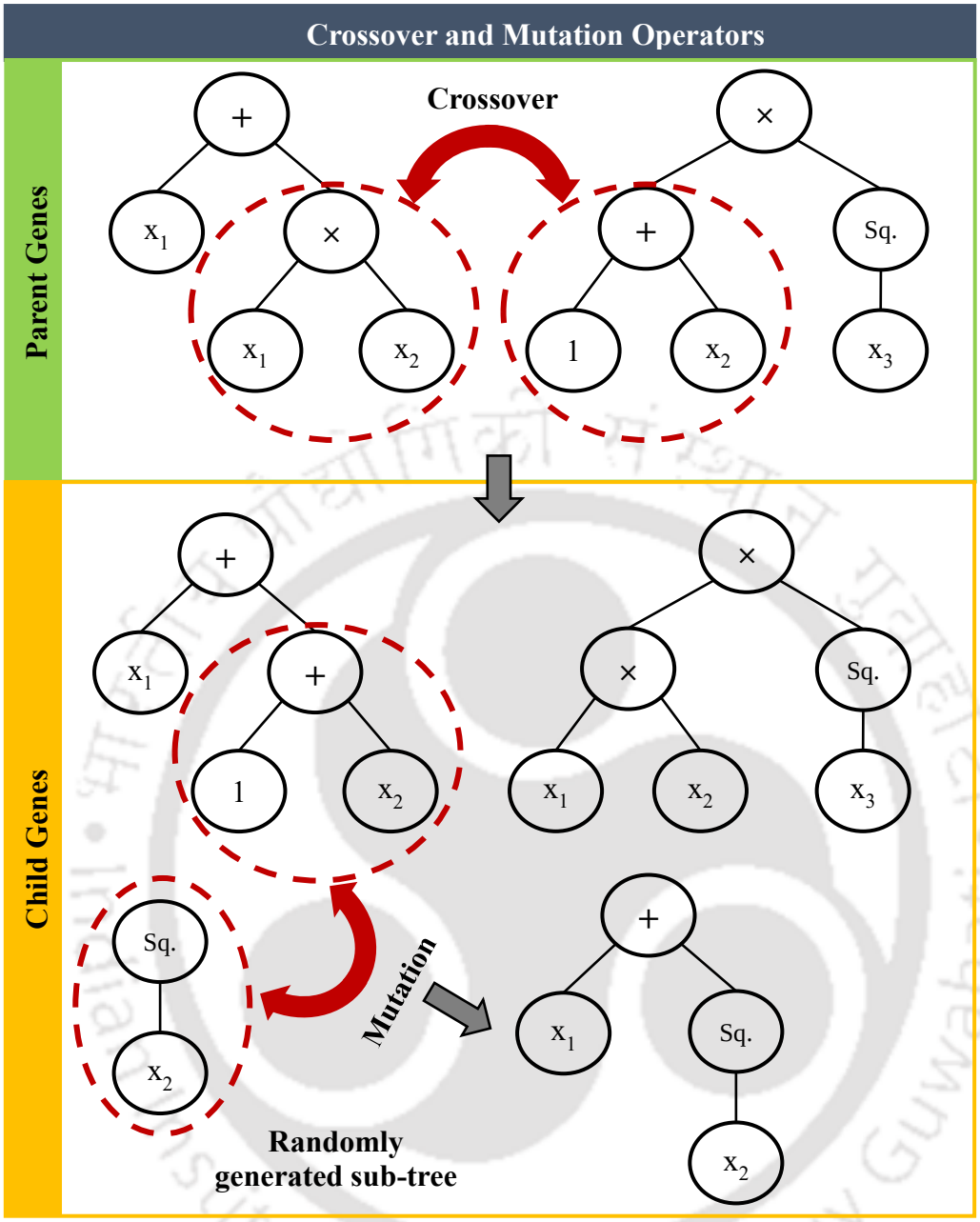

Figure 5.15: Typical example of crossover and mutation

5.6.2 Dataset for model formulation using MSGP

To predict test results, 80% of the total data presented in **Section 5.3** were selected as a training dataset for MSGP. The rest 20% were used as a testing dataset to validate the developed model. Each of the input parameters and test results was described with respect to the control mix (mix C1) to remove the biasedness of results due to the magnitude of input and output values. For instance, for mix C32, the TSA, EC, and WC were 1.15 ($TSA_{mix\ C32}$ / $TSA_{control\ mix}$ =11.7/10.2), 0.89 ($EC_{mix\ C32}$ / $EC_{control\ mix}$ =12.5/14), and 1.16 ($WC_{mix\ C32}$ / $WC_{control\ mix}$ =5.4/6.4), respectively.

5.6.3 Parameter effect on MSGP based model

Initially, the parameters were varied over a wide range of values to improve the model performance, i.e., minimize error. A trial-and-error-based technique was used to find the best set of parameters. The parameters were varied one by one while keeping the other parameters constant. For each varied parameter, the RMSE was calculated, and the set of parameters with minimum RMSE were selected.

In this study, initial values of parameters were kept at the default values of the GPTIPS toolbox, and the parameters were varied one by one. The population size (number of models generated in a single generation) and the number of generations (iterations) was varied from 10-1000 and 10-300 respectively, to ensure higher accuracy (reduces with lower population size) within reasonable computational effort (increases with higher population size). Next, the values of G_{max} and D_{max} were selected from the range of 2-4. Even though higher G_{max} and D_{max} might capture the non-linear behavior better, but the chances of overfitting the training data increases (Gandomi & Alavi, 2012).

Subsequently, tournament size (%) was varied from 5-70 to control the selection pressure. Higher tournament size allows a fast convergence rate due to high parent selection pressure, but there is a risk of obtaining a locally optimal solution. Then, elitism, a technique where the individuals are copied unchanged from one generation to the next, was selected. The elite fraction (elite size / population size) was varied between 0.05 to 1.

The probability of mutation and crossover were varied between 0.1-0.3 and 0.88-0.68, respectively. Increasing the probability of mutation allows finding the solution outside the subspace, thus increasing the diversity of the population. Crossover provides the convergence of a solution within the subspace. The probability of direct reproduction was kept at the default value, i.e., 0.02. The sum of mutation, crossover, and direct reproduction probability was kept 1. At every selection event, i.e., selecting individuals for mutation, crossover, or direct reproduction, the probability of the Pareto tournament is selected from 0-1.

The variation of R^2 with different model parameter values for all the performance parameters are illustrated in **Appendix B**. The parameter values were selected based on R^2 and are described in **Table 5.6**. The models were developed considering the parameter values selected for the input parameters.

Table 5.6: Parameter settings for modeling using MSGP

Parameter	Parameter settings for model development with MSGP					
	CT	***CH_{30}***	***CH_{60}***	***AL***	***LD***	***SA***
Population size	1000	1000	1000	1000	500	400
Number of generations	150	150	150	150	100	100
Maximum genes	4	4	4	4	4	4
Maximum tree depth	4	4	4	4	4	4
Tournament size	10	10	10	20	15	10
Elite fraction	0.15	0.15	0.15	0.15	0.15	0.15
M-C-D probability*	M = 0.14 C = 0.84 D = 0.02	M = 0.30 C = 0.68 D = 0.02	M = 0.14 C = 0.84 D = 0.02	M = 0.14 C = 0.84 D = 0.02	M = 0.14 C = 0.84 D = 0.02	M = 0.14 C = 0.84 D = 0.02
Probability of Pareto tournament	0	0	0.15	0	0.20	0

* **Note:** *CT = Consistency; CH_{30} = Cohesion at 30 minutes; CH_{60} = Cohesion at 60 minutes; AL = Abrasion Loss; LD = Lateral Displacement; SA = Sand adhesion; M-C-D probability = Probability of mutation, crossover and direct reproduction respectively.*

5.6.4 Development and testing of MSGP based models

Using the parameters in **Table *5.6***, the model was developed using the MSGP algorithm. The set of primitive functions used for model development include multiplication (times), subtraction (minus), addition (plus), division (rdivide), square (square), exponential (exp), square root (sqrt), and natural logarithm (log). The model developed using these primitive functions with the least error for the training and test dataset, and lower equation complexity was selected as the best MSGP model.

The mathematical expressions for describing consistency, cohesion at 30-min and 60-min, abrasion loss, lateral displacement and sand adhesion in terms of TSA, EC and WC are provided in **Equation 5.8** to **5.13**, respectively.

$$\begin{aligned} CT = {} & 17.43 \times TSA - 15.37 \times EC - 10.93 \times WC - 19.24 \times EC^2 \times WC^2 \\ & - 21.2 \times TSA \times EC - 21.2 \times TSA \times WC \\ & + 21.2 \times EC \times WC + 14.8 \times EC \times WC^2 + 6.493 \times EC^3 \\ & + 23.67 \times TSA \times EC \times WC + 5.411 \end{aligned} \tag{5.8}$$

$$\begin{aligned} CH_{30} = {} & 0.08932 \times EC + 0.08932 \times WC + 0.8231 \times ln(EC) \\ & - 0.2217 \times TSA \times EC + 0.08932 \times EC^2 \\ & - \frac{8.876 \times ln(EC)}{9.007 \times \left(TSA^2 + ln(WC)\right)} - \frac{0.2217 \times TSA \times EC^2}{WC} \\ & + \frac{0.2217 \times TSA \times EC^2}{WC^2} \\ & + 0.5016 \times TSA \times WC^3 \times ln(TSA) + 0.9477 \end{aligned} \tag{5.9}$$

$$\begin{aligned} CH_{60} = {} & \frac{-1.196 \times TSA^2 + 2.392 \times WC}{1441 \times (EC + WC) - \frac{2.914}{WC}} - 0.02452 \times \left(e^{TSA^2} + e^{e^{EC}}\right) \\ & - 0.2334 \times WC + \frac{0.5386}{WC} - 0.2334 \times \sqrt{EC} \\ & + 0.07342 \times TSA \times WC \times e^{2 \times EC} + 0.8341 \end{aligned} \tag{5.10}$$

$$AL = 5.893 \times ln\left(\frac{WC}{TSA}\right) - 2.946 \times ln(WC) + 0.3712 \times e^{2\times EC} \times (-1 \times WC^2 + TSA \times WC) + \frac{0.643 \times TSA^2}{EC^2} - 214.9 \times \left(ln(EC)\right)^2 \times \left(ln(WC)\right)^2 + 0.4224 \quad (5.11)$$

$$LD = 8.47 \times (TSA + EC)^2 - 0.8128 \times e^{2\times TSA\times EC} - 32.59 \times ln\left(ln(TSA + EC)\right) + 0.8631 \times EC^2 \times WC^2 \times (-WC^2 + WC + EC) - 39.59 \quad (5.12)$$

$$SA = 0.1327 \times e^{\left(TSA(WC+2.689)\right)} - 0.9221 \times e^{\left(\frac{EC^2}{TSA}\right)} + 0.6544 \times e^{\left(\frac{EC^3}{TSA}\right)} - 5.474 \times \sqrt{TSA \times (WC + 2.256)} + 11.05 \quad (5.13)$$

where, CT = Consistency; CH_{30}= Cohesion at 30-min; CH_{60}= Cohesion at 60-min; AL = Abrasion Loss; LD = Lateral displacement; SA = sand adhesion; TSA = Total surface area of aggregates; EC = Emulsion content; and WC = Water content.

The RMSE and R^2 for both the training and testing dataset is shown in **Figure 5.16** and **Figure 5.17**. It could be observed that the model developed using MSGP had a good performance, with the R^2 of both training and test data being more than 0.9 for all test parameters except abrasion loss, where R^2 was more than 0.78. Hence, the model developed using MSGP was able to capture the influence of process control parameters on the performance of the microsurfacing mix.

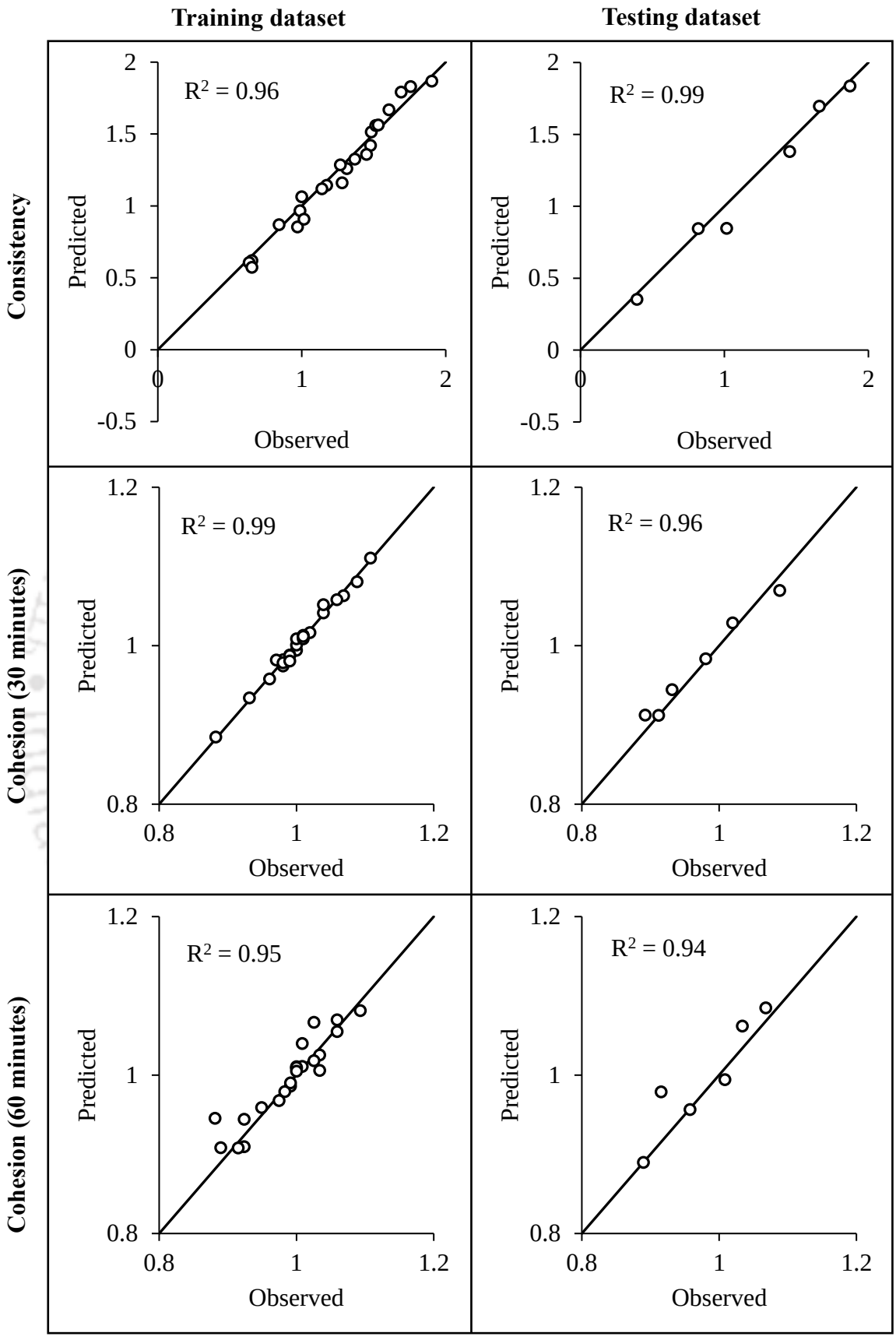

Figure 5.16: MSGP predicted and observed consistency and cohesion

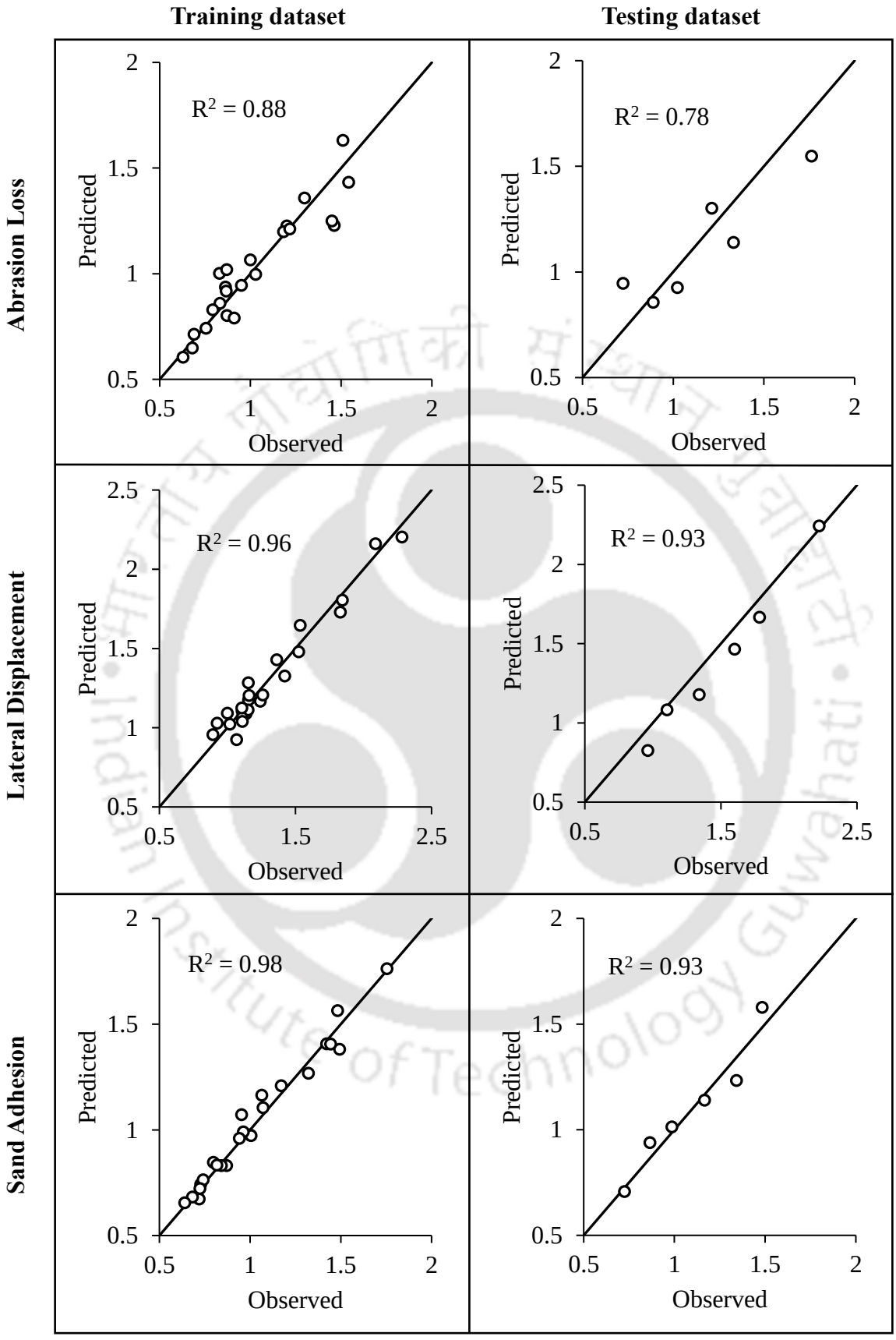

Figure 5.17: MSGP predicted and observed raveling, rutting and bleeding

5.6.5 Sensitivity analysis

Sensitivity analysis was used to interpret the influence of input parameters on the output variable. The architecture for sensitivity analysis is shown in **Figure 5.18**. The value of i = 1 represented the value of process control parameters for control mix, i.e., Mean of Type II gradation for aggregate gradation, OEC for emulsion content and OWC for water content. The range of variation considered for sensitivity analysis was ±20% of control mix. So, the values of input parameters were varied one by one from 0.80-1.20 at an increment of 0.005. For each input parameter value, the value of the output parameter was computed.

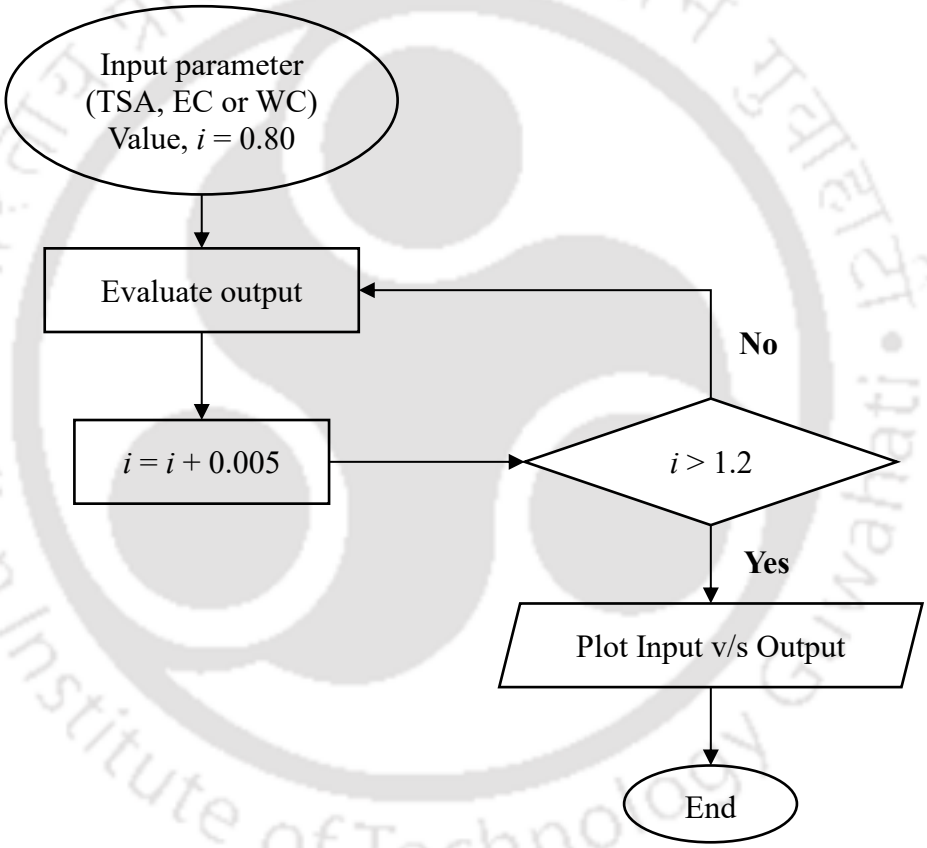

Figure 5.18: Architecture for sensitivity analysis

Results of sensitivity analysis are illustrated in **Figure 5.19**. The analysis was divided into a total of 18 combinations including 6 tests and 3 input parameters. The values 1 to 6 were assigned for tests and alphabets (a) to (c) were assigned for input parameters. For instance, in **Figure 5.19(4b)** depicts the effect of emulsion content on the raveling of microsurfacing mix.

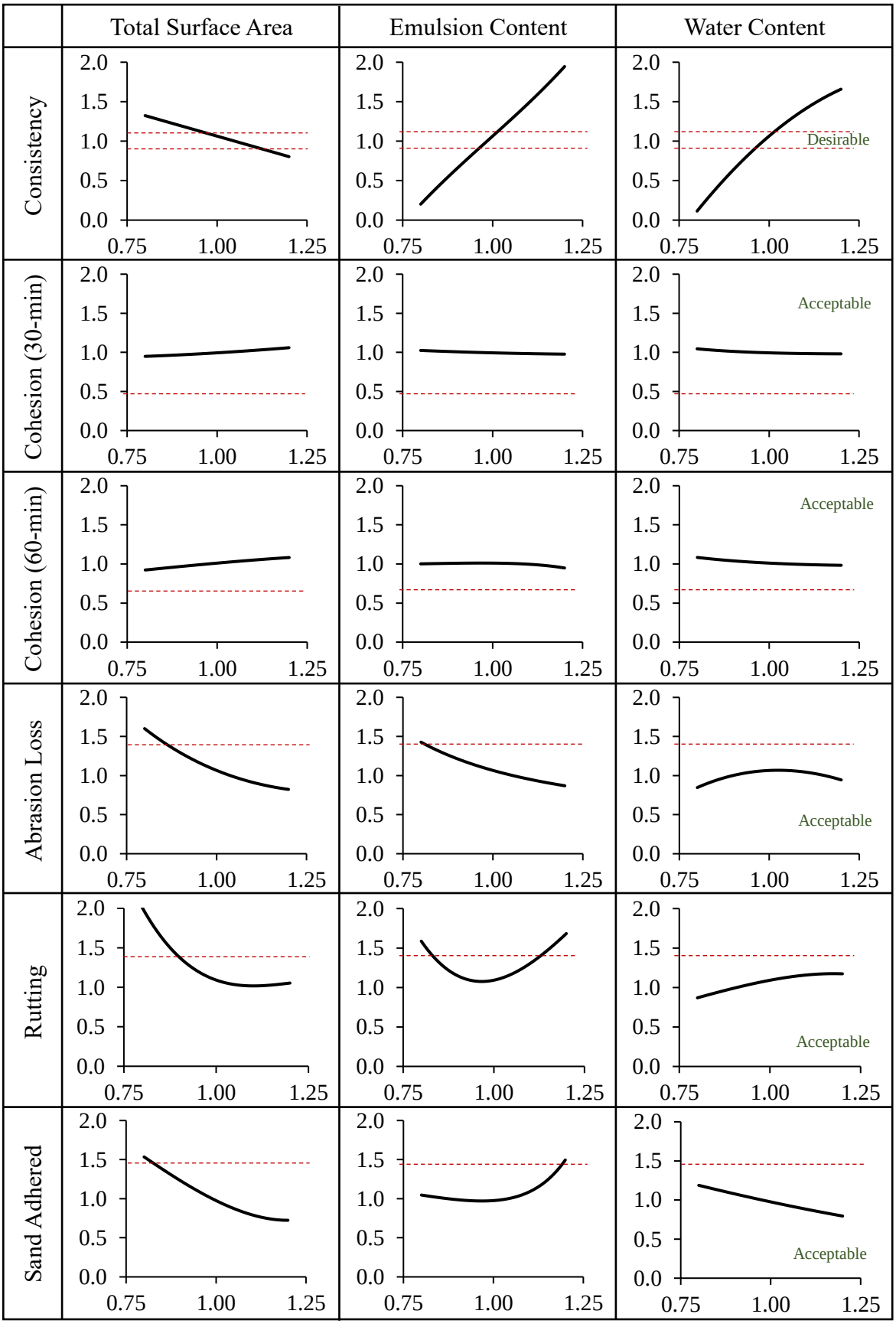

Figure 5.19: Sensitivity analysis of MSGP model formulation

It could be observed from **Figure 5.19(1)** that all the parameters had a substantial impact on consistency, whereas cohesion did not vary substantially, as shown in **Figure 5.19(2)** and **Figure 5.19(3)**. Consistency varied in the range of 0.11-1.95, whereas variation was only 0.92-1.08 for cohesion. Consistency constantly increased with the decrease in TSA and increased emulsion and water content. On the other hand, cohesion constantly increased with the increase in TSA (finer gradation) and decreased with the increase in water content.

With the increase in TSA and emulsion content, **Figure 5.19**(**4a**) and **Figure 5.19**(**4b**) shows that the abrasion loss initially decreased at a rapid rate. Subsequently, the rate of reduction of abrasion loss was reduced with a further increase in TSA and emulsion content. For water content, the abrasion loss initially increased and then decreased, as shown in **Figure 5.19**(**4c**).

The increase in TSA till mean resulted in a rapid reduction in the lateral displacement, whereas after optimum, further increase in TSA had minimal impact the lateral displacement, as illustrated in **Figure 5.19(5a)**. In terms of emulsion content, **Figure 5.19(5b)** shows that there exists an optimal value for which the lateral displacement was minimum. Lateral displacement increased with the reduction in water content, as shown in **Figure 5.19(5c)**.

Figure 5.19(6a) and **Figure 5.19(6c)** shows that the sand adhesion constantly decreases with the increase in TSA and reduction in water content, respectively. Sand adhesion didn't vary substantially below OEC, whereas there was a rapid increase in the sand adhesion when the emulsion content was increased above OEC, as shown in **Figure 5.19(6b)**.

Hence, from the sensitivity analysis of models developed using MSGP, the following scenarios were identified as the critical combinations for which the risk of the failure of microsurfacing mix increases substantially.

- Coarser gradation having relatively lower mineral filler content – Highly workable mix leading to segregation, raveling, rutting and bleeding of microsurfacing mix.
- Finer gradation having relatively higher mineral filler content – Rapid breaking of emulsion.
- Lower emulsion content – Rapid breaking of emulsion, raveling and rutting.

- Higher emulsion content – Highly workable mix, rutting and bleeding.
- Lower water content – Rapid breaking of emulsion and bleeding.
- Higher water content – Highly workable mix (potentially segregation) and rutting.

Here, it is important to note that the predictive models can only be used to predict the response using variables that are within the range of the original data used to develop the model themselves. For this study, the model is applicable for the following range of input variables:

- Aggregate gradation = Mid-point of Type II gradation ± tolerance limits
- Emulsion content = OEC ± 1.5%
- Water content = OWC – 1% to OWC + 2%

5.7 Reliability of microsurfacing mix design

Performance assessment and analysis using ANN and MSGP highlighted the risk of failure associated with the production of microsurfacing mix having critical combinations of process control parameters. So, it is vital to identify the set of critical combinations for which the risk of failure is maximum and quantify the extent of acceptable variability.

One of the approaches to understand the extent of acceptable variability is the consideration of reliability-based assessment. Reliability analysis describes the probability of the pavement satisfying the performance criteria throughout its design life. It is important to increase the reliability by restricting the variation in performance without a substantial increase in the cost associated with very stringent quality control.

In this study, reliability was used as a qualitative measure to assess the repeatability of microsurfacing performance. However, unlike the conventional practice of keeping all the parameters consistent, variation in aggregate gradation, emulsion content and water content was considered in the study to accommodate inherent variability of process control parameters during the material handling and production of microsurfacing mix.

The performance parameters included in reliability analysis were cohesion at 60 minutes, abrasion loss, lateral displacement, and sand adhesion. Reliability was defined through the limits of performance parameters as per ISSA guidelines (ISSA A143, 2010). The following steps were followed to determine reliability.

- Assigning frequency distribution
- Determining goodness-of-fit
- Evaluating the reliability of mix through the specified performance limits

Assigning frequency distribution

Gravetter and Wallnau (2016) defined frequency distribution as "an organized tabulation of the number of individuals located in each category on the scale of measurement." In this study, the number of intervals (N_i) and bin size for each performance parameter was evaluated using **Equation 5.14** and **5.15**, respectively. The frequency of observations within each class interval was determined, and the % frequency in each group (f_i) was calculated using **Equation 5.16** for cohesion, abrasion loss, lateral deformation and sand adhesion. Then, the mean and standard deviation of the dataset was calculated using **Equation 5.17** and **5.18,** respectively.

$$N_i = \sqrt{Number\ of\ observations} \tag{5.14}$$

$$Bin\ Size = \frac{Maximum\ data\ point - Minimum\ data\ point}{N_i} \tag{5.15}$$

$$f_i = \frac{Observed\ frequency}{Total\ frequency} \times 100 \tag{5.16}$$

$$\mu = \frac{\sum f_i\, u_i}{\sum f_i} \tag{5.17}$$

$$\sigma = \sqrt{\frac{n_i \times (u_i - \mu)^2}{N - 1}} \tag{5.18}$$

where, μ = Mean; σ = Standard deviation; f_i = % Frequency in the group i; u_i = Mid-point of the range for group i; n_i = Observed frequency in group i; N = Total number of observations.

Determination of the goodness-of-fit

The distribution was assumed to be a normal distribution. The chi-square (χ^2) test was used for testing goodness-of-fit. In the test, a bin range similar to frequency distribution was assigned and observed frequency (O_i) were noted down. Then, the expected frequency (E_i) were determined using the fitted distributions for each class interval.

The degree of freedom (DOF) was assigned to all parameters using **Equation 5.19**, after which $\chi^2_{calculated}$ was evaluated using **Equation 5.20**.

$$DOF = n_{ra} - p_{ra} - 1 \tag{5.19}$$

$$\chi^2_{calculated} = \sum_{i=1}^{n} \frac{(O_i - E_i)^2}{E_i} \tag{5.20}$$

where n_{ra} = number of class intervals; p_{ra} = number of model parameters (= 2), respectively. The probability associated with chi-square distribution was assumed as 0.95 and $\chi^2_{critical}$ was determined using DOF and probability for all performance parameters.

Evaluating reliability

After testing for goodness-of-fit, reliability, $R(m)$, was evaluated in terms of probability, $P_{ra}(n)$, of performance test results falling within specification limits (Chakroborty *et al.*, 2009). For determining the probability, **Equation 5.21** was used.

$$P_{ra}(n) = \int_a^b f_n(x)dx \tag{5.21}$$

where $f_n(x)$ = joint probability density function (PDF) obtained after developing a frequency distribution, fitting distribution, and testing for goodness-of-fit.

5.7.1 Influence of process control parameters on reliability

Initially, to determine reliability, the dataset was divided into different groups based on the range of test results. The bin range calculated using **Equation 5.15** is shown in **Table 5.7**. Then, the corresponding observed frequency and % frequency was determined for each group, as shown in **Table 5.8**.

Table 5.7: Bin range for different parameters

Parameter	Minimum	Maximum	Bin range
Cohesion, kg-cm	26.0	32.3	1.04
Raveling, g/m^2	237.9	668.0	71.68
Rutting, %	3.15	8.04	0.82
Bleeding, g/m^2	235.1	645.5	68.40

Table 5.8: Determination of frequency distribution

Parameters	Lower Limit	Upper Limit	Middle, u_i	Observed Frequency	% Frequency in Group, f_i	$f_i \times u_i$	$f_i \times (u_i - \mu)^2$
Cohesion	26.0	27.0	26.5	6	20.0	159.1	41.8
	27.0	28.1	27.6	3	10.0	82.7	7.7
	28.1	29.1	28.6	3	10.0	85.8	0.9
	29.1	30.2	29.6	9	30.0	266.8	2.1
	30.2	31.2	30.7	5	16.7	153.4	11.7
	31.2	32.3	31.7	4	13.3	126.9	26.4
Raveling	237.9	309.5	273.7	6	20.0	1642.2	115231.9
	309.5	381.2	345.4	9	30.0	3108.5	40283.2
	381.2	452.9	417.1	4	13.3	1668.3	91.3
	452.9	524.6	488.8	5	16.7	2443.8	29230.4
	524.6	596.3	560.4	4	13.3	2241.7	87782.6
	596.3	668.0	632.1	2	6.7	1264.2	96643.1
Rutting	3.1	4.0	3.6	11	36.7	39.1	15.8
	4.0	4.8	4.4	8	26.7	35.0	1.2
	4.8	5.6	5.2	4	13.3	20.7	0.8
	5.6	6.4	6.0	2	6.7	12.0	3.1
	6.4	7.2	6.8	3	10.0	20.5	12.8
	7.2	8.0	7.6	2	6.7	15.3	16.6
Bleeding	235.1	303.5	269.3	9	30.0	2423.6	103341.1
	303.5	371.9	337.7	9	30.0	3039.1	13520.0
	371.9	440.3	406.1	4	13.3	1624.3	3513.8
	440.3	508.7	474.5	3	10.0	1423.4	28833.2
	508.7	577.1	542.9	4	13.3	2171.5	110800.2
	577.1	645.5	611.3	1	3.3	611.3	55145.4

For the dataset, the mean and standard deviation calculated using **Equations 5.17** and **5.18** are provided in **Table 5.9**. Subsequently, a hypothesis was made that the test results follow normal distribution for all performance parameters. For proving the hypothesis, goodness-of-fit for the distribution was assessed using the chi-square (χ^2) test.

Table 5.9: Mean and standard deviation for different parameters

Parameter	Mean	Standard deviation
Cohesion, kg-cm	29.2	1.8
Raveling, g/m^2	412.3	112.8
Rutting, %	4.75	1.3
Bleeding, g/m^2	376.4	104.2

In chi-square test, the first step is the determination of the expected frequency (E_i). In this regard, the upper limit (UL_i) for standard normal (z_d) was determined using **Equation 5.22**.

$$z_d = \frac{UL_i - \mu}{\sigma} \tag{5.22}$$

The probability of $z \leq z_d$ was determined using a standard normal distribution table. The probability of occurrence in each group was calculated by subtracting the probability of $z \leq z_d$ of the corresponding group from the previous group. Expected frequency was evaluated by multiplying the total number of observations by the probability of an occurrence in that group.

Finally, using **Equation 5.20**, $\chi^2_{calculated}$ was evaluated for each group and the results are shown in **Table 5.10**. The sum of $\chi^2_{calculated}$ for all groups in a particular test was defined as the $\chi^2_{calculated}$ for that test. **Table 5.11** shows the results of $\chi^2_{calculated}$ for all the test parameters. It could be observed from **Table 5.11** that all the $\chi^2_{calculated}$ were less than $\chi^2_{critical}$. Hence, the hypothesis that the dataset follows normal distribution could not be rejected. So, for further analysis, the test results were considered to be normally distributed.

Table 5.10: Determination of calculated Chi-square

Parameters	Upper Limit	Observed Frequency (O_i)	Upper Limit (Std. Normal), z_d	Probability of $z \leq z_d$	Probability of occurrence in group	Expected Frequency (E_i)	$\chi^2_{calculated}$
Cohesion	27.0	6	-1.199	0.12	0.12	3.5	1.9
	28.1	3	-0.609	0.27	0.16	4.7	0.6
	29.1	3	-0.020	0.49	0.22	6.6	2.0
	30.2	9	0.570	0.72	0.22	6.7	0.8
	31.2	5	1.159	0.88	0.16	4.8	0.0
	32.3	4	1.749	0.96	0.08	2.5	0.9
Raveling	309.5	6	-0.911	0.18	0.18	5.4	0.1
	381.2	9	-0.275	0.39	0.21	6.3	1.1
	452.9	4	0.360	0.64	0.25	7.5	1.6
	524.6	5	0.995	0.84	0.20	6.0	0.2
	596.3	4	1.630	0.95	0.11	3.2	0.2
	668.0	2	2.266	0.99	0.04	1.2	0.5
Rutting	4.0	11	-0.599	0.27	0.27	8.2	0.9
	4.8	8	0.021	0.51	0.23	7.0	0.1
	5.6	4	0.641	0.74	0.23	6.9	1.2
	6.4	2	1.260	0.90	0.16	4.7	1.6
	7.2	3	1.880	0.97	0.07	2.2	0.3
	8.0	2	2.500	0.99	0.02	0.7	2.3
Bleeding	303.5	9	-0.700	0.24	0.24	7.3	0.4
	371.9	9	-0.044	0.48	0.24	7.2	0.4
	440.3	4	0.612	0.73	0.25	7.4	1.6
	508.7	3	1.268	0.90	0.17	5.0	0.8
	577.1	4	1.925	0.97	0.08	2.3	1.3
	645.5	1	2.581	1.00	0.02	0.7	0.2

Table 5.11: Comparison of calculated and critical chi-square

Parameter	$\chi^2_{calculated}$	$\chi^2_{critical}$	Parameter follows normal distribution
Cohesion	6.2	7.8	Yes
Raveling	3.7	7.8	Yes
Rutting	6.5	7.8	Yes
Bleeding	4.8	7.8	Yes

The reliability analysis includes the determination of the probability of performance parameters satisfying the ISSA guidelines using **Equation 5.21**. The function, $f_n(x)$, being normally distributed, can be represented as shown in **Equation 5.23**. The distribution parameters mean (μ) and standard deviation (σ), described in **Table 5.9**, were determined using **Equation 5.17** and **5.18,** respectively. The frequency distribution adopted for all the test parameters are shown in **Equations 5.24-5.27**.

$$f_n(x) = \frac{1}{\sqrt{2\pi\sigma^2}} e^{-\frac{(x-\mu)^2}{2\sigma^2}} \tag{5.23}$$

$$f_n(CH_{60}) = \frac{1}{4.4} e^{-\frac{(CH-29.2)^2}{6.2}} \tag{5.24}$$

$$f_n(AL) = \frac{1}{283} e^{-\frac{(AL-412.3)^2}{25466}} \tag{5.25}$$

$$f_n(LD) = \frac{1}{3.3} e^{-\frac{(LD-4.7)^2}{3.5}} \tag{5.26}$$

$$f_n(SA) = \frac{1}{261} e^{-\frac{(SA-376.4)^2}{21735}} \tag{5.27}$$

The next step is integrating the function subjected to upper and lower limits as per ISSA recommendations (ISSA A143, 2010). In this study, the probability integral ($\varphi(z)$), as shown in **Equation 5.28**, was used for integrating the function and determining the reliability (Lebedev, 1965).

$$\varphi(z) = \frac{2}{\sqrt{\pi}} \int_0^z e^{-t^2} dt \tag{5.28}$$

where $z = (x-\mu)/(\sqrt{2}\sigma)$ and $t = (x-\mu)$. The results of the reliability analysis are shown in **Table 5.12**. The reliability of cohesion, raveling and bleeding was more than

85%. It highlights that the mix attains suffiecient strength and the risk of raveling and bleeding minimizes if the production parameters are within the tolerance limits. However, the reliability of rutting was relatively low, i.e., 0.57, which shows that the risk of rutting is high in microsurfacing.

Table 5.12: Reliability of microsurfacing mix

Parameter	Limits		Reliability
	Lower	Upper	
Cohesion	20	N/A	1.00
Raveling	0	538	0.87
Rutting	0	5	0.57
Bleeding	0	538	0.94

* *N/A – Not applicable*

5.7.2 Improvement in reliability with elimination of critical combinations

For improving reliability, it was assumed that the scenarios exhibiting maximum rutting were avoided during quality control of microsurfacing production. So, the 3 mixes having maximum rutting, i.e., mix C23, C24 and C35, were removed from reliability calculations. For the dataset (27 combinations), the mean and standard deviation calculated using **Equations 5.17** and **5.18** are provided in **Table 5.13**.

Compared to the test results before eliminating critical combinations (**Table 5.12**), the cohesion, raveling, rutting and bleeding improved by 0.9%, 8.4%, 8.5% and 2.2%, respectively. Subsequently, similar to **Section 5.7.1**, it was assumed that the data follows a normal distribution, and the goodness-of-fit for the distribution was assessed using the chi-square (χ^2) test. The results of the chi-square test are provided in **Table 5.14** and **Table 5.15**.

Table 5.13: Mean and standard deviation after modification

Parameter	Unit	Mean	Standard deviation
Cohesion	kg-cm	29.4	1.7
Raveling	g/m^2	377.7	93.1
Rutting	%	4.35	0.8
Bleeding	g/m^2	368.1	102.7

Table 5.14: Determination of calculated Chi-square after modification

Parameters	Upper Limit	Observed Frequency (O_i)	Upper Limit (Std. Normal), z_d	Probability of $z < z_d$	Probability of occurrence in group	Expected Frequency (E_i)	$\chi^2_{calculated}$
Cohesion	27.0	4	-1.422	0.08	0.08	2.1	1.7
	28.1	2	-0.798	0.21	0.13	3.6	0.7
	29.1	3	-0.173	0.43	0.22	5.9	1.4
	30.2	9	0.451	0.67	0.24	6.6	0.9
	31.2	5	1.076	0.86	0.18	5.0	0.0
	32.3	4	1.700	0.96	0.10	2.6	0.7
Raveling	295.5	5	-0.883	0.19	0.19	5.1	0.0
	353.2	9	-0.264	0.40	0.21	5.6	2.1
	410.8	4	0.355	0.64	0.24	6.6	1.0
	468.4	4	0.974	0.84	0.20	5.3	0.3
	526.1	2	1.593	0.94	0.11	3.0	0.3
	583.7	3	2.212	0.99	0.04	1.1	3.1
Rutting	3.7	6	-0.758	0.22	0.22	6.1	0.0
	4.3	9	-0.101	0.46	0.24	6.4	1.1
	4.8	5	0.556	0.71	0.25	6.8	0.5
	5.4	2	1.213	0.89	0.18	4.8	1.6
	5.9	2	1.870	0.97	0.08	2.2	0.0
	6.5	2	2.528	0.99	0.02	0.7	2.6
Bleeding	303.5	9	-0.629	0.26	0.26	7.1	0.5
	371.9	8	0.037	0.51	0.25	6.7	0.2
	440.3	4	0.703	0.76	0.24	6.6	1.0
	508.7	2	1.368	0.91	0.16	4.2	1.2
	577.1	3	2.034	0.98	0.06	1.7	0.9
	645.5	1	2.700	1.00	0.02	0.5	0.6

It could be observed from **Table 5.15** that all the $\chi^2_{calculated}$ were less than $\chi^2_{critical}$. Hence, the hypothesis that the dataset follows normal distribution could not be rejected. So, for further analysis, the test results were considered to be normally distributed.

Table 5.15: Comparison of calculated and critical chi-square after modification

Parameter	$\chi^2_{calculated}$	$\chi^2_{critical}$	Parameter follows normal distribution
Cohesion	5.6	7.8	Yes
Raveling	6.8	7.8	Yes
Rutting	5.8	7.8	Yes
Bleeding	4.4	7.8	Yes

The reliability analysis was conducted similar to **Section 5.7.1,** considering the limits specified in the ISSA guidelines (ISSA A143, 2010). Since the dataset follows a normal distribution, $f_n(x)$ was represented as **Equation 5.23**. The frequency distribution adopted for cohesion at 60-min (CH_{60}), abrasion loss (AL), lateral displacement (LD) and sand adhesion (SA) are shown in **Equations 5.29-5.32**.

$$f_n(CH_{60}) = \frac{1}{4.2}\, e^{-\frac{(CH - 29.4)^2}{5.6}} \tag{5.29}$$

$$f_n(AL) = \frac{1}{233}\, e^{-\frac{(AL - 378)^2}{17343}} \tag{5.30}$$

$$f_n(LD) = \frac{1}{2.1}\, e^{-\frac{(LD - 4.3)^2}{1.4}} \tag{5.31}$$

$$f_n(SA) = \frac{1}{258}\, e^{-\frac{(SA - 368)^2}{21112}} \tag{5.32}$$

Finally, to determine the reliability, **Equation 5.28** was used to integrate the function for the limits specified by ISSA. Results of the reliability analysis are shown in **Table 5.16**. It could be observed from **Table 5.16** that the reliability of raveling and bleeding increased to more than 0.95 with the elimination of 3 critical combinations. The reliability of rutting increased from 0.57 (**Table 5.12)** to 0.78 (**Table 5.16**), i.e., the reliability improved by 0.21. Hence, it is vital to avoid the combination of coarser

gradation having relatively lower mineral filler content and lower emulsion content to ensure that the risk of failure of microsurfacing mix is minimized.

Table 5.16: Modified reliability of microsurfacing mix

Parameter	Limits		Reliability
	Lower	Upper	
Cohesion	20	N/A	1.00
Raveling	0	538	0.96
Rutting	0	5	0.78
Bleeding	0	538	0.95

* *N/A – Not applicable*

5.7.3 Overall reliability

Apart from assessing the individual reliability, the overall reliability of the mix was also determined. But, before determining the overall reliability, it is important to analyze the dependency among test parameters. For this purpose, the mechanism for each test parameter is explained below.

- Cohesion – Measure of resistance to torque when a sudden shear action is applied.
- Abrasion loss – Measure of adhesion between aggregate and asphalt binder when a constant shearing action is applied onto the surface of the mix.
- Lateral displacement – Measure of stiffness of the mix when dynamic compressive stress is applied.
- Sand adhesion – Measure of asphalt flushing under heavy traffic loads when cohesionless sand is allowed to adhere to mix under dynamic compressive stress.

From the above discussion, it could be inferred that the mechanism and purpose behind each test parameter were different. Since all the test parameters were independently assessed and the testing mechanism was different, the overall reliability was determined by multiplying the probability of satisafactory performance of all parameters (Chakroborty *et al.*, 2009), as shown in **Equation 5.33**.

$$R(M) = P(CH_{60}) \times P(AL) \times P(LD) \times P(SA) \quad (5.33)$$

where, $R(M)$ = Reliability of mix; $P(CH_{60})$ = Probability of cohesion at 60-min; $P(AL)$ = Probability of abrasion loss; $P(LD)$ = Probability of lateral displacement; $P(SA)$ = Probability of sand adhesion. All the parameter of **Equation 5.33** describes the probability of mix passing the ISSA specified limits (ISSA A143, 2010).

For the materials tested in the study, the overall reliability was only 47%. The reliability increased to 71% when mixes C23, C24 and C35 were excluded from the reliability assessment. Hence, avoiding critical combinations during the production stage improves the reliability of the microsurfacing mix substantially.

5.8 Summary

In this chapter, the influence of process control parameters on the performance of microsurfacing mix was investigated. The parameters considered were aggregate gradation, emulsion content and water content. The performance was expressed in terms of workability, strength evolution, raveling, rutting and bleeding. A total of 35 different combinations of aggregate gradation, emulsion content, and water content were selected. In these combinations, the aggregate gradation was varied within tolerance limits, emulsion content was varied from optimum by ±1.5%, and water content was varied from optimum by -1% to +2%. The following conclusions were drawn from the laboratory investigations.

- Workability was dependent on the TSA of aggregates and total fluid content present in the mix. Lower TSA and higher total fluid content resulted in an increase in workability up to 87%. Alternatively, the workability reduced up to 59% for higher TSA and lower total fluid content.
- Mix strength was predominantly influenced by aggregate gradation, where the strength at 60-min for coarser gradation (TSA = 8.7 m^2/kg) was 12% lower than control mix.
- Aggregate gradation and emulsion content had a substantial impact on raveling. Rutting was predominantly influenced by aggregate gradation and emulsion content. The combination of emulsion content and water content had a substantial influence on bleeding of microsurfacing mix.

- Assessment of synergistic effect of process control parameters highlighted the following scenarios that should be avoided during production.
    - Workability – *Water content variation to more than ±1% from optimum and/or combination of finer aggregate gradation and lower emulsion content.*
    - Strength – *Coarser aggregate gradation with low mineral filler content*.
    - Raveling and rutting – *Combination of coarser aggregate gradation and lower emulsion content.*
    - Bleeding – *Combination of coarser gradation, higher emulsion content and relatively lower water content.*

Subsequently, relative contribution of process control parameters on the performance was determined using ANN and Garson's algorithm. MSGP was used to formulate the model, and sensitivity analysis was used to interpret the model developed. Finally, the reliability of mix performance was determined. From the analysis of the test results, the following conclusions were drawn.

- The findings from ANN and MSGP are illustrated in **Figure 5.20**. Using ANN, the process control parameters predominantly affecting performance were assessed by evaluating its relative contribution on performance. MSGP was used as an effective tool to quantify the effect of predominant factors.

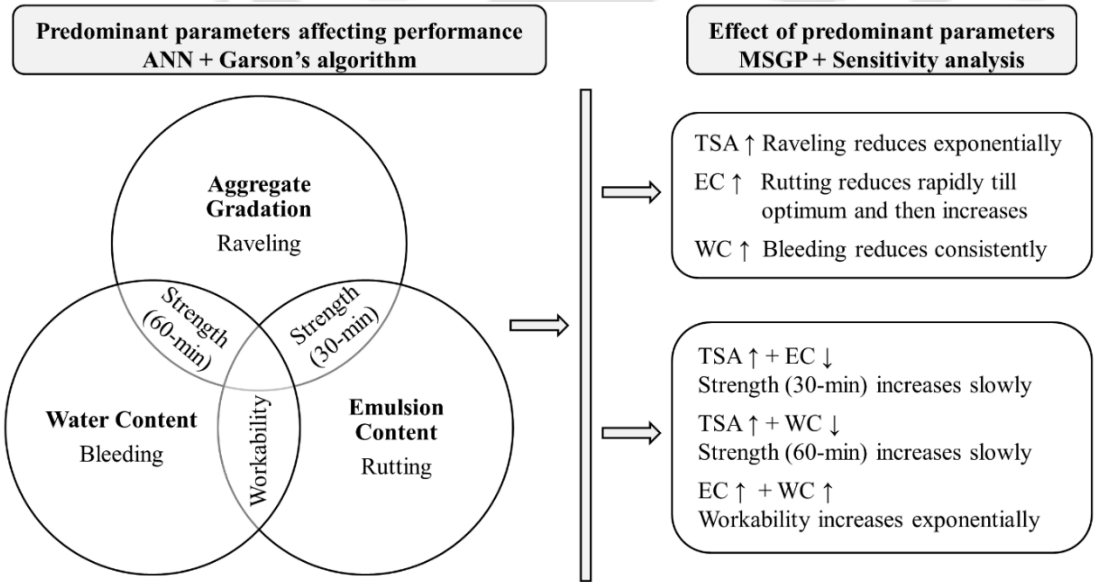

Figure 5.20: Summarizing results from ANN and MSGP

- Relative contribution assessment showed that the parameter having relative contribution of more than 35% includes the following.
  - Aggregate gradation – Strength (cohesion at 30-min and 60-min) and raveling.
  - Emulsion content – Workability, strength (cohesion at 30-min) and rutting.
  - Water content – Workability, strength (cohesion at 60-min) and bleeding.
- Using MSGP model formulation, the effect of process control parameters having highest impact on performance could be quantified as follows.
  - With the increase in emulsion content and water content from -10% to +10% of optimum, workability increased exponentially from -75% to +74% with respect to control mix.
  - Strength at 30-min gradually increased from -6% to +2% with respect to control mix with the combined increase in TSA from -10% to +10% of TSA for control mix and reduction in emulsion content from +10% to -10% of optimum.
  - Strength at 60-min gradually increased from -6% to +7% with respect to control mix with the combined increase in TSA from -10% to +10% of TSA for control mix and reduction in water content from +10% to -10% of optimum.
  - Raveling reduced exponentially from +29% to -9% with respect to control mix with the increase in TSA from -10% to +10% of TSA for control mix.
  - Rutting was minimum at optimum emulsion content. Reduction of emulsion content by 10% of optimum led to a increase in rutting by 15%. Alternatively, if emulsion content was increased by 10% of optimum, rutting was found to increase rapidly by 30%.
  - Bleeding reduced consistently from +8% to -12% with respect to control mix with the increase in water content from -10% to +10% of optimum.
- Reliability analysis showed that the probability of failure due to rutting was the highest when the process control parameters were varied within the tolerance limits. Overall, reliability increased from 47% to 71% with the exclusion of critical combinations from reliability analysis, i.e, combination of coarser gradation having relatively lower mineral filler content and lower emulsion content.

CHAPTER 6

Durability Assessment of Microsurfacing Mix

6.1 Introduction

This chapter presents the durability of the microsurfacing mix. The two environmental factors including aging and moisture damage were considered. A total of 30 combinations of aging and moisture conditioning protocols were considered. Performance was quantified in terms of raveling. Multiple linear regression analysis was used to model the test output and quantify the dependence of mix durability on aging and moisture.

6.2 Methodology

In this study, aging and moisture damage were selected for quantifying the durability of microsurfacing mix. The reason behind the selection of these parameters that during service life, aging causes an increase in the stiffness of the asphalt binder with time which results in the adhesion at the aggregate binder interface. In addition, the ingress of moisture into the mix causes softening of binder at the aggregate-binder interface. It ultimately results in loss of adhesion and the mix becomes susceptible to stripping and raveling. Hence, different aging and moisture conditioning protocols were considered in the study and the performance of the microsurfacing mix was assessed in terms of raveling resistance.

A brief illustration of the methodology adopted in the study is described in **Figure 6.1**. The methodology was divided into two stages.

- **Stage 1 – Aging and moisture conditioning**: For long-term aging of asphalt mixture, AASTHO R30 (2019) recommends placing the compacted specimen in a forced-draft oven at a temperature of 85°C for a duration of 5 days. Since microsurfacing is also a surface course, similar conditioning protocol was considered as the benchmark. But, due to its thin application and difference in chemistry with respect to HMA, the influence of variation in aging conditions was studied. Aging time was varied from 1 to 5 days (Mix A1 to A5) whereas aging temperature was varied from 85°C to 105°C (Mix A5 to A7). It was assumed that

the exposure of microsurfacing specimen to aging would initially result in moisture loss from the specimen followed by an increase in the stiffness of the mix and finally, the specimen would exhibit loss of adhesion. The reason behind the selection of these protocols was to determine the aging protocol for which the mix starts to exhibit loss of adhesion, i.e., raveling increases.

According to ISSA recommendation, the assessment of moisture damage in microsurfacing is conducted at a temperature of 25°C for 6 days. But, it is important to understand the progression of moisture damage, i.e., how the ingress of moisture in microsurfacing mix results in the loss of adhesion. In this regard, the moisture conditioning time was varied from 1 to 8 days (Mix M1 to M5) and the loss of adhesion was monitored in terms of loss of adhesion at 1, 2, 4, 6 and 8 day. Since the rate of moisture damage is also dependent on the temperature of moisture conditioning, the loss of adhesion due to higher moisture conditioning temperature was also studied. The range of moisture conditioning temperature selected was 25°C to 60°C (Mix M4, M6 and M7).

Since aging and moisture co-occur in the field, the synergistic influence of aging and moisture was also studied. For each conditioning protocol, 2 levels were selected based on the results and significance analysis of the investigations on the individual effect of aging and moisture on raveling. A total of 16 combinations were selected based on 2^4 full factorial design (Mix AM1 to AM16). The detailed description of the combinations selected and the notations used is described in **Table 6.1**.

- **Stage 2 – Analysis and model development**: Statistical analysis was conducted using a *t*-test to determine the difference in raveling due to aging and moisture conditioning protocols considered. Then, for the 16 combinations tested for assessing the synergistic influence of aging and moisture damage, ANOVA was used to determine the parameters having a statistically significant impact on the raveling resistance of microsurfacing mix. Subsequently, significant parameters were selected to formulate the model using regression analysis.

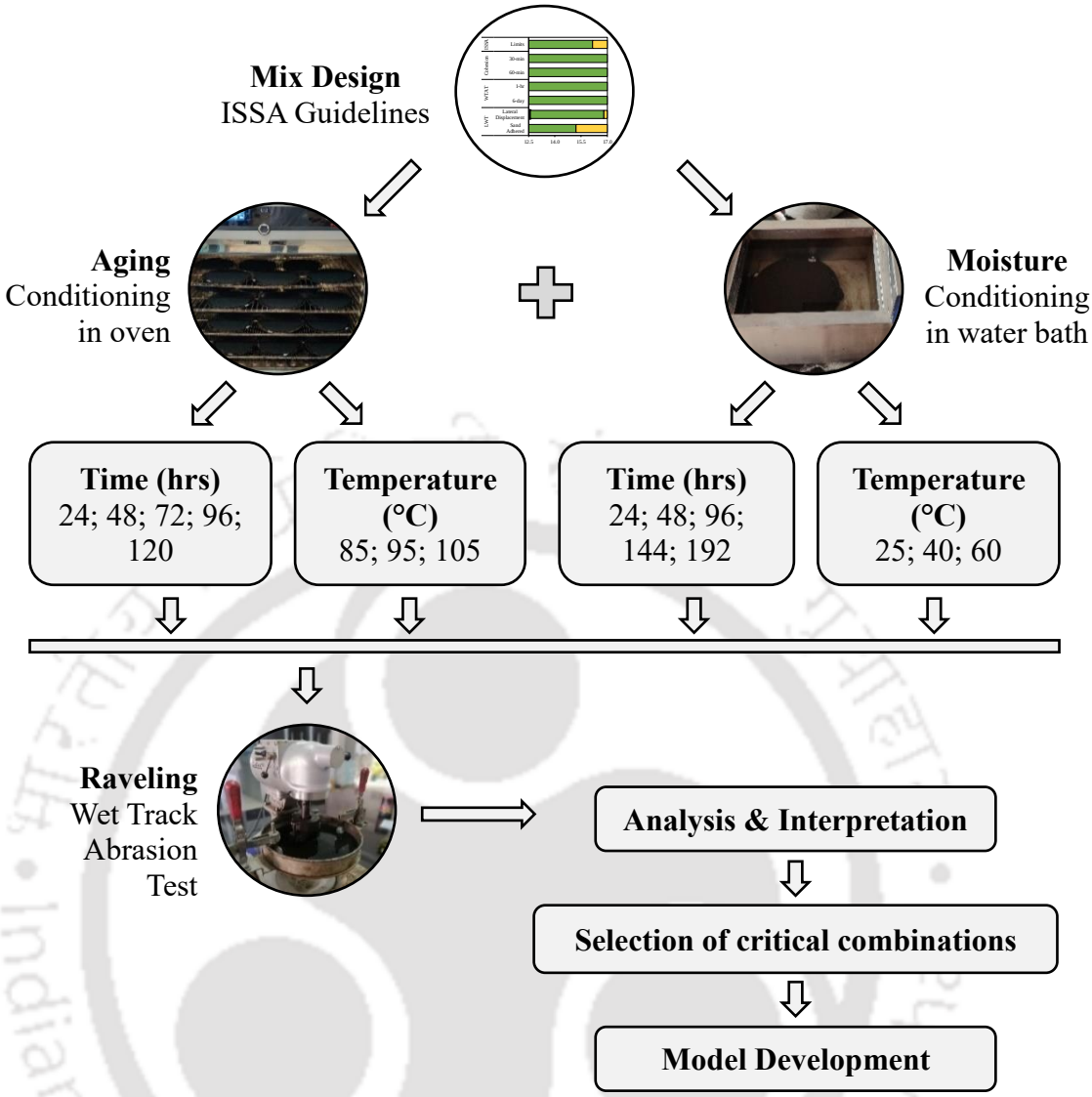

Figure 6.1: Methodology for durability assessment

6.3 Conditioning protocols

Aging was conducted by placing the cured specimens in a forced-draft oven (**Figure 6.2a**) for the temperature and time mentioned in **Table 6.1**. On the other hand, the specimens for moisture conditioning were placed in a water bath (**Figure 6.2b**) for the desirable time and temperature (**Table 6.1**). During moisture conditioning, at least 12.5 mm of water cover was ensured to be present above the surface of the specimen. The specimens were first aged and then subjected to a moisture conditioning process for the combination of aging and moisture. Subsequently, the specimens were allowed to cool down to room temperature before subjecting them to abrasion using WTAT.

Table 6.1: Detailed description of conditioning parameters

Mix ID	Aging		Moisture		Mix ID	Aging		Moisture	
	Temp. (°C)	Time (hrs.)	Temp. (°C)	Time (hrs.)		Temp. (°C)	Time (hrs.)	Temp. (°C)	Time (hrs.)
A1	85	24	--	--	**M1**	--	--	25	24
A2	85	48	--	--	**M2**	--	--	25	48
A3	85	72	--	--	**M3**	--	--	25	96
A4	85	96	--	--	**M4**	--	--	25	144
A5	85	120	--	--	**M5**	--	--	25	192
A6	95	120	--	--	**M6**	--	--	40	144
A7	105	120	--	--	**M7**	--	--	60	144
AM1	85	48	25	48	**AM9**	105	48	25	48
AM2	85	48	25	144	**AM10**	105	48	25	144
AM3	85	48	40	48	**AM11**	105	48	40	48
AM4	85	48	40	144	**AM12**	105	48	40	144
AM5	85	120	25	48	**AM13**	105	120	25	48
AM6	85	120	25	144	**AM14**	105	120	25	144
AM7	85	120	40	48	**AM15**	105	120	40	48
AM8	85	120	40	144	**AM16**	105	120	40	144

** Note: Temp. = Temperature; hrs. = hours.*

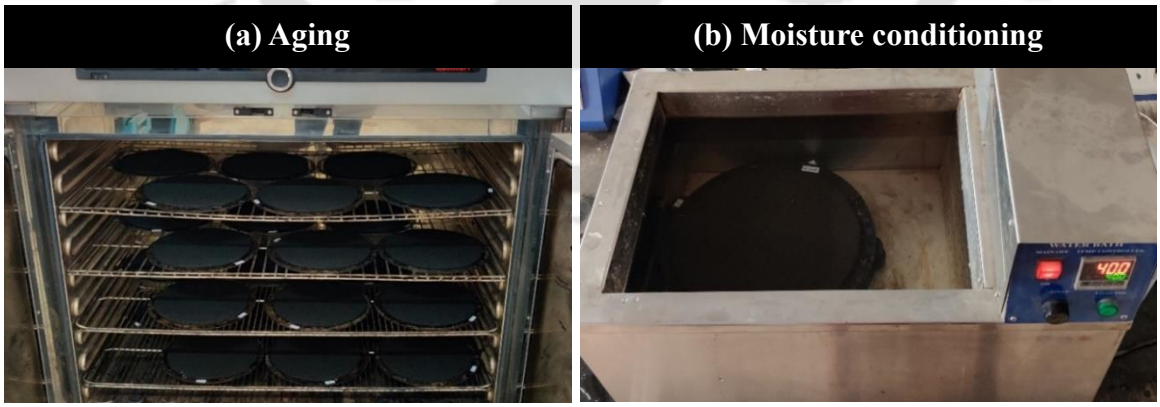

Figure 6.2: Conditioning set-up for (a) aging and (b) moisture conditioning

6.4 Individual effect of conditioning protocols on raveling resistance

6.4.1 Effect of aging

The effect of aging on the durability of microsurfacing mix was assessed in terms of raveling resistance by subjecting the WTAT specimens to conditioning in the oven for different times and temperatures. Results from the laboratory investigations are presented in **Figure 6.3**. Error bars refer to ± standard deviation. The repeatability of the test results was investigated in terms of CoV. For the 7 combinations tested (with 4 replicates), the CoV varied from 4.3-13.2%, with the average CoV being 9.2%. It could be observed from **Figure 6.3** that the raveling resistance decreased with the increase in aging time and temperature.

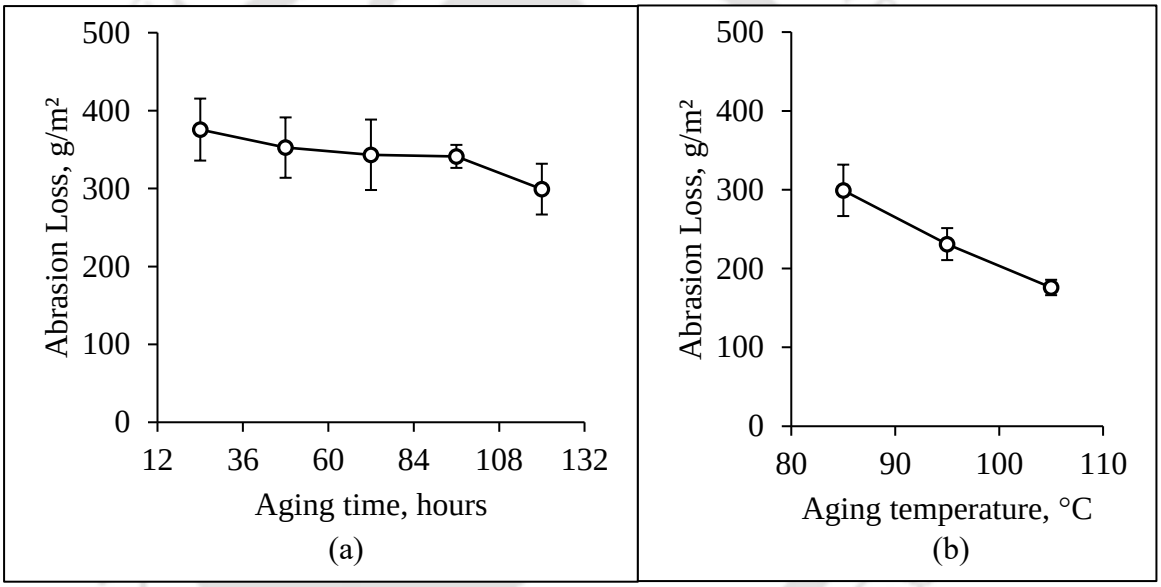

Figure 6.3: Effect of aging, (a) time and (b) temperature, on raveling

The abrasion loss reduced from 379 g/m^2 for the control mix (without aging) to 299 g/m^2 after aging at 85°C for 5 days, as shown in **Figure 6.3a**. On average, the abrasion loss reduced by 2.6% after 24 hours of aging at 85°C until 4 days. However, for the fifth day, the abrasion loss was reduced by 12.3%. In order to explain the sudden decrease in the abrasion loss, the moisture loss during aging was determined. For this purpose, the weight of the specimen after curing at 60°C $(W_{a,aging})$ and the weight of specimen after aging $(W_{b,aging})$ was noted down. Then, percentage moisture loss during aging was determined using **Equation 6.1**.

$$Moisture\ loss\ (\%) = \frac{W_{b,aging} - W_{a,aging}}{W_{b,aging}} \times 100 \qquad (6.1)$$

Results of the moisture loss due to aging are presented in **Figure 6.4.** Error bars refer to ± standard deviation. It could be observed from **Figure 6.4a** that the moisture loss increased consistently from 0.04% for 1-day aging to 0.22% for 4 days of aging at 85°C. After that, for the fifth day, no additional moisture loss was observed. In terms of aging temperature, **Figure 6.3b** shows that with the increase in aging temperature from 85°C to 105°C, the abrasion loss reduced by 41%. But, the difference in moisture loss was minimal (less than 0.02%), as shown in **Figure 6.4b**.

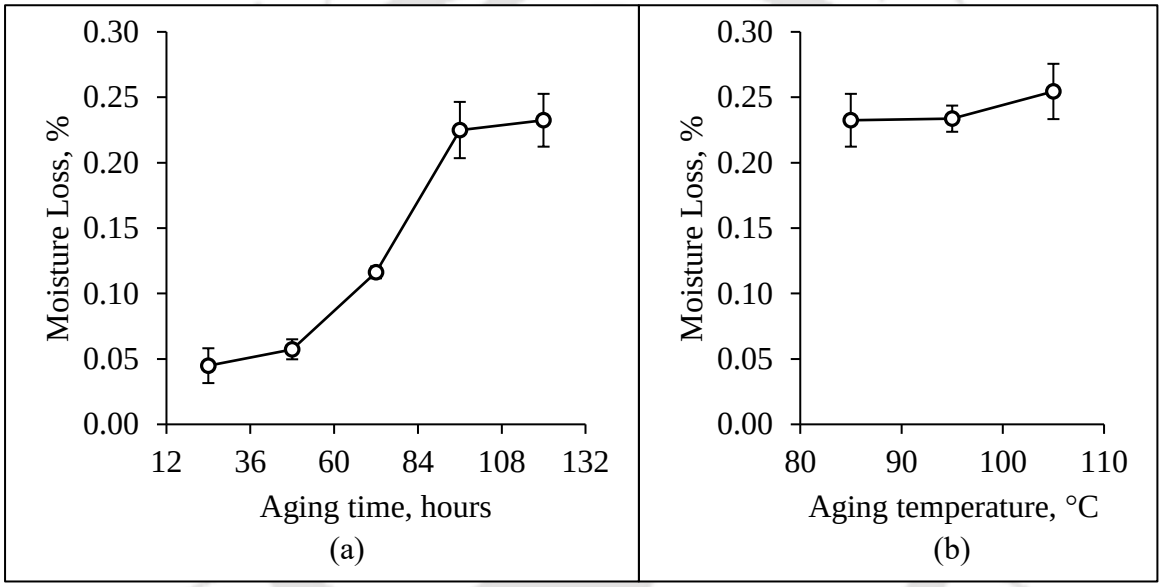

Figure 6.4: Effect of aging, (a) time and (b) temperature, on moisture loss

The decrease in abrasion loss with aging could be explained in two stages. In the first stage, with the increase in aging time, the reduction in abrasion loss could be attributed to the loss of water from the specimen. Thiriet *et al.* (2021) reported that the mix stiffness increases with the loss of water for the cold mix. In turn, the resistance to shear stresses increases and relatively lower raveling was observed. In the second stage, when the mix had achieved maximum moisture loss, aging tends to increase the mix stiffness. With the rapid increase in the mix stiffness, the magnitude of shear stress required to scour the mix increases. As a result, the raveling resistance of the mix improves substantially.

6.4.2 Effect of moisture conditioning

Results of the investigations on the effect of moisture conditioning on raveling are illustrated in **Figure 6.5**. Error bars refer to ± standard deviation. The repeatability of the test results was investigated in terms of CoV. For the 7 combinations tested (with 4 replicates), the CoV varied from 2.9-11.3%, with the average CoV being 7.3%.

It could be observed from **Figure 6.5a** that the abrasion loss increased by 14% with the increase in conditioning temperature from 24 hours to 144 hours. Subsequently, the abrasion loss did not increase with the increase in conditioning time from 144 hours to 196 hours. The moisture intrusion in the mix results in the loss of adhesive properties and softening of the binder (Little & Jones, 2003). Hence, when shear stress was applied to the specimen, the weakened bond breaks faster, and higher raveling was observed.

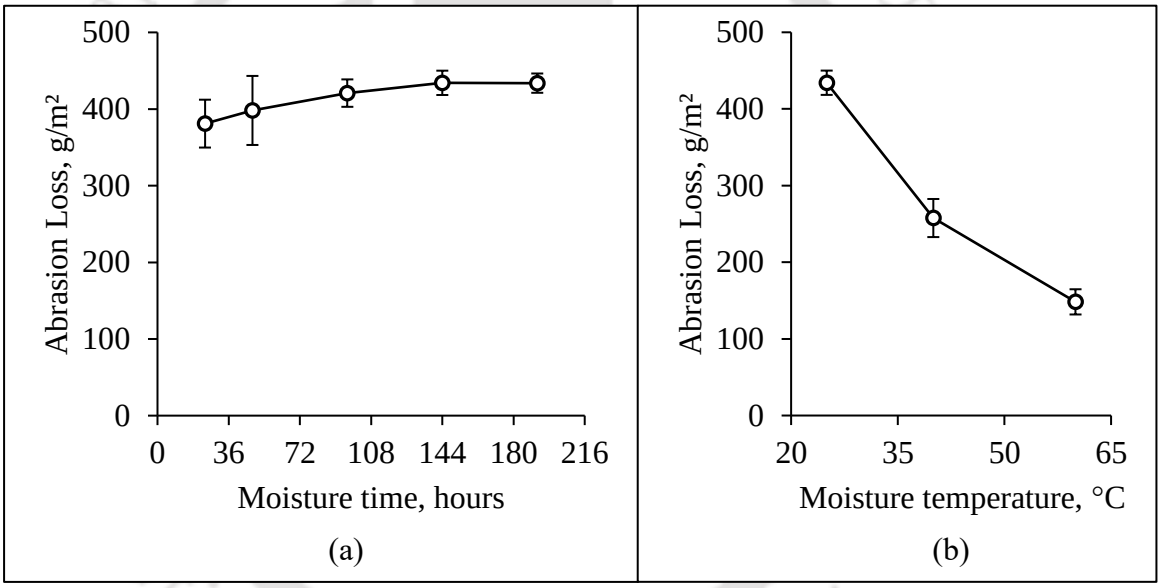

Figure 6.5: Effect of moisture, (a) time and (b) temperature, on raveling

The increase in moisture conditioning temperature from 25°C to 60°C led to a 66% reduction in abrasion loss, as shown in **Figure 6.5b**. The lower raveling for higher moisture conditioning temperature could be due to a combination of factors including the strength gain mechanism associated with higher temperature, improved properties of mix ingredients including cement and flyash with curing at higher temperature, and oxidation of asphalt in the presence of moisture (Deschner *et al.*, 2013; Noguera *et al.*, 2014; Thiriet *et al.*, 2021). Further investigations would help in better understanding of

the role of each mechanism on the reduction in raveling with the increase in moisture temperature.

6.4.3 Statistical analysis on individual effect of aging and moisture on raveling

The variation in abrasion loss due to different aging and moisture conditioning protocols was statistically analyzed using a *t*-test at a significance level of 5%. Results of the statistical analysis are presented in **Table 6.3**. The following observations were made based on the statistical analysis.

- **Aging time**: The difference in raveling due to aging time was not statistically significant until 96 hours of oven conditioning (mix A4) at 85°C with respect to control mix. After 120 hours of oven conditioning (mix A5), the difference in raveling with respect to control mix was significant. This shows that after initial curing of specimen at 60°C for 23-24 hours, the increase in raveling resistance due to additional moisture loss was not significant. However, the combination of maximum possible moisture loss and the increase in the specimen's stiffness due to additional aging results in a significant reduction of raveling of microsurfacing.
- **Aging temperature**: The increase in the temperature of aging from 85°C to 105°C led to a significant reduction of raveling of microsurfacing. It could be attributed to the increased stiffness of the microsurfacing mix.
- **Moisture conditioning time**: Increasing the time of moisture conditioning, even up to 192 hours did not have a significant effect on the raveling of microsurfacing mix. This highlights that the raveling resistance of microsurfacing mix was not affected by moisture conditioning at ambient temperature.
- **Moisture conditioning temperature**: Raveling reduced significantly with the increase in temperature of moisture conditioning. The significant reduction in raveling points out the importance of strength gain mechanism.

Table 6.2: Statistical analysis for assessing the effect of conditioning protocols

Parameter	ID	Significant							
		A1	**A2**	**A3**	**A4**	**A5**	**A5**	**A6**	**A7**
Aging Conditioning time	CM	No	No	No	No	Yes			
	A1		No	No	No	Yes			
	A2			No	No	No		N/A	
	A3				No	No			
	A4					No			
Aging Conditioning temperature	CM						Yes	Yes	Yes
	A5			N/A				No	Yes
	A6								Yes
		M1	**M2**	**M3**	**M4**	**M5**	**M4**	**M6**	**M7**
Moisture Conditioning time	M1	No	No	No	No	No			
	M2		No	No	No	No			
	M3			No	No	No		N/A	
	M4				No	No			
	M5					No			
Moisture Conditioning temperature	CM						No	Yes	Yes
	M4			N/A				Yes	Yes
	M6								Yes

Note: CM = Control mix; N/A = Not applicable.

6.5 Synergistic effect of aging and moisture damage

Apart from assessing the individual effect of aging and moisture, it is vital to understand the synergistic effect of aging and moisture damage in order to quantify the durability of microsurfacing mix. For this purpose, the raveling resistance was determined for the 16 combinations including mix AM1 to AM16 (**Table 6.1**). Results of the laboratory investigations are described in **Figure 6.6**. Error bars refer to ± standard deviation. The repeatability of the test results was investigated in terms of CoV. For the 16 combinations tested (with 4 replicates), the CoV varied from 0.6% to 12.9%, with the average CoV being 7.3%.

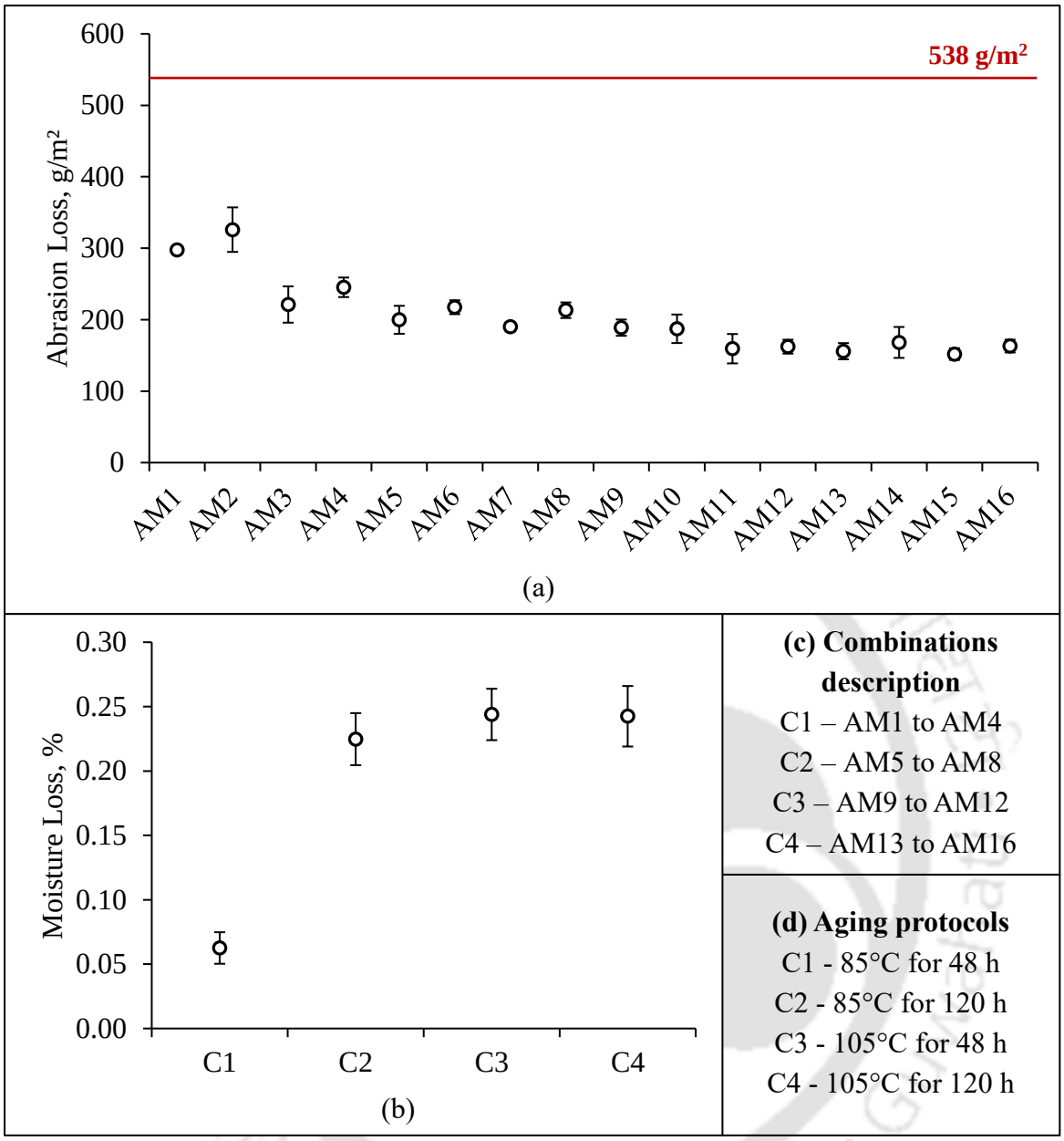

Figure 6.6: (a) Synergistic influence of aging and moisture on raveling; (b) Moisture loss due to aging; (c) Combinations description and (d) Aging protocol

It could be observed from **Figure 6.6a** that overall, the abrasion loss varied from 152 g/m^2 to 326 g/m^2, which was lower than the control mix. It shows that the microsurfacing mix produced at ambient temperature gains strength with time due to water loss. Subsequently, during the curing process and its service life, the carbonyl and sulfoxide oxidation index increases and improves mechanical behavior (Thiriet *et al.*, 2021). Thus, the strength development in microsurfacing mix is continuous and evolutive, until the maximum strength is achieved.

To further understand the effect of conditioning protocols, the difference in abrasion loss for different conditioning protocols is quantified in **Table 6.3**. Here, the difference was expressed as a percentage decrease in abrasion loss. For instance, the difference due to aging time between mix AM1 and AM5 was quantified using **Equation 6.2**.

$$Difference_{AM1-AM5}\,(\%) = \frac{(Abrasion\ Loss)_{AM1} - (Abrasion\ Loss)_{AM5}}{(Abrasion\ Loss)_{AM1}} \times 100 \quad (6.2)$$

Table 6.3: Variation in raveling due to combined effect of aging and moisture

Parameter	Conditioning time		Conditioning temperature	
	Combination	Difference (%)	Combination	Difference (%)
Aging	AM1-AM5	33	AM1-AM9	37
	AM2-AM6	33	AM2-AM10	43
	AM3-AM7	14	AM3-AM11	28
	AM4-AM8	13	AM4-AM12	34
	AM9-AM13	17	AM5-AM13	22
	AM10-AM14	10	AM6-AM14	23
	AM11-AM15	5	AM7-AM15	20
	AM12-AM16	-1	AM8-AM16	24
Moisture	AM1-AM2	-10	AM1-AM3	26
	AM3-AM4	-11	AM2-AM4	25
	AM5-AM6	-9	AM5-AM7	5
	AM7-AM8	-12	AM6-AM8	2
	AM9-AM10	1	AM9-AM11	16
	AM11-AM12	-2	AM10-AM12	13
	AM13-AM14	-8	AM13-AM15	3
	AM15-AM16	-7	AM14-AM16	3

Aging time had a substantial influence on raveling, especially when the mix was not fully cured, i.e., the moisture was still present in the specimen. For instance, when the aging time was increased from 48 hours at 85°C to 120 hours at 85°C, the abrasion loss was reduced by 33% for mix subjected to moisture conditioning at 25°C (**Table 6.3**). After maximum possible moisture loss, the effect of aging on raveling reduces with the increase in the aging time. In addition, the effect of aging time was prominent at 85°C than 105°C. Hence, it could be said that once the mix is fully cured and the bond at the

aggregate-binder interface achieves the maximum possible strength, subjecting the mix to further aging does not contribute to bond strength. Similar observations were reported by Yuan *et al.* (2020).

Aging temperature had the highest influence among the four parameters considered. The reduction in abrasion loss with the increase in aging temperature from 85°C to 105°C was prominent when the aging time was 48 hours and moisture conditioning temperature was 25°C. The abrasion loss reduced by 37% for mix AM1 to AM9 and 43% for mix AM2 to AM10. Overall, the difference in abrasion loss was more than 20% for all cases (**Table 6.3**). The reason for the substantial difference in raveling is the combination of rate of moisture loss from the mix and close relationship between aging kinetics and oxidation temperature. Higher moisture loss ensures better bond strength, as explained earlier. with the increase in aging temperature, the carbonyl oxidations products formed are relatively more (Petersen *et al.*, 1993). As a result, the oxidation of the binder is accelerated. Hence, the better bond strength and the additional stiffness imparted by the relatively higher oxidation of binder leads to improved raveling resistance with the increase in aging time.

In terms of moisture conditioning time, **Figure 6.6a** shows that after aging the specimens, increasing the moisture conditioning time led to an increase in the abrasion loss. However, with the increase in aging temperature from 85°C to 105°C, the effect of moisture conditioning time on raveling reduced, especially when the aging time was 48 hours. For instance, when the mixes were subjected to moisture conditioning at 40°C, the abrasion loss increased with increase in moisture conditioning time from 48 to 144 hours by 11% for aging at 85°C whereas the increase in abrasion loss was only 2% when the aging temperature was 105°C (**Table 6.3**). Hence, it could be said that the effect of moisture conditioning time reduces with the increase in the mix stiffness.

In addition, **Figure 6.6a** shows that after aging the specimens, increasing the moisture conditioning temperature led to a reduction in abrasion loss for all cases. When the specimens were conditioned in oven at 85°C for 48 hours, moisture conditioning temperature had a substantial influence on the raveling. In particular, a reduction of 26% was observed for mix AM1 to AM3. Similarly, there was a 25% reduction in abrasion loss for mix AM4 in comparison to mix AM2. But, when the aging temperature was increased to 105°C for 48 hours, the difference in the raveling reduced

to 16% and 13% respectively (**Table 6.3**). The reduction in the difference in raveling with the increase in conditioning temperature of aging could be attributed to the additional moisture loss. It could be observed from **Figure 6.6b** that the moisture loss increased from 0.06% to 0.24% with the increase in aging conditioning temperature from 85°C to 105°C for 48 hours. After aging for 120 hours at 85°C or 105°C, the difference in abrasion loss due to moisture conditioning temperature reduced to less than 5% for all cases (**Table 6.3**). Hence, it could be said until the specimen is cured, raveling is influenced by moisture conditioning temperature. But, once the specimen is fully cured and subjecting to further aging, the effect of moisture conditioning temperature on raveling becomes minimal.

6.5.1 Statistical Analysis on synergistic effect of aging and moisture on raveling

Univariate ANOVA test was used to statistically analyze the test results at a 5% significance level. The following observations were derived from results presented in **Table 6.4.**

Table 6.4: Statistical analysis for combinations AM-1 to AM-16

Conditioning	Raveling		
	F	***p*-value**	**Significant**
Aging			
Time	311.540	0.000	Yes
Temperature	101.880	0.000	Yes
Time * Temperature	42.083	0.000	Yes
Moisture			
Time	52.063	0.000	Yes
Temperature	13.171	0.001	Yes
Time * Temperature	0.021	0.886	No

- **Aging**: Interaction and individual effect of aging time and temperature had a significant influence on raveling of microsurfacing mix. In terms of *F*-value, aging had relatively higher influence on raveling compared to moisture conditioning.

- **Moisture**: Interaction of moisture conditioning time and temperature did not contribute significantly to raveling. However, the individual effect of both moisture conditioning time and temperature had a significant influence.

6.5.2 Model development using regression analysis

In order to develop a statistical model for determining the effect of aging and moisture on raveling, the significant parameters from **Table 6.4** were considered. The "Regression Learner" app in MATLAB 2019a was used to determine the model parameters and the significance of each parameter. The estimated values of coefficients of model parameters along with *p*-value are described in **Table 6.5**. It could be observed that, in Case 1, apart from moisture conditioning time, all the model parameters had a significant effect on the predicted output. So, the model was formulated again without considering the moisture conditioning time. In case 2, all the parameters considered showed significant influence on the predicted output.

Table 6.5: Model parameters for relating raveling to aging and moisture

Equation term	Case 1			Case 2		
	Estimate	***p*-Value**	**Sig.**	**Estimate**	***p*-Value**	**Sig.**
Intercept	932.8	0.000	Yes	947.5	0.000	Yes
A_T	-6.66	0.000	Yes	-6.66	0.000	Yes
A_t	-4.05	0.012	Yes	-4.05	0.014	Yes
M_T	-1.96	0.014	Yes	-1.96	0.017	Yes
M_t	0.15	0.167	No	*NA*	*NA*	*NA*
$A_T \times A_t$	0.04	0.024	Yes	0.04	0.028	Yes

** Note: Sig. = Significant; A_T = Aging temperature (°C); A_t = Aging time (hours); M_T = Moisture conditioning temperature (°C); M_t = Moisture conditioning time (hours).*

The final model formulation is shown in **Equation 6.3**. The relation between the predicted and observed abrasion loss (AL_{am}) is shown in **Figure 6.7**. The value of adjusted R^2 was 0.83, which shows that the formulated model could predict the synergistic effect of aging and moisture conditioning on the raveling resistance of the microsurfacing mix.

$$AL_{am} = 947.5 - 4.05 \times A_t - 6.66 \times A_T + 0.04 \times A_t \times A_T - 1.96 \times M_T \quad (6.3)$$

From **Equation 6.3**, it is evident that with the increase in aging time, aging temperature, and moisture conditioning temperature, the abrasion loss decreases, i.e., raveling resistance improves. The lower value of the coefficient highlights that the interaction of aging time and temperature had a minimal influence on raveling. Hence, while assessing the durability of microsurfacing mix, it is vital to consider the aging time and temperature along with moisture conditioning temperature.

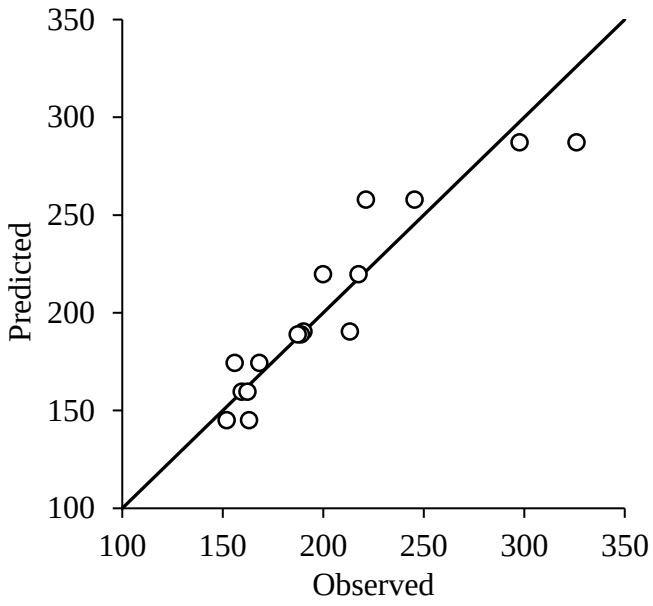

Figure 6.7: Correlation between the predicted and observed abrasion loss

6.6 Summary

The durability of the microsurfacing mix was assessed by investigating the synergistic effect of aging and moisture conditioning on the raveling resistance of the microsurfacing mix. A total of 30 combinations of conditioning protocols were considered. The following conclusions were drawn from the laboratory investigations and analysis conducted in the study.

- With the increase in aging time, the raveling reduced. An increase in the aging temperature from 85°C to 105°C leads to a 41% reduction in raveling.
- The effect of moisture conditioning time on raveling was not significant, even for 8 days at 25°C. Increasing the moisture conditioning temperature from 25°C

to 60°C for 6 days resulted in a 66% reduction in the raveling of microsurfacing mix.

- In terms of the synergistic effect of aging and moisture, aging time had the highest influence on the raveling, especially when the aging time was 48 hours and moisture conditioning temperature was 25°C. It highlights that the curing of mix and additional stiffness imparted by the increased aging time leads to improved raveling resistance.
- Subjecting the aged mix to moisture conditioning highlighted that raveling is influenced by moisture conditioning temperature until the specimen is fully cured. In contrast, the effect of moisture conditioning time is minimal. Once the specimen is fully cured and is subjected to further aging, the effect of both moisture conditioning time and temperature on raveling becomes minimal.
- The model developed using regression analysis confirms the durability of microsurfacing mix is significantly affected by aging time and temperature and moisture conditioning temperature.

CHAPTER 7

Conclusions and Recommendations

In this study, the factors influencing the performance of microsurfacing mix during the mix design stage, production stage and in-service life were evaluated. During the mix design stage, the parameters were filler type, mineral filler type and dosage, emulsifier dosage, asphalt binder type, and solvent.

Process control parameters including aggregate gradation, emulsion, and water content were considered for the production stage. During in-service life, environmental conditions including aging and moisture were considered. The performance was evaluated in terms of workability, strength, compatibility, adhesion, raveling, rutting and bleeding.

From the laboratory investigations and analysis, the following conclusions were drawn.

7.1 Mix design stage

- Compatibility of the microsurfacing mix was found to be dependent on the filler characteristics. Acceptable workability (mix time > 120 sec) was observed with the incorporation of filler having lower clay content (Sand Equivalent Value > 65, and MBV < 5).
- Varying emulsifier dosage resulted in the difference in cohesion, raveling and rutting upto 43%, 58% and 14% respectively. Study recommends assessment of the variation in performance whenever the emulsifier dosage is varied to adjust the breaking and curing time.
- Incorporation of harder binder grade improved the rutting resistance by 36% but resulted in unacceptable raveling. In such scenarios, study recommends the use of solvent during emulsion production to maintain asphalt at equiviscous temperature (200 cP viscosity) while ensuring the outlet temperature to be less than 95°C.
- Mix characteristics including cohesion at 60-minute, adhesion, and compatibility (abrasion loss) had a good correlation with the raveling and rutting. The study recommend to establish these mix characteristics during mix design to identify suitable type and optimum dosage of mineral filler.

- Findings propose a narrow range diagram accounting for cohesion at 30-min and 60-min, abrasion loss, lateral displacement and sand adhesion to obtain the job mix formula. Implementing a narrow range diagram would give an idea to the practitioners about the consequences of deviation from design formulation.

7.2 Production stage

- Individual effect of process control parameters and the range of variation with respect to control mix is summarized in **Table 7.1**. Substantial variation was observed in workability, raveling, rutting and bleeding whereas the range of variation was minimal for strength.

Table 7.1: Summarizing effect of process control parameters on performance

Performance parameter	Influence of increase in the value of process control parameter		
	Aggregate gradation (in terms of TSA)	**Emulsion content**	**Water content**
Workability	Decrease (-16% to +31%)	Increase (-35% to +48%)	Increase (-61% to +87%)
Strength	Increase (-12% to +4%)	Minimal variation (-2% to +1%)	Minimal variation (-3% to +3%)
Raveling	Decrease (-17% to +54%)	Decrease (-28% to +46%)	Decrease (-25% to +2%)
Rutting	Decrease (-8% to +53%)	Optimum (0% to +42%)	Optimum (0% to +16%)
Bleeding	Decrease (-27% to +49%)	Increase (-4% to +7%)	Decrease (-28% to +17%)

- The synergistic variation of process control parameters, even within the tolerance limits, substantially influenced the performance. **Table 7.2** presents a summary of the critical combinations of process control parameters for which unacceptable performance was noticed as per ISSA guidelines.

Table 7.2: Critical combinations of process control parameters

Parameter	Critical scenarios
Workability	• Water content > OWC + 1% • Water content = OWC – 1% & Emulsion content = OEC – 1.5% • Aggregate gradation = UL & Emulsion content = OEC – 1.5%
Raveling	• Aggregate gradation = LL & Emulsion content = OEC – 1.5%
Rutting	• Aggregate gradation = LL & Water content ≥ OWC
Bleeding	• Aggregate gradation = LL; Emulsion content > OEC; & WC < OWC

- Analysis using ANN showed that the relative contribution of aggregate gradation on strength and raveling, emulsion content on workability, strength at 30-min and rutting, and water content on workability, strength at 60-min and bleeding was more than 35%.
- Model developed using MSGP effectively quantified the effect of process control parameters on performance. Among all the parameters, workability exhibited highest variability whereas the variation in strength was minimal. Raveling and rutting increased exponentially for coarser gradation and higher emulsion content, respectively. The variation in bleeding was relatively lower than raveling and rutting, where bleeding increased by 8% with a 10% increase in water content with respect to optimum.
- Reliability analysis highlighted that the highest probability of failure of microsurfacing mix was due to rutting (Reliability = 57%). Controlling the scenarios for which the risk of rutting was highest improved the overall reliability from 47% to 71%. Utilizing such analysis during the mix design stage would help in establishing a decision on the quality control tolerance limits to maximize the performance within the budgetary constraints.

7.3 In-service stage

- The effect of environmental conditions on raveling is summarized in **Table 7.3**. Reduction in raveling due to increase in the aging time and temperature was statistically significantly. However, the raveling increased with the increase in the moisture conditioning time or decrease in the moisture temperature.

Table 7.3: Summarizing individual effect of environmental conditions on raveling

Conditioning	Influence of increment in conditioning protocol on raveling	
	Time	**Temperature**
Aging	• Decreased by 21% in 120 h • Significant – After 120 h	• Decreased by 41% – 85 to 105°C • Significant – 85 to 105°C
Moisture	• Increased by 14% in 196 h • Not significant	• Decreased by 66% – 25 to 60°C • Significant – 25 to 60°C

- Synergistic variation of aging and moisture conditioning protocols showed that the loss of moisture and gain in mix stiffness due to aging improves the resistance to raveling and moisture damage. This highlights that higher temperature for a longer duration promotes the development of strength. Hence, the microsurfacing mix should be applied during hot weather conditions to ensure durability.

7.4 Application

Process control in microsurfacing is confined to the individual monitoring of parameters that exhibit inherent variability during production including aggregate gradation, mineral filler content, emulsion content and water content. This study demonstrates the synergistic influence of these parameters and lays down a procedure for identification and quantification of critical combinations that increases the risk of failures. The outcomes of the laboratory investigation highlighted that controlling the parameters within the tolerance limits might not be sufficient to ensure desirable characteristics. In particular, mix produced with the combination of coarse aggregate gradation having lower mineral filler content and lower emulsion content had the highest risk of failure.

Hence, it is recommended that the performance should be examined in terms of workability, strength, raveling, rutting and bleeding, for the extreme limits of tolerance range during the mix design stage. Special remarks should be provided to highlight the scenarios for which the performance reaches to an unacceptable limit. Avoiding such scenarios during QC/QA would ensure that the risk of failure of the microsurfacing mix is minimized during its design life. In addition, the accumulation of different project-specific findings could potentially help in generalizing the findings of this study.

CHAPTER 8

Limitations and Future Scope

The study included variations generally encountered in field during production. However, certain limitations were associated with this study due to time and laboratory constraints. Some of the limitations and associated future scope for research is discussed below.

- In this study, conventional laboratory investigations were carried out with a single microsurfacing mix formulated to meet the specification requirements. The model development to understand the performance could be influenced by the mix ingredients and design formulation. The performance of microsurfacing mix is highly dependent on the aggregate-emulsion interaction. Conducting laboratory investigations on aggregates with different physical and mineralogical properties would help in further generalizing the conclusions drawn from the study.
- Mineral filler types and dosages were found to be critical aspect of microsurfacing performance. The results were based on the macroscopic investigations conducted on the mix produced in laboratory. In order to understand the mechanism behind the findings of the research, there is a need to explore microscopic tests like X-ray powder diffraction (XRD), Fourier-transform infrared spectroscopy (FTIR), and environmental scanning electron microscope (ESEM), among many others.
- The range of process control parameters explored in this research was based on the tolerance limits specified by ISSA. The range should be verified with the variability observed in field. Accordingly, conclusions and recommendations from this study could be utilized to fine-tune the quality control during production.
- Study on raveling behavior with environmental conditions during service life was assessed. Investigations on other critical performance parameters like rutting and cracking is important. Also, there is a need to explore the aging kinetics and moisture damage mechanism associated with microsurfacing mix.

Publications

Journals

1. Bhargava, N., Siddagangaiah, A. K., & Ryntathiang, T. L. (2022). Evaluating the Workability and Strength Evolution of Microsurfacing Mix. *Transportation Research Record*, 1-14.
2. Bhargava, N., Siddagangaiah, A. K., & Ryntathiang, T. L. (2022). Modelling the Factors Influencing the Rutting and Bleeding Characteristics of Microsurfacing Mix. *Journal of Materials in Civil Engineering*, *34*(4), 04022026.
3. Bhargava, N., Siddagangaiah, A. K., & Ryntathiang, T. L. (2022). Effect of Cement and Fly ash Dosages on the Performance of Microsurfacing Mix. *Journal of Materials in Civil Engineering*, *34*(2), 04021441.
4. Bhargava, N., Siddagangaiah, A. K., & Ryntathiang, T. L. (2022). Relative Contribution of Process Control Parameters on the Raveling Resistance of Microsurfacing Mix. *Transportation Research Record*, *2676*(2), 743-753.
5. Bhargava, N., Siddagangaiah, A. K., & Ryntathiang, T. L. (2021). Systematic approach to address challenges in microsurfacing mix design. *Construction and Building Materials*, *270*, 121759.
6. Bhargava, N., Siddagangaiah, A. K., & Ryntathiang, T. L. (2021). Sustainable Development with Microsurfacing: A Review. *Journal of Testing and Evaluation*, *49*(2), 1284-1306.
7. Bhargava, N., Siddagangaiah, A. K., & Ryntathiang, T. L. (2020). Reliability of Microsurfacing Mix Subjected to Variation in Aggregate Gradation. *Transportation Research Record*, *2674*(11), 720-730.
8. Bhargava, N., Siddagangaiah, A. K., & Ryntathiang, T. L. (2020). State of the art review on design and performance of microsurfacing. *Road Materials and Pavement Design*, *21*(8), 2091-2125.

International conference

1. Bhargava, N., Siddagangaiah, A. K., & Ryntathiang, T. L. (2022). *Effect of Process Control Parameters on the Workability and Strength Characteristics of Microsurfacing Mix.* Transportation Research Board, 101st Annual Meeting 2022, Washington D. C., USA.
2. Bhargava, N., Siddagangaiah, A. K., & Ryntathiang, T. L. (2021). *Sustainability Assessment of Microsurfacing with Incorporation of Fly Ash*. International Conference on Resource Sustainability - Sustainable Pavement Technologies, Tirupati, India.

Under review

1. Bhargava, N., Siddagangaiah, A. K., & Ryntathiang, T. L. *Influence of Aging and Moisture Conditions on the Raveling Resistance of Microsurfacing Mix.* Road Materials and Pavement Design.

References

Abo-Qudais, S., & Al-Shweily, H. (2007). Effect of aggregate properties on asphalt mixtures stripping and creep behavior. *Construction and Building Materials, 21*(9), 1886-1898.

Alavi, A. H., Hasni, H., Zaabar, I., & Lajnef, N. (2017). A new approach for modeling of flow number of asphalt mixtures. *Archives of Civil and Mechanical Engineering, 17,* 326-335.

American Coal Ash Association. (2003). *Fly ash facts for highway engineers.* Report No. FHWA-IF-03-019. US Department of Transportation, Federal Highway Administration.

Andrews, E. M. (1994). *The evaluation of micro-surfacing mixture design procedures and the effects of material variation on the test responses.* Doctoral dissertation, Texas A&M University.

ASTM D2397. (2020). *Standard Specification for Cationic Emulsified Asphalt.* West Conshohocken, PA: ASTM International.

ASTM D5148. (2010). *Standard test method for centrifuge Kerosine equivalent.* West Conshohocken, PA: ASTM International.

ASTM D6372. (2015). *Standard Practice for Design, Testing, and Construction of Microsurfacing.* West Conshohocken, PA: ASTM International.

ASTM D6930. (2019). *Standard Test Method for Settlement and Storage Stability of Emulsified Asphalts.* West Conshohocken, PA: ASTM International.

ASTM D6933. (2018). *Standard Test Method for Oversized Particles in Emulsified Asphalts (Sieve Test).* West Conshohocken, PA: ASTM International.

ASTM D7496. (2018). *Standard test method for viscosity of Emulsified asphalt by Saybolt Furol Viscometer*. West Conshohocken, PA: ASTM International.

Aurangzeb, Q., & Al-Qadi, I. (2014). Asphalt pavements with high reclaimed asphalt pavement content: economic and environmental perspectives. *Transportation Research Record: Journal of the Transportation Research Board, 2456,* 161-169.

Babashamsi, P., Yusoff, N., & Hainin, M. (2016). The effect of preservation maintenance activities in asphalt concrete pavement sustainability. *Jurnal Teknologi, 78*(4), 117-124.

Bae, A., & Stoffels, S. M. (2008). Economic effects of microsurfacing on thermally-cracked pavements. *KSCE Journal of Civil Engineering, 12*(3), 177-185.

Baker, R. F. (1990). Asphalt Emulsion Slurry Seal and Wheelpath Inlay. *Asphalt Emulsions, ASTM STP 1079*, 65-79.

Baladi, G., Svasdisant, T., Van, T., Buch, N., & Chatti, K. (2002). Cost-effective preventive maintenance: Case studies. *Transportation Research Record: Journal of the Transportation Research Board, 1795*, 17-26.

Barnes, G., & Langworthy, P. (2003). *The Per-Mile Costs of Operating Automobiles and Trucks. MN/RC 2003-19.* St. Paul, MN: Minnesota Department of Transportation.

Baumgardner, G. L. (2006). Asphalt emulsion manufacturing today and tomorrow. In *Asphalt Emulsion Technology* (pp. 15-26). Transportation Research Circular E-C102.

Bennert, T., Hanson, D., Maher, A., & Vitillo, N. (2005). Influence of pavement surface type on tire/pavement generated noise. *Journal of Testing and Evaluation, 33*(2), 94-100.

Borwankar, R. P., Lobo, L. A., & Wasan, D. T. (1992). Emulsion stability - Kinetics of flocculation and coalescence. *Colloids and Surfaces, 69*(2-3), 135-146.

Bouteiller, É. l. (2010). Asphalt Emulsions for Sustainable Pavements. *First International Conference on Pavement Preservation* (pp. 627-640). California Department of Transportation, Federal Highway Administration, Foundation for Pavement Preservation.

Broughton, B., & Lee, S.-J. (2012a). *Microsurfacing in Texas (Report No. FHWA/TX-12/0-6668-1).* Austin, Texas: Texas Department of Transportation.

Broughton, B., & Lee, S.-J. (2012b). Microsurfacing as a Preventative Maintenance Program in Texas. *International Journal of Pavement Research and Technology, 5*(6), 405-410.

Broughton, B., Lee, S.-J., & Kim, Y.-J. (2012). 30 Years of Microsurfacing: A Review. *ISRN Civil Engineering*.

BS EN 12273. (2008). *Slurry surfacing – requirements.* British Standards.

BS EN 12274-3. (2002). *Slurry surfacing – test methods – Part 3: Consistency.* British Standards.

BS EN 12274-4. (2003). *Slurry surfacing – test methods – Part 4: Determination of cohesion of the mix.* British Standard.

BS EN 12274-5. (2003). *Slurry surfacing – test methods – Part 5: Determination of wearing.* British Standard.

BS EN 12274-7. (2005). *Slurry surfacing – test methods – Part 7: Shaking abrasion test.* British Standard.

BS EN 12274-8. (2005). *Slurry surfacing – test methods – Part 8: Visual assessment of defects.* British Standard.

Buss, A., & Pinto, I. (2019). *Scientific Innovations in Microsurfacing and Slurry Seal Mixture Design (Report No. IHRB Project TR-755).* Ames, Iowa: Institute for Transportation, Iowa State University.

Button, J. W. (1996). Permeability of Asphalt Surface Seals and Their Effect on Aging of Underlying Asphalt Concrete. *Transportation Research Record: Journal of the Transportation Research Board, 1535*, 124-130.

Caltrans. (2004). *Slurry Seal / Micro-Surface Mix Design Procedure - Phase I Report.* Fugro Consultant, Inc. and Mactec, California Department of Transportation (Caltrans).

Caltrans. (2009). Chapter 9 - Micro-Surfacing. In *MTAG Volume I Flexible Pavement Preservation 2nd Edition.* California: Caltrans Division of Maintenance.

Caltrans. (2010). *Slurry Seal / Micro-Surface Mix Design Procedure - Phase II Report.* California: Fugro Consultant, Inc. and Mactec, California Department of Transportation (Caltrans).

Caltrans. (2015). *Standard specifications.* California: California State Transportation Agency, Department Of Transportation.

Chakroborty, P., Das, A., & Ghosh, P. (2009). Determining reliability of an asphalt mix design: case of Marshall method. *Journal of Transportation Engineering, 136*(1), 31-37.

Chan, S., Lane, B., Kazmierowski, T., & Lee, W. (2011). Pavement preservation: A solution for sustainability. *Transportation Research Record: Journal of the Transportation Research Board, 2235*, 36-42.

Chatti, K., & Zaabar, I. (2012). *Estimating the effects of pavement condition on vehicle operating costs. NCHRP Report 720*. Washington, DC: Transportation Research Board of the National Academies.

Chehovits, J., & Galehouse, L. (2010). Energy usage and greenhouse gas emissions of pavement preservation processes for asphalt concrete pavements. In *Proceedings on the 1st International Conference of Pavement Preservation*, (pp. 27-42).

Cheng, D., Hicks, R. G., Parsons, A., Zubeck, H., Liu, J., & Mullin, A. (2013). Development of Enhanced Alaska Pavement Preservation Program and Strategy Selection Guide. *Transportation Research Record: Journal of the Transportation Research Board, 2361*, 44-55.

Copeland, A. (2011). *Reclaimed asphalt pavement in asphalt mixtures: State of the practice.* No. FHWA-HRT-11-021.

Cui, D., & Pang, J. (2017). The Effect of pH on the Properties of a Cationic Bitumen Emulsifier. *Tenside Surfactants Detergents, 54*(5), 386-392.

Cui, P., Wu, S., Xiao, Y., Yang, C., & Wang, F. (2020). Enhancement mechanism of skid resistance in preventive maintenance of asphalt pavement by steel slag based on micro-surfacing. *Construction and Building Materials, 239*, 117870.

Das, S., Raju, N., Maurya, A. K., & Arkatkar, S. (2020). Evaluating lateral interactions of motorized two-wheelers using multi-gene symbolic genetic programming. *Transportation research record, 2674*(9), 1120-1135.

Deschner, F., Lothenbach, B., Winnefeld, F., & Neubauer, J. (2013). Effect of temperature on the hydration of Portland cement blended with siliceous flyash. *Cement and concrete research, 52*, 169-181.

Dong, Q., Chen, X., Huang, B., & Gu, X. (2018). Analysis of the Influence of Materials and Construction Practices on Slurry Seal Performance Using LTPP Data. *Journal of Transportation Engineering, Part B: Pavements, 144*(4), 04018046.

Dong, Q., Huang, B., Richards, S. H., & Yan, X. (2013). Cost-effectiveness analyses of maintenance treatments for low-and moderate-traffic asphalt pavements in Tennessee. *Journal of Transportation Engineering*, *139*(8), 797-803.

Du, H., Dong, Q., & Ni, F. (2018). Performance and Effectiveness Evaluation of Pavement Maintenance Treatments through Data Mining. In *International Conference on Transportation and Development, Airfield and Highway Pavements (pp. 371-381)*. Pittsburgh, Pennsylvania: ASCE.

Du, S. (2013). Effect of different fillers on performance properties of asphalt emulsion mixture. *Journal of Testing and Evaluation*, *42*(1), 126-134.

Du, S. (2014). Interaction mechanism of cement and asphalt emulsion in asphalt emulsion mixtures. *Materials and structures*, *47*(7), 1149-1159.

Ducasse, K., Distin, T., & Osborne, L. (2004). The use of microsurfacing as a cost effective remedial action for surface rutting. In *8th Conference on Asphalt Pavements for Southern Africa (CAPSA'04) (pp. 11)*. Sun City, South Africa.

Elvik, R. (2000). How much do road accidents cost the national economy? *Accident Analysis & Prevention*, *32*(6), 849-851.

Erwin, T. C. (2007). *Safety Effects of Preventative Maintenace: Microsurfacing: A Case Study*. Master's thesis, University of Waterloo.

Esfahani, M. A., & Khatayi, A. (2020). Effect of type and quantity of emulsifier in bitumen polymer emulsion on microsurfacing performance. *International Journal of Pavement Engineering*, 1-15.

Fang, X., Garcia-Hernandez, A., & Lura, P. (2016). Overview on cold cement bitumen emulsion asphalt. *RILEM Technical Letters*, *1*, 116-121.

Firouzinia, M., & Shafabakhsh, G. (2018). Investigation of the effect of nano-silica on thermal sensitivity of HMA using artificial neural network. *Construction and Building Materials*, *170*, 527-536.

Fooladi, A., & Hesami, S. (2021). Experimental Investigation of the Effect of Types of Fillers on the Performance of Microsurfacing Asphalt Mixture. *Journal of Materials in Civil Engineering*, *33*(7), 04021139.

Frederick, G., & Tario, J. D. (2009). *Quantify the Energy and Environmental Effects of Using Recycled Asphalt and Recycled Concrete for Pavement Construction, Phase I Final Report, Agreement No. 10629/C-08-02.* Albany, NY: New York State Energy Research and Development Authority.

Galehouse, L., Moulthrop, J. S., & Hicks, R. G. (2003). Principles of pavement preservation: Definitions, benefits, issues, and barriers. *TR News*, *228*.

Gandomi, A. H., & Alavi, A. H. (2012). A new multi-gene genetic programming approach to non-linear system modeling. Part II: geotechnical and earthquake engineering problems. *Neural Computing and Applications*, *21*(1), 189-201.

Gandomi, A. H., & Atefi, E. (2020). Software review: the GPTIPS platform. *Genetic Programming and Evolvable Machines*, *21*(1), 273-280.

García, A., Lura, P., Partl, M. N., & Jerjen, I. (2013). Influence of cement content and environmental humidity on asphalt emulsion and cement composites performance. *Materials and structures*, *46*(8), 1275-1289.

Garfa, A., Carter, A., & Dony, A. (2018). Rutting Resistance of HMA Rehabilitated with Micro-Surfacing. *Open Journal of Civil Engineering*, *8*(2), 245-255.

Garfa, A., Dony, A., & Carter, A. (2016). Performance evaluation and behavior of microsurfacing with recycled materials. *6th Eurasphalt & Eurobitume Congress*. Prague, Czech Republic.

GDOT. (2013). *Standard specifications construction of transportation systems.* Georgia Department of Transportation. State Transportation Board.

Geiger, D. R. (2005). *Pavement Preservation Definitions.* U.S. Department of Transportation, Federal Highway Administration. Retrieved April 15, 2018, from https://www.fhwa.dot.gov/pavement/preservation/091205.cfm

Gevrey, M., Dimopoulos, I., & Lek, S. (2003). Review and comparison of methods to study the contribution of variables in artificial neural network models. *Ecological modelling*, *160*(3), 249-264.

Giustozzi, F., Crispino, M., & Flintsch, G. W. (2012). Preventive Maintenance on Road Pavements: Performance and Environmental Assessment of Strategies. In *SIIV Roma MMXII - Fifth International Congress* (pp. 1-11). Italy: SIIV.

Gorman, J. L., Crawford, R. J., Stannard, P., & Harding, I. H. (1998). The role of aggregate surface chemistry in bitumen emulsion--aggregate interactions. *Road & Transport Research, 7*(4), 3-12.

Gransberg, D. D. (2010). *NCHRP Synthesis 411: Microsurfacing; a synthesis of highway practices.* Washington, DC: Transportation Research Board of the National Academies.

Gransberg, D. D., Pittenger, D. M., & Tighe, S. M. (2012). Microsurfacing best practices in North America. In *Seventh International Conference on Maintenance and Rehabilitation of Pavements and Technological Control (Vol. 51, pp. 1-9).* Auckland, New Zealand.

Gravetter, F. J., & Wallnau, L. B. (2016). *Statistics for the behavioral sciences.* Cengage Learning.

Gujar, R. S., & Chauhan, K. A. (2013). Feasibility of Rice Husk Ash as Optional Mineral Filler in Microsurfacing incorporating Type III Aggregate. *American Journal of Environmental Engineering, 3*(2), 95-99.

Gujar, R. S., Chauhan, K. A., & Dadhich, G. (2013). Microsurfacing - An Eco-Efficient Tool for Road Safety and Pavement Maintenance. *International Journal of Sustainable Construction Engineering and Technology, 4*(2), 47-51.

Gujar, R., & Vakharia, V. (2019). Prediction and validation of alternative fillers used in micro surfacing mix-design using machine learning techniques. *Construction and Building Materials, 207,* 519-527.

Guo, J., Ye, Y., Cai, C., & Zhao, W. (2017). Effects of Fineness of Rubber Powder on Micro-Surfacing Performance. In *IOP Conference Series: Materials Science and Engineering (Vol. 216, pp. 012031).* Seoul, Korea: IOP Publishing.

Habeeb, H., Chandra, S., & Nashaat, Y. (2014). Estimation of moisture damage and permanent deformation in asphalt mixture from aggregate gradation. *KSCE Journal of Civil Engineering, 18*(6), 1655-1663.

Hafezzadeh, R., & Kavussi, A. (2021). Application of microsurfacing in repairing pavement surface rutting. *Road Materials and Pavement Design, 22*(5), 1219-1230.

Hagan, M. T., & Menhaj, M. B. (1994). Training Feedforward Networks with the Marquardt Algorithm. *IEEE transactions on Neural Networks, 5*(6), 989-993.

Han, Z., Porras-Alvarado, J. D., Stone, C., & Zhang, Z. (2019). Incorporating uncertainties into determination of flexible pavement preventive maintenance interval. *Transportmetrica A: Transport Science, 15*(1), 34-54.

Harbi, S., Margni, M., Loerincik, Y., & Dettling, J. (2015). Life cycle management as a way to operationalize sustainability within organizations. In *Life cycle management* (pp. 23-33). Dordrecht: Springer.

Hein, D. K., Emery, J. J., & Ippolito, R. D. (1994). Microsurfacing urban pavements. *Civil Engineering, 64*(5), 55-57.

Heritage, R. (2011). Micro Surfacing Solves Hurricane-Induced Rutting. *Progressive Railroading, 5*(1), 22-23.

Hicks, R. G., Dunn, K., & Moulthrop, J. (1997). Framework for selecting effective preventive maintenance treatments for flexible pavements. *Transportation Research Record: Journal of the Transportation Research Board, 1597*, 1-10.

Hixon, C. D., & Ooten, D. A. (1993). Nine Years of Microsurfacing in Oklahoma. In *Proceedings, Transportation Research Board, National Research Council (Vol. 1392, pp. 13-19)*. Washington, D.C.

Hogendoorn, S. (2016). Chemistry of Asphalt Emulsion and Emulsion Systems. In *31 Annual Slurry Systems Workshop*. Las Vegas, Nevada: ISSA.

Holleran, G., Reed, J. R., & Van Kirk, J. (1997). The use of crumb rubber in slurry and microsurfacing and chip seals. In *AAPA International Flexible Pavements Conference*. Perth, Western Australia.

Hou, S., Chen, C., Zhang, J., Shen, H., & Gu, F. (2018). Thermal and mechanical evaluations of asphalt emulsions and mixtures. *Construction and Building Materials, 191*, 1221-1229.

Humphries, E., & Lee, S.-J. (2015). Evaluation of Pavement Preservation and Maintenance Activities at General Aviation Airports in Texas: Practices, Perceived Effectiveness, Costs, and Planning. *Transportation Research Record: Journal of the Transportation Research Board, 2471*, 48-57.

Hunter, R. N., Self, A., & Read, J. (2015). *The Shell Bitumen (6th ed.).* London: ICE Publishing.

Ibrahim, H. E.-S. (1998). *Assessment and design of emulsion-aggregate mixtures for use in pavements.* Doctoral dissertation, University of Nottingham.

Ilias, M. (2015). *Development of Performance-Related Specification for Fresh Emulsions Used for Surface Treatments and Performance Study of Chip Seals and Microsurfacing.* Raleigh, North Carolina.

Ilias, M., Adams, J., Castorena, C., & Kim, Y. R. (2017). Performance-Related Specifications for Asphalt Emulsions Used in Microsurfacing Treatments. *Transportation Research Record: Journal of the Transportation Research Board, 2632*, 1-13.

InstroTek, Inc. (n.d.). *ACT: Asphalt Compatibility Tester. Operating Manual.* Retrieved from https://web.archive.org/web/20190724125928/https://cdn.shopify.com/s/files/1/1245/4913/files/ACT_Manual_ver_3.pdf?20

IRC: SP: 16. (2004). *Guidelines for the surface eveness of highway pavements.* Indian Roads Congress.

IRC: SP: 81. (2008). *Tentative Specifications for Slurry Seal and Microsurfacing.* New Delhi, India: Indian Roads Congress.

Irfan, M., Khurshid, M. B., Ahmed, A., & Labi, S. (2011). Scale and condition economies in asset preservation cost functions: case study involving flexible pavement treatments. *Journal of Transportation Engineering, 138*(2), 218-228.

ISSA A143. (2010). *Recommended Performance Guideline For Micro Surfacing.* Glen, Ellyn, IL: International Slurry Surfacing Association.

ISSA TB No. 100. (2017). *Laboratory Test Method for Wet Track Abrasion of Slurry Surfacing Systems.* Glen, Ellyn, IL: International Slurry Surfacing Association.

ISSA TB No. 106. (2015). *Test Method for Measurement of Slurry Seal Consistency.* Glen, Ellyn, IL: International Slurry Surfacing Association.

ISSA TB No. 109. (2005). *Test Method for Measurement of Excess Asphalt In Bituminous Mixtures by Use of a Loaded Wheel Tester and Sand Adhesion.* Glen, Ellyn, IL: International Slurry Surfacing Association.

ISSA TB No. 111. (2005). *Outline Guide Design Procedure for Slurry Seal.* Glen, Ellyn, IL: International Slurry Surfacing Association.

ISSA TB No. 113. (2017). *Test method for Determining Mix Time for Slurry Surfacing Systems.* Glen, Ellyn, IL: International Slurry Surfacing Association.

ISSA TB No. 115. (2005). *Determination of Slurry System Compatibility.* Glen, Ellyn, IL: International Slurry Surfacing Association.

ISSA TB No. 118. (2005). *Surface Area Method of Slurry Seal Design.* Glen, Ellyn, IL: International Slurry Surfacing Association.

ISSA TB No. 139. (2017). *Test Method to Determine Set and Cure Development of Slurry Surfacing Systems by Cohesion Tester.* Glen, Ellyn, IL: International Slurry Surfacing Association.

ISSA TB No. 144. (2013). *Test Method for Classification of Slurry Surfacing Materials Compatibility by Schulze-Breuer and Ruck Procedures.* Glen, Ellyn, IL: International Slurry Surfacing Association.

ISSA TB No. 147. (2005). *Test Method for Measurement of Stability and Resistance to Compaction, Vertical and Lateral Displacement of Multilayered Fine Aggregate Cold Mixes.* Glen, Ellyn, IL: International Slurry Surfacing Association.

ISSA TB No. 149. (2005). *Test Method for Boiling Compatibility of Slurry Seal Mixes.* Glen, Ellyn, IL: International Slurry Surfacing Association.

Jada, A., Florentin, C., & Mariotti, S. (2004). Study of the electrical properties of cationic bitumen emulsions by microelectrophoresis. *Advances in colloid and interface science, 108-109*, 127-132.

Jahren, C. T., Nixon, W. A., Bergeson, K. L., Al-Hammadi, A., Celik, S., Chung, J. W., Lau, G., Quintero, H., Thorius, J. (2003). *Thin Maintenance Surfaces Phase*

Two Report with Guidelines for Winter Maintenance on Thin Maintenance Surfaces. No. Project TR-435.

Jahren, C., & Behling, K. (2004). Thin maintenance surface treatments: Comparative study. *Transportation Research Record: Journal of the Transportation Research Board, 1866*, 20-27.

James, A. (2006). Overview of asphalt emulsion. *Asphalt emulsion technology* (pp. 1-15). Transportation Research Circular E-C102.

Jamion, N., Hainin, M. R., & Yaacob, H. (2014). Performance of Micro Surfacing on Expressway. *Jurnal Teknologi, 70*(7), 125–129.

Ji, Y., Nantung, T., Tompkins, B., & Harris, D. (2013). Evaluation for Microsurfacing as Pavement Preservation Treatment. *Journal of Materials in Civil Engineering, 25*(4), 540-547.

Johnson, E., Wood, T., & Olson, R. (2007). Flexible slurry-microsurfacing system for overlay preparation: Construction and seasonal monitoring at Minnesota road research project. *Transportation Research Record: Journal of the Transportation Research Board, 1989*, 321-326.

Kazmierowski, T. J., & Bradbury, A. (1995). Microsurfacing: Solution for deteriorated freeway surfaces. *Transportation Research Record, 1473*, 120-130.

Khan, M. I. (1998). *Performance optimization and modeling of slurry seal and micro surfacing utilizing steel slag aggregates.* Saudi Arabia: Doctoral dissertation, King Fahd University of Petroleum and Minerals.

Kim, Y. J., Lim, J. K., Son, H. J., Kwon, S. A., Hong, J. C., & Shin, H. J. (2013). Field Evaluation of Surface Treatments on Existing Asphalt Pavement in National Highway. *Advanced Materials Research, 723*, 745-752.

Kim, Y. R., Adams, J., Castorena, C., Ilias, M., Im, J. H., Bahia, H., Chaturabong, P., Hanz, A., Johannes, P. T. (2017). *Performance-Related Specifications for Emulsified Asphaltic Binders Used in Preservation Surface Treatments. NCHRP 837 - No. Project 09-50*. Washington, DC: Transportation Research Board of the National Academies.

Koza, J. R. (1992). *Genetic programming: on the programming of computers by means of natural selection (Vol 1).* London: MIT Press.

Krishnan, J. M., & Rao, C. L. (2001). Permeability and bleeding of asphalt concrete using mixture theory. *International Journal of Engineering Science, 39*(6), 611-627.

Kucharek, A. S., Davidson, J. K., Moore, T., & Linton, T. (2010). Performance Review of Micro Surfacing and Slurry Seal Applications in Canada. In *CTAA Annual Conference Proceedings-Canadian Technical Asphalt Association (Vol. 55, pp. 311-330).* Quebec City, Canada: Canadian Technical Asphalt Association.

Kumar, B., Jha, A., Deshpande, V., & Sreenivasulu, G. (2014). Regression model for sediment transport problems using multi-gene symbolic genetic programming. *Computers and Electronics in Agriculture, 103*, 82-90.

Kumar, R., & Ryntathiang, T. L. (2012). Rural Road Preventive Maintenance with Microsurfacing. In *International Conference on Emerging Frontiers in Technology for Rural Area (EFITRA)* (pp. 4-8). International Journal of Computer Applications® (IJCA).

Kumar, R., & Ryntathiang, T. L. (2016). New Laboratory Mix Methodology of Microsurfacing and Mix Design. In *Transportation Research Procedia (pp. 488-497)*. Mumbai, India.

Labi, S., & Sinha, K. C. (2005). Life-cycle evaluation of flexible pavement preventive maintenance. *Journal of Transportation Engineering, 131*(10), 744-751.

Lambert, M., Piau, J. M., Gaudefroy, V., Millien, A., Dubois, F., Petit, C., & Chaignon, F. (2018). Modeling of cold mix asphalt evolutive behaviour based on nonlinear viscoelastic spectral decomposition. *Construction and Building Materials, 173*, 403-410.

Lebedev, N. N. (1965). *Special functions and their applications.* Prentice Hall, Inc.

Lee, J., Edil, T., Tinjum, J., & Benson, C. (2010). Quantitative assessment of environmental and economic benefits of recycled materials in highway construction. *Transportation Research Record: Journal of the Transportation Research Board, 2158*, 138-142.

Lesueur, D., & Josè Potti, J. (2004). Cold mix design: a rational approach based on the current understanding of the breaking of bituminous emulsions. *Road Materials and Pavement Design, 5*(1), 65-87.

Li, X.-j., Wang, C., Bi, W.-l., & Shi, F.-z. (2019). Study on Road Durability of Multilevel Built-In Waterborne Epoxy Micro-Surfacing. *Journal of Highway and Transportation Research and Development (English Edition), 13*(4), 1-8.

Li, Y., Lyv, Y., Fan, L., & Zhang, Y. (2019). Effects of Cement and Emulsified Asphalt on Properties of Mastics and 100% Cold Recycled Asphalt Mixtures. *Materials, 12*(5), 754.

Little, D. N., & Jones, D. R. (2003). Chemical and mechanical processes of moisture damage in hot-mix asphalt pavements. In *National seminar on moisture sensitivity of asphalt pavements (pp. 37-70)*. Sand Diego, California.

Little, D. N., & Petersen, J. C. (2005). Unique effects of hydrated lime filler on the performance-related properties of asphalt cements: Physical and chemical interactions revisited. *Journal of Materials in Civil Engineering, 17*(2), 207-218.

Liu, B., & Hou, W. (2017). Influence of storage conditions on the stability of asphalt emulsion. *Petroleum Science and Technology, 35*(12), 1217-1223.

Liu, F., Zheng, M., Fan, X., Li, H., & Wang, F. (2021). Performance evaluation of waterborne epoxy resin-SBR compound modified emulsified asphalt micro-surfacing. *Construction and Building Materials, 295*, 123588.

Liu, J., Yan, K., Liu, J., & Zhao, X. (2018). Using Artificial Neural Networks to Predict the Dynamic Modulus of Asphalt Mixtures Containing Recycled Asphalt Shingles. *Journal of Materials in Civil Engineering, 30*(4), 04018051.

Liu, M., Han, S., Wang, Z., Ren, W., & Li, W. (2019). Performance evaluation of new waterborne epoxy resin modified emulsified asphalt micro-surfacing. *Construction and Building Materials, 214*, 93-100.

Loeber, L., Alexandre, S., Muller, G., Triquigneaux, J., Jolivet, Y., & Malot, M. (2000). Bituminous emulsions and their characterization by atomic force microscopy. *Journal of Microscopy, 198*, 10-16.

Lonbar, M. S., & Nazirizad, M. (2016). Laboratory Investigation of Materials Type Effects on the Microsurfacing Mixture. *Civil Engineering Journal, 2*(3), 86-94.

Lonbar, M., Nasrazad, S., & Shafaghat, A. (2014). Evaluation of aggregate types and adhesive materials effect on the microsurfacing skid resistance. In *Proceedings*

2nd International Congress on Structure, Architecture and Urban Development. Tabriz, Iran.

Lonbar, M., Nasrazad, S., & Shafaghat, A. (2015). Investigation of aggregate and binder types effects on the microsurfacing rutting properties. In *International Conference on Civil Engineering Architecture and urban infrastructure, 15th Annual Meeting*. Tabriz, Iran.

Luo, Y., Zhang, K., Xie, X., & Yao, X. (2019). Performance evaluation and material optimization of Micro-surfacing based on cracking and rutting resistance. *Construction and Building Materials, 206*, 193-200.

Lyon, C., Persaud, B., & Merritt, D. (2018). Quantifying the safety effects of pavement friction improvements - results from a large-scale study. *International journal of pavement engineering, 19*(2), 145-152.

Mamlouk, M. S., & Zaniewski, J. P. (1998). Pavement preventive maintenance: Description, effectiveness, and treatments. *Flexible Pavement Rehabilitation and Maintenance, ASTM STP 1348*, 121-135.

Mamlouk, M. S., & Zaniewski, J. P. (2001). Optimizing pavement preservation: An urgent demand for every highway agency. *International Journal of Pavement Engineering, 2*(2), 135-148.

McNerney, M. T., Landsberger, B., Turen, T., & Pandelides, A. (1998). Comparative field measurements of tire pavement noise of selected Texas pavements. *Transportation Research Record: Journal of the Transportation Research Board, 1626*, 78-84.

Menapace, I., Masad, E., Bhasin, A., & Little, D. (2015). Microstructural properties of warm mix asphalt before and after laboratory-simulated long-term ageing. *Road Materials and Pavement Design, 16*(S1), 2-20.

Mercado, R., & Fuentes, L. (2017). Measure of asphalt emulsions stability by oscillatory rheology. *Construction and Building Materials, 155*, 838–845.

Mirmiran A, Shahawy M, Nanni A, Karbhari V, Yalim B, & Kalayci A. (2008). *Recommended construction specifications and process control manual for repair and retrofit of concrete structures using bonded FRP composites*.

NCHRP Report 609. Washington, DC: Transportation Research Board of the National Academies.

MnDOT. (2016). *MnDOT'S Experience: Efforts to Improve Micro Surfacing Performance.* Minnesota Department of Transportation.

Morian, D. A. (2011). *Cost benefit analysis of including microsurfacing in pavement treatment strategies & cycle maintenance.* No. FHWA-PA-2011-001-080503. Pennsylvania Department of Transportation, Harrisburg.

MoRT&H. (2013). *Ministry of Road Transport & Highway- Specifications of Road and Bridge Works, Fifth Revision.* New Delhi, India: Indian Road Congress.

Mosier, R. D., & Gransberg, D. D. (2015). Carbon footprint cost index: a pavement case study. *Procedia engineering (Vol. 118, pp. 781-786).*

Moulthrop, J., Day, L., & Ballou, W. (1996). Initial improvement in ride quality of jointed, plain concrete pavement with microsurfacing: case study. *Transportation Research Record: Journal of the Transportation Research Board, 1545*, 3-10.

MS-19. (2008). *A Basic Asphalt Emulsion Manual.* Ibadan, Nigeria: Asphalt Institute Manual Series No. 19, Fourth Edition.

Nair, H., Lane, D. S., & McGhee, K. K. (2020). *Use of Surface Treatments to Extend Pavement Life: A Case Study on US 301, Sussex County, Virginia.* Charlottesville, Virginia: Virginia Transportation Research Council.

Nikolaides, A., & Oikonomou, N. (2000). The use of fly ash as a substitute of cement in microsurfacing. *Waste Materials in Construction, 1*, 234-240.

Noguera, J. A., Quintana, H. A., & Gómez, W. D. (2014). The influence of water on the oxidation of asphalt cements. *Construction and Building Materials, 71*, 451-455.

ODOT. (2018). *Construction and material specifications.* Columbus, OH: State of Ohio, Department of Transportation.

OkDOT. (2009). *Section 707 Thin surface Courses.* Oklahoma: Department of Transportation.

Olden, J. D., & Jackson, D. A. (2002). Illuminating the ‘‘black box’’: a randomization approach for understanding variable contributions in artificial neural networks. *Ecological modelling, 154*(1-2), 135-150.

Ozsahin, T. S., & Oruc, S. (2008). Neural network model for resilient modulus of emulsified asphalt mixtures. *Construction and Building Materials, 22*(7), 1436-1445.

Pandey, S., Sangita, & Pundhir, N. K. (2011). Micro-Surfacing: An eco-friendly bailout for Indian roads. In *8th All India People Technology Congress.* Kolkata.

Patel, N., & Gujar, R. (2017). Evaluation of Performance of High Calcium Fly Ash as a Mineral Filler in Mix Design of Microsurfacing of Road Pavement. *Civil Engineering and Urban Planning: An International Journal (CiVEJ), 4*(2), 49-58.

Patrick, S. (2018). *Guidelines and Specifications for Microsurfacing.* Austroads Research Report AP-R569-18. Sydney, Australia.

Pattanaik, M. L., Choudhary, R., & Kumar, B. (2020). Prediction of frictional characteristics of bituminous mixes using group method of data handling and multigene symbolic genetic programming. *Engineering with Computers, 36*(4), 1875-1888.

PD 6689. (2009). *Surface treatments – guidance on the use of BS EN 12271 and BS EN 12273.* Published Document. BSI British Standards.

Pederson, C. M., Schuller, W. J., & Hixon, C. D. (1988). Microsurfacing with Natural Latex-Modified Asphalt Emulsion: A Field Evaluation. *Transportation Research Record: Journal of the Transportation Research Board, 1171*, 108-112.

Pellecuer, L., Assaf, G. J., & St-Jacques, M. (2014). Life cycle environmental benefits of pavement surface maintenance. *Canadian Journal of Civil Engineering, 41*(8), 695-702.

Peshkin, D. G., Hoerner, T. E., & Zimmerman, K. A. (2004). *NCHRP Report 523 Optimal timing of pavement preventive maintenance treatment applications.* Washington, DC: Transportation Research Board of the National Academies.

Petersen, J. C., & Glaser, R. (2011). Asphalt oxidation mechanisms and the role of oxidation products on age hardening revisited. *Road Materials and Pavement Design, 12*(4), 795-819.

Petersen, J. C., Branthaver, J. F., Robertson, R. E., Harnsberger, P. M., Duvall, J. J., & Ensley, E. K. (1993). Effects of physicochemical factors on asphalt oxidation kinetics. *Transportation Research Record, 1391*, 1-10.

Pittenger, D. (2011). Evaluating sustainability of selected airport pavement treatments with life-cycle cost, raw material consumption, and Greenroads standards. *Transportation Research Record: Journal of the Transportation Research Board, 2206*, 61-68.

Poulikakos, L. D., Cannone Falchetto, A., Wang, D., Porot, L., & Hofko, B. (2019). Impact of asphalt aging temperature on chemo-mechanics. *RSC Advances, 9*(21), 11602-11613.

Poursoltani, M., & Hesami, S. (2020). Performance evaluation of microsurfacing mixture containing reclaimed asphalt pavement. *International Journal of Pavement Engineering, 21*(12), 1491-1504.

Rajagopal, A. (2010). *Effectiveness of chip sealing and micro surfacing on pavement serviceability and life.* Infrastructure Management and Engineering Inc.

Ram, P. V., & Peshkin, D. G. (2014). Performance and Benefits of Michigan Department of Transportation's Capital Preventive Maintenance Program. *Transportation Research Record: Journal of the Transportation Research Board, 2431*, 24-32.

Raza, H. (1992). *An Overview of Surface Rehabilitaion Techniques for Asphalt Pavements.* Washington, D.C.: Federal Highway Administration.

Raza, H. (1994). *State-of-the-practice Design, Construction, and Performance of Micro-Surfacing. FINAL REPORT. No. FHWA-SA-94-051.* Washington, D.C.: Federal Highway Administration.

Reinke, G. H., Ballou, W. R., Engber, S. L., & O'Connell, T. M. (1990). Studies of Polymer-Modified Microsurfacing Materials in Highway Maintenance. *Asphalt Emulsions, ASTM STP 1079*, 80-105.

Robati, M. (2014). *Evaluation and improvement of micro-surfacing mix design method and modelling of asphalt emulsion mastic in terms of filler-emulsion interaction.* Montreal: PhD thesis.

Robati, M., Carter, A., & Perraton, D. (2013a). Incorporation of reclaimed asphalt pavement and post-fabrication asphalt shingles in micro-surfacing mixture. In *Proceedings of the Fifty-Eighth Annual Conference of the Canadian Technical Asphalt Association (CTAA).* St. John's, Newfoundland and Labrador.

Robati, M., Carter, A., & Perraton, D. (2013b). Repeatability and reproducibility of micro-surfacing mixture design tests and effect of aggregates surface areas on test results. *Australian Journal of Civil Engineering, 11*(1), 41-56.

Robati, M., Carter, A., & Perraton, D. (2013c). Evaluation of test methods and selection of aggregate grading for type III application of micro-surfacing. *International Journal on Pavement Engineering & Asphalt Technology, 14*(2), 11-66.

Robati, M., Carter, A., & Perraton, D. (2015a). New conceptual model for filler stiffening effect on asphalt mastic of microsurfacing. *Journal of Materials in Civil Engineering, 27*(11), 04015033.

Robati, M., Carter, A., & Perraton, D. (2015b). Evaluation of a modification of current microsurfacing mix design procedures. *Canadian journal of civil engineering, 42*(5), 319-328.

Rodríguez-Valverde, M. A., Ramón-Torregrosa, P., Páez-Dueñas, A., Cabrerizo-Vílchez, M. A., & Hidalgo-Álvarez, R. (2008). Imaging techniques applied to characterize bitumen and bituminous emulsions. *Advances in colloid and interface science, 136*(1-2), 93-108.

Ronald, M., & Luis, F. P. (2016). Asphalt emulsions formulation: State-of-the-art and dependency of formulation on emulsions properties. *Construction and Building Materials, 123*, 162-173.

Salleh, S., Muhamad, R., Abdillah, M. H., & Shahimi, A. F. (2019). Performance of pavement preservation with Ralumac Micro surfacing at LATAR highway. In *IOP Conference Series: Materials Science and Engineering (Vol. 512, pp. 012049).* IOP Publishing.

Sangiorgi, C., Bitelli, G., & Lanti, C. (2012). A study on texture and acoustic properties of cold laid microsurfacings. In *Procedia-Social and Behavioral Sciences (Vol. 53, pp. 223-234)*.

Santos, J., Flintsch, G., & Ferreira, A. (2017). Environmental and economic assessment of pavement construction and management practices for enhancing pavement sustainability. *Resources, Conservation and Recycling, 116*, 15-31.

Searson, D. (2015). GPTIPS 2: an open-source software platform for symbolic data mining. In A. H. Gandomi, A. H. Alavi, & C. Ryan, *Handbook of Genetic Programming Applications.* New York: Springer International Publishing.

Searson, D. P., Leahy, D. E., & Willis, M. J. (2010). GPTIPS: An open source genetic programming toolbox for multigene symbolic regression. In *Proceedings of the International MultiConference of Engineers and Computer Scientists (Vol. 1, pp. 77-80)*. Hong Kong: Citeseer.

Serigos, P. A., Smit, A., & Prozzi, J. A. (2017). *Performance of Preventive Maintenance Treatments for Flexible Pavements in Texas. Report No. FHWA/TX-16/0-6878-2.* Washington, DC: Federal Highway Administration.

Shackil, G., Ali, A., Mehta, Y., & Papuc, D. (2020). Evaluating the laboratory cracking performance of pavement preservation materials using the Texas overlay tester. *Construction and Building Materials, 262*, 120802.

Sharaf, E. A., & Mandeel, F. M. (1998). An Analysis of the Impact of Different Priority Setting Techniques on Network Pavement Condition. In *Proceedings of the Fourth International Conference on Managing Pavements* (pp. 159-168). Pretoria, South Africa: CSIR Transportek.

Sholar, G. A., & Kim, S. (2013). *Performance Report of Micro-surfacing Experimental Project US-319/SR-369 in Leon County.* State Materials Office, State of Florida.

Simões, D., Almeida-Costa, A., & Benta, A. (2017). Preventive maintenance of road pavement with microsurfacing - an economic and sustainable strategy. *International Journal of Sustainable Transportation, 11*(9), 670-680.

Sivanandam, S. N., & Deepa, S. N. (2006). *Introduction to neural networks using Matlab 6.0.* New Delhi, India: Tata McGraw-Hill Education.

Smith, R., & Beatty, C. (1999). Microsurfacing usage guidelines. *Transportation Research Record: Journal of the Transportation Research Board, 1680*, 13-17.

Smith, R., Beatty, C., Button, J., Stacy, S., & Andrews, E. (1994). *Use of Micro-Surfacing in Highway Pavements. Final Report (No. FHWA/TX-95/1289-2F).* Washington, DC: Federal Highway Administration.

Spray, A., Parry, T., & Huang, Y. (2014). Measuring the Carbon Footprint of Road Surface Treatments. In *International Symposium on Pavement LCA.* Davis, California.

Start, M. R., Kim, J., & Berg, W. D. (1998). Potential safety cost-effectiveness of treating rutted pavements. *Transportation research record, 1629*(1), 208-213.

Susanto, H. A., Yang, S.-H., & Chou, H.-H. (2019). Mechanical Properties of Thin Surface Treatment for Pavement Maintenance. *The Baltic Journal of Road and Bridge Engineering, 14*(2), 136–157.

Tabatabaee, N., Ziyadi, M., & Shafahi, Y. (2012). Two-Stage Support Vector Classifier and Recurrent Neural Network Predictor for Pavement Performance Modeling. *Journal of Infrastructure Systems, 19*(3), 266-274.

Takamura, K. (2001). Portland cement-free microsurfacing. In *International Slurry Seal Association Annual Meeting*. Maui, Hawaii.

Takamura, K., & James, A. (2015). Paving with asphalt emulsions. *Advances in asphalt materials*, 393-426.

Takamura, K., Lok, K. P., Wittlinger, R., & Aktiengesellschaft, B. A. (2001). Microsurfacing for preventive maintenance: Eco-efficient strategy. In *International Slurry Seal Association Annual Meeting (pp. 5)*. Maui, Hawaii.

Tanzadeh, J., & Otadi, A. (2019). Testing and Evaluating the Effect of Adding Fibers and Nanomaterials on Improving the Performance Properties of Thin Surface Asphalt. *Journal of Testing and Evaluation, 47*(1), 654-677.

Tarefder, R. A., White, L., & Zaman, M. (2005). Neural network model for asphalt concrete permeability. *Journal of Materials in Civil Engineering, 17*(1), 19-27.

Temple, W., Shah, S., Paul, H., & Abadie, C. (2002). Performance of Louisiana's chip seal and microsurfacing program, 2002. *Transportation Research Record: Journal of the Transportation Research Board, 1795*, 3-16.

Thiriet, A., Gaudefroy, V., Chailleux, E., Piau, J. M., Delfosse, F., & Leroy, C. (2021). Effects of curing on emulsion cold mix asphalts and their extracted binder. *Functional Composite Materials, 2*(1), 1-14.

Thomas, M. D. (2007). *Optimizing the use of fly ash in concrete (Vol. 5420).* Skokie, IL: Portland Cement Association.

Tighe, S. L., & Gransberg, D. D. (2012). *Sustainable Pavement Maintenance Practices. NCHRP Research Results Digest 365.* Washington, DC: Transportation Research Board of the National Academies.

Topçu, İ. B., & Saridemir, M. (2008). Prediction of rubberized concrete properties using artificial neural network and fuzzy logic. *Construction and Building Materials, 22*(4), 532-540.

TxDOT. (2014). *Standard specifications for construction and maintenance of highways, streets, and bridges.* Austin, TX: Texas Department of Transportation.

Uhlam, B., Andrews, J., Kadrmas, A., Egan, L., & Harrawood, T. (2010). *Micro Surfacing Eco-efficiency Analysis Final Report - July 2010.* BASF Corporation, Florham Park, NJ, Tech. Rep. Submission for Verification of Eco-efficiency Analysis Under NSF Protocol P352, Part B.

Uhlman, B. W., & Saling, P. (2010). Measuring and Communicating Sustainability Through Eco-efficiency Analysis. *Chemical Engineering Progress, 106*(12), 17-26.

Uzarowski, L., Maher, M., & Farrington, G. (2005). Thin Surfacing-Effective Way of Improving Road Safety within Scarce Road Maintenance Budget. In *2005 Annual Conference of the Transportation Association of Canada.* Calgary, Alberta.

Van Dam, T., Harvey, J., Muench, S., Smith, K., Snyder, M., Al-Qadi, I., Ozer, H., Meijer, J., Ram, P. V., Roesler, J. R., Kendall, A. (2015). *Towards sustainable*

pavement systems: A reference document. Washington DC: Federal Highway Administration.

Vargas-Nordcbeck, A. (2019). 6-Year Study on Micro Surfacing Performance. In *International Airfield and Highway Pavements Conference, pp. 189-197*. Chicago, Illinois.

Wang, A., Shen, S., Li, X., & Song, B. (2019). Micro-surfacing mixtures with reclaimed asphalt pavement: Mix design and performance evaluation. *Construction and Building Materials, 201*, 303-313.

Wang, F., Liu, Y., Zhang, Y., & Hu, S. (2012). Experimental study on the stability of asphalt emulsion for CA mortar by laser diffraction technique. *Construction and building materials, 28*(1), 117-121.

Wang, G., Morian, D., & Frith, D. (2012). Cost-benefit analysis of thin surface treatments in pavement treatment strategies and cycle maintenance. *Journal of Materials in Civil Engineering, 25*(8), 1050-1058.

Wang, Y., Wang, G., & Mastin, N. (2011). Costs and effectiveness of flexible pavement treatments: experience and evidence. *Journal of Performance of Constructed Facilities, 26*(4), 516-525.

Wang, Z., Gao, J., Ai, T., & Zhao, P. (2014). Laboratory investigation on microwave deicing function of micro surfacing asphalt mixtures reinforced by carbon fiber. *Journal of Testing and Evaluation, 42*(2), 498-507.

Watson, D., & Jared, D. (1998). Georgia department of transportation's experience with microsurfacing. *Transportation Research Record: Journal of the Transportation Research Board, 1616*, 42-46.

West, K., & Smith, R. (1996). *Micro-surfacing: Guidelines for Use and Quality Assurance.* Texas Transportation Institute.

Wijnen, W., & Stipdonk, H. (2016). Social costs of road crashes: An international analysis. *Accident Analysis & Prevention, 94*, 97-106.

Wood, T. J., & Geib, G. (2001). *1999 Statewide Micro Surfacing Project. Report No. MN/RC-2001-11*. Minnesota Department of Transportation.

Wu, G., Yu, M., & Tan, W. (2011). Study on the water damage resistance performance of micro-surfacing. *Applied Mechanics and Materials*, *97*, 162-166.

Wu, Z. (2015). Research on Fiber Micro-Surfacing Mixture Design and Pavement Performance in Interchange's Connections. In *MATEC Web of Conferences*, *25*. EDP Sciences.

Wu, Z., Groeger, J. L., Simpson, A. L., & Hicks, R. G. (2010). *Performance Evaluation of Various Rehabilitation and Preservation Treatments. Report No. FHWA-HIF-10-020.* Washington DC: Federal Highway Administration.

Xiao, F., Amirkhanian, S., & Juang, C. H. (2009). Prediction of fatigue life of rubberized asphalt concrete mixtures containing reclaimed asphalt pavement using artificial neural networks. *Journal of Materials in Civil Engineering, 21*(6), 253-261.

Xiao, Y., Wang, F., Cui, P., Lei, L., Lin, J., & Yi, M. (2018). Evaluation of Fine Aggregate Morphology by Image Method and Its Effect on Skid-Resistance of Micro-Surfacing. *Materials, 11*(6), 920.

Yan, J., Zhang, Z., Ding, W., & Li, F. (2014). Cost-Benefit Analysis of Preventive Maintenance Treatments for Semi-rigid Base Asphalt Pavement in Jiangsu, China: A Pilot Study. In *93rd Transportation Research Board Annual Meeting.* Washington DC.

Yang, S.-H., & Liu, G.-W. (2017). Using packing theory to improve micro-surfacing mix design procedure and evaluating its long term performance. In *96th Transportation Research Board Annual Meeting.* Washington, D.C.

Yang, Y., Yang, Y., & Qian, B. (2019). Performance and microstructure of cold recycled mixes using asphalt emulsion with different contents of cement. *Materials, 12*(16), 2548.

Yao, L., Dong, Q., Ni, F., Jiang, J., Lu, X., & Du, Y. (2019). Effectiveness and Cost-Effectiveness Evaluation of Pavement Treatments Using Life-Cycle Cost Analysis. *Journal of Transportation Engineering, Part B: Pavements, 145*(2), 04019006.

Ye, Y., Guo, J., & Hou, F. (2017). Effects of Aggregate Gradation on Drying MicroSurfacing added by Waste Rubber Powders. In *IOP Conference Series (Vol. 216, pp. 012030)*. Seoul, Korea: Materials Science and Engineering.

Yu, J., Zhang, X., & Xiong, C. (2017). A methodology for evaluating micro-surfacing treatment on asphalt pavement based on grey system models and grey rational degree theory. *Construction and Building Materials, 150*, 214-226.

Yuan, Y., Zhu, X., & Chen, L. (2020). Relationship among cohesion, adhesion, and bond strength: From multi-scale investigation of asphalt-based composites subjected to laboratory-simulated aging. *Materials & Design, 185*, 108272.

Zalnezhad, M., & Hesami, E. (2020). Effect of steel slag aggregate and bitumen emulsion types on the performance of microsurfacing mixture. *Journal of Traffic and Transportation Engineering (English Edition), 7*(2), 215-226.

Zaniewski, J. P., & Mamlouk, M. S. (1996). *Pavement Maintenance Effectiveness - Preventive Maintenance Treatments. Report No. FHWA-SA-96-027*. Washington DC: Federal Highway Administration.

Zhai, H., & Rosales, A. (2017). Accelerating micro surfacing mix design process. In *AEMA-ARRA-ISSA annual meeting, pavement preservation and recycling alliance, (pp. 1-6)*. Tucson, Arizona.

Zhao, F., Wang, K., & Zhang, S. (2010). Application of Micro-Surfacing in Pavement Preventive Maintenance for Shen-Shan Freeway. In *E-Product E-Service and E-Entertainment (ICEEE), 2010 International Conference (pp. 1-4)*. Henan, China: IEEE.

Zuniga-Garcia, N., Martinez-Alonso, W., Smit, A. d., Hong, F., & Prozzi, J. A. (2018). Economic Analysis of Pavement Preservation Techniques. *Transportation Research Record, 2672*(12), 10-19.

Appendix A

Correlation between observed and ANN predicted test results

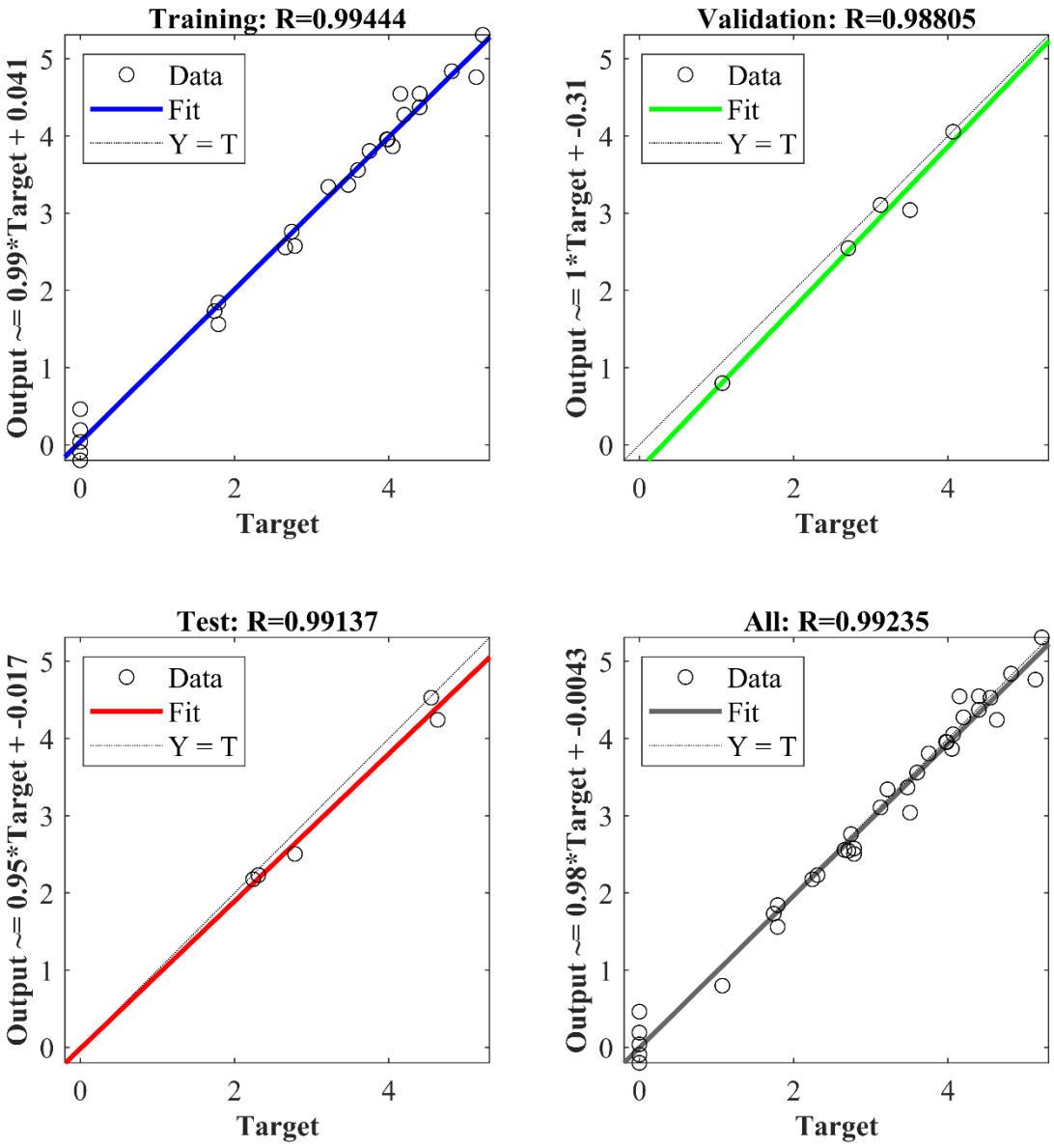

Figure A.1: Correlation between observed and ANN predicted consistency

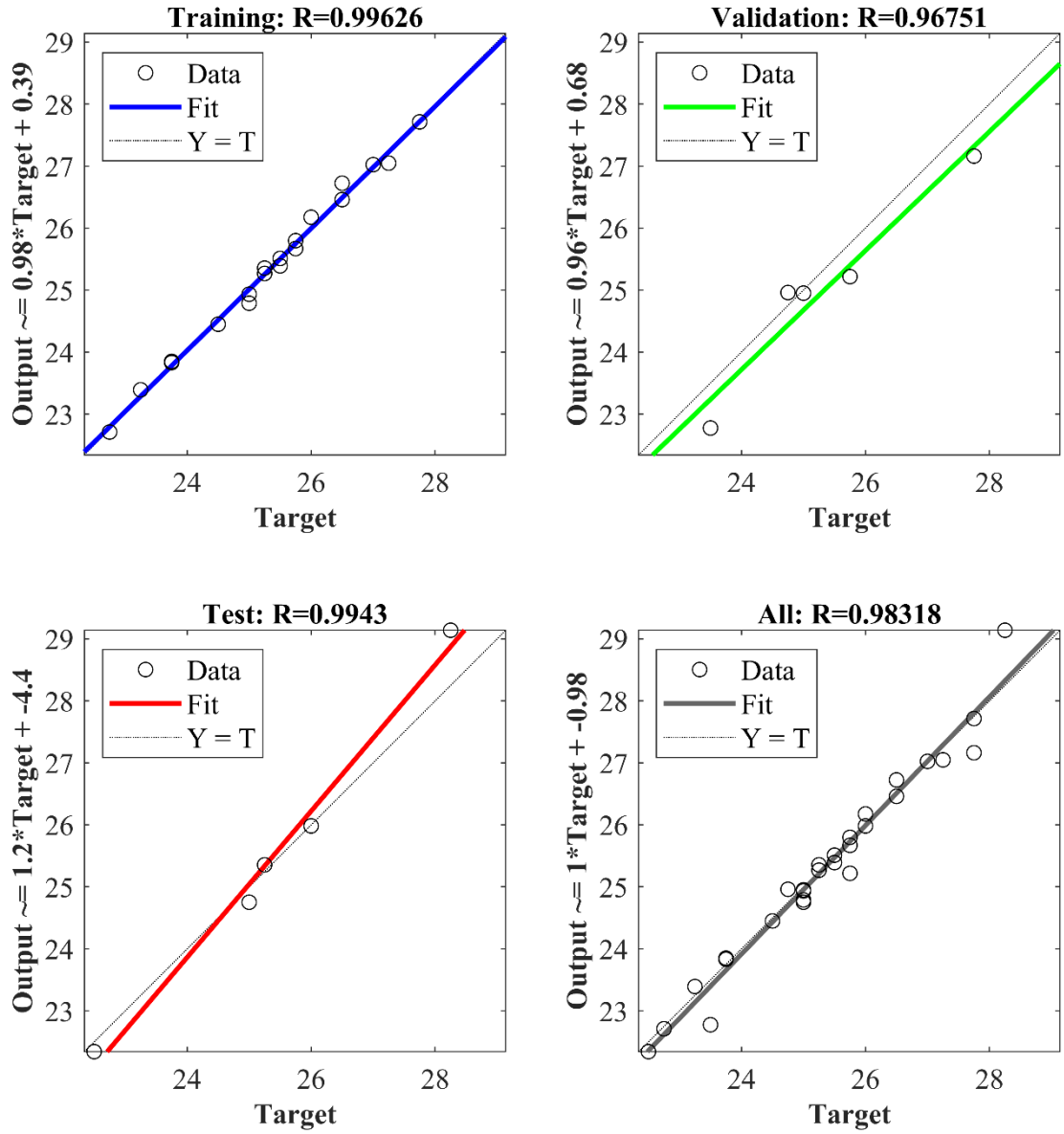

Figure A.2: Correlation between observed and ANN predicted cohesion (30-min)

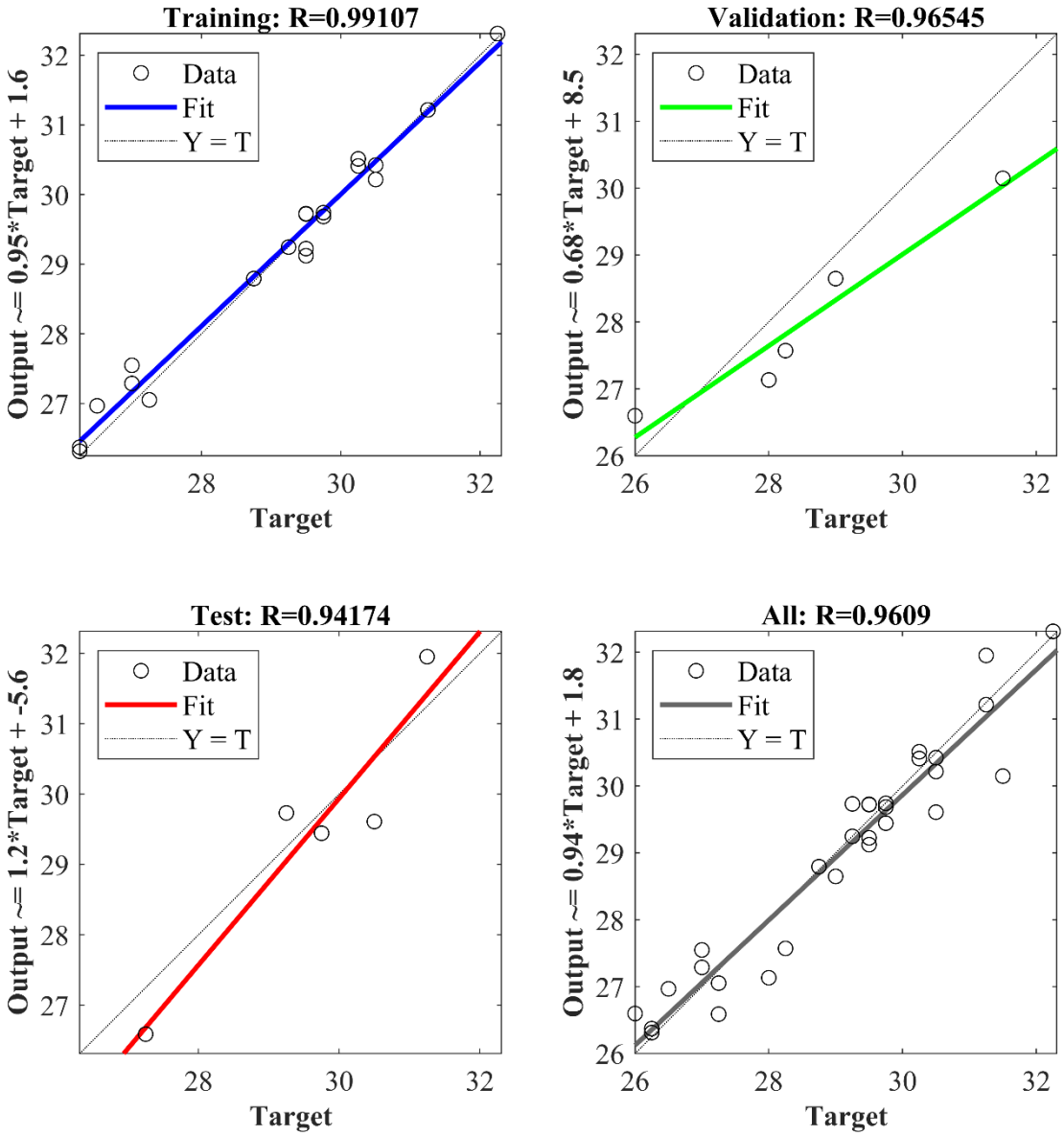

Figure A.3: Correlation between observed and ANN predicted cohesion (60-min)

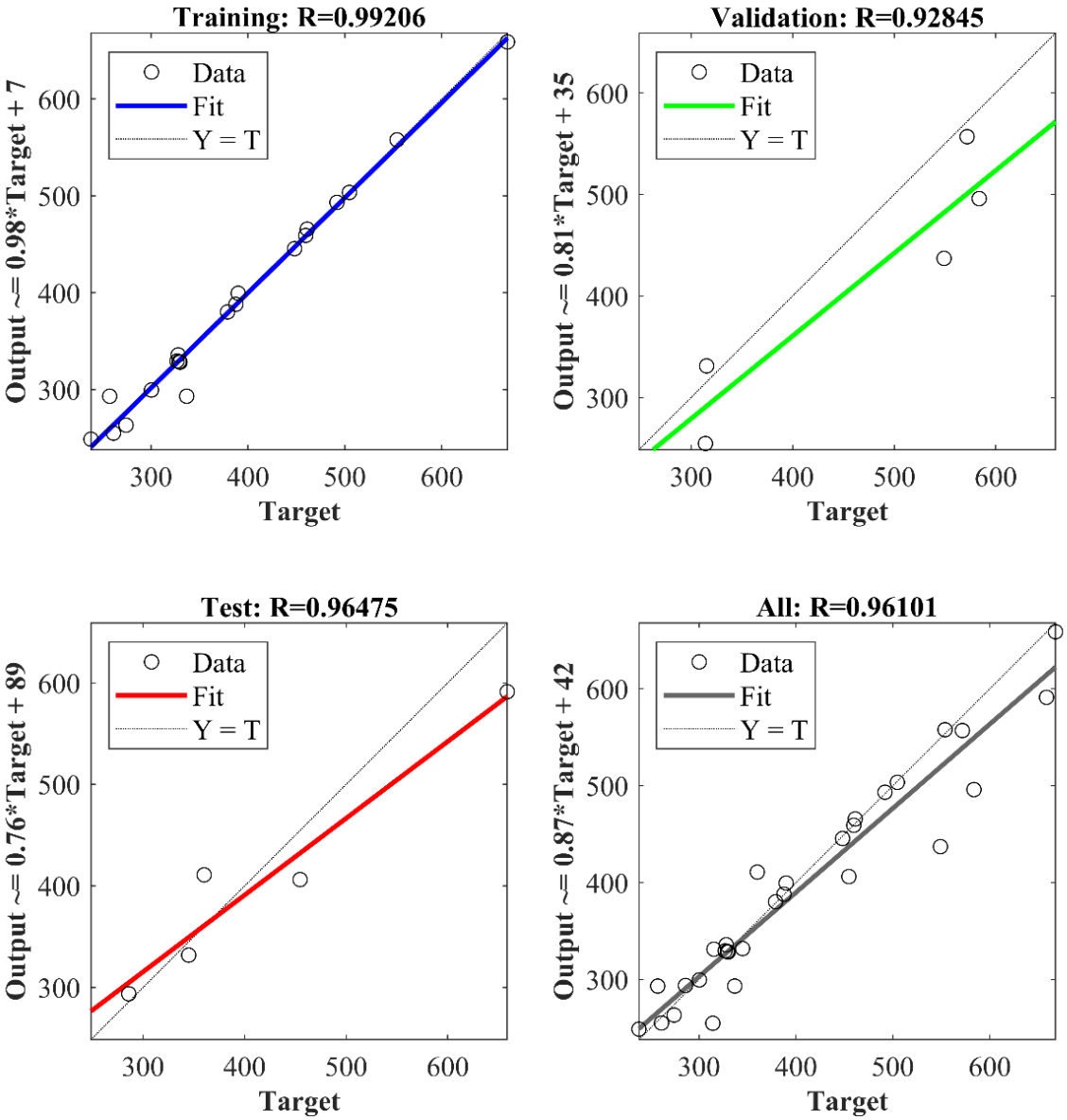

Figure A.4: Correlation between observed and ANN predicted abrasion loss

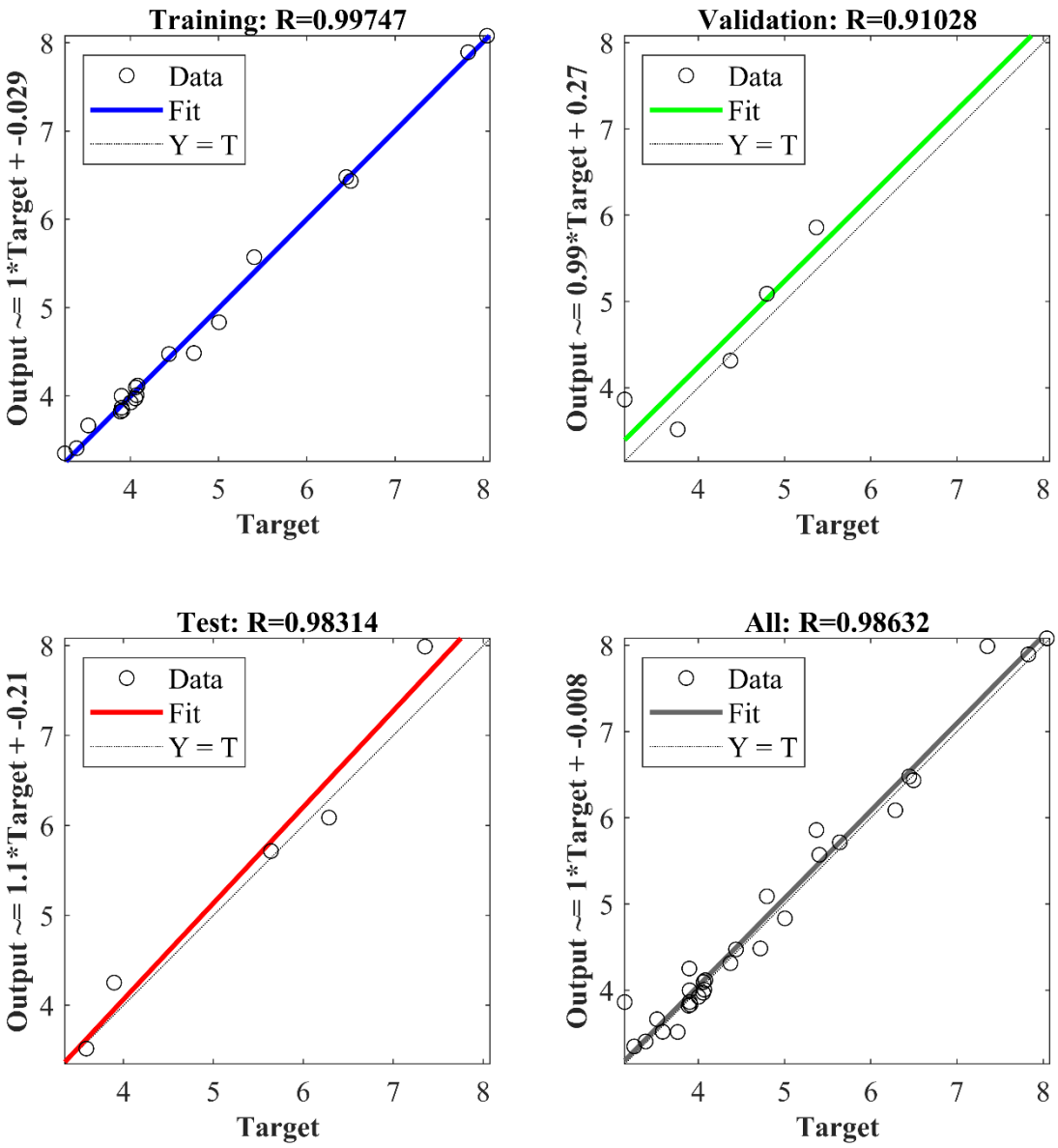

Figure A.5: Correlation between observed and ANN predicted lateral displacement

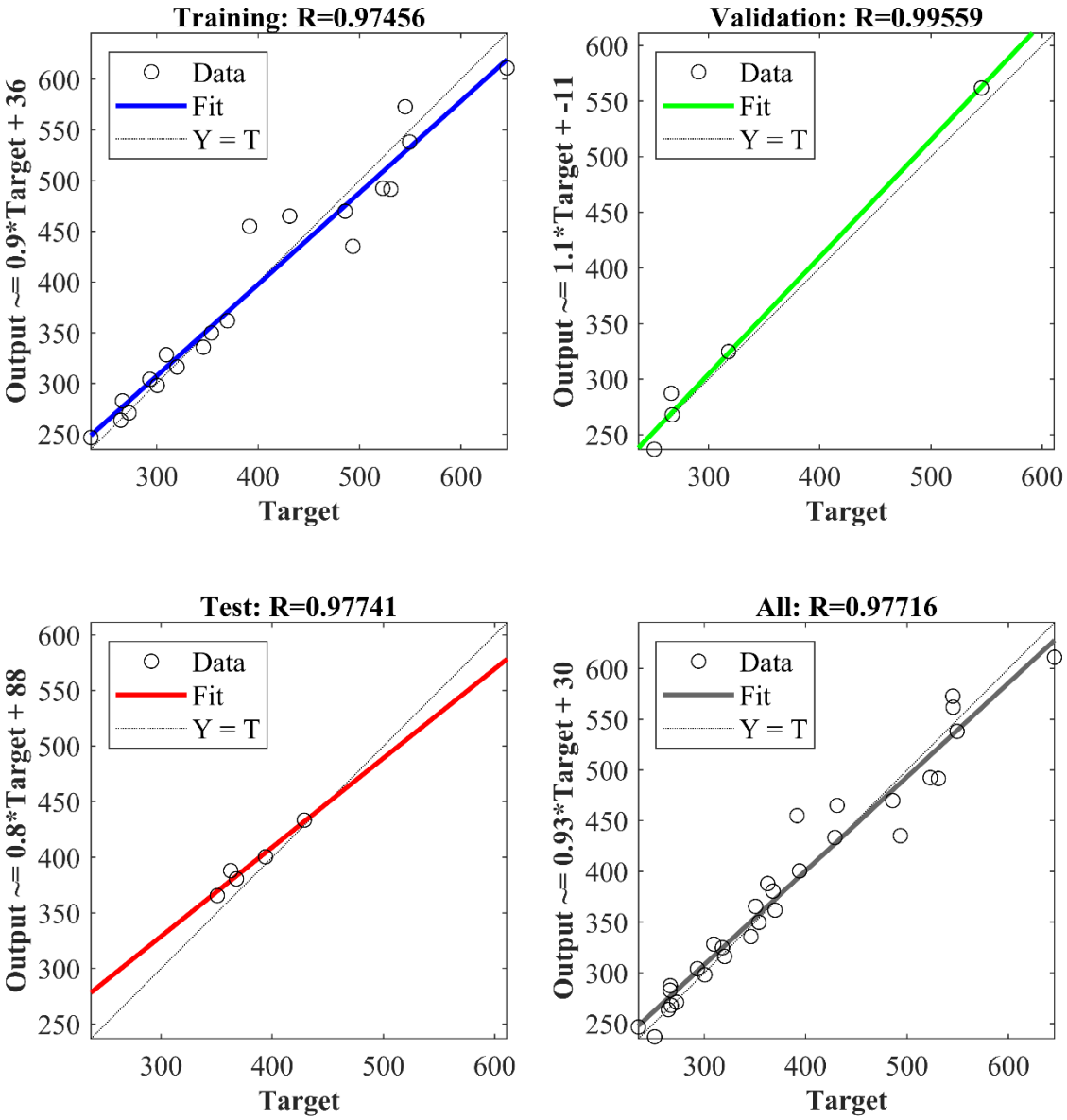

Figure A.6: Correlation between observed and ANN predicted sand adhesion

Appendix B

Selection of parameters for modeling using MSGP

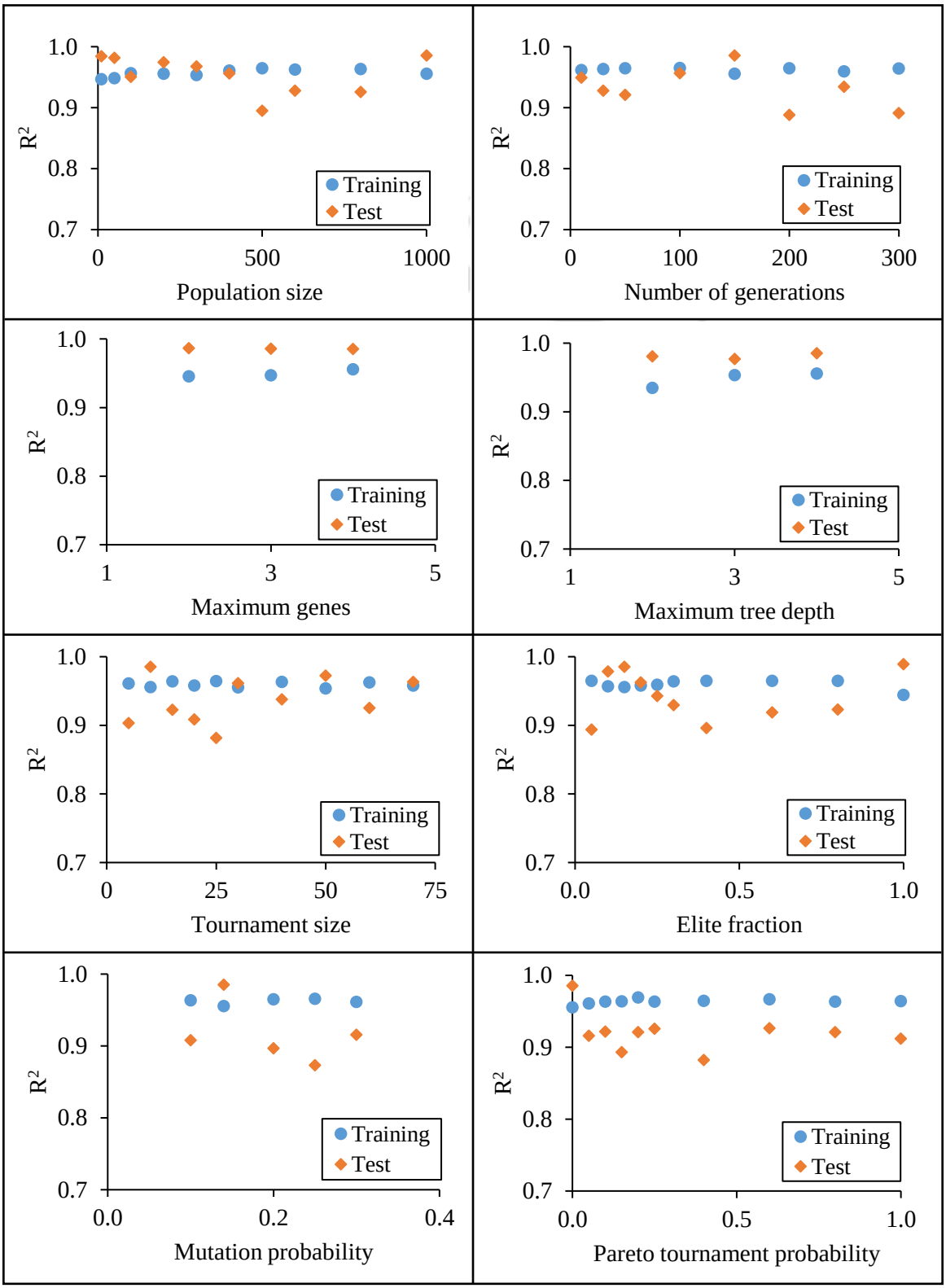

Figure B.1: Selection of parameters for modeling consistency using MSGP

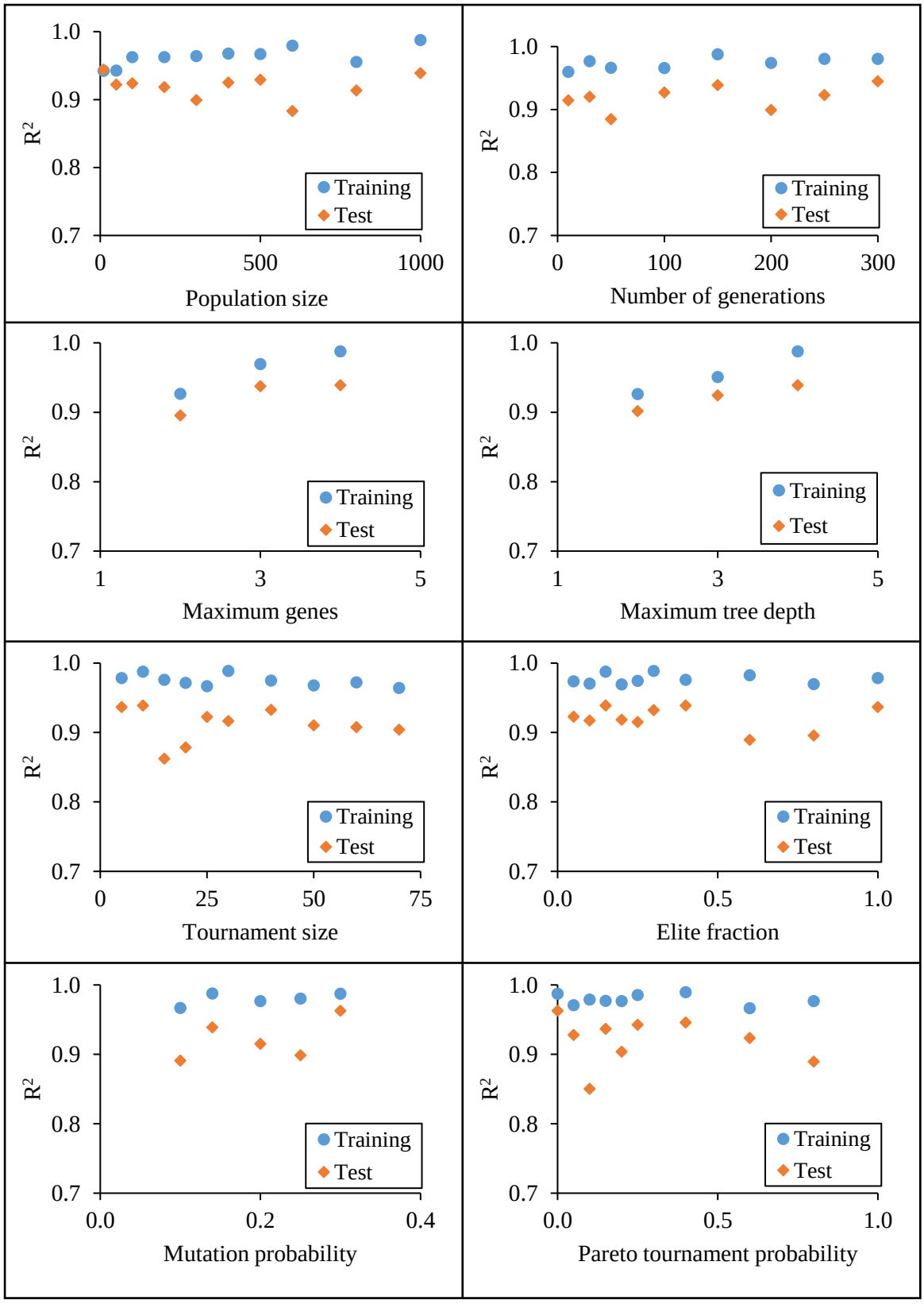

Figure B.2: Selection of parameters for modeling cohesion at 30-min using MSGP

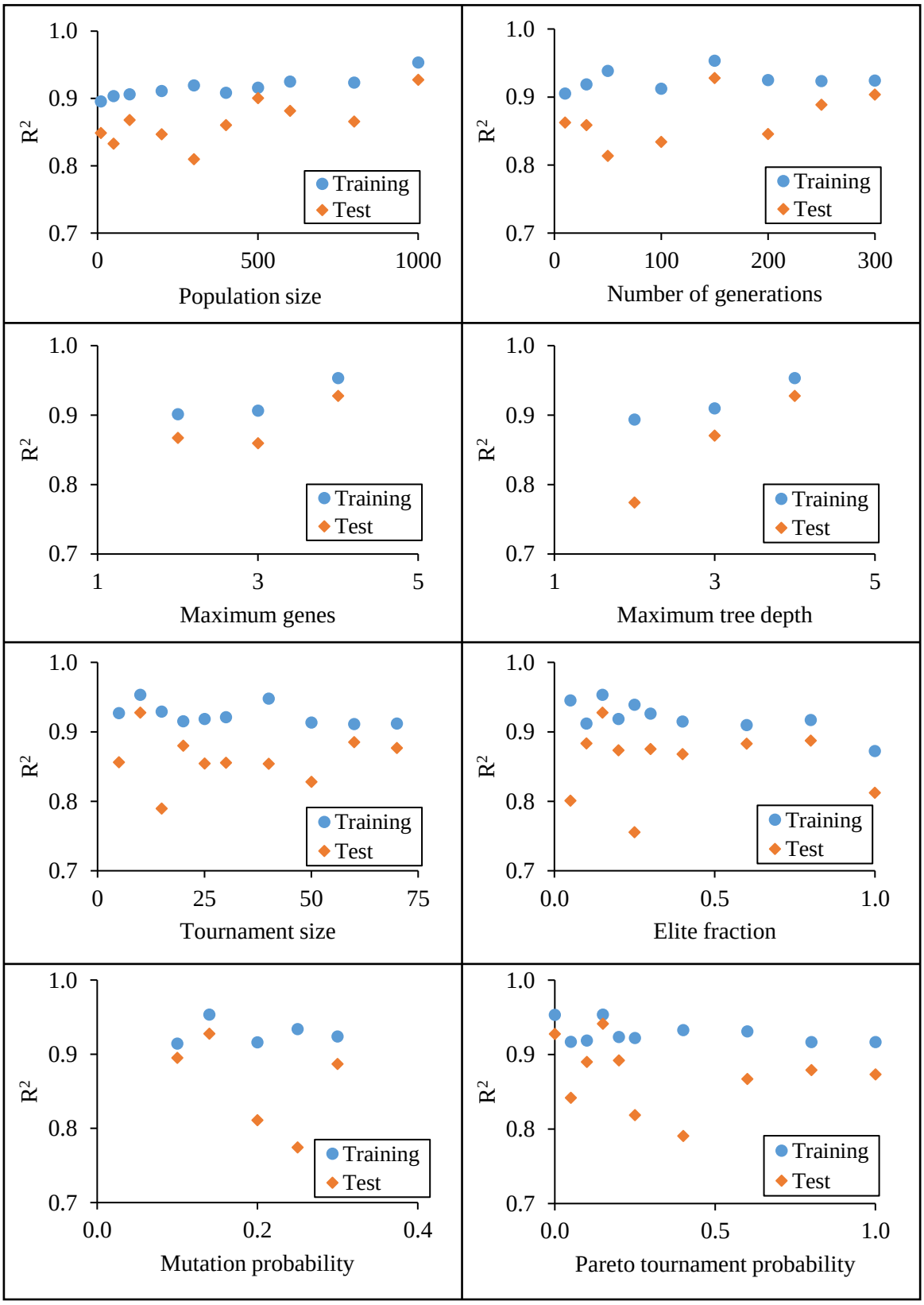

Figure B.3: Selection of parameters for modeling cohesion at 60-min using MSGP

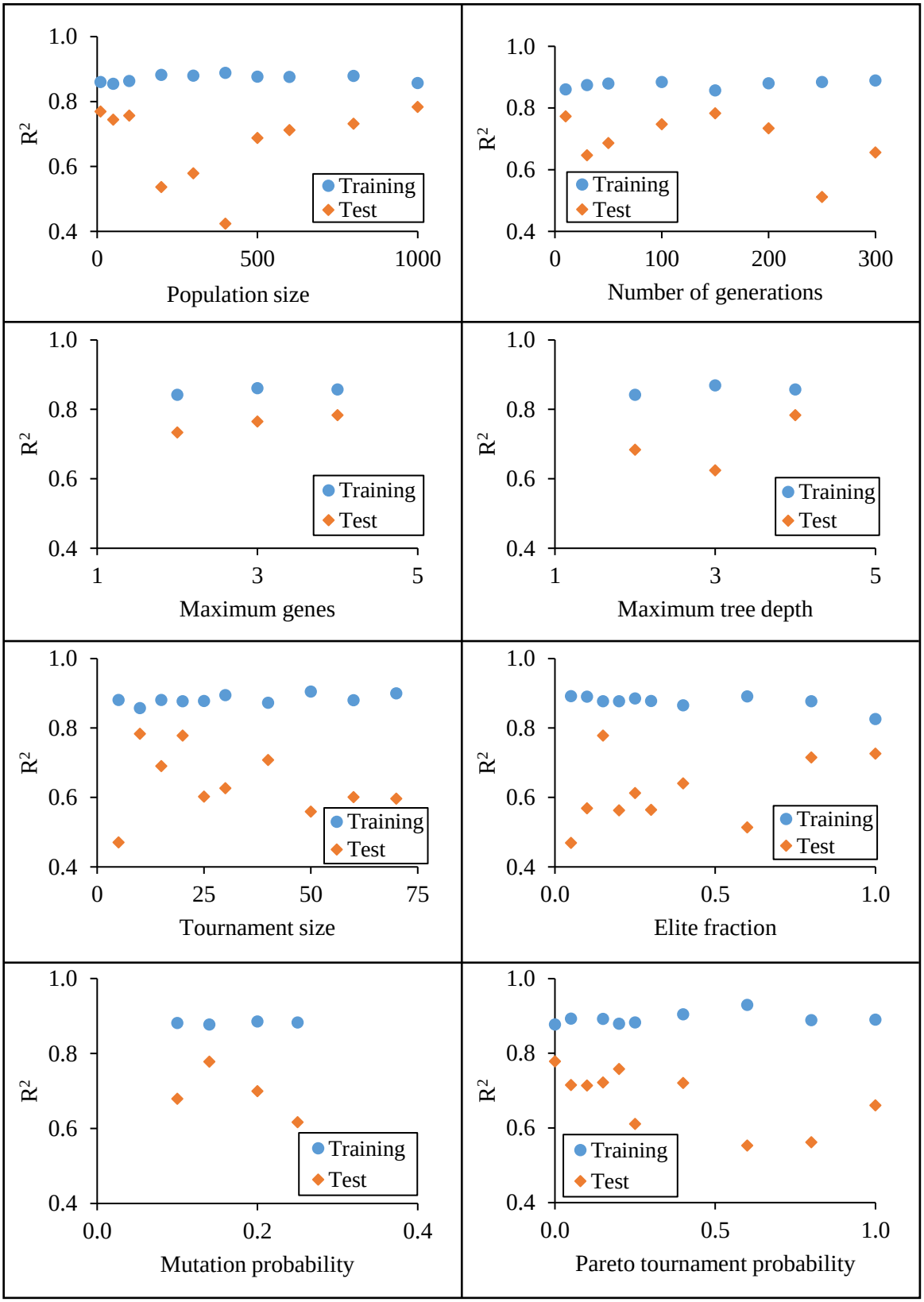

Figure B.4: Selection of parameters for modeling abrasion loss using MSGP

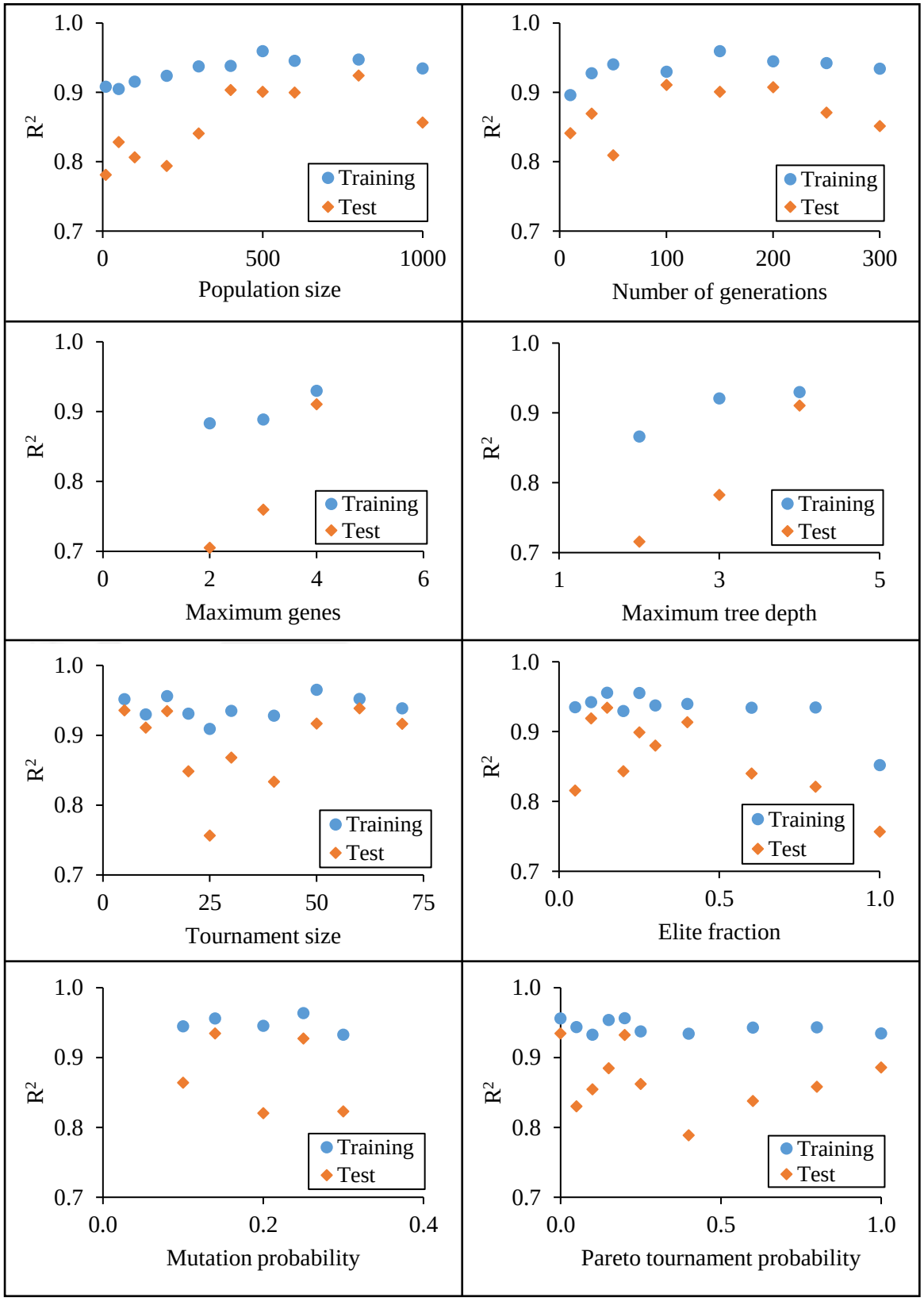

Figure B.5: Selection of parameters for modeling lateral displacement using MSGP

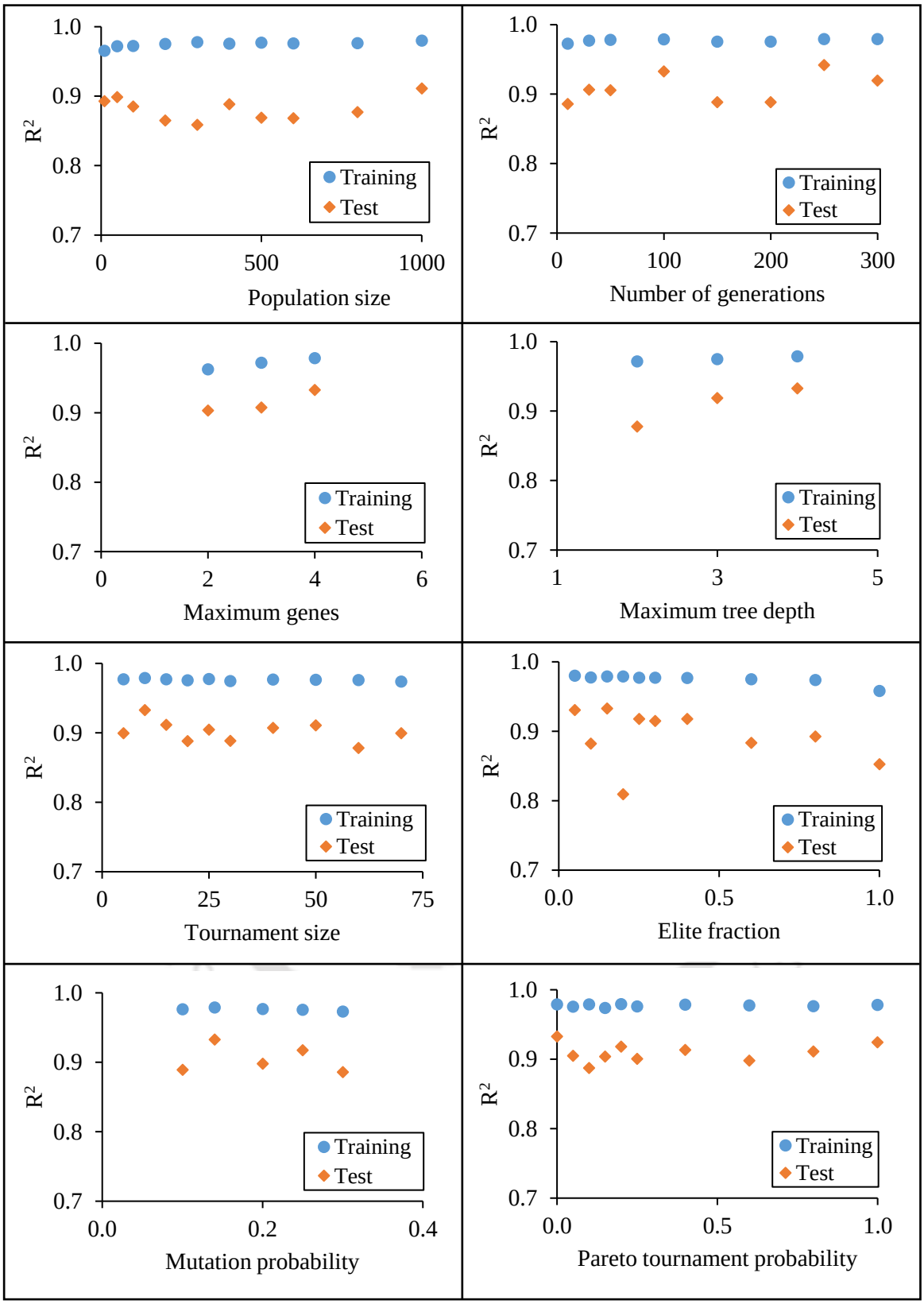

Figure B.6: Selection of parameters for modeling sand adhesion using MSGP